UNIVERSITAT DE BARCELONA

Design of peptides able to modulate Protein-protein interactions (PPIs) in mutated p53

Federica Nicolini

Federica Nicolini

Design of peptides able to modulate Protein-Protein Interactions (PPIs) in mutated p53

2022

Design of peptides able to modulate Protein-Protein Interactions (PPIs) in mutated p53

Federica Nicolini

UNIVERSITAT DE BARCELONA

Programa de doctorat de Química Orgànica

Design of peptides able to modulate Protein-Protein Interactions (PPIs) in mutated p53

Federica Nicolini

Tesi doctoral dirigida per:

Prof. Ernest Giralt Lledó

Institut de Recerca Biomèdica,
IRB Barcelona

Prof. Xavier Salvatella Giralt

Institut de Recerca Biomèdica,
IRB Barcelona

Tutor:

Prof. Antoni Riera Escalé

Universitat de Barcelona i
Institut de Recerca Biomèdica, IRB Barcelona

Barcelona, 2022

ACKNOWLEDGEMENTS

Primero de todo, me gustaria agradecer a Ernest. No hay palabras suficientes para describir lo bonito que ha sido trabajar contigo por tu enorme paciencia, curiosidad, disponibilidad y grandísima pasión que pones en tu trabajo y en todo lo que haces. Quien trabaja contigo percibe eso y es una gran suerte. Gracias por dejar siempre la puerta de tu despacho abierta. Si no hubiese sido por ti, nunca hubiera llevado a termine mi doctorado. De corazón, ¡muchísimas gracias!

También quiero agradecer a Xavier por la posibilidad que me dio de terminar mi trabajo en su grupo.

A lo largo de mi doctorado tuve la suerte de encontrar y trabajar al lado de personas maravillosas y, de verdad, os agradezco a todos porque cada uno a su maniera contribuyó en esta tesis y en este camino.

Nunca olvidaré los almuerzos y los café junto con el mejor grupo de trabajo. Así que muchas gracias Macarena, Salva, Leo, Adam, Toni, Daniela, Mark, Cris G., Cristina Fuster, Cristina Diaz, Shauna, Huguito, Ignacio, Alejandro, Karen, Monica, Xavi. Un gracias especial también es por Eva.

Luego me fui una temporada en la Pompeu Fabra donde me sentí muy a gusto y “en mi casa”. Y todo eso gracias al magnifico grupo de David Andreu. Primero quiero agradecer a David la grande oportunidad que me dio a trabajar con ellos. Y por supuesto a todo el grupo: Adam, Toni, Maria, Giusi, Javi, Roberto, Eduard, Edgar, Patrizia, Yolanda y Sira. Simplemente ha sido fantástico encontrar a nuevos amigos.

Y luego a mi grupo actual: Mireia, Isabel, Jomi, Mateusz, Levi, Stase, Borja, Jesús, Carla, Michael, Paula, Melina, Maria. Especialmente quiero agradecer a Mireia por su grande disponibilidad y hospitalidad.

Un gracias muy grande va también a las facilities del masa y del RMN del IRB. Especialmente quiero agradecer a Mireia, Mar y Marta por sus enormes ayudas y disponibilidad.

Luego quiero agradecer a todos mis amigos y compañeros que estuvieron a mi lado a lo largo de este camino. En particular quiero agradecer a Laura, Maria, Giusi, Petra, Nevenka, Fabio, Jeremy, Luca, Lucia, Milosz, Sol, Pato, Veronica, Dani, Israel y Uri.

Un gracias muy especial va a mis compañeras de acroyoga con las cuales tuvimos momentos realmente bonitos y enriquecedores. Muchas gracias Cindy, Carla y Bea, os quiero mucho.

Per ultimo, ma non per importanza, voglio ringraziare di cuore la mia famiglia. Grazie babbo per tutto quello che hai fatto e continui a fare per me. Grazie Franci per essere la mia roccia, per esserci sempre e sapermi ascoltare come nessun altro sa fare. Grazie mamma per la tua grande sensibilitá e disponibilitá sempre e comunque per me. Grazie Cello e Gia per sapermi fare ridere e cogliere il lato divertente delle cose. Grazie Gell per la tua apertura alla nostra cultura e famiglia. Ed infine, GRAZIE Gianni e Amanda, le emozioni che provo per voi sono davvero uniche e speciali. Vi voglio bene, tanto bene.

Fatti non foste a viver come bruti,

ma per seguir virtute e canoscenza.

Versi 119-120, Canto XXVI dell'Inferno, Divina Commedia

Dante Alighieri

CONTENTS

ABBREVIATIONS

aa	Amino acids
ACN	Acetonitrile
AcOH	Acetic acid
Boc	*Tert*-butoxycarbonyl
BSA	Bovine serum albumin
COSY	Correlation spectroscopy
Da	Dalton
DCM	Dichloromethane
DIPEA	*N,N*-diisopropylethylamine
DIC	Diisopropylcarbodiimide
DMEM	Dulbecco's modified eagle medium
DMF	Dimethylformamide
DMSO	Dimethylsulfoxide
DTT	D,L-dithiothreitol
EDC	*N*-(3-dimethylaminopropyl)-*N'*-ethylcarbodiimide hydrochloride
eq	equivalents
ESI	Electrospray ionisation
EtOH	Ethanol
FBS	Fetal bovine serum
Fmoc	9-fluorenylmethoxycarbonyl
HEPES	4-(2-hydroxyethyl)piperazine-1-ethanesulfonic acid
HOAt	1-hydroxy-7-azabenzotriazole
HPLC	High-performance liquid chromatography
HPLC-MS	High-performance liquid chromatography with mass spectrometry detection
HSQC	Heteronuclear single quantum coherence spectroscopy

K_d	Dissociation constant
MD	Molecular dynamics
MeOH	Methanol
MS	Mass spectroscopy
MST	Microscale thermophoresis
MW	Molecular weight
NHS	*N*-hydroxysuccinimide
NMR	Nuclear magnetic resonance
NOE	Nuclear Overhauser effect
NOESY	Nuclear Overhauser effect scectroscopy
Pbf	2,2,4,5,7-pentamethyldihydrobenzofurane-5-sulfonyl
PBS	Phosphate-buffered saline
PDA	Photodiode array
PDB	Protein data bank
PyBOP	1H-Benzotriazol-1-yloxytris(pirrolidino)phosphonium
PPI	Protein-protein interaction
RT	Room temperature
SAW	Surface acoustic wavelength
SD	Standard deviation
SDS	Sodium dodecylsulfate
SEC	Size exclusion chromatography
SPPS	Solid-phase peptide synthesis
TBTU	*O*-(Benzotriazole-1-yl)-1,1,3,3-tetramethyluronium tetrafluoroborate
*t*Bu	*Tert*-butyl
TD	Tetramerisation domain

TFA	Trifluoroacetic acid
TIPS	Triisopropylsilane
T_m	Melting temperature
TOCSY	Total correlation spectroscopy
t_R	Retention time
Trt	Trityl
UPLC	Ultrahigh-performance liquid chromatography
UPLC-MS	Ultrahigh-performance liquid chromatography with mass spectrometry detection
UV	Ultraviolet
WT	Wild type

Proteinogenic amino acids

A
Ala
L-Alanine

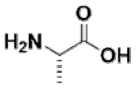

C
Cys
L-Cysteine

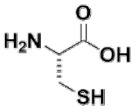

D
Asp
L-Aspartic acid

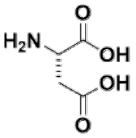

E
Glu
L-Glutamic acid

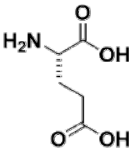

F
Phe
L-Phenylalanine

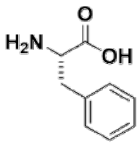

G
Gly
Glycine

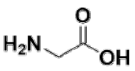

H
Hys
L-Histidine

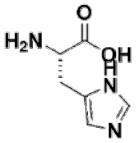

I
Ile
L-Isoleucine

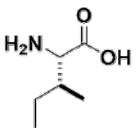

K
Lys
L-Lysine

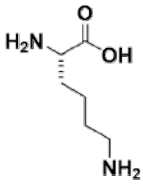

L
Leu
L-Leucine

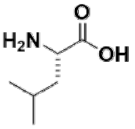

M
Met
L-Methionine

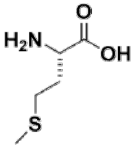

N
Asn
L-Asparagine

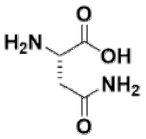

P
Pro
L-Proline

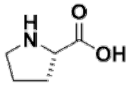

Q
Gln
L-Glutamine

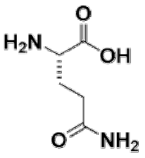

R
Arg
L-Arginine

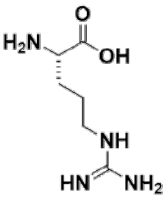

S
Ser
L-Serine

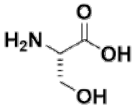

T
Thr
L-Threonine

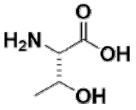

V
Val
L-Valine

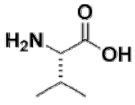

W
Trp
L-Tryptophan

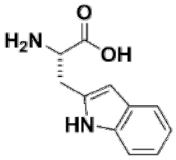

Y
Tyr
L-Tyrosine

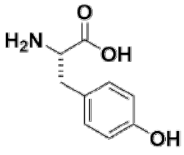

Non-proteinogenic amino acids

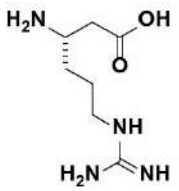

β-3-arginine *S*

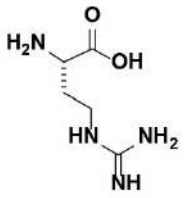

Rab

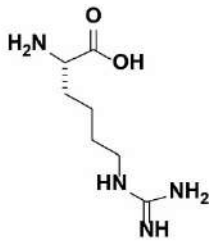

Rys

Protecting groups

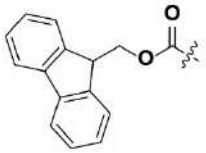

Fmoc

9-Fluorenylmethoxycarbonyl

***t*Bu**

Tert-Butyl

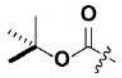

Boc

Tert-Butoxycarbonyl

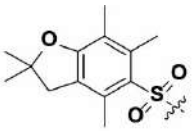

Pbf

2,2,4,5,7-pentamethyldihydro benzofurane-5-sulfonyl

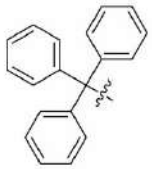

Trt

Trityl

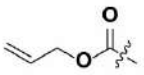

Alloc

Allyloxycarbonyl

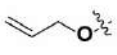

OAl

Allyl

Resins

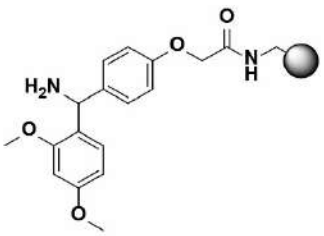

RinkAmide-ChemMatrix resin

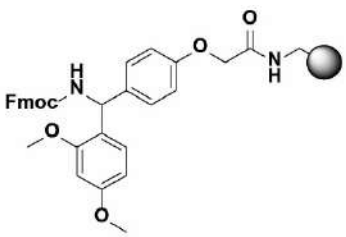

RinkAmide-Protide resin

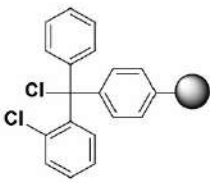

2-chlorotrityl resin

Coupling reagents and additives

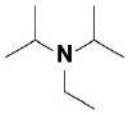

DIPEA

N,N-diisopropylethylamine

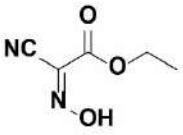

Oxyma

Ethyl ciano-glyoxylate-2-oxime

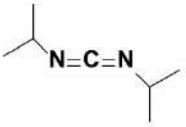

DIC

Diisopropylcarbodiimide

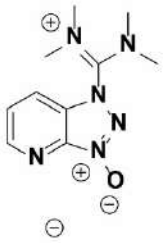

HATU

1-(Bis(dimethylamino)methylene)-1H-1,2,3-triazolo[4,5-b]pyridinium 3-oxide hexafluorophosphate

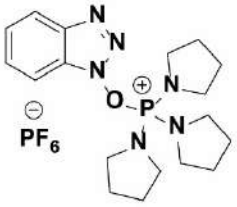

PyBOP

1H-Benzotriazol-1-yloxytris (pyrrolidino)phosphonium hexafluorophosphate

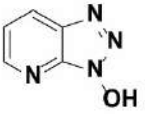

HOAt

1-hydroxy-7-azabenzo triazole

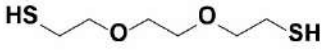

EDT

2,2'-(Ethylenedioxy)diethanethiol

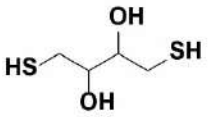

DTT

D,L-dithiothreitol

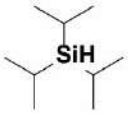

TIPS

Triisopropylsilane

BisNPys

2,2'-dithiobis(5-nitropyridine)

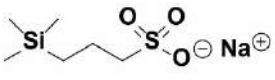

DSS

Sodium trimethylsilyl propanesulfonate

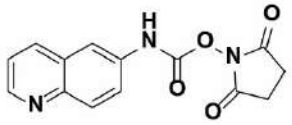

AccQ Reagent

6-Aminoquinolyl-
N-hydroxysuccinimidyl Carbamate

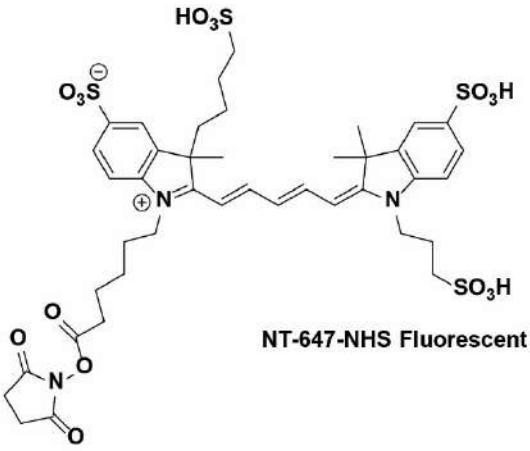

NT-647-NHS Fluorescent dye

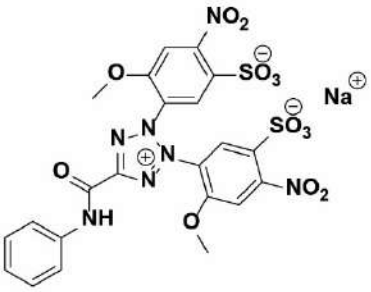

XTT Reagent

2,3-bis-(2-methoxy-4-nitro-5-sulfophenyl)-
2H-tetrazolium-5-carboxanilide

INTRODUCTION

Protein-Protein Interactions (PPIs)

Proteins play a crucial role in a myriad of cellular processes, therefore they are essential biomolecules for life. As matter of fact, the word 'protein' comes from the greek word 'proteios', which means 'of primary importance'. Biomolecules are classified mainly in four types of compounds, each one having its own functionality. Nucleic acids are the *storage of genetic information* and carbohydrates are the *source of the energy*. Lipids are essential structural compounds of biologicals membranes and proteins are the *agent of action* in the cells.[1]

Proteins and peptides are main players in a variety of cellular activities, such as enzymatic catalysis, physiological regulation, transport, cell signalling, immune response, structural composition and support among others. The key characteristic for the functional diversity is their ability to recognise and bind other molecules, including other proteins, sugars, fatty acids, nucleic acids, small ligands or ions. Within the cell, protein-protein interactions (PPIs) are organised into a high complex network, named *interactome*,[2] where proteins are represented as nodes and interactions as edges (Figure 1). Essential proteins are more connected (hubs) than non-essential ones, constituting the structural basis of the network. The deletion of a hub protein is likely lethal for the organism, although the deletion of a non-hub protein could be detrimental too. In this huge and complex network, some proteins have tens, hundreds or thousands of links. This high level of connectivity is reflected in the protein structure because the diversity in the interaction is achieved by intrinsic structural flexibility.[3–6]

Figure 1. Protein interaction network map. Each colour dot represents a node.[2]

This network of interaction is crucial to maintain the homeostasis inside the cells, thus healthy conditions of the whole organism. Malfunctions in this network in many cases causes pathologies, among them various types of cancer. For this reason, PPIs constitute important targets in therapeutic outcomes. The design of molecules able to modulate PPIs is a prominent and challenging strategy for new pharmaceutics. Understanding how proteins interact between each other would facilitate our comprehension of the pathogenic mechanism involved in diseases enabling the possible development of therapeutic agents.

Several examples are reported in the literature in which the aim was to impede interactions between proteins.[7–14] Normally, this strategy is based on the design of peptides or small molecules that act as inhibitor binding to the interface of the interested protein involved in the interaction with its receptor, impeding in this way the PPI. For examples, it is well known that cancer cells are hyper-metabolic active and they overproduce growth factors growing faster than normal cells. Therefore, a possible approach to face cancer growth, is to inhibit the interaction between the epidermal growth factor (EGF) with its receptor.[15] Moreover, cancer cells are hyper-vascularised having in this way many nutrients reaching them and allowing a fast growth. Another strategy to face cancer growth is the isolation of tumour cells impeding new vascularisation around them. Therefore, in this case, the aim is to inhibit the interaction of the vascular endothelial growth factor (VEGF) with its receptor.[16] A third strategy aims to target p53, which plays a crucial role in the cancer development. The idea is to reduce its degradation that is mediated by interaction with MDM2. This binding promotes p53 nuclear expulsion and degradation, constituting a negative control of the protein function. The inhibition of this interaction is a promising strategy for the development of new cancer therapeutics, favouring p53 anti-tumour activity.[13,14]

On the contrary, in this thesis we aim to stabilise PPIs, although not many examples are reported regarding this strategy. In these cases, the protein studied normally is a homo-oligomeric protein that self-interacts with other chains of itself. In particular, in this project, we focused on p53, a homo-tetrameric transcription factor protein.

p53

The transcription factor p53 is a tumour suppressor, which plays a crucial role in many biological processes. It is called 'genome guardian' due to its ability to bind the DNA and check its integrity.[17] In response to stress, p53 transactivates a variety of genes by binding to specific DNA sequences, promoting repairing damaged DNA, cell-cycle arrest, or apoptosis.[18] It contributes to the protection of the genome as well by favouring senescence in order to maintain genome stability.[19]

p53 is inserted in a very sophisticated network of protein-protein interactions (PPIs) and cellular signalling. The activity of p53 is very precisely regulated by several factors that include protein stability, cellular localisation, and tetramerisation. The protein is mainly located in the cytosol and it is shuttled inside the nucleus after stress signals. It is still unclear if the protein is shuttled inside the nucleus as small oligomer and then the tetramerisation occurs in the nucleus, or if it enters directly as a tetramer.[20,21] Factors that damage DNA - such as hypoxia, shortening of the telomeres, and activation of oncogenes - induce post-translational modifications that fast stabilise p53 and increase its concentration, promoting protein oligomerisation. Phosphorylation of more than 20 different sites stabilises the protein and avoids its degradation.[22] Inside the nucleus, p53 binds to DNA through a specific sequence and the affinity to this sequence is 1000-time increased by tetramerisation of the protein. It is suggested that the oligomerisation of p53 occurs step-wise in different times and different areas of the cell. In particular, the dimerization occurs co-translationally on the polysome, whereas the tetramerisation is a post-translational event that takes place in solution.[23] Depending on the severity of the DNA damage, p53 is able to decide to activate different cellular processes, such as DNA repair, senescence, cell-cycle arrest, or apoptosis. The degradation of p53 occurs by MDM2-ubiquitous-mediated pathway that promotes nuclear exclusion and proteasome degradation. A schematic drawing of p53 network is shown in Figure 2.

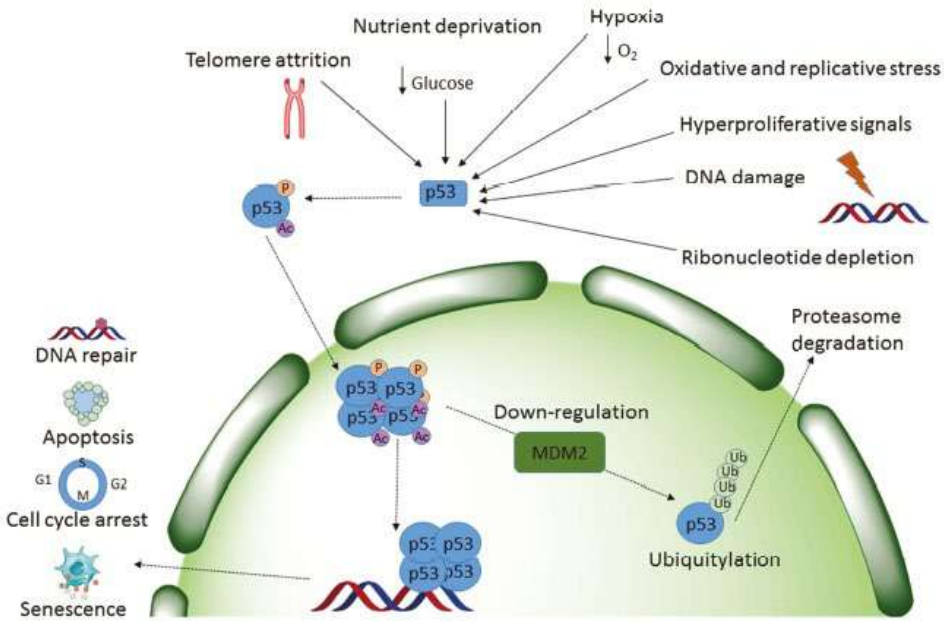

Figure 2. Illustrative p53 network inside the cell. Image adapted from García.[24]

p53 tetramerisation

p53 is a homo-tetrameric protein where each monomer is composed of 393 amino acids. The first time high-molecular weight p53 complexes have been reported was in 1981, when complexes of roughly 200 kDa were identified to interact with SV40 large-T antigen.[25] Later, the tetrameric nature of p53 was confirmed by Friedman *et al*.[26] by gel filtration chromatography, chemical cross-linking, and zonal velocity gradient centrifugation. The protein is composed of an unfolded transactivation domain (TAD), the DNA binding region (DBD), an unfolded linker, the tetramerisation domain (TD), and the *C*-terminus (Figure 3 A). The structure of the TD has been resolved by X-ray crystallography[27] and NMR experiments.[28] They found that the secondary structure of the monomer is composed by a β-strain and an α-helix linked together by a little turn, the Gly residue 334 (Figure 3 B). The monomer has a V-shape and the tetramer is a dimer of dimers. Two monomers dimerise through the anti-parallel β-strain and the dimers tetramerise by interactions of the α-helixes. In the dimer formation the hydrogen bonds have a crucial role, whereas the tetramer is mainly stabilised by hydrophobic interactions (Figure 3 C). The *C*-terminus of the protein contains specific sequences, which have the function of localise p53 in the cell. In particular, there are three nuclear localization sequences (NLSs) (res 316-325, 369-375 and 379-384) and a nuclear exporting sequence (NES)

(res 340-351), which is inaccessible when the protein is in its tetrameric form.[29] The presence of a TD (res 325-353)[30] is fundamental for the tetramerisation of the protein, which enhances the affinity of the protein itself with specific DNA sequences.[31] The DBD recognises and binds specific sequences of DNA, and the tetramerisation of the protein is essential for the stability of the protein-DNA complex. Weinber *et al*.[32] showed that the binding to the DNA is highly co-operative, and oligomerisation of the protein increase its affinity to the DNA. The binding affinity of the tetramer to the DNA, in fact, is 1000-time high than that of the monomer, but it is only 6-time higher than that of the dimer. It has been suggested that the TD and the *C*-terminus play a crucial role for the binding of the protein to the DNA, not only due to the tetramerisation, but as well to the long-range inter-domain communication between the DBD and the TD and the influence of the latter on the conformation of the first.[33]

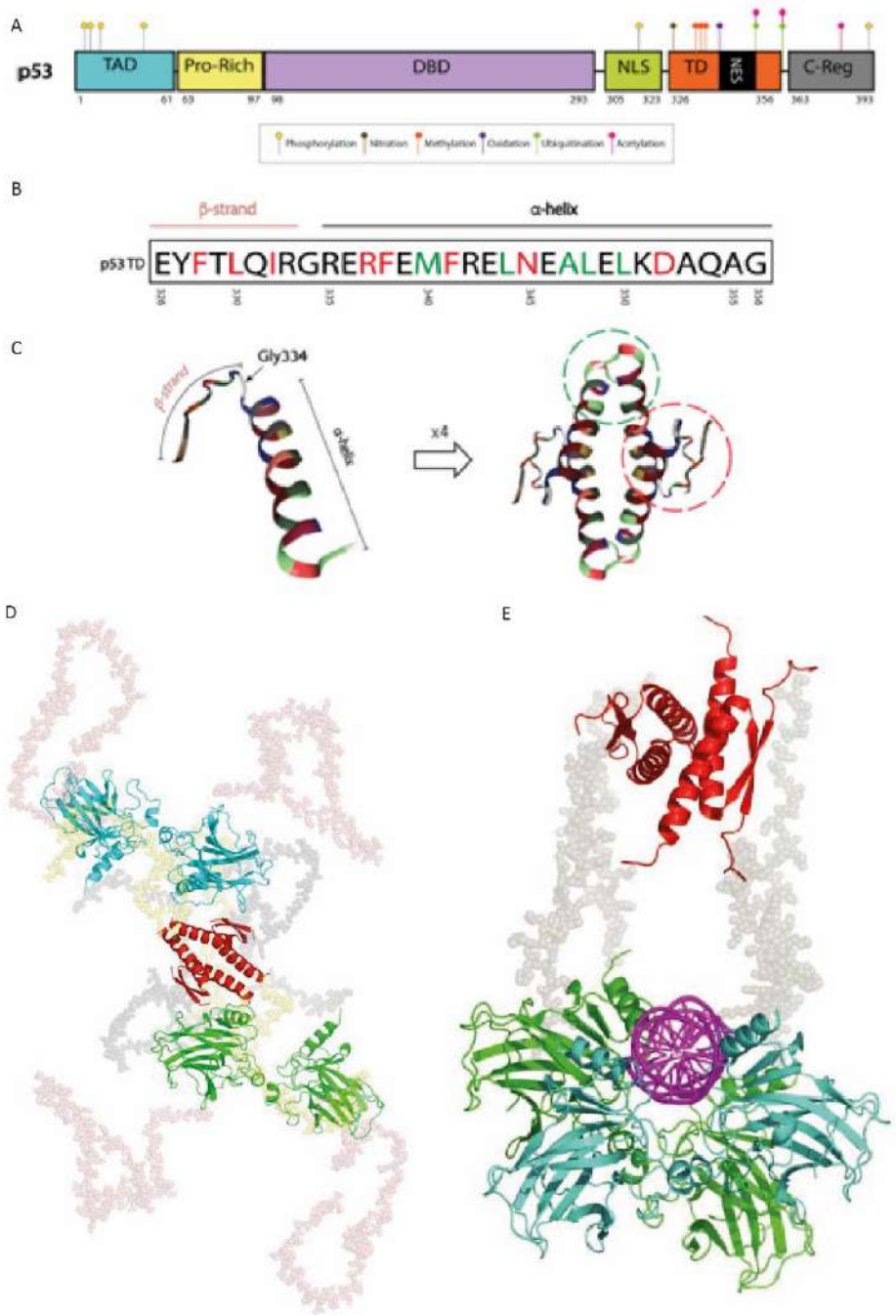

Figure 3. p53 structure of the whole protein and of the tetramerisation domain. (A) Map of p53 protein; PTM: post-translational modifications. p53TD sequence (B) and structure (C). Quaternary structure of p53 (D) and of the DNA-p53 complex (E). Images adapted from Gencel-Augusto *et al*.[34] and Tidow *et al*.[35]

Although it is universally recognised that p53 acts as a homo-tetramer protein, the mechanism of tetramerisation is not completely understood yet. Different models have been proposed describing an interaction between the *C* and *N*-terminus in murine p53 as key interactions for the tetramerisation of the protein. Nevertheless, for human p53 the model suggests that the tetramerisation occurs prevalently by the presence of the TD.[30] In a healthy cell, the levels of p53 are quite low and the protein is located mainly in the cytosol. It is proposed that different stoichiometries of p53 oligomers coexist in solution, *i.e.* monomers, dimers, and tetramers are in equilibrium.[36] Until recently, it has been proposed that the protein was mainly tetrameric, as tetramers have been found interacting with DNA.[37] More recently, several studies reported that in unstressed conditions the protein is mainly dimeric. Fluorescence correlation spectroscopy (FCS) experiments *in vitro*[36] and in cells[38] consistently suggest the dimer as the most abundant oligomer, although a large cell-to-cell variation has been reported in cell-assays.[38] Recent studies have pointed out that the dimer has biological functions as well. Fischer and coworkers reported that the oligomerisation of p53 is crucial in the cell fate decisions of growth, cell cycle arrest or apoptosis.[39] The tetramerisation is required to induce apoptosis, but the dimer is still able to arrest the cell growth. It has been proposed that, although the protein is mainly dimeric in unstressed conditions, it fully fulfil its functions in a tetrameric state. As a matter of fact, it has been found as 93% tetrameric in cells after DNA damage, meaning that tetramerisation is required for its function.[38] Therefore, the regulation of the tetramerisation plays a crucial role for p53 biological functions and cell fate. Many factors contribute to p53 tetramerisation, such as DNA damage, post-translational modifications, and increase of protein concentration. Despite these evidences, Gaglia *et al*.[40] found functional tetramers in cells before protein concentration increasing and DNA damage.

Regulation of p53 tetramerisation

p53 oligomerisation is sophisticatedly regulated, in fact, post-translational modification of p53 as well as several protein-protein interactions inside the wide network of the protein can either stabilise or avoid protein tetrameristion. The protein MYBBP1A is involved in rRNA transcriptional regulation and process. It is able to bind and stabilise p53, as in the presence of this protein, p53 was found oligomerised giving high-molecular complexes. This does not occur when MYBBP1A is mutated and the mutant is unable to bind p53, suggesting a stabilisation effect after MYBBP1A binding.[41] BCCIP is a protein that interacts with BRCA2 and CDKN1A and it is required for the transactivation activity of wild type p53. p53 does not bind effecintely promoters of CDKN1A (p21) and MDM2 after DNA damage in the cells that have low level of BCCIP, meaning that this protein is modulating p53 activity,

although direct binding with p53 has not been observed. Probably the binding between the proteins is unstable or the modulation is indirect.[42] RhoGAPs is a domain of ArhGAP11A protein that is able to bind p53TD only in its tetrameric form. This interaction probably stabilises the tetramer enhancing the DNA-binding.[43] Another protein, Atg7, which is essential for cell degradation and its recycling, is able to bind p53 and modulates its transcriptional activity. Cells with continued metabolic stress lack Atg7 and they increase apoptotic responses mediated by p53, suggesting a correlation between the amount and activity of the two proteins.[44] Finally, 14-3-3 is a family of conserved proteins that are able to bind to diverse signaling proteins, such as kinases, phosphatases, and transmembrane receptors. Some proteins belonging to 14-3-3 family as well promote p53 dimers to form tetramers at lower concentration and, as consequence, enhance the binding of p53 to sequence-specific DNA.[45]

S100 is a family of calcium-binding proteins and some proteins belonging to this family are able to bind p53 in several domains of the protein. In particular, S100A and S100B proteins can bind either to the intrinsically disordered TAD and *C*-terminus or to the TD. Since TAD and *C*-terminus domains are subjected to post-translational modifications, the binding of S100 protein is modulated and depends on these modifications of p53.[46] On the other hand, S100 proteins that bind to the TD, can bind either the monomer or higher oligomers. Therefore, the effect of the binding is different. In particular, the proteins that bind monomeric p53 impede the tetramerisation of the protein. However, other proteins bind more tightly the tetramer than the monomer. Therefore, depending on the concentration of p53 and the member of the S100 family, binding can shift the balance between monomer and tetramer in either direction.[47] Another protein that inhibits p53 oligomerisation is RBEL1A, a Ras-like GTPase that is overexpressed in cancers. It interacts with the p53TD suppressing oligomer formation in unstressed cells and cells exposed to DNA damage. Silencing of RBEL1A significantly enhances the formation of p53 complexes and RBEL1A knockdown increases the expression of p53 target genes.[48] Finally, multiple cancer cells induce expression of ARC. This protein binds p53 inside the nucleus and promotes p53 exposure of the nuclear exporting sequence (NES), causing a re-localisation of p53 in the cytosol, and, as consequence, avoiding p53-mediated apoptosis. ARC knockdown in breast cancer cells results in tetramerisation of p53, accumulation in the nucleus and expression of p53 target genes.[49]

Post-translational modifications (PTM) as well modulate p53 tetramerisation. Many PTM are reported to occur in p53 but not all of them have been studied in term of tetramerisation propensity. Mainly they occur in the *C*-terminus, which is a regulatory domain of the protein. For example, phosphorylation of S392 promotes protein tetramerisation, whereas phosphorylation of S315 has an opposite effect.[50]

When nitration of Y327 occurs, p53 tetramers are stabilised and its transcriptional activity is increased.[51] On the contrary, when M340 is oxidised the tetramers are destabilised by structural changes that make the protein more sensitive to enzyme degradation.[52] It has been proposed that lysine residues in the C-terminus regulatory domain do not modulate the tetramerisation, as by substituting them with a glutamine or arginine residue there is no effect on the tetramerisation of the protein.[53]

Regulation of p53 activity

There are many levels of p53 regulation, among them p53 localisation, stability, tetramerisation, and cell fate decisions play a crucial role. In unstressed conditions, the protein is instable, with a half-life between 20 and 50 minutes.[36] PTMs stabilise the protein promoting in this way the oligomerisation. Additionally, the quaternary structure of p53 favour as well PTMs that cause p53 activation. The main negative control of p53 is MDM2-mediated ubiquitination.[54] The binding between the two proteins is dependent on the oligomeric state of p53, so tetrameric protein binds better than monomeric or dimeric p53. Lower oligomeric species of mutant p53 are shown to be mainly degraded by ubiquitin independent 20S proteasome.[55–57]

Another level of regulation is protein localisation in the cell. The TD contains a nuclear export sequence (NES, res 340-351) that are accessible when the protein is in non-tetrameric form and it is buried when the protein tetramerises, avoiding thus its expulsion from the nucleus. Some PTMs in the TD favour or inhibit p53 nuclear export. The cancer-related mutation K351N was found to abrogate lysine ubiquitination and, as consequence, p53 nuclear export.[58,59] Moreover, the substitution of Arg residues 333, 335, and 337 by lysine residues affect the protein localisation. Most probably, arginine methylation favours its cytoplasmic localisation reducing the transcriptional activity.[60] A possible therapeutic strategy could be the blocking of the hyperactive export of p53 from the nucleus favouring its activity.

A third level of regulation is tetramerisation of the protein. Although it is largely recognised that the protein is active in its tetrameric form, the tetramerisation event as well as its oligomeric state is still under investigation.[36] Accurate values of dissociation constants between the oligomers are not available in literature, which are fundamental in order to assign the oligomeric state of the protein in normal and cancer cells.

p53 initiates several cellular outcomes, such as apoptosis, cell-cycle arrest, and senescence. How the protein is able to make these decisions remains ununderstood.

Some evidences suggest that PTMs in some TD residues can switch p53 responses of apoptosis or cell-cycle arrest. For example, a triple mutant where Arg residues 333, 335, and 337 are replaced by Lys residues, is unable to undertake arginine methylation, resulting in the inability to activate cell-cycle arrest, but not apoptosis in SAOS-2 cells.[60] Acetylation of C-terminal lysine residues is important for cell fate and it is dependent on tetramer formation. Itahana *et al*.[61] showed that the acetyltransferase p300 acetylates only the tetrameric form of p53 and non-tetrameric mutants, which are non-acetylated, are unable to induce apoptosis. Therefore, PMTs deeply influence p53 activity and protein interactions. The TD is an essential domain for protein regulation, protein functionality and cell fate decisions. Cancer-related TD mutants, thus, need to be investigated to better understand their potential in regulating p53 function.

p53 mutations

Cancer onset is frequently associated to p53 mutations, in fact, more than half of human cancers lose p53 function due to mutations.[62] Tumours with inactive mutated p53 normally are aggressive and resistant to ionising radiation and chemotherapy. In spite of the complex regulatory network, mutations of p53 can affect dramatically the oligomeric state of the protein. The majority of these cancer-related mutations occurs in the DNA binding domain (DBD) (Figure 4). These mutations alter the interaction between p53 and DNA, although can also modulate the aggregation state of the protein.[63] Nevertheless *ca.* 20% of cancer-associated mutations occur in the TD[64,65] having a direct impact on the oligomeric state of p53. Mutations in TD could impact the oligomeric state of p53 modulating the secondary structure of this folded domain and, as a consequence, also its quaternary structure. Changes in the oligomeric state of p53 have been reported to affect the activity of the protein as well.[66] Considering the lengths of the two domains, DBD ≈ 200 residues and TD ≈ 30 residues, the probability to missense mutations is similar, suggesting that both domains are essential for p53 function and that the TD as well has a key role in tumour suppression.

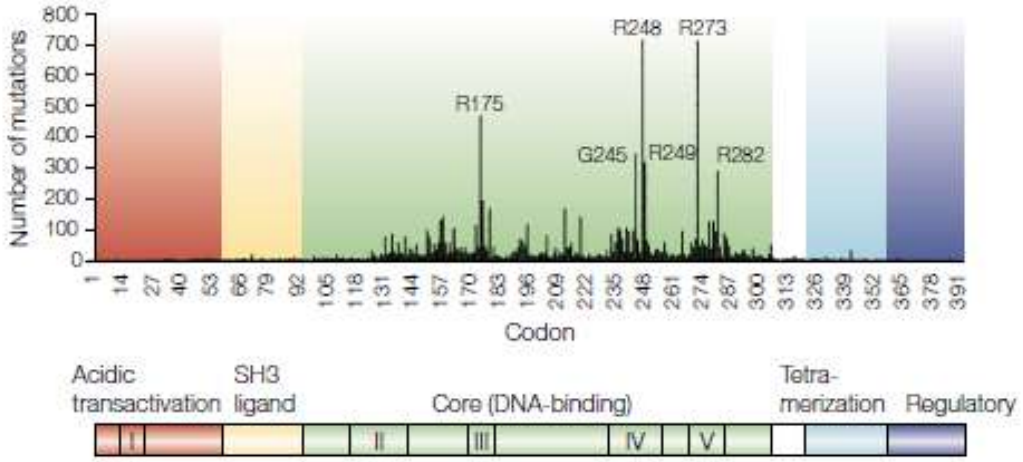

Figure 4. Frequency and distribution of p53 mutations. Image adapted from Bullock *et al.*[62]

The majority of the TD residues are found to be mutated in cancer and these substitutions affect the oligomerisation of the protein, with different extents depending on the position of the mutation and on the nature of the amino acid replacement (Figure 5). Several *in vitro* approaches have been used to determine the oligomeric state of the mutated TDs.[67,68] Moreover, these systems have been studied as well in yeast looking at eight p53 target genes. They found that the oligomerisation of the mutated p53 is related to its activity, although with some exception.[18,69] For example, p53I332T is able to form tetramers but it is transcriptionally inactive. One explication could be that this mutation in the TD causes conformational changes in the DBD, resulting in the impairment of the gene transcription. On the other hand, p53N345K/Y/H are unable to tetramerise but they are transcriptionally active. Finally, some mutants are tetramers and hyperactive, as for example p53R335H, which has been found in cancer patients as well. It is still unclear how a cancer cell can tolerate a hyperactive form of p53. Probably, the mutation affects the interactions with other proteins or p53 localisation in the cell.[70,71] A class of 43 mutants have been studied in mammalian cells, finding that those that are predominantly monomeric do not have transcriptional activity.[70] Moreover, a group of 49 cancer-related mutations have been studied by Kamada *et al*.[64] assigning the oligomeric state of the peptides by gel chromatography. They found that mutations in the hydrophobic part of the tetramer are more destabilising compared to these occurring in solvent-exposed residues.

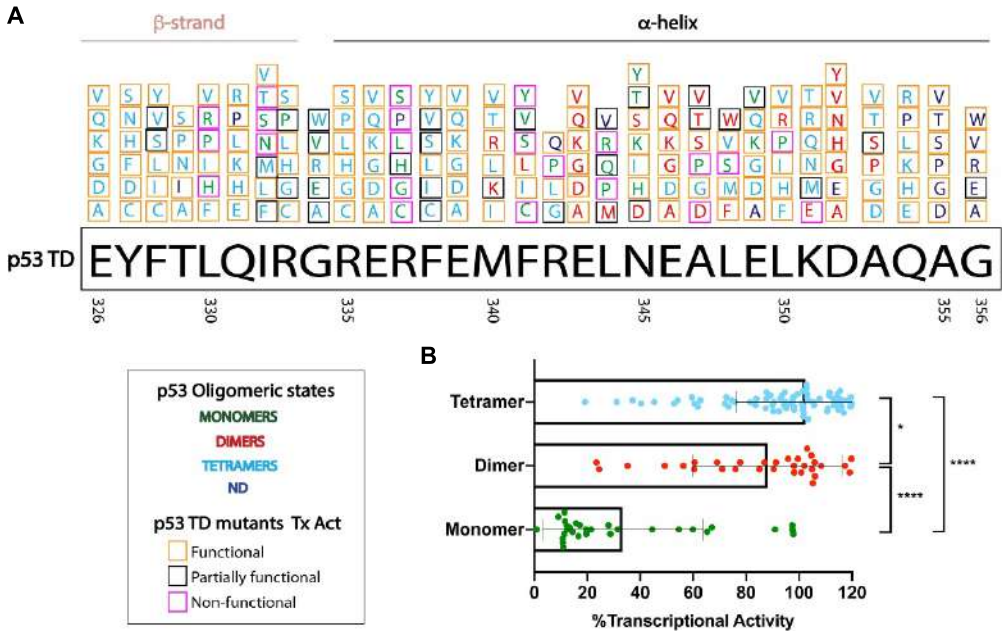

Figure 5. p53TD missense mutations and their outcomes. Image adapted from Gencel-Augusto *et al*.[34]

Even though these studies are extremely important to determine the oligomeric state of mutant p53 and how this is related to protein activity, the limitation is that these experiments were done overexpressing the proteins, or at temperatures different to the physiological one, or at different system-specific environment having been performed in yeast or mammalian cells. As consequence of this, PTM and the presence of proteins that interact with p53 may be affected. The only *in vivo* model currently studied is p53R337H, which corresponds to the most common mutation in the TD. It is related to Li-Fraumeni syndrome (LFS) or LFS-like syndrome and it is particularly widespread in southern Brazil.[72,73] LFS is a cancer predisposition syndrome associated with high risks for a diverse spectrum of onset malignancies in children and adults. There are mainly five cancers associated to this syndrome, such as adrenocortical carcinomas, breast cancer, central nervous system tumours, osteosarcomas, and soft-tissue sarcomas. Moreover, LFS is associated to increased risk for other types of cancers, in particular leukemia, lymphoma, gastrointestinal cancers, cancers of head and neck, kidney, larynx, lung, melanoma, ovary, pancreas, prostate, testis, and thyroid.[74] People affected of LFS normally develop cancers in the first years of their lives, and, those that survive have an increased risk for multiple primary cancers. It has been found that p53R337H is related to adrenocortical carcinomas, mostly in southern Brazil, affecting thus cells where physiologically the pH is basic. The reason of this may be related to the protein stability. By substituting the Arg residue to a His, the protein stability is dependent

on the pH, having a higher destabilising effect at basic pH with un-protonated imidazole group.[75] *In vivo* models of this mutation, which corresponds to p53R334H in mice, showed that the protein is predominantly monomeric and its transcriptional activity is compromised.[76] Jeffers *et al*.[77] found that mutant p53R334H mice developed tumours with long latency and incomplete penetrance, consistent with human carriers data of LFS risk. These results suggest that additional cooperating genetic alterations are important in the long-term clinical.

Although it has been shown that p53 oligomerisation and activity has a strong impact on tumour suppression, it is still unclear how the altered function of mutated p53 is related to cancer development. Some explanations have been proposed in this topic, as PTMs and cellular localisation of p53 can contribute to changes in interdomain and intermolecular interactions, modifying its behaviour. Therefore, mutations in the TD may promote tumour development despite potential transcriptional ability. It is still unclear how different oligomerization states affect p53 interactions with other proteins of its network, as well as PTMs and DNA binding. Moreover, a duality behaviour of p53 function have been shown and deserve further investigation to understand how this protein is working. It has been suggested that mutant p53 acts as a guardian of cancer cells by protecting the cancer cells from the rewiring of their metabolic pathways, normally actuated after stress stimuli.[78] Therefore, more studies are needed in this field to develop important therapeutic applications.

Small molecules interacting with p53

One possible strategy to restore the WT activity is the design of small molecule to interact with a particular domain of the protein. An example of this is reported by Bykov *et al*.[79] that screened a library of small molecules to rescue the WT protein activity of mutated p53. They found that a candidate, PRIMA-1 (Figure 6), is capable of inducing apoptosis in human tumour cells through restoration of the transcriptional transactivation function of mutant p53. The ligand is able to rescue the sequence-specific DNA contacts, as well as the active conformation of mutant p53. They tested this molecule in vivo and it showed an anti-tumour activity with no toxicity in mice.

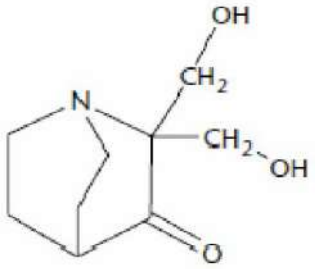

Figure 6. Structure of PRIMA-1.

Some examples are reported as well studying the TD, as Gordo *et al*.[80] and Kamada *et al*.[81] showed the ability of calixarene molecules, or more precisely calix[n]arene, to bind the TD and stabilise the mutated form R337H (Figure 7). Calix[n]arene molecules are compounds that, as the name suggests, have the shape of a 'calix', formed by a different number of arene rings, four or six in these reported cases (Figure 7). From the arene groups of this rigid crown of the molecule, it is defined *lower rim* the narrow part below the arene rings and *upper rim* the wider part on top of them. In these studies, different groups are linked on the *upper rim*, such as guanidinium, imidazole or pyrazole groups, whereas hydrophobic groups are linked in the *lower rim*. These molecules have been designed to interact with p53TD by hydrophobic interaction between the *lower rim* of the ligands with the hydrophobic pocket of the protein domain. Guanidinium, imidazole or pyrazole groups are fully or partially protonated at physiological pH and are meant to interact with Glu residues of p53TD. The complex formation of these molecules and p53TD was studied *in vitro* by NMR, thermal stability CD, and ITC, at different experimental conditions. Calix[4]arene with guanidinium groups (Figure 7b) resulted to be the best candidate, increasing the thermal stability of the TD mutated form R337H of *ca*. 10 degrees. The binding orientation and the apparent k_D were determined by NMR experiments.[80] The binding was occurring only in water, whereas the interaction was lost in buffer, suggesting that the electrostatic interactions play an important role in this system.[80,81]

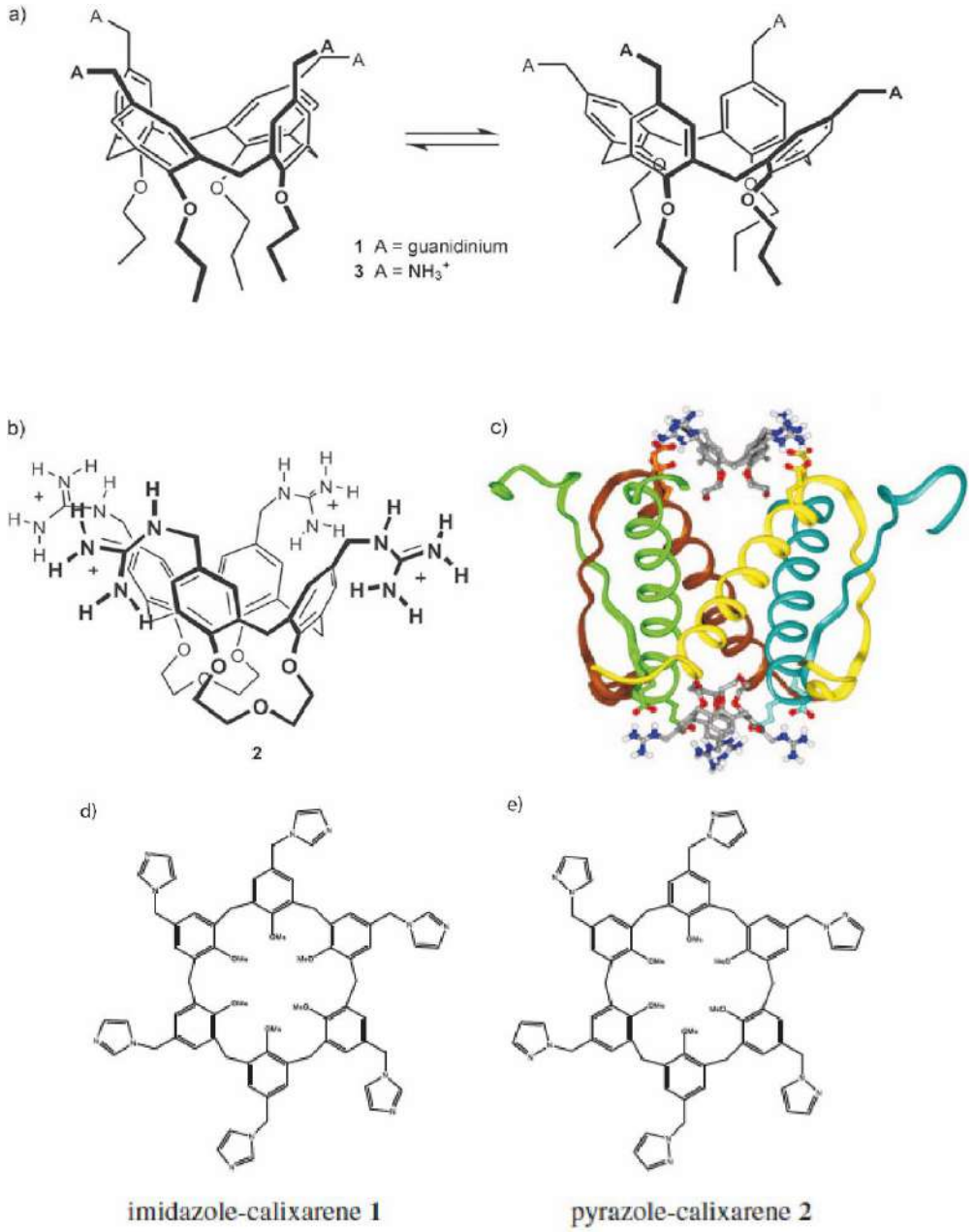

Figure 7. Calix[4]arene and calix[6]arene ligands that bind p53TD. Images adapted from Gordo *et al*.[82] and Kamada *et al*.[81]

Additionally, molecules that interact with p53 could be used as therapeutic strategy in cancer that still express p53 WT. Moreover, molecules that bind to different oligomeric states of p53 can be exploit with distinct strategies. If a ligand binds to the tetrameric form of the protein, it can be used as stabiliser of the active state,

promoter of PMTs and interactions for p53 functions. For example, Gabizon *et al*.[83] reported a PKCα-derived peptide that is able to bind the *C*-terminus in its tetrameric form and to stabilise the tetramer *in vitro*.[84] On the contrary, molecules that preferentially binds to lower oligomeric state of p53, could be used to trap mutated form of the protein, avoiding in this way that mutants oligomerise with the WT and blocking their dominant-negative effect.

Targeting PPIs using peptides

In the design of molecules to modulate PPIs, peptides present several advantages compared to small molecule or bigger biomolecules, such as antibodies (Figure 8). They are flexible, therefore they are able to adapt better to large surfaces; they are characterised by easy modularity, which increases structural diversity allowing higher selectivity and potency. They have a size that limits accumulation in tissues and they are totally biocompatible, therefore they normally have low toxicity in human cells. All these characteristics contribute to make peptides increasing attractive in targeting PPIs.[85]

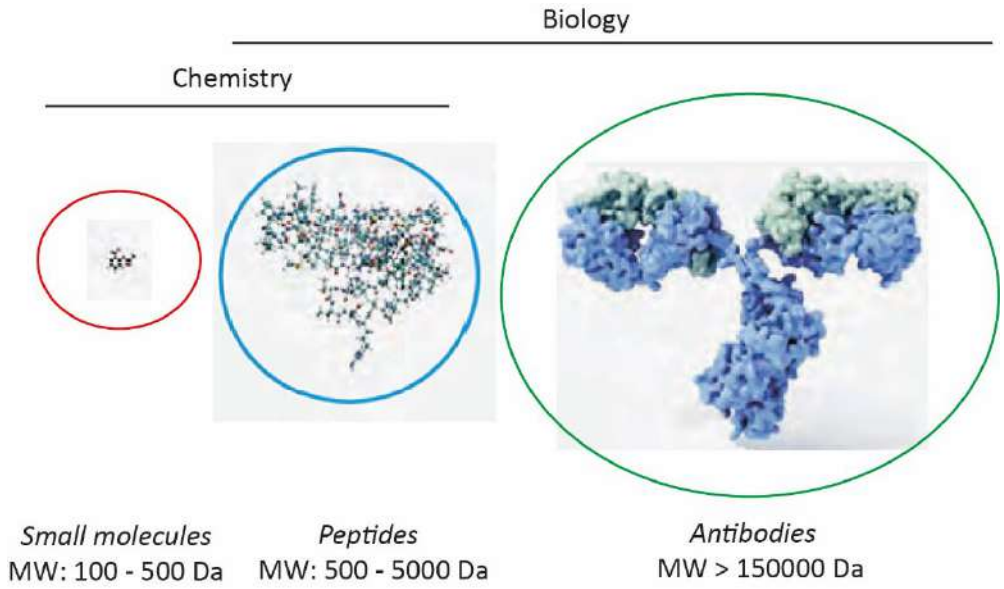

Figure 8. Peptides bridge the gap between small molecules and proteins.

Nevertheless, they have drawbacks that need to be considered at the stage of the design of new peptides as therapeutics. The main ones are their low protease resistance, potential immunogenicity, and fast circulation expulsion. In order to avoid these drawbacks, some strategies have been developed and mainly they consist on the cyclisation of the peptides, either forming stapled peptides or head-

to-tail cyclisation, and the modification of the backbone, introducing for example β-amino acids or peptoids (Figure 9).[8] The introduction of these non-natural building blocks and various chemical scaffolds can be exploited to create a wide range of chemical diversity and functionality. These tricks to tackle the bottlenecks allowed to get a large number of peptides or peptide derivatives as pharmaceutics. In addition to features that allow cell and tissue permeability, many chemical modifications and smart linker conjugations have been introduced into PPI modulators in order to reduce proteolytic degradation and improve bioavailability.

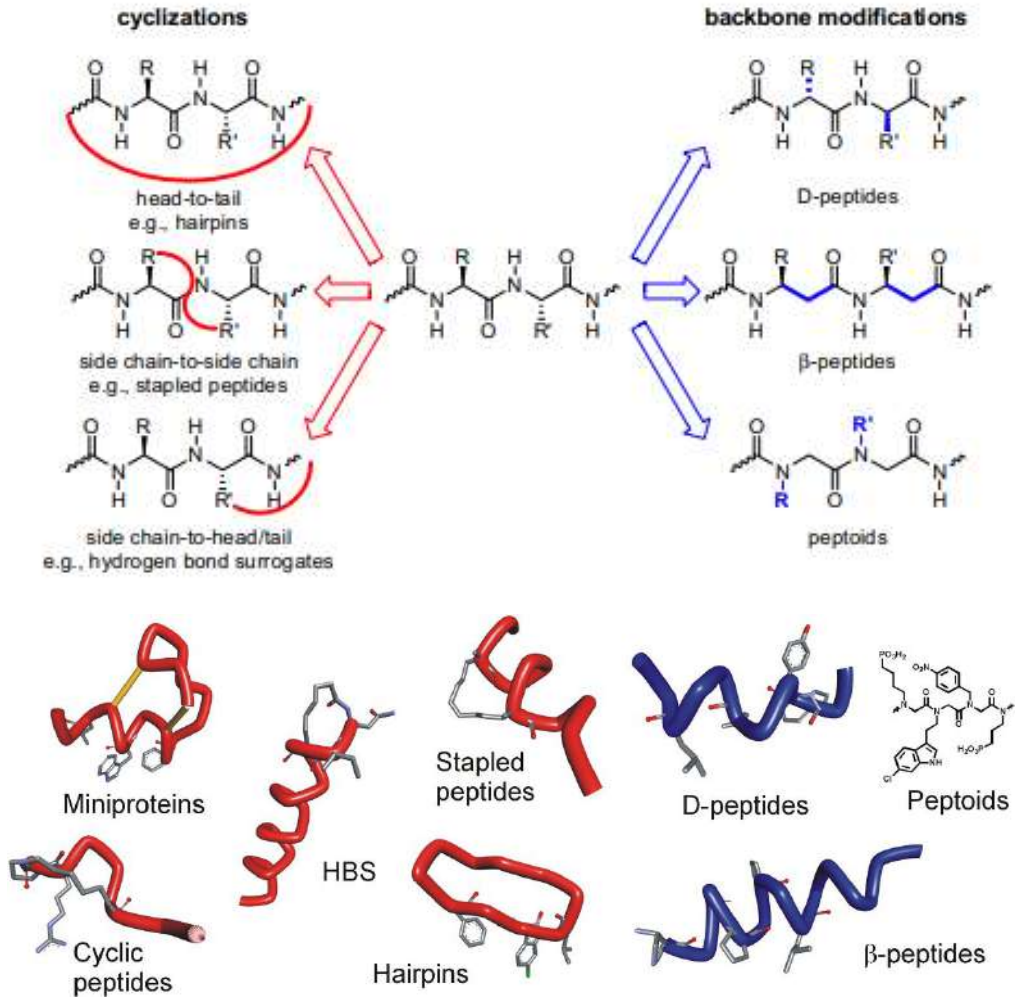

Figure 9. Major modification types of peptide-based PPIs inhibitors. Image adapted from Wójcik *et al*.[8]

These major modifications aiming at getting peptide-based inhibitors less prone to protein degradation, less immunogenic and more prone to tissue penetration are

promising and attractive as many examples of peptide-based drugs already reached the market. These drugs were designed to face different pathologies, among them, hypertension, blood coagulation disorders, type 2 diabetes, and neurophatic pain. The peptides used as drugs derive from animal venoms.[86]

Perspectives

Having a crucial role in the development of cancer, p53 is a very interesting target protein. Although it is widely recognised that it is biologically active as a homo-tetramer, there are still many open questions in the topic of the tetramerisation. It is still not clear which oligomeric state is more abundant in healthy cells and precise dissociation constants are not known. Oligomerisation plays a key role in cell fate decision, although p53 makes these decisions depending on many others factors that are not fully understood. Therefore, it is still not known how mutations impact on the tetramerisation of the protein and consequently on its function. Many studies have been carried out *in vitro* to better understand the tetramerisation. In this work, we defined a short version of the TD minimising the flanking regions, and we selected the WT and six cancer-related mutations to delve into the phenomenon of tetramerisation. To do so, we applied a variety of innovative biophysical techniques for this system, such as native MS, CD, NMR, and thermophoresis. Previous studies focused on the TD defined different lengths of the peptide. Moreover, for the nature of these equilibria, it is very difficult to isolate the dimer and investigate on its structure. It would be interesting having a dimeric peptide maintaining the WT secondary structure, as well as a stable tetramer avoiding the equilibria with the lower molecular weight species. A few strategies have been proposed, such as mutating specific positions to avoid tetramerisation or designing two fused monomers sequences. Here, we propose cross-linking of two monomers to achieve our target peptides.

Targeting a PPI is a challenging objective, mostly if the aim is to stabilise the interaction. Based on the previous studies on small molecules able to interact and stabilise the mutated form R337H of p53TD, it would be interesting having other classes of molecules targeting this PPI. We designed peptides to achieve our goal for the advantages that peptides molecules intrinsically have. We applied some strategies to tackle their drawbacks, such as cyclisation, modification of the backbone, using β-amino acids, or modification of the side chain of the arginine residues.

OBJECTIVES

The goal of this thesis is the study of the oligomerisation of p53 tetramerisation domain (TD) and in particular, the investigation of the way p53TD species are in equilibrium with each other and how these equilibria can be shifted by peptides as ligands. To achieve this goal, we need to meet the following objectives:

1. Study of the equilibrium between p53TD species, i.e. monomer, dimer and tetramer of a short version of the tetramerisation domain. This study involves the wild type sequence (WT) as well as 6 cancer-related mutations. We compare the behaviour of these short lengths TDs combining innovative techniques for this system, such as native MS, NMR and thermophoresis.

2. Design of p53TD mutants to stabilise either the dimer or the tetramer by cross-linking between monomers.

3. Design and synthesis of peptides as ligands able to bind the hydrophobic pocket of p53TD and to rescue the stability of the mutated tetramers.

4. Study of the interaction between p53TDs and the ligands by several biophysical techniques.

RESULTS AND DISCUSSION

EQUILIBRIUM BETWEEN P53TD SPECIES

Tumour suppressor p53 is a homo-tetramer protein, which oligomerises through the tetramerisation domain (TD) (res 325-353).[30] The monomer of this domain has a V-shape and comprises a β-strand (res 326-333), a turn (G334), and an α-helix (res 335-354) (Figure 10 and 11 A). The tetramer is a dimer of dimers and it has D2 symmetry (Figure 10 A). Several interactions are involved in the stabilisation of the dimer and tetramer. Among them, the salt bridge between R337 of one monomer and D352 of the other monomer of the same dimer (Figure 10 B) stabilises the dimer. The tetramer is stabilised mainly by hydrophobic interactions between the side chains of the residues that form the α-helix (F338, M340, F341, L344, L348, L350). Cancer-related mutations in the TD may alter the oligomeric state of the protein, thus compromising its biological function. It has been shown that the probability of somatic mutations occurring in the TD is similar to that in the DNA-binding domain (DBD), taking into account that the TD is roughly 6 times shorter than the DBD (TD ~35 residues vs. DBD ~200 residues).[64,65,34] Given these considerations, many studies have centred on the oligomeric state of the TD in an attempt to understand how the replacement of wild-type (WT) residues affects the equilibrium between the species. In this chapter, we focus on the oligomeric state of p53TD of the WT and 6 cancer-related mutations. We designed a short version of the TD to compare the oligomeric states of our TD sequences, which have the same length and were chemically synthesised. We applied unconventional techniques for this system, such as native MS, NMR and thermophoresis. Here we present the design of the TD and the selection of the mutations. We studied the folding of our peptides by circular dichroism and the oligomeric states by native MS in the gas phase and NMR in solution. Finally, we determined the K_d of the binding through thermophoresis.

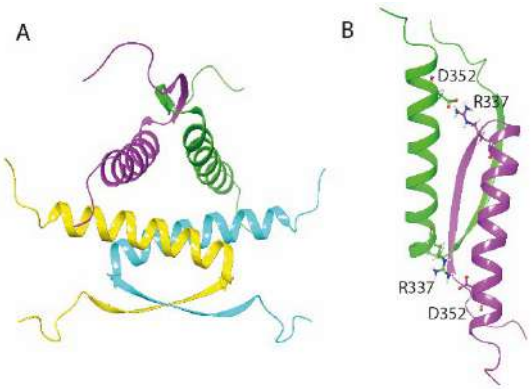

Figure 10. (A) Cartoon representation of the WT (dimer of dimers) from its NMR structure,[28] PDB ID 1OLG. (B) Cartoon representation of the dimer showing location of the salt bridge between R337 and D352.

Definition of the TD and selection of the mutations

There is no single definition of the p53 TD, and its length differs slightly depending on the study (Table 1).

Residues	Reference
323-353	Bista *et al.*[30]
325-355	Rajagopalan *et al.*[36]
326-356	Gaglia *et al.*[38]
323-360	Tidow *et al.*[35]
320-356	García[24], Gordo[87]
319-358	Kamada *et al.*[64]

Table 1. Definition of the TDs.

In our study, we worked with peptides spanning 37 amino acids (res 320-356) to maintain a folded TD, thereby minimising the effects of the flanking region.[24,87] These peptides are named 37TDs. To study the equilibrium between p53TD species by native MS and NMR, we selected the wild-type (37TD-WT, Figure 11 A) and 6 cancer-related mutations[64] (Figure 11)—all with the same length— which were all chemically synthesised. The chosen mutations involve the residues of the salt bridge (R337H and D352H), residues on the α-helix (R342L, L344R and L344P) and a residue on the β-strand (T329I) (Figure 11 A and B). R337H is the most common mutation in the TD and it has been found mostly in children in South Brazil. This mutation is associated with Li-Fraumeni syndrome, which gives rise to several types of cancer. Due to its correlation with cancer, this mutation has been widely studied and characterised.[75,80,88] Di Giammarino and co-workers reported that R337H strongly destabilises the tetramer, but the stability of the latter is partially recovered by decreasing the pH to acidic values.[75] In D352H mutant, the original salt bridge R337-D352 is replaced by R337-H352. Since a His residue has been introduced, the stability of the tetramer may also depend on the pH. However, in this case, by protonating the imidazole group, two positive charges (from R337 and H352) would interact, reducing the stability of the tetramer. We selected R342L because it is the second most common mutation in the TD. The replacement of the R342 by a Leu residue impedes stabilisation of the α-helix by interactions between the side chain of R342, which is positively charged, with negative charges on E339 and E346, which correspond to *i,i-3* and *i,i+4* interactions. T329I is a mutation on the β-strand that enhances the thermal stability of the domain compared to the WT (Figure 11).[64] Finally, L344R and L344P were introduced since it has been proposed that they promote the monomeric and dimeric forms, respectively (Figure 11).[39,64] L344 residue in the WT is involved in stabilising interactions of the tetramer, this residue being at the dimer-dimer interface. In particular, hydrophobic interactions between

the L344 side chain of a monomer with the same residue on another monomer of the other dimer stabilise the tetramer. By replacing L344 by an Arg residue, two positive charges will be close in space destabilising the tetramer. The introduction of a Pro residue, L344P, into the α-helix potentially disrupts the structure, resulting in an unfolded peptide.[39,64]

All 37TDs were chemically synthesised by SPPS (Solid Phase Peptide Synthesis) (Figure 11). 37TD-WT and 37TD-R337H were manually synthesised and they were obtained using either a normal methionine or ^{13}C-methyl methionine to facilitate NMR studies. All the other mutants were synthesised by microwave-assisted SPPS using ^{13}C-methyl methionine (Figure 11). In this thesis, we refer to the isotope-labelled sequences, unless stated otherwise. The data corresponding to the characterisation of the 37TDs are reported in the section 'Product characterisation' at the end of the manuscript (Figures S1-S5).

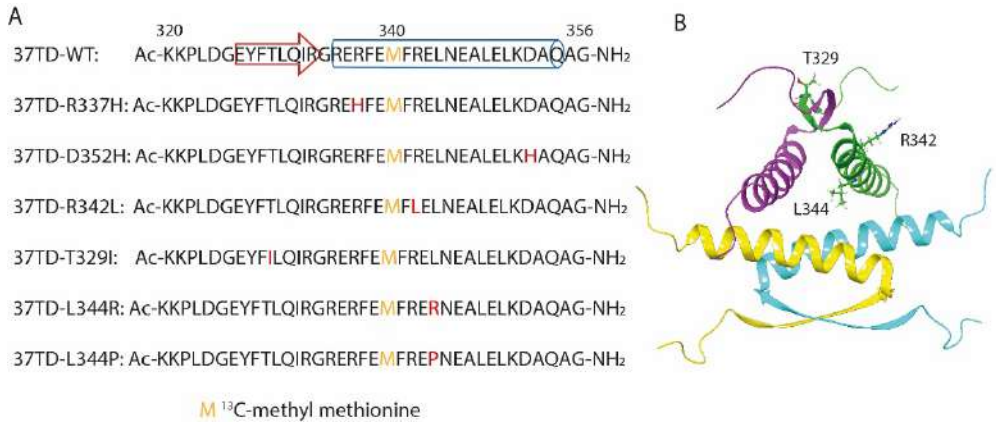

Figure 11. (A) Sequences of the 37TDs. The red residues correspond to the positions of the mutations and the yellow Met indicates the isotope-labelled residue. The β-strand and the α-helix are represented with an arrow and a cylinder, respectively, in the WT sequence. For 37TD-WT and 37TD-R337H, only the isotope-labelled sequences are shown. (B) Cartoon representation of the WT from its NMR structure,[28] PDB ID 1OLG, showing location, only in one monomer, of the residues that are mutated (T329, R342 and L344).

Secondary structure of the 37TDs

With the peptides in hand, we first studied their folding by circular dichroism (CD) experiments. This technique allows measurement of the ellipticity (θ) of a circular polarised beam after having passed through an optically active sample. The profile of the spectrum is related to the secondary structure of the protein or peptide. In the UV region of the spectrum, the typical profile of an α-helix structure corresponds

to two negative bands at 208 and 222 nm and a positive one at 190 nm; the β-sheet structure gives less intense bands, with two negative ones at 217 and 180 nm and a positive one at 195 nm. The random coil profile is characterised by a negative band at 195 nm.[89] We studied our system in two distinct environments, namely water and phosphate buffer, both at neutral pH, to check whether ionic strength participates in peptide folding. The results show that the peptides have the same structure under these conditions, as the spectra obtained are practically identical (Figure 12). In these experiments, non-isotope-labelled sequences of 37TD-WT and 37TD-R337H were used. The WT sequence and T329I mutant showed very similar profiles, typical of an α-helix, with two negative bands at 208 and 222 nm (Figure 12), meaning that both peptides are well folded and structured. Two peptides, 37TD-R337H and 37TD-R342L, present a more pronounced contribution of the β-sheet compared to the other 37TDs. The overall profile of the spectra is changed because the typical β-sheet band at 217 nm is more intense than the two bands of the α-helix. 37TD-D352H and 37TD-L344R adopt an α-helix structure, but they are less helical than the other 37TDs as the intensity of the bands is almost half that of 37TD-WT. Finally, the introduction of a proline residue in the α-helix in 37TD-L344P results in a random coil profile, thereby indicating that the peptide is unstructured.

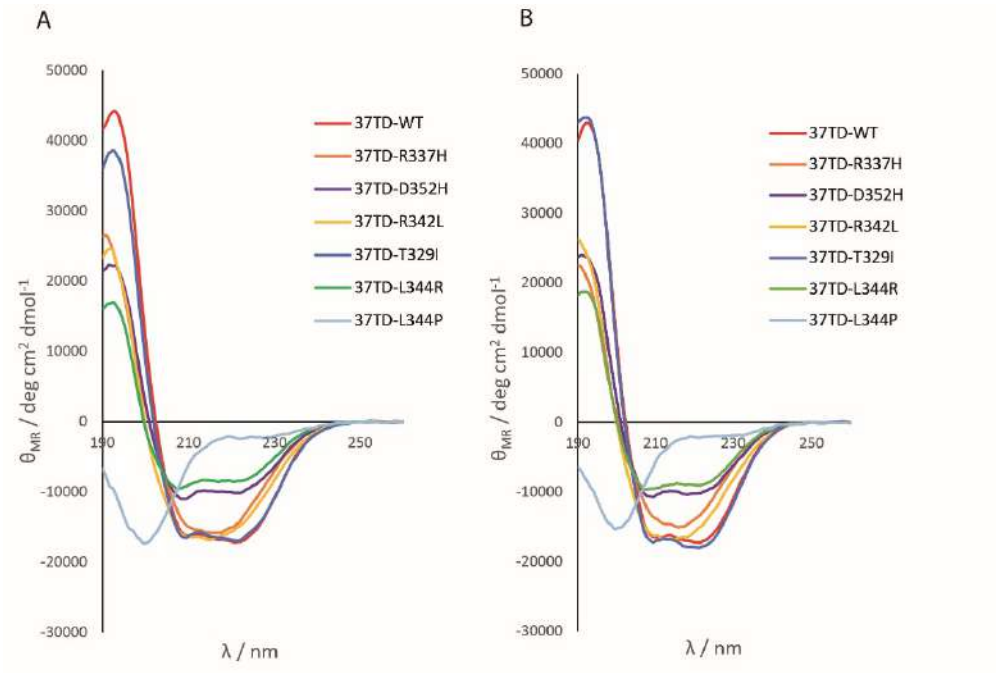

Figure 12. Circular dichroism spectra of the 37TDs. The spectra correspond to a monomer concentration of 20 μM of each peptide in 50 mM sodium phosphate buffer, pH 7 (A) and water, pH 7 (B). For 37TD-WT and 37TD-R337H, non-isotope-labelled peptides were used.

Determination of the oligomeric state by native MS

One of the main challenges in structural biology is the determination of the binding between a target and a ligand, as well as understanding the structure of the complexes. In this field, dramatically increased interest has arised on native MS due to its ability to detect protein-protein and protein-ligand complexes in their native conformation. We performed native MS experiments to determine the oligomeric state of our 37TDs. This technique allows the detection of non-covalent complexes using soft conditions of ionisation, such as electrospray ionisation (ESI).[90] The sample is dissolved in non-denaturing buffer and ionised in the source of the instrument. ESI has increased its applicability for biomolecules analysis as coated glass capillaries with a diameter of 1-5 µm are now used. This allows a droplet size one order of magnitude smaller than traditional ESI. Named nanoESI, this lower flow rate ESI source is the most widely used in native MS due to its ability to reduce sample consumption, increase salt and buffer tolerance, and allow softer conditions of ionisation to desolvate the analyte.[91] Optimised instrumental parameters are set with the aim to preserve protein folding structures during the creation and ejection of ions from solution to the gas phase. Conditions of voltage in the source and the different parts of the instrument, such as the trap and the transfer, are optimised for the system studied, as well as the source temperature and the vacuum. In native MS, nanoESI is most often coupled to a Time of Flight (TOF) analyser, since it allows the detection of high molecular weight biomolecules without compromising the sensitivity and resolution of the spectra.[92] The experiments can be performed using a TOF analyser or Ion Mobility (IM) coupled to the TOF. IM analysis allows the addition of an orthogonal measure to the MS information, separating by drift times ions with the same m/z value but distinct shapes.[93,94] The drift tube is filled with an inert gas and ions are separated on the basis of their ability to 'surf' on the gas. The drift time at which an ion reaches the detector depends on the physical properties of the molecule, such as charges, shape and size. The peaks were assigned from both the MS spectra and IM-MS analysis. In particular, ions with the same m/z value were distinguished in the IM spectrum due to their different drift times (Figure 13).

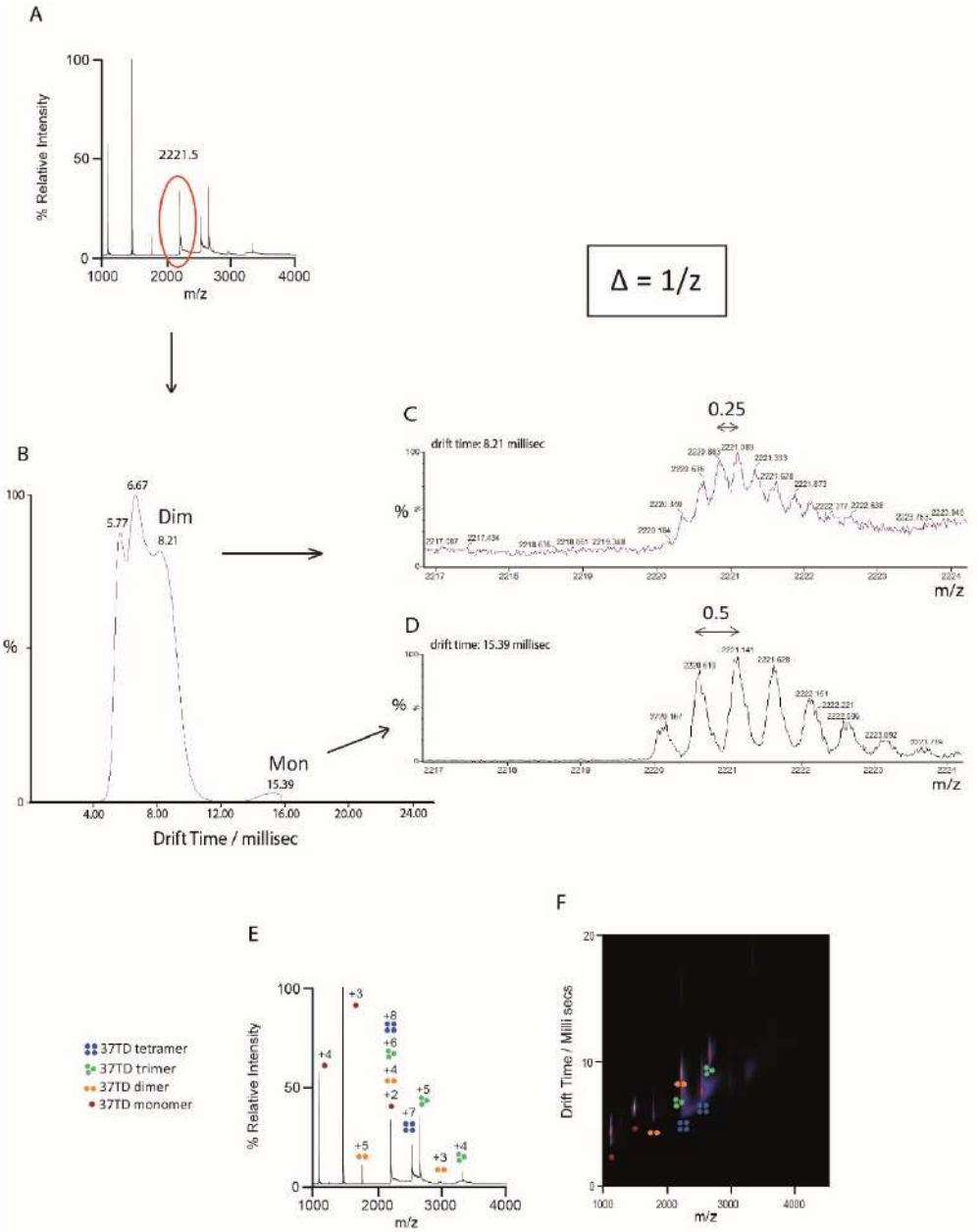

Figure 13. Native MS and IM-MS experiments at 120 V of 37TD-WT at a monomer concentration of 20 µM in ammonium bicarbonate 20 mM, pH 7. (A) Native MS spectrum with a peak of 2221.5 m/z in evidence. (B) Total ion chromatogram corresponding to the 2221.5 m/z peak in the IM-MS experiment. Mon: monomer; Dim: dimer. (C, D) MS spectra of the peaks at 8.21 millisec (C) and 15.39 millisec (D). (E) Native MS spectrum with peaks assigned. (F) IM mobilogram with peaks assigned.

37TD-WT

MW 4441.02

		Monomer	Dimer	Trimer	Tetramer
Charge	1	4442.02	8883.04	13324.06	17765.08
	2	2221.51	4442.02	6662.53	8883.04
	3	1481.34	2961.68	4442.02	5922.36
	4	1111.26	2221.51	3331.76	4442.02
	5	889.20	1777.41	2665.61	3553.82
	6	741.17	1481.34	2221.51	2961.68
	7	635.43	1269.86	1904.29	2538.72
	8	556.13	1111.26	1666.38	2221.51
	9	494.45	987.89	1481.34	1974.79
	10	445.10	889.20	1333.31	1777.41

Table 2. Mass-to-charge ratio (m/z) of the different 37TD-WT species, i.e. monomer, dimer, trimer and tetramer. Red indicates the ion 2221.5 m/z, which, as an example of the assignation, can correspond to different 37TD-WT species. MW: molecular weight.

The peak at 2221.5 m/z in the MS spectrum (Figure 13 A) may correspond to a monomer with charge +2, a dimer with charge +4, a trimer with charge +6, or a tetramer with charge +8 (Table 2). To assign the correct species, we looked at the total ion chromatogram from the IM-MS experiment (Figure 4 B). In this case, we can see 4 peaks with different drift times, most probably corresponding to the different species (monomer, dimer, trimer, tetramer). Looking at the MS of each peak, if they are resolved, the different species can be assigned by measuring the distance between the peaks (Δ) (Figure 4 C and D). There is a direct relation between the Δ and the charge of the ion (z), in particular $\Delta = 1/z$. In this example, in Figure 4 C, Δ is 0.25 corresponding to z = 4. This peak, with a drift time of 8.21 millisec, thus corresponds to the dimer, with a charge +4 and a m/z = 2221.5. The peak at 15.39 millisec corresponds to the monomer with charge +2. We used this methodology for the assignment of all the native MS and IM spectra, as shown in Figure 4 E and F as example.

We studied a range of concentrations and applied different cone voltages for each sample. Starting from the most native condition of 37TD-WT (80 µM, and low voltage, 40 V) (Figure 14), three consecutive charge states corresponding to the tetramer (+9, +8, +7) were detected. The contribution to different charge states was further validated by the ion mobilogram, which suggested that the most abundant species in the sample was the tetramer (Figure 14). However, signals of further oligomerisation were also detected, in particular octamers and decahexamers (16 monomers). Although these larger oligomers showed low abundance since their peaks were not detected in the MS analysis, their presence may be explained by peptide aggregation.

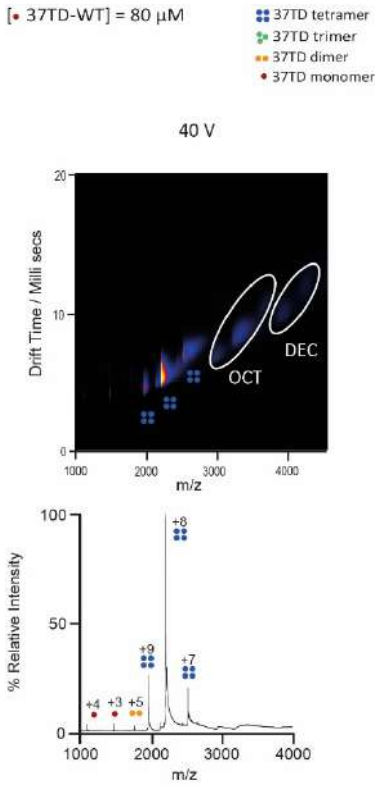

Figure 14. Native MS and IM spectra of 80 µM 37TD-WT at a cone voltage of 40 V. Non-isotope-labelled peptide was used. The concentration reported refer to the monomer. The sample was dissolved in 200 mM ammonium acetate buffer, pH 7. OCT: octamer; DEC: decahexamer (16 monomers).

To further test this hypothesis and to study how the oligomeric state depends on the sample concentration, we diluted the sample to 20 µM of monomeric 37TD-WT (Supplementary native MS, Figure S18). Under these conditions, the tetramer was still the species giving the most intense peaks, whereas larger oligomers were detected with a reduced contribution. In the TOF spectrum (Figure 15 A), low-intensity peaks of both monomer (+4 and +3) and dimer (+5) were detected. Given the very low intensity of these peaks, their presence is interpreted as products of sample ionisation.

To study the dissociation of the tetramer, the cone voltage was increased up to 80, 100 and 120 V. At high voltages, the tetramer was disrupted into smaller oligomers (Figure 15 A and Supplementary native MS, Figure S17), reaching a most abundant monomer species at 120 V (+4, +3 and +2 charges). The tetramer, although still present in both the MS and IM-MS spectra, was dissociated mainly into monomers, but also into trimers and dimers. Given that p53TD is a dimer of dimers (Figure 10

A), dimers were initially expected to be detected as major species upon dissociation of the tetramer. However, the dissociation went directly towards the monomer. We interpret our results as an intrinsic instability of the dimer in this system. The dissociation constants are low, at the limit of detection,[36] making the dimer unstable and difficult to detect.[39] Kamada *et al*. analysed the oligomeric state of a slightly longer TD (Table 1) by gel filtration chromatography and reported a mixture of tetramers and monomers for the WT in solution.[64] On the other hand, the presence of the trimer in our experiments is considered a product of ionisation in the gas phase. We interpret the dissociation event as highly charged tetramers dissociating asymmetrically into trimers and monomers. Other complexes also behave in a similar manner, separating a highly charged unit as a result of high coulombic repulsion and leaving the rest of the complex in a more stable form.[95,96]

The behaviour of 37TD-R337H differed. With this mutant, at 100 µM and 40 V (Figure 15 B and Supplementary native MS, Figure S19), the tetramer peaks were the most intense of the spectrum, but at the same time, the monomer peaks were already more prominent compared to the WT. Similarly, as in the case of 37TD-WT, the tetramer dissociated mainly into monomers when the voltage was increased up to 100 V. However, peaks corresponding to trimers and dimers were also present. By diluting the sample to 25 µM, the monomer was probably the most abundant species as its peaks were the most intense in the spectrum, although the tetramer was still present (Figure 15 B and Supplementary native MS, Figure S20). These results confirm that the tetramer is strongly destabilised by the R337H mutation, as reported by others.[75,80,88]

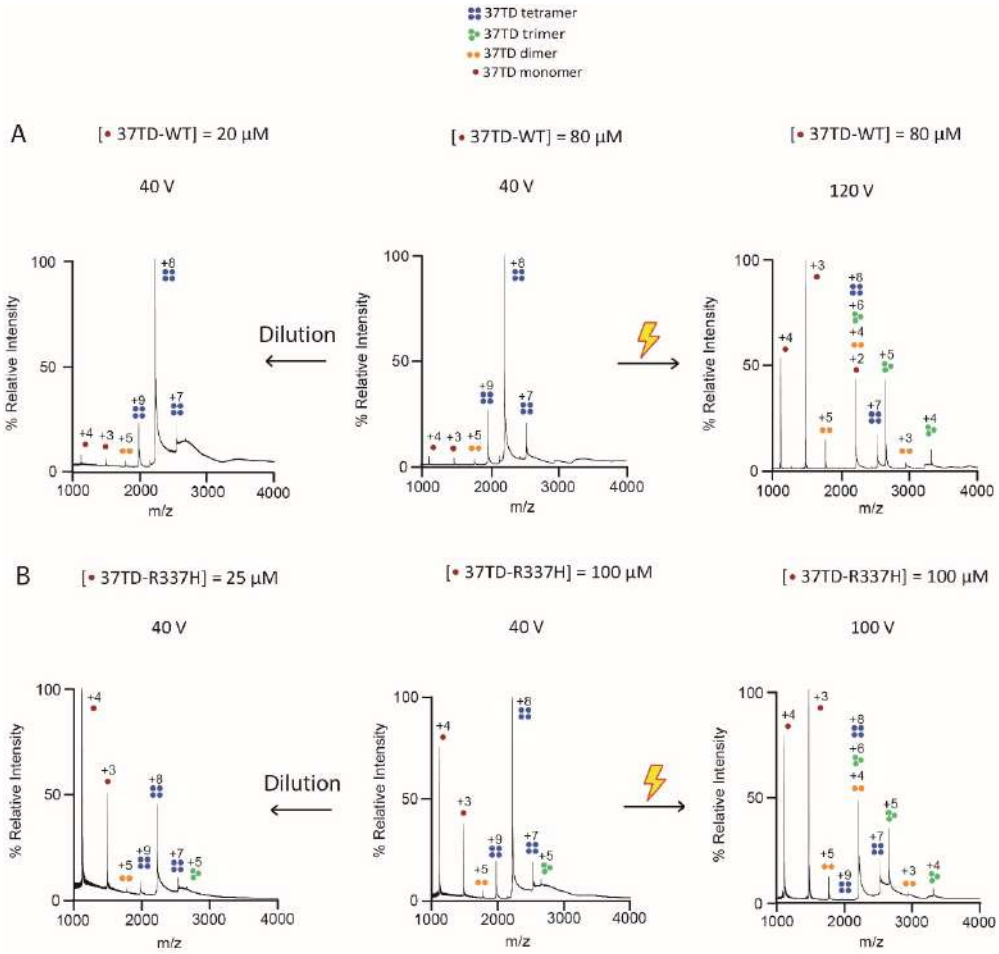

Figure 15. Native MS spectra of 37TD-WT (A) and 37TD-R337H (B). For both 37TDs, non-isotope-labelled peptides were used. The concentrations reported refer to the monomer. Starting from the central panel, which corresponds to the most native conditions of high concentration and low voltage, towards left is the spectrum of a more diluted sample and towards right a spectrum at higher voltage. The samples were dissolved in 200 mM ammonium acetate buffer, pH 7.

A similar analysis was performed with the other mutants. 37TD-T329I, 37TD-D352H and 37TD-R342L were found to be mainly tetrameric, whereas 37TD-L344R and 37TD-L344P were predominantly monomeric (Supplementary native MS, Figure S21-S30). Overall, the tetramer of all the 37TDs dissociated into smaller oligomers by increasing the voltage. The dissociation occurred similarly to 37TD-WT, generating mainly monomers, as well as trimers and dimers. Regarding 37TD-T329I, it was found to be mainly tetrameric at high concentration (80 µM) and low voltage (40 V); however, the monomer peaks were more intense compared to 37TD-WT (Figure 16 A and B). When the sample was diluted, the spectrum did not change

(Supplementary native MS, Figure S25-S26), but the tetramer dissociated with increased activating conditions, as occurred with the other mutants. Thus, we conclude that this mutation does not stabilise the tetramer in the gas phase.

Regarding the L344R and L344P mutations, we expected to detect the dimer and the monomer as the most abundant species, respectively. The tetramer, which is a dimer of dimers, is stabilised mainly by hydrophobic interactions between the side chains of the residues that form the α–helix at the dimer-dimer interface. Among these residues, L344 also participates in these interactions and, in particular, two L344 residues from two distinct dimers interact with each other. By mutating L344 this interaction is lost and, in addition, the introduction of an Arg residue brings two positive charges close together, thereby destabilising the tetramer. On the other hand, when L344 is replaced by a Pro residue, the structure of the domain is compromised by the latter, thereby preventing the formation of the helix and thus peptide folding. We expected to detect monomers with this mutant as the oligomerisation occurs when the domain is structured and folded. The MS spectra of the mutants L344R and L344P showed a mixture of monomers and dimers, where the monomer was the most abundant species (Figure 16 C and D). Regarding 37TD-L344R, the results indicate that the dimers are not stable enough in the gas phase and they dissociate into monomers despite the application of low voltages and modified vacuums for ion cooling.[97] In the case of 37TD-L344P, although this domain is unfolded due to the disruption of the secondary structure by the Pro residue, as the CD results showed (Figure 12), some further oligomerisation is still possible. Our results thus reveal similar behaviour of these two mutants in the gas phase.

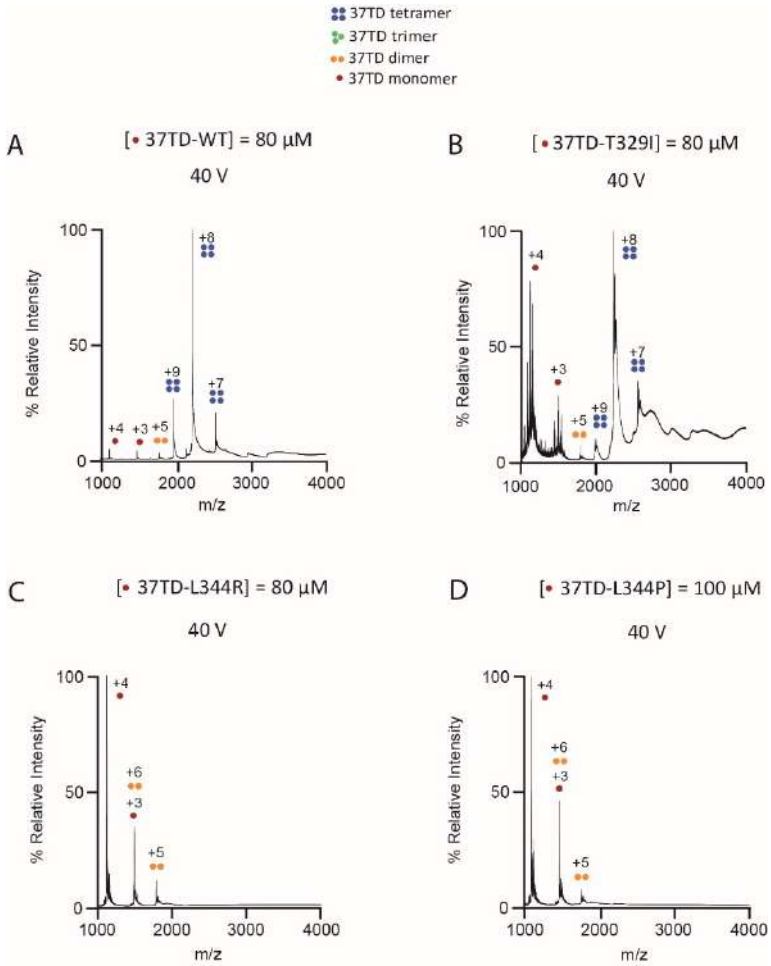

Figure 16. Native MS spectra of 37TD-WT (A), 37TD-T329I (B), 37TD-L344R (C) and 37TD-L344P (D). For 37TD-WT, a non-isotope-labelled sequence was used. The concentrations reported refer to the monomer. The samples were dissolved in 200 mM ammonium acetate buffer, pH 7. The tetramer to monomer ratio is compared in panels A and B, whereas the dimer to monomer ratio is compared in panels C and D.

Regarding 37TD-D352H and 37TD-R342L, the monomer was the most abundant species even at high concentration, meaning that these two mutations strongly destabilise the tetramer, even more dramatically than 37TD-R337H (Supplementary native MS, Figure S19-S24). D352 forms a salt bridge with R337 in the WT. The salt bridge in the WT is a key stabilising interaction for dimer formation and consequently also for the tetramer. Therefore, the mutation of either Arg337 or Asp352 has a strong destabilising effect on this domain. Having replaced one residue or the other by His, the stability of the tetramer might depend on the pH, affecting the protonation or deprotonation of the imidazole group. Finally, in the presence of

R342L mutation, helical stability may be compromised by the loss of the original intra-helical interactions of the Arg side chain with Glu residues (E339 and E346), which correspond to interactions *i, i-3* and *i, i+4*. The tetramer may be less stable due to the reduced helical character of the domain, as inferred from the CD profile (Figure 12).

Study of the equilibrium between oligomers by NMR

We conducted 2D Heteronuclear Single Quantum Coherence (HSQC) NMR experiments to assign the oligomeric state of 37TDs in solution and to study how the equilibrium between p53 species shifts in response to a change in concentration, temperature or pH. In the $^{1}H,^{13}C$-HSQC spectrum, each signal corresponds to a proton linked to the heteronucleus considered, in this case ^{13}C. We selectively introduced a ^{13}C-methyl group on Met340 of our 37TDs (Figure 11) and the resulting $^{13}C^{\varepsilon}$-Met340-labelled 37TDs were monitored by NMR experiments. Each monomer contains only one Met residue and, upon oligomerisation, only one methyl signal was observed in the HSQC spectra due to the symmetry of the tetramer. Met340 is located in the tetramerisation interface and the NMR signal of its methyl group is sensitive to the oligomerisation state of the TD, as reported by Bista *et al.*[30] We analysed our 37TDs at a range of sample concentrations and temperatures in order to favour either small or large oligomers. For the mutations that introduce a His residue, we also examined how the stability of the tetramer was affected by a change in pH. Dr. Jesús García conducted all the NMR experiments, which were performed in D_2O, pH 7, unless stated otherwise.

Starting from 37TD-WT, we defined an area of the spectrum as the region of folded and tetrameric peptides. The spectra corresponding to the two concentrations studied (20 and 100 µM) showed only one peak (Figure 17 A and C). We assigned this peak to the tetrameric form of 37TD-WT, since the chemical shift (^{1}H 1.50 ppm, ^{13}C 13.53 ppm) matches that previously reported for the tetramer[30] (BMRB code 7251[98]). We studied the WT system at different temperatures and pH (Supplementary NMR, Figure S35). Although these changes caused small chemical shift perturbations in the tetramer signal, the tetramer was the only species detected in all the conditions tested.

A second region of the spectrum where the signal of unfolded monomeric peptides appeared was defined by the study of 37TD-L344P. The NMR spectra of 37TD-L344P were typical of unfolded peptides and they showed very low signal dispersion. This observation is consistent with the CD and native MS results and with the fact that Pro residues disrupt secondary structures. Regarding the methyl region of the 1D ^{1}H

spectra (0.8-0.9 ppm), a clear difference was observed when comparing 37TD-WT and 37TD-L344P. While some methyl ^{1}H protons located in the hydrophobic interface of the tetramer were shifted upfield in the 1D ^{1}H spectra of 37TD-WT (Ile332 δH^{δ} = 0.78 ppm, Leu344 δH^{δ} = 0.74 ppm, Leu330 δH^{δ} = 0.54 ppm) (Supplementary NMR, Figure S42), all the methyl groups of 37TD-L344P virtually completely overlapped and resonated at *ca.* 0.9 ppm. The ^{1}H,^{15}N HSQC spectrum of 37TD-L344P, obtained at natural abundance, showed a similar lack of signal dispersion for the amide NH resonances (Supplementary NMR, Figure S43), thereby further confirming the unstructured nature of this peptide. In the ^{1}H,^{13}C-HSQC spectrum of 37TD-L344P (Figure 17 A), a single cross-peak resonating at 2.05 ppm was detected, close to the expected value (2.10 ppm) for a random coil peptide.[99] This area of the spectrum was thus defined as the region where the signal of an unfolded monomeric 37TD peptide appears. When the temperature was decreased to 5 ºC, a second small peak appeared (^{1}H 1.74 ppm, ^{13}C 13.99 ppm) in a region between the monomer and the tetramer (Supplementary NMR, Figure S41). Therefore, this peak should correspond to an intermediate oligomer, most probably a dimer, since in the MS experiments some signals of the dimer were detected. Our results suggest that, although this peptide is unstructured, oligomerisation events can occur in the gas phase or at low temperature.

Having defined the regions of folded and unfolded peptides, we analysed the different oligomeric species detected in the ^{1}H,^{13}C-HSQC spectra of the other 37TDs. Upon 37TD mutation, if the domain remains folded, the methyl cross-peak may, to some extent, be shifted with respect to that of the tetrameric WT due to differences in the chemical environment of Met340. On the other hand, on unfolded peptides, due to conformational averaging, the methyl signal should appear close to the expected random coil value (2.10 ppm) and should not vary much between mutants.

In the case of 37TD-R337H, at 100 µM, a single peak that resonated at the position close to that of the tetrameric WT (^{1}H 1.64 ppm, ^{13}C 13.67 ppm) was detected and an additional weak cross-peak (^{1}H 2.02 ppm, ^{13}C 14.19 ppm) appeared upon dilution of the sample (20 µM) (Figure 17 B and D). By increasing the temperature and/or the pH, the relative intensity of the smaller cross-peak increased (Supplementary NMR, Figure S20). Given that tetramer formation is not favoured by increasing the temperature and the tetramer is destabilised by the deprotonation of the imidazole group,[75] we assigned the main cross-peak signal to the tetramer and the weak cross-peak signal to a smaller oligomer. Comparison of the ^{1}H,^{13}C-HSQC spectra (Figure 17 A and B) revealed that the weak 37TD-R337H cross-peak was very close to the signal of 37TD-L344P. Together with the MS results (Figure 15 B), where a mixture of tetramer and monomer was detected, we assigned this peak to the 37TD-R337H monomer. Therefore, our NMR experiments confirm that the R337H mutation

strongly destabilises the tetramer, thus complementing our previous native MS results. Our findings using these two techniques suggest that the disruption of the tetramer proceeds towards the monomer, whereas the dimer is probably unstable or its concentration is below the limit of detection.

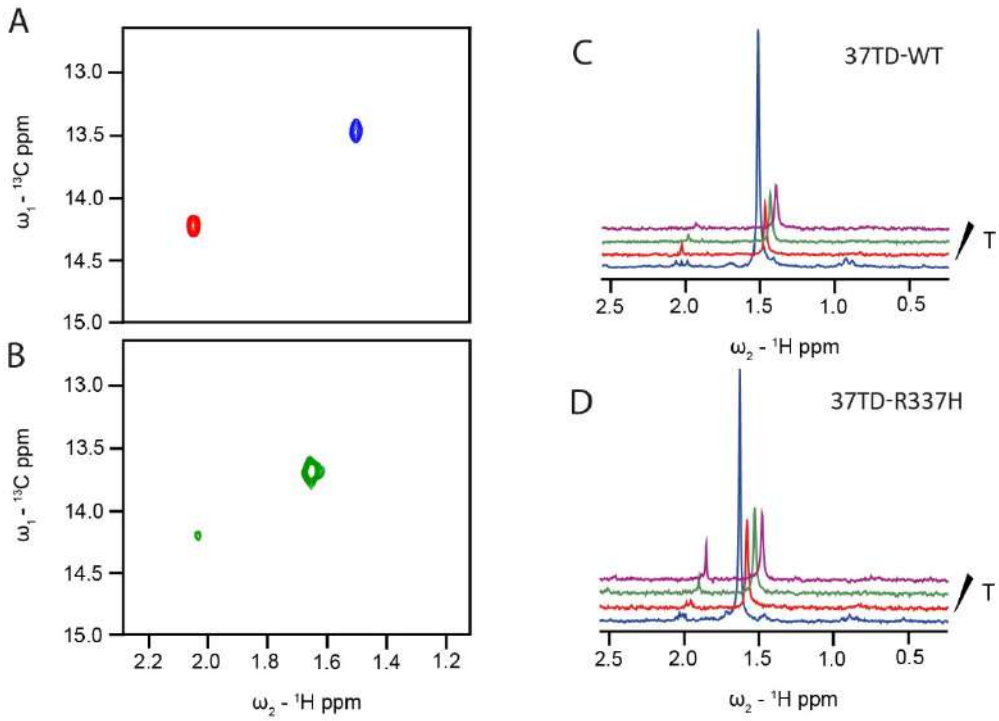

Figure 17. (A) 2D $^{1}H,^{13}C$ HSQC spectra at 25 °C of 37TD-WT (blue) and 37TD-L344P (red) at a monomer concentration of 20 µM. (B) 2D $^{1}H,^{13}C$ HSQC spectrum at 25 °C of 37TD-R337H (green) at a monomer concentration of 20 µM. ^{1}H projections of $^{1}H,^{13}C$ HSQC spectra are represented in (C) for 37TD-WT and in (D) for 37TD-R337H. ^{1}H projections of $^{1}H,^{13}C$ HSQC spectra of 100 µM 37TDs obtained at 25 °C (blue) and of 20 µM 37TDs acquired at 25 °C (red), 32 °C (green) and 40 °C (purple) (C, D).

The T329I mutation is reported to have a stabilising effect on the tetramer.[64] The mayor peak of the HSQC of 37TD-T329I overlapped with the signal of 37TD-WT, thereby indicating that this peptide was also mainly tetrameric, as expected. However, also at high concentration, a small peak in the unfolded region was present as well (Supplementary NMR, Figure S39). Therefore, we conclude that this mutant behaves in a WT-like manner, consisting of a structured and folded domain, but the replacement of the Thr residue by Ile does not stabilise the tetramer in the gas phase or in solution.

In the HSQC of 37TD-D352H, a mixture of tetramer and monomer was detected even at high peptide concentration (Supplementary NMR, Figure S37), thereby indicating

that the tetramer is destabilised by this mutation. The peak corresponding to the folded 37TD-D352H species was significantly shifted downfield with an increase in temperature. On the other hand, the protonation of the imidazole group did not seem to affect the oligomerisation of 37TD-D352H, as the HSQC spectra recorded at pH 7 and 5 were almost identical.

Regarding the R342L mutation, a mixture of monomer and tetramer was detected in the HSQC spectra of 37TD-R342L, and the relative peaks had a similar intensity. By changing the concentration and the temperature, 37TD-R342L behaved in a similar manner to 37TD-D352H (Supplementary NMR, Figure S38).

Finally, in the HSQC spectra of 37TD-L344R two peaks were present (Supplementary NMR, Figure S40). One (^{1}H 2.04 ppm, ^{13}C 14.24 ppm) corresponded to the unfolded monomeric peptide whereas the other (^{1}H 1.58 ppm, ^{13}C 13.52 ppm) resembled that of the folded tetrameric species. However, our MS experiments showed a mixture of monomer and dimer for this peptide, in agreement with a previous study, where this mutant was described as mainly dimeric.[64] To further study the size of the oligomeric species present in solution, we performed X-STE NMR diffusion experiments.

X-STE NMR diffusion experiments

Heteronuclear stimulated echo (X-STE) experiments measure the translational diffusion coefficients (D) of molecules containing ^{1}H nuclei attached to magnetically active heteronuclei.[100] A magnetic field gradient is applied to the system and the magnetisation is stored in the *z*-axis. Due to the diffusion of the molecules in solution, the signals decay at each experiment performed (Figure 18 D). Diffusion experiments can be combined with the ^{1}H,^{13}C-HSQC. In our case, the HSQC was recorded without decoupling, so the ^{1}H coupled to ^{13}C, resulting in the splitting of the cross-peak signals (Figure 18 B). On the basis of the D values obtained by diffusion NMR, it is possible to estimate the hydrodynamic radius (R_H) of the species analysed, as shown in Equation 1-3. In our study, we exploited the ^{13}C-methyl group of Met340 to independently monitor the molecular diffusion of each 37TD-L344R species present in solution. To assign the oligomeric states of the species, we also measured the diffusion coefficients of 37TD-WT and 37TD-L344P and compared them to the values obtained with 37TD-L344R (Table 3).

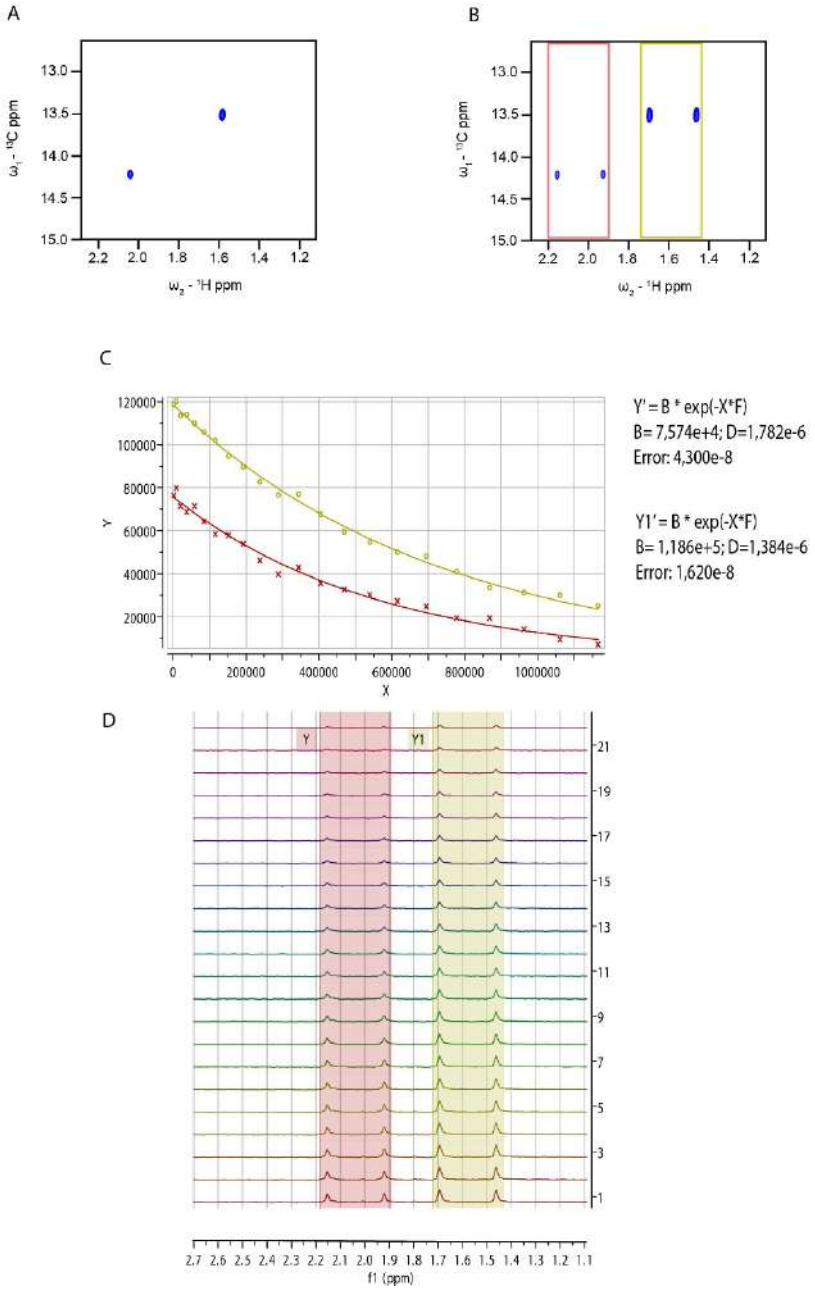

Figure 18. X-STE NMR diffusion of 37TD-L344R monitoring the size of the species containing ^{13}C-attached ^{1}H nuclei. (A) 2D ^{1}H,^{13}C-HSQC. (B) ^{13}C-coupled 2D ^{1}H,^{13}C-HSQC illustrating the splitting of the Met340 $^{1}H^{\varepsilon}$ signal ($^{1}J_{HC}$ ≈140 Hz). (C,D)) X-STE NMR diffusion experiments. The decay in signal intensity of the Met340 $^{1}H^{\varepsilon}$ signal (panel D) was fitted to a mono exponential function to obtain the coefficient diffusion. X-STE experiments were performed without decoupling and the Met340 $^{1}H^{\varepsilon}$ signal split into a doublet ($^{1}J_{HC}$ ≈140 Hz). The spectra were recorded at 25 °C using a monomer concentration of 100 µM (D_2O, pH 7).

37TDs	D x 10^{-10} / m^2 s^{-1}	R_H / Å experimental	R_H / Å predicted
37TD-WT	1.00 ± 0.02	22.2	20.3[a]
37TD-L344P	1.45 ± 0.01	15.3	14.6[b]
37TD-L344R			
Dimer	1.38 ± 0.02	16.1	16.5[c]
Monomer	1.78 ± 0.04	12.5	14.1[b]

Table 3. Diffusion coefficients (D) and hydrodynamic radius (R_H) of 37TD-WT, 37TD-L344P, and 37TD-L344R. For 37TD-L344R, the two species were independently analysed. Predicted R_H values were calculated from Marsh *et al*.[101]

[a] Value calculated for a folded tetramer (Eq. 2).
[b] Value calculated for a disordered monomer (Eq. 3).
[c] Value calculated for a folded dimer (Eq. 2).

Experimental hydrodynamic radii of 37TDs (R_H^{37TD}) were calculated using equation 1, where 1,4-dioxane is a standard reference:

$$R_H^{37TD} = (D^{diox}/D^{37TD}) * R_H^{diox} \quad \textbf{Eq. 1}$$

assuming that R_H^{diox} is 2.12 Å.[102]

Predicted hydrodynamic radii were calculated from empirical equations for folded proteins:[101]

$$R_H = 4.75 * N^{0,29} \quad \textbf{Eq. 2}$$

and for disordered proteins:

$$R_H = (1.24 * P_{Pro} + 0.904) * (0.00759 * |Q| + 0.963) * 2.49* N^{0,509} \quad \textbf{Eq. 3}$$

where N is the number of residues (37, 74, and 148 for monomer, dimer, and tetramer, respectively), P_{Pro} is the fraction of proline residues, and |Q| the absolute net charge. |Q| was calculated at pH 7 using the Protein Calculator v3.4 software (http://protcalc.sourceforge.net).

The diffusion experiment spectra of 37TD-WT and 37TD-L344P are shown in the 'Product characterisation' section at the end of this thesis (Supplementary NMR, Figure S44 and S45). The diffusion coefficient determined for 37TD-WT was D = (1.00 ± 0.02) x 10^{-10} m^2 s^{-1}, which provided an experimental R_H of 22.2 Å, close to the expected value (20.3 Å) for a globular protein of the size of tetrameric 37TD (148 residues) (Table 3).[101] Regarding 37TD-L344P, the values obtained were D = (1.45 ± 0.01) x 10^{-10} m^2 s^{-1} and R_H = 15.3 Å, in agreement with the R_H predicted (14.6 Å) for a disordered 37-residue peptide (Table 3).[101] In the case of 37TD-L344R, the monomeric species provided values of D = (1.78 ± 0.04) x 10^{-10} m^2 s^{-1} and R_H = 12.5 Å. The experimental hydrodynamics radii were smaller than the radius predicted for a disordered 37-residue peptide (14.6 Å) (Table 3), thereby suggesting that the monomeric 37TD-L344R peptide has some degree of compaction. On the other hand, the 37TD-L344R species resonating at δ^1H =1.58 ppm and δ^{13}C=13.52 ppm,

provided a D = (1.38 ± 0.02) x 10^{-10} m^2 s^{-1} and a R_H = 16.1 Å. This hydrodynamic radii value suggests that this second species is dimeric because it was in good agreement with the value predicted (16.5 Å) for a globular protein of the size of dimeric 37TD (74 residues) (Table 3). These results indicate that monomeric and dimeric 37TD-L344R co-exist in solution.

As a summary of the NMR results, a qualitative scheme illustrating the equilibrium between different species of the 37TDs based on NMR data at a monomer concentration of 20 µM and 40 °C is shown in Figure 19. The arrows indicating the equilibrium are proportional to the intensity of the peaks in the NMR spectra. On the basis of the NMR experiments, we can conclude that all the mutations studied destabilise the tetramer in solution.

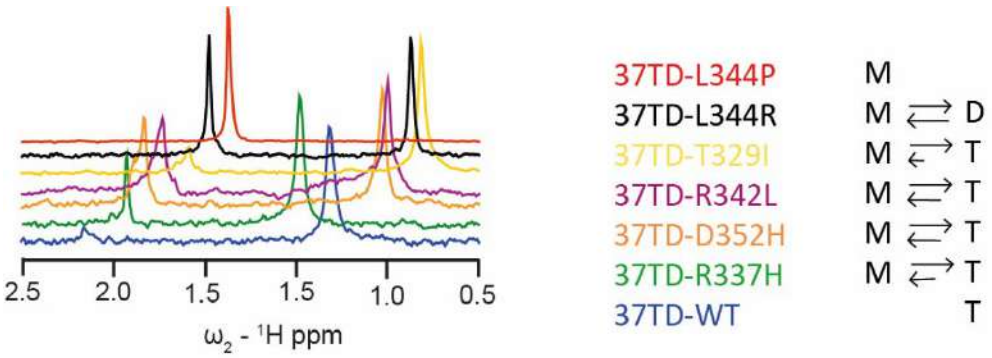

Figure 19. ^{1}H projections of HSQC spectra of 37TDs at 40 °C at a monomer concentration of 20 µM. A scheme illustrating the oligomeric 37TD species (T: tetramer, D: dimer, M: monomer) detected by NMR is shown on the right panel.

Determination of the K_d of tetramerisation by thermophoresis

We performed thermophoresis experiments to determine the constant of dissociation (K_d) of the tetramerisation event for the 37TDs. Microscale thermophoresis (MST) is a powerful technique that allows the detection of a variety of bio-molecular interactions and the relative dissociation constants. This technique is based on thermophoresis, which consists of the motion of molecules in a temperature gradient caused by an infrared laser.[103,104] The movement depends on several properties of the analyte, such as size, shape, charge, hydration shell and conformation, and it is sensitive to small changes of these molecular properties, consequent to the binding (Figure 20 B and C).[105] Although microscopic thermophoresis is poorly understood, it is very sensitive to changes in the solvation shell of molecules caused by binding. Therefore, it is a very useful technique to study the binding of small molecules to proteins, where there may not be a big alteration

in the total charge or size of the whole protein, but the solvation of the protein changes upon binding. This technique detects and quantifies the movement of the molecules by the fluorescence of a covalently bonded fluorophore or the intrinsic fluorescence of the analyte. K_d is determined by the scan of 16 capillaries filled with solutions where the amount of the fluorescent protein is constant and the protein is titrated by an increasing concentration of the ligand (Figure 20 A and D).

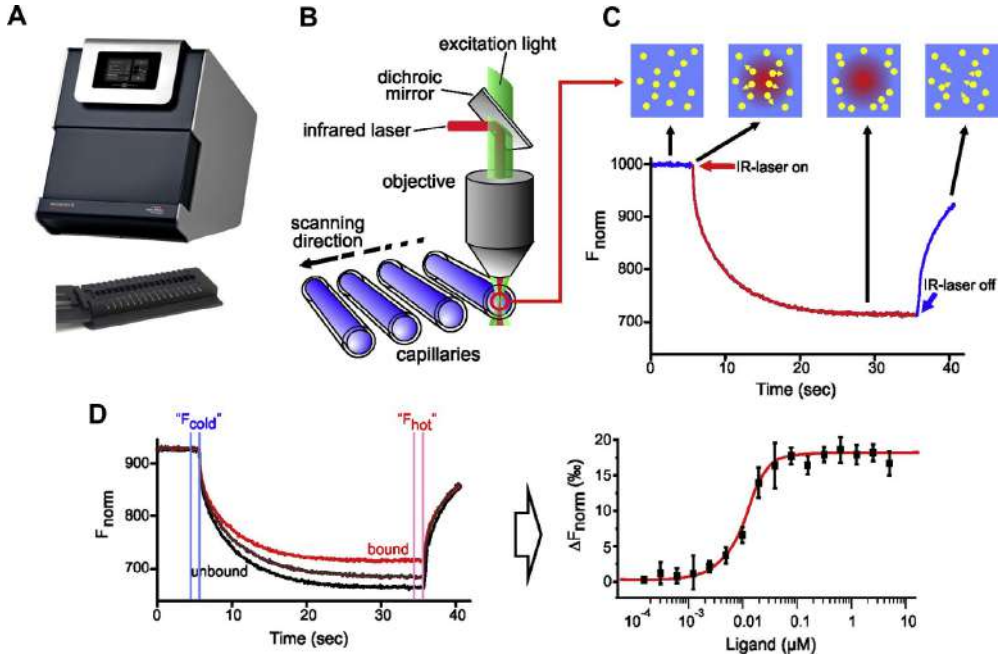

Figure 20. Schematic representation of MST experiment. Image adapted from Jerabek-Willemsen *et al.*[105] for illustrative purposes.

In our experiments, we studied the homo-tetramerisation phenomenon for each 37TD. To achieve this, 37TDs were labelled with the NT-647-NHS fluorescent dye, which binds to the Lys side chains. These peptides, our targets, were named with an asterisk, indicating that carried a fluorescent label. We first performed the *pretest* experiment to find the lowest concentration of the target that gives a fluorescence signal high enough to carry on the experiment. After that, the targets were titrated with an increasing amount of 'cold' peptide — our ligands — meaning that they were not fluorescently labelled. We performed a *binding check* experiment to find the highest concentration of the ligand to detect the binding. Having found these experimental conditions, a *binding affinity* experiment was performed to determine the K_d of the tetramerisation (Figure 21).

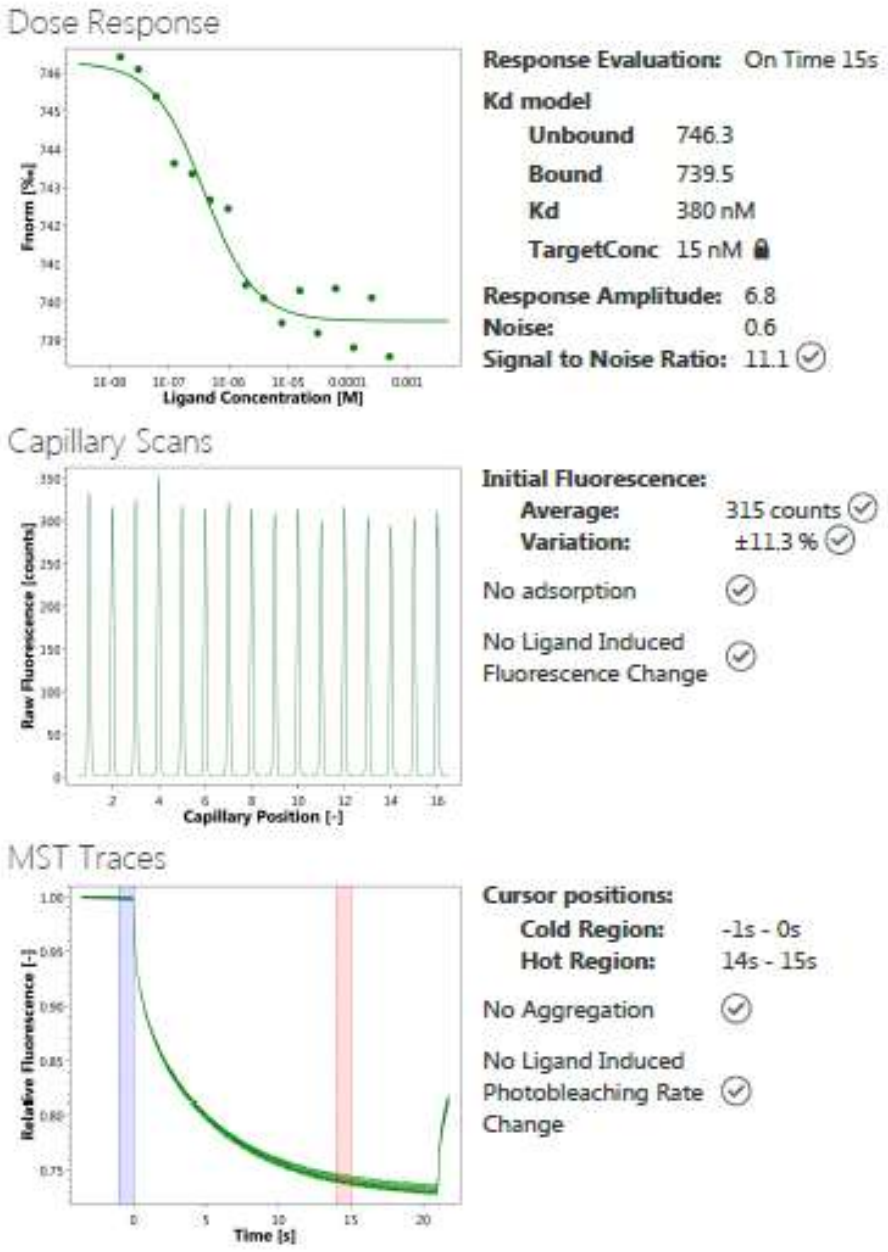

Figure 21. MST experiment of 37TD-WT. The concentration of 37TD-WT* (target) was 15 nM and the highest concentration of 37TD-WT (ligand) was 500 µM.

The dose-response panel in Figure 21 shows the fitting data of the 16 points to calculate the K_d. In the case of 37TD-WT, it was 380 nM. MST experiments of the other 37TDs are shown in the 'Supplementary MST' section (Figure S51-S60). Before

and after performing the MST experiment itself, the capillaries were scanned (Capillary scans panel, Figure 21) to check there was no absorption of the sample on the capillary walls and to check that the fluorescence did not vary upon addition of the ligand. The MST experiment is shown in the last panel of Figure 21 (MST Traces). From the profile of the traces, technical parameters can be proved, such as aggregation and photobleaching rate changes induced by the ligand. If these phenomena do not occur, the calculated value of the K_d from the experiment is reliable, otherwise some technical changes in the preparation of the sample should be considered, such as the addition of detergent to the buffer. The dissociation constants of the 37TDs are reported in Table 4.

Peptide	pH	k_D
37TD-WT	7	380 nM
37TD-R337H	5.3	36.5 µM
	7	959 nM
	8	1.51 µM
37TD-D352H	5.3	186 µM
	7	70.2 µM
	8	4.51 µM
37TD-R342L	7	11.2 µM
37TD-T329I	7	14.7 µM
37TD-L344R	7	87.2 µM
37TD-L344P	7	N/A

Table 4. Dissociation constants of the tetramerisation of 37TDs found by MST.

37TD-WT was the peptide that gave the lowest constant of dissociation, meaning that this tetramer was the most stable of those studied. On the other hand, with 37TD-L344P any K_d was found because the peptide is unstructured, thus unable to tetramerise. For the mutants in which a His residue was introduced, *i.e.* 37TD-R337H and 37TD-D352H, different pH conditions were studied to check how the tetramerisation was affected by the protonation or deprotonation of the imidazole group. In the case of 37TD-R337H, we expected the stability of the tetramer to recover by protonating the imidazole group, thus at acidic pH. However, the results did not show a clear tendency with the change of the pH and they are not consistent with those of previous studies reported[75] nor with our NMR data. In the case of 37TD-D352H, we expected an opposite dependency on the pH compared to 37TD-R337H. When the Asp residue was replaced by His, the original salt bridge R337-D352 of the WT was replaced by R337-H352. Therefore, at acidic pH, two positive charges, from R337 and H352, would be close having a destabilising effect. We found that K_d increased when the pH was decreased. Regarding 37TD-R342L, the results showed a destabilising effect of this mutation on the tetramer, as expected and in

agreement with our results from native MS and NMR. From our MST experiments, we conclude that the mutation T329I has a destabilising effect. Although it is consistent with our results from native MS and NMR, the K_d found suggests a destabilisation comparable to other mutations, such as R337H and R342L. Finally, for 37TD-L344R we found a high K_d, which was interpreted as the constant of dimerisation.

In summary, in this chapter, we studied the oligomerisation of p53TD. To this end, we selected the WT and six mutations with biological relevance and value as structural models because their populations involve distinct oligomeric states. The secondary and quaternary structures were defined by CD, native MS, and NMR, and the dissociation constants were calculated by MST. From our experiments, we conclude that 37TD-WT is tetrameric in all the conditions studied and that it is the most stable tetramer among our 37TDs. The tetramer dissociates in the gas phase when the voltage was increased, and the equilibrium moves towards the monomer. Overall, the mutations studied in this chapter have a destabilising effect on the tetramer, although to a different extent. In particular, R337H, D352H and R342L mutations strongly destabilise the tetramer. They probably adopt a distinct structure from that of the WT, with 37TD-R337H and 37TD-R342L having a major β-sheet contribution, and 37TD-D352H having weaker bands. Like the WT, the dissociation of the tetramer proceeds directly to the monomer. 37TD-R337H presents an equilibrium between distinct oligomers that is dependent on the pH, forming a more stable tetramer at acidic pH in NMR experiments. T329I is the mutation that has the weakest destabilising effect on the tetramer. 37TD-T329I has a similar CD profile to the WT. It is mainly tetrameric both in the gas phase and in solution, but a monomeric population is also present in the MS and NMR spectra. Surprisingly, the dissociation constant found in the MST experiments is similar to that found for the strong destabilising mutants. Finally, 37TD-L344R and 37TD-L344P were unable to tetramerise, resulting in dimer and monomer, respectively. These results have been achieved by applying a variety of biophysical techniques that allow the problem to be tackled from different perspectives and physical states. Taken together, our results contribute to a deeper understanding of the equilibrium between the oligomers of p53TD and to a more precise assignment of the oligomeric state of p53TD mutations.

DESIGN OF A ‘SUPER’ TETRAMER AND A ‘SUPER’ DIMER OF P53TD

In this chapter, we want to study deeper the equilibrium between p53 species defining and isolating dimeric and tetrameric p53TD species in order to reduce the number of p53 oligomers, thus the equilibria among them, simplifying our system. In order to achieve our goal, we have introduced one cysteine residue in specific positions of the monomer to form disulphide bridges between monomers. The mutations we have introduced, namely L330C and L344C, are not cancer related, but they were designed to selectively stabilise the dimer in one case (L330C) and the tetramer in the other case (L344C). In principle, the mutant L330C was designed to stabilise the dimer by cross-linking two monomers, but still allowing the tetramerisation. In this way thus, the monomer-dimer equilibrium is avoided, but the dimer-tetramer equilibrium is still allowed and it can be shifted by changing the conditions of the experiments, such as the temperature and the concentration. Isolating the dimer is not easy because it is normally not stable enough. Nevertheless, some previous studies reported p53 TD as dimeric. For example, mutations in the hydrophobic residues of the α-helix favour the dimeric form. Bista *et al.*[30] and Mateu *et al.*[67] reported the mutant L348A as dimeric, as well as mutants F341C, L344R and A347T are described as dimeric.[34,64] Another approach to stabilise the dimer was described by Poon *et al.*[106] and Fischer *et al.*[39] They designed a sequence composed by the DNA-binding region followed by two oligomerisation domains joined together by a linker. After the folding of the domain, the monomer already adopted the geometry of the dimer. The oligomerisation of this species, which consisted of a dimerisation, allowed the geometry of the tetramer (dimer of dimers). Instead, we propose a cross-linking approach to isolate the p53 species of our interest. The mutant L344C was designed to stabilise the tetramer linking together two monomers belonging to different dimers. In this case as well, only the dimer-tetramer equilibrium is allowed and can be shifted by changing the experimental conditions.

Having our peptides in hands, we studied first the folding of the peptides by circular dichroism. Afterwards, the oligomerisation state of these peptides was determined by native MS, whereas the secondary and quaternary structure by NMR. The dissociation constants of tetramerisation were calculated by thermophoresis and finally, a theoretical study aimed to determine the secondary and quaternary structures of these mutants in the presence of the disulphide bridge was achieved by molecular dynamics (MD), performed by Dr. Salvador Guardiola.

Design of the mutants

In order to stabilise the dimer in one case and the tetramer in the other case, we designed two mutations (L330C and L344C) that introduce cysteine residues to form the disulphide bridge (Figure 22). As for 37TDs, the monomer sequence has been defined from residues 320-356. In this case, two monomers are covalently linked by the disulphide bridge, thus the peptides are composed by 74 residues and they are named 74TDs (Figure 22).

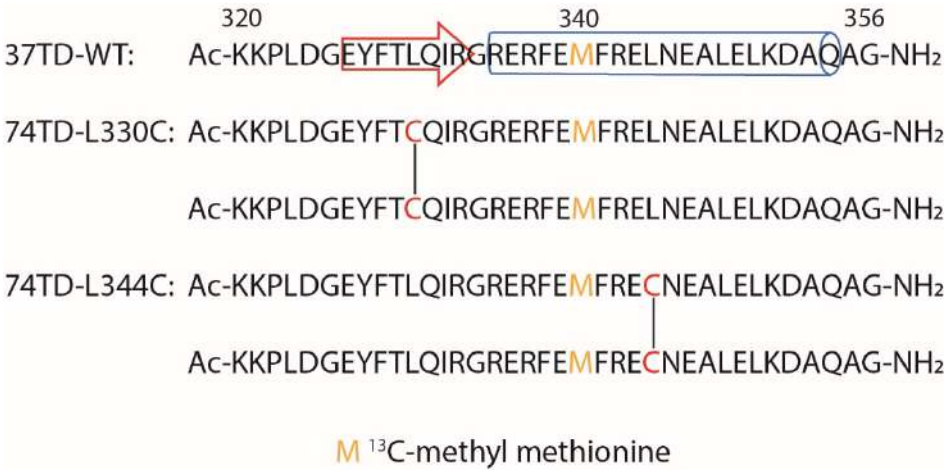

Figure 22. Sequences of the 74TDs and 37TD-WT. The red residues correspond to the positions of the mutations and the yellow Met indicates the isotope-labelled residue. The β-strand and the α-helix are represented with an arrow and a cylinder, respectively, in the WT sequence.

The L330C mutation was introduced in the β-strand of the domain (res 326-333) because it has been reported that L330 is involved in the stabilisation of the dimer and a residue on one chain is close in space to the respective residue of another chain belonging to the same dimer[107,108] (Figure 23). We thus designed this mutant introducing a cysteine residue to link together two monomers of the same dimer, with the purpose of stabilising the dimer. The L344C mutation, on the contrary, was introduced in the α-helix of the domain (res 335-354). The L344 residue is part of the hydrophobic core in the dimer-dimer interface and it is involved in the stabilisation of the tetramer.[107,108] The side chains of the four L344 residues in the tetramer are close to each other, but, considering one monomer, the side chain of L344 is closer to the side chain of the respective residue on a monomer belonging to the other dimer (Figure 24). By substituting the L344 with a cysteine, after forming the disulphide bridge, ideally two monomers of different dimers would be covalently bonded, thus stabilising the tetramer.

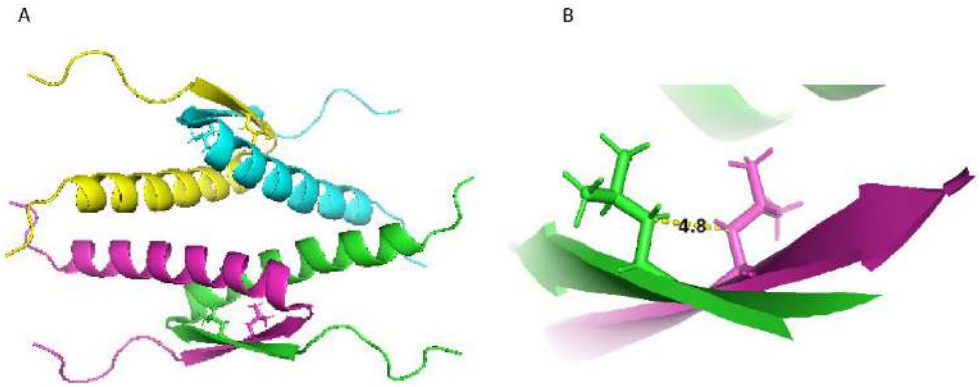

Figure 23. (A) Cartoon representation of the WT from its NMR structure,[28] PDB ID 1OLG, showing location of the residues L330. (B) Zoom of the same image showing the distance (4.8 Å) between residues.

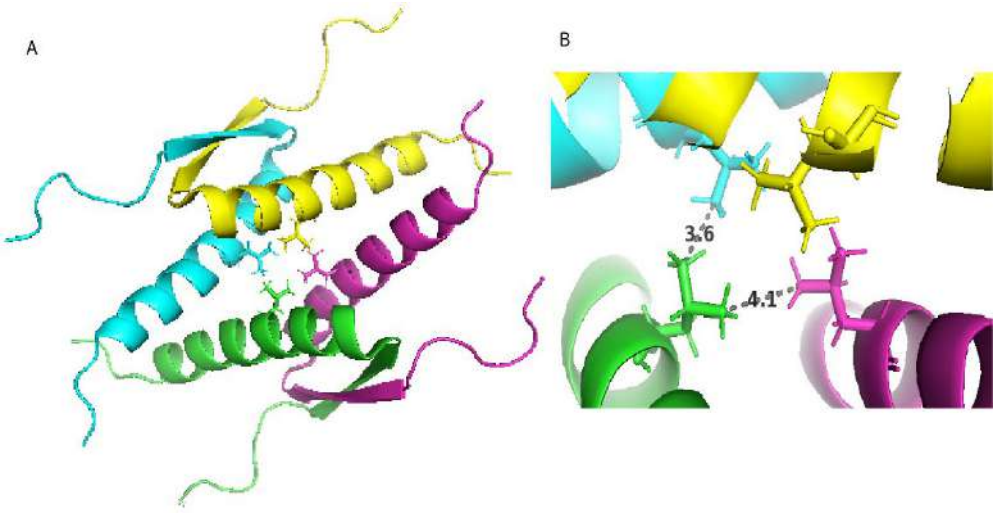

Figure 24. (A) Cartoon representation of the WT from its NMR structure,[28] PDB ID 1OLG, showing location of the residues L344. (B) Zoom of the same image showing the distances (3.6 and 4.1 Å) between residues.

The 74TDs were chemically synthesised by microwave-assisted SPPS (Solid Phase Peptide Synthesis) using a ^{13}C-methyl methionine to perform NMR experiments. After having purified the monomers, the disulphide bridge was formed in solution using BisNPys as activator reagent, giving the dimers as products. The data corresponding to the characterisation of the 74TDs are reported in the section 'Product characterisation' at the end of the thesis (Figure S6-S7).

Secondary structure of the 74TDs

Having the peptides in hands, we first studied their folding by circular dichroism (CD) experiments. We compared the results with 37TD-WT, as a reference for a tetrameric folded peptide. Both 74TDs were folded and their spectra presented a helical structure profile. Nevertheless, they showed bands less intense compared to the WT (Figure 25). This may suggest that the helical degree of these peptides was reduced. Moreover, for 74TD-L330C, the band at 208 nm was more intense than the band at 222 nm, changing the ratio θ_{222} / θ_{208}. The reasons way this ratio changes are quite controversial and the interpretation of the data is not always straightforward. A possible scenario in the case of a ratio θ_{222} / θ_{208} close to 0.8, is that the peptide is helical, but the helices are not interacting with each other.[109] On the contrary, when the ratio is close to 1, the helices are interacting in a structure as stranded coiled coil.[110] Another possible scenario, in case the band at 208 nm is bigger than the one at 222 nm, is that the peptide is less structured with a higher contribution of the random coil.

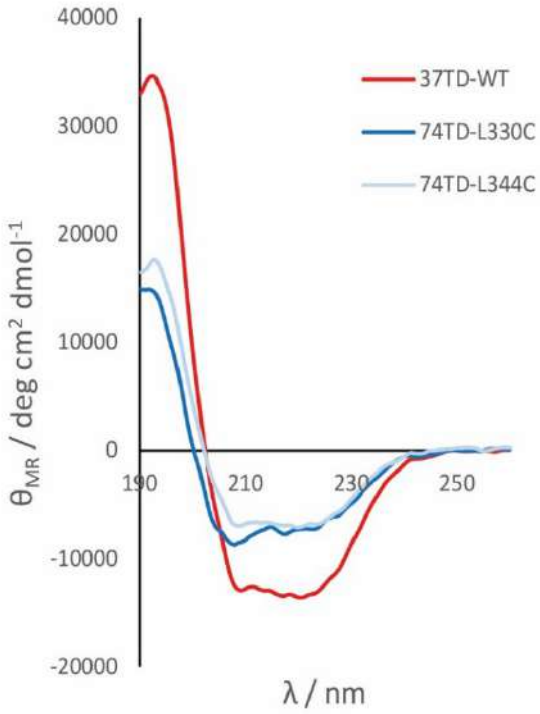

Figure 25. Circular dichroism spectra of the 74TDs compared to 37TD-WT. The spectra correspond to a monomer concentration of 20 µM of each peptide in water, pH 7. For 37TD-WT, non-isotope-labelled peptide was used. The spectra were recorded at 25 °C.

Determination of the oligomeric state by native MS

In order to determine the oligomeric state of the 74TDs, native MS experiments were performed in a similar way as for 37TDs. The TOF and IM-MS spectra of 74TDs are shown in the 'Supplementary native MS' section (Figure S31-S34). For 74TD-L330C, it was found that this peptide was mainly dimeric (Figure 26). Although this mutation was introduced to stabilise the dimer, this peptide was expected to be mainly tetrameric. On the contrary, the MS results suggested it was mainly dimeric, but the dimer coexisted with the tetramer in the gas phase. One explanation for this evidence can be that the introduction of the cysteine in the β-strand and the formation of the disulphide bridge constrain the peptide in a structure that is not particularly prone to tetramerising. By increasing the voltage, the spectrum did not change much, as expected. Since at the most native condition of high concentration and low voltage (100 µM, 40 V), the peptide was predominantly dimeric, by increasing the voltage, it could not disrupt, since it is two monomers covalently bonded to each other.

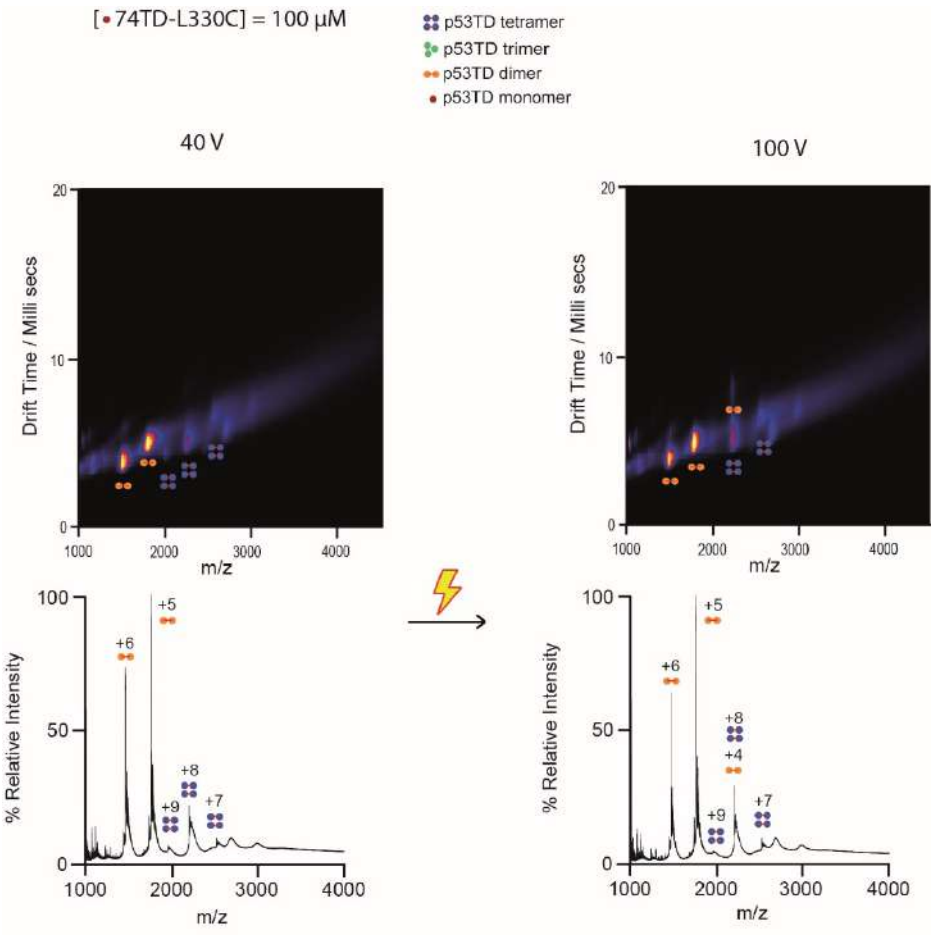

Figure 26. Native Mass Spectrometry and Ion Mobility spectra of 100 µM 74TD-L330C at a cone voltage of 40 and 100 V. The concentration reported refer to the monomer. The sample was dissolved in 200 mM ammonium acetate buffer, pH 7.

For 74TD-L344C, the results suggested that the peptide was mainly tetrameric in the gas phase. After diluting the sample or increasing the voltage even up to 120 V, the peptide remained tetrameric. By comparing the results of low concentration and high voltage (20 µM and 120 V) of 74TD-L344C and 37TD-WT (Figure 27), the tetramer of L344C mutant was clearly more resistant to the high voltage than the WT, where the latter disrupted at these conditions. These promising results motivated us to further study this system in solution by NMR experiments.

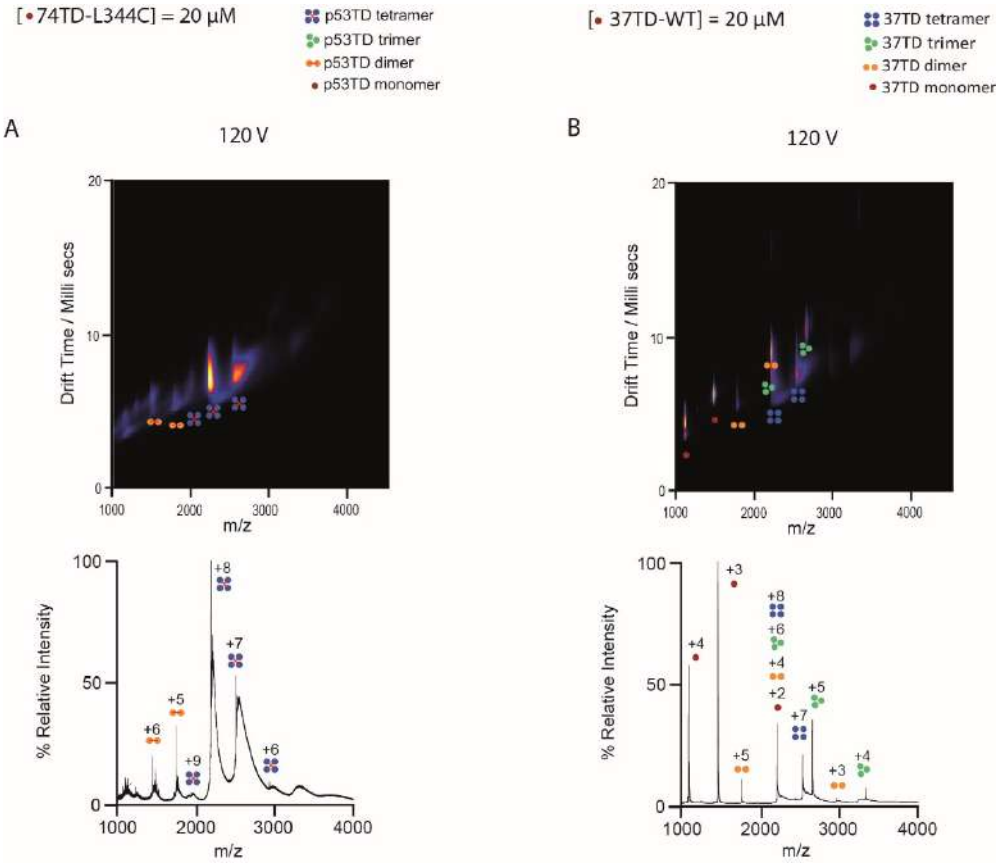

Figure 27. Native Mass Spectrometry and Ion Mobility spectra of 20 µM 74TD-L344C (A) and 37TD-WT (B) at a cone voltage of 120 V. The concentration reported refer to the monomer. For 37TD-WT non-isotope-labelled peptide was used. The sample was dissolved in 200 mM ammonium acetate buffer, pH 7.

Study of the equilibrium between oligomers by NMR

Similarly as for the study of 37TDs, we acquired 2D HSQC NMR experiments to assign the oligomeric state of 74TDs in solution and to study how the population of the oligomeric species changed by modifying the temperature and the concentration. Starting with 74TD-L330C, three peaks were present in the spectrum at 100 µM (Figure 28 B). Two of them (^{1}H 2.05 ppm, ^{13}C 14.19 ppm; ^{1}H 1.98 ppm, ^{13}C 14.31 ppm) were in the region of unfolded monomeric peptides, close to the signal of 37TD-L344P (Figure 28). One cross-peak (^{1}H 1.62 ppm, ^{13}C 13.86 ppm) instead resonated in the region of structured folded peptides, close to the tetrameric signal of 37TD-R337H (Figure 28). By increasing the temperature up to 40 °C the peak corresponding to a folded peptide disappeared, whereas by decreasing the temperature to 5 °C the cross-peak in the unfolded region resonating at ^{1}H 1.98 ppm, ^{13}C 14.31 ppm disappeared. We interpreted our results as three different populations, where the two cross-peaks in the region of unfolded peptides corresponded both to the dimer, one unfolded (^{1}H 1.98 ppm, ^{13}C 14.31 ppm) and the other one folded (^{1}H 2.05 ppm, ^{13}C 14.19 ppm). One explanation why, although folded, the dimer signal has a chemical shift in the unfolded region may be that the presence of the disulphide bridge constrained the peptide to folding in a different way than the wild type. The cross-peak (^{1}H 1.62 ppm, ^{13}C 13.86 ppm) that disappeared when increasing the temperature, instead, may correspond to the signal of the tetramer. In order to prove this hypothesis, we performed CD experiments at 100 µM and different temperatures, such as 5, 25 and 40 °C (Figure 32). The results showed that 74TD-L330C had a lower thermal stability compared to 37TD-WT and 74TD-L344C, as at 40 °C the contribution of the random coil was more prominent than for the other peptides. These results are in agreement with the fact that the peak we assigned to the tetramer disappeared at 40 °C since probably there was no tetrameric peptide at this temperature. On the other hand, the cross-peak corresponding to the unfolded dimer disappeared at 5 °C, consistently with the fact that at low temperature the conformational equilibrium is shifted towards the more stable conformer. The peaks corresponding to the folded dimer and to the tetramer shifted by decreasing the temperature. In particular, the peak of the tetramer moved towards the position of the wild type, whereas the peak of the folded dimer shifted upfield in the axe of ^{13}C signal. By diluting the sample to 20 µM of monomer concentration, the spectra did not change significantly (Supplementary NMR, Figure S46)

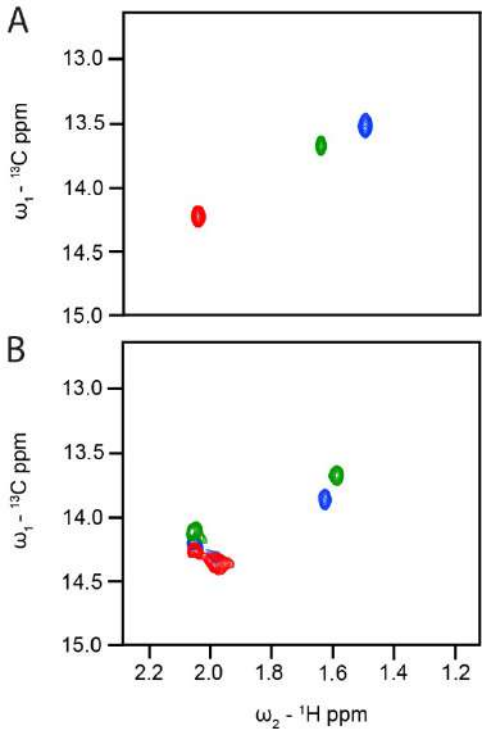

Figure 28. (A) 2D $^{1}H,^{13}C$ HSQC spectra at 25 °C of 37TD-WT (blue), 37TD-L344P (red) and 37TD-R337H (green) at a monomer concentration of 100 µM. (B) 2D $^{1}H,^{13}C$ HSQC spectrum at 25 °C (blue), 40 °C (red) and 5 °C (green) of 74TD-L330C at a monomer concentration of 100 µM.

Concerning 74TD-L344C, the HSQC spectra showed broad signals in the unfolded region. Changing the temperature or the concentration did not modify the spectra much (Figure 29 and Supplementary NMR, Figure S47). Considering the CD results (Figure 25) and the MS results (Figure 27) we did not expect to find signals in the unfolded region, because the CD spectrum showed a profile of an α-helix and in the MS spectra the tetramer signals were detected even at high voltage. Nevertheless, in this mutant, the mutation introduced (L344C) is close to the Met residue (M340), which is the only residue detected in the NMR experiments, thus the Met signals may appear in different positions due to the change in the chemical environment around it.

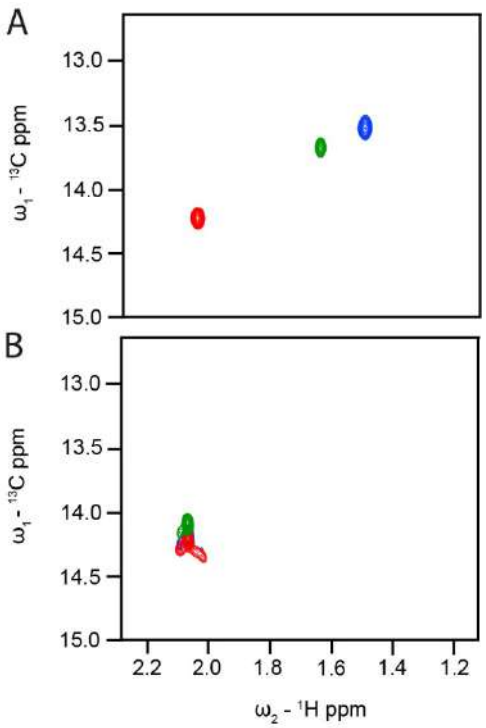

Figure 29. (A) 2D $^{1}H,^{13}C$ HSQC spectra at 25 °C of 37TD-WT (blue), 37TD-L344P (red) and 37TD-R337H (green) at a monomer concentration of 100 µM. (B) 2D $^{1}H,^{13}C$ HSQC spectrum acquired at 25 °C (blue), 37 °C (red), and 5 °C (green) of 74TD-L344C at a monomer concentration of 100 µM at 25 and 5 °C and at a monomer concentration of 20 µM at 37 °C.

In order to investigate the folding of this peptide in solution more in depth, we acquired 1D ^{1}H spectrum of 74TD-L344C at a monomer concentration of 100 µM and we compared the results deriving from similar analysis of 37TD-WT and 37TD-L344P. As discussed in the previous chapter, the wild type is a folded tetrameric peptide, whereas the L344P mutant is an unfolded monomeric peptide. Looking at the methyl region (0.8-0.9 ppm) (Figure 30), the signals of the wild type were shifted upfield and they appeared in the region of 0.5-0.8 ppm. On the contrary, the signals of L344P mutant virtually overlapped and they resonated around 0.9 ppm in a broad signal. The profile of 74TD-L344C was an intermediate situation between them two, thus indicating that this peptide probably adopts the conformation of a molten globule. The molten globule conformation is characterised by a secondary structure very similar to the native folding, a lower level of compactness with a radius of the protein not larger than a 10-30% of the original folded structure and a more flexible hydrophobic core.[111–113] The profile of the NMR spectra suggests a molten globule structure of this mutant and a similar situation was found looking at the signals of the NHs of the backbone residues (6.5 - 9.5 ppm) (Figure 30). The wild type presents

sharp and defined signals because the NH of the residues that form the hydrophobic core do not exchange the proton with the deuterium of the solvent, being not solvent exposed. These signals disappeared in the mutant L344P, being this peptide unstructured and having the whole residues exposed to the solvent. Again, an intermediate behaviour was observed for the mutant L344C meaning that it is partially structured but most likely it adopts a different conformation than the wild type.

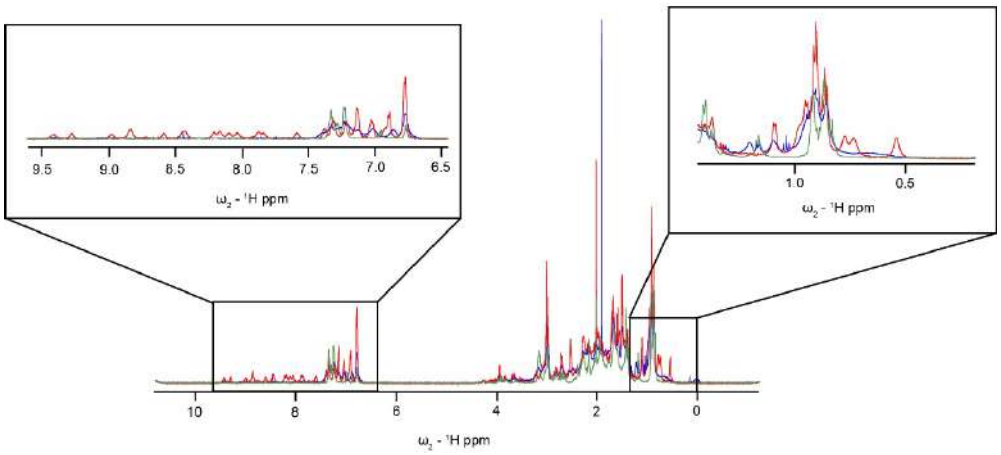

Figure 30. (A) 1D ^{1}H spectra at 25 °C of 37TD-WT (red), 37TD-L344P (green), and 74TD-L344C (blue) at a monomer concentration of 100 µM.

In order to further investigate the oligomeric state of L344C mutant, we performed X-STE NMR diffusion experiments, as described in the previous chapter. The results of 74TD-L344C are shown in Figure 22 and the hydrodynamic radii of the WT, L344P, L344R and L344C peptides are compared in Table 5.

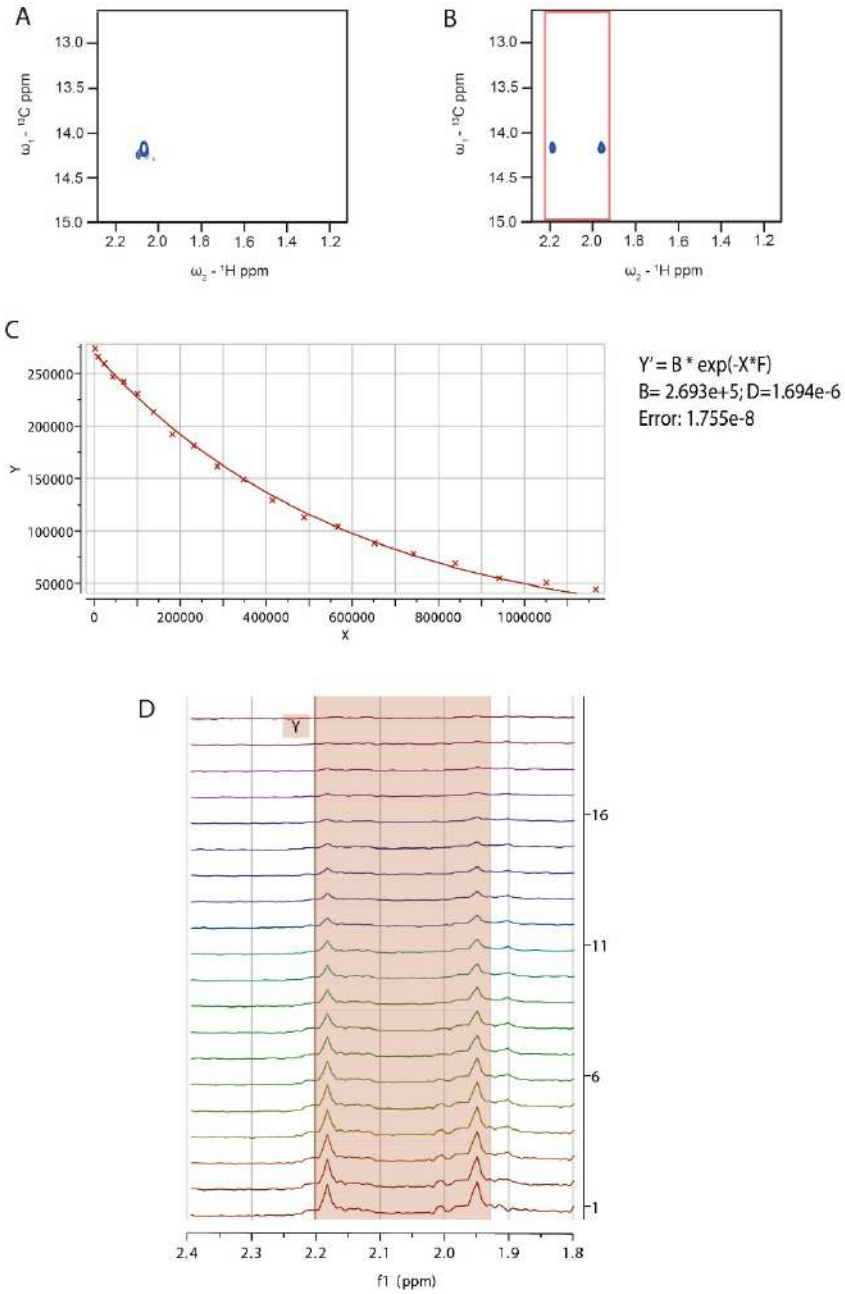

Figure 31. X-STE NMR diffusion of 74TD-L344C monitoring the size of the species containing ^{13}C-attached ^{1}H nuclei. (A) 2D ^{1}H,^{13}C-HSQC. (B) ^{13}C-coupled 2D ^{1}H,^{13}C-HSQC illustrating the splitting of the Met340 $^{1}H^{\varepsilon}$ signal ($^{1}J_{HC}$ ≈140 Hz). (C,D)) X-STE NMR diffusion experiments. The decay in signal intensity of the Met340 $^{1}H^{\varepsilon}$ signal (panel D) was fitted to a mono exponential function to obtain the coefficient diffusion. X-STE experiments were acquired without decoupling and the Met340 $^{1}H^{\varepsilon}$ signal splits into a doublet ($^{1}J_{HC}$ ≈140 Hz). The spectra were recorded at 25 °C using a monomer concentration of 100 µM (D_2O, pH 7).

Peptides	D x 10^{-10} / m^2 s^{-1}	R_H / Å experimental	R_H / Å predicted
37TD-WT	1.00 ± 0.02	22.2	20.3[a]
37TD-L344P	1.45 ± 0.01	15.3	14.6[b]
37TD-L344R			
Dimer	1.38 ± 0.02	16.1	16.5[c]
Monomer	1.78 ± 0.04	12.5	14.1[b]
74TD-L344C	1.69 ± 0.02	13.1	20.3[a]

Table 5. Diffusion coefficients (D) and hydrodynamic radius (R_H) of 37TD-WT, 37TD-L344P, 37TD-L344R and 74TD-L344C. For 37TD-L344R, the two species are independently analysed. Predicted R_H are calculated from Marsh *et al*.[101]

[a] Value calculated for a folded tetramer (Eq. 2).
[b] Value calculated for a disordered monomer (Eq. 3).
[c] Value calculated for a folded dimer (Eq. 2).

The hydrodynamic radius of 74TD-L344C expected was around 20 Å, the value predicted for a tetramer, according to the MS data. Nevertheless, a much smaller value was found (13.1 Å, Table 5). This value is an intermediate value between the hydrodynamic radius of the monomer and of the dimer of 37TD-L344R. Therefore, we interpreted our results as a dimeric peptide of 74TD-L344C, which maybe was more compacted than the dimer of 37TD-L344R. A dimeric 74TD-L344C is the smallest species possible for this peptide as it cannot be monomeric. In order to analyse the structure of both 74TDs more in depth, we performed molecular dynamic studies of these systems as well as circular dichroism at the same concentrations and temperature as for the NMR experiments.

The CD results from spectra acquired at 5, 25 and 40 °C at a monomer concentration of 100 µM of the 74TDs are shown in Figure 32 and they are compared to the wild type. As commented above in this chapter, 74TD-L344C was structured according to the CD results, but the bands were less intense than the wild type. This mutant was stabile during thermal denaturation, at least up to 40 °C, because the CD profile did not change significantly increasing the temperature. The magnitude of change in the band intensity was comparable to that of the WT (Figure 32). On the other hand, 74TD-L330C probably adopts a different conformation having a different CD profile and it was much less stabile during thermal denaturation, as at 40 °C the contribution of the random coil was much more pronounced than for the other peptides.

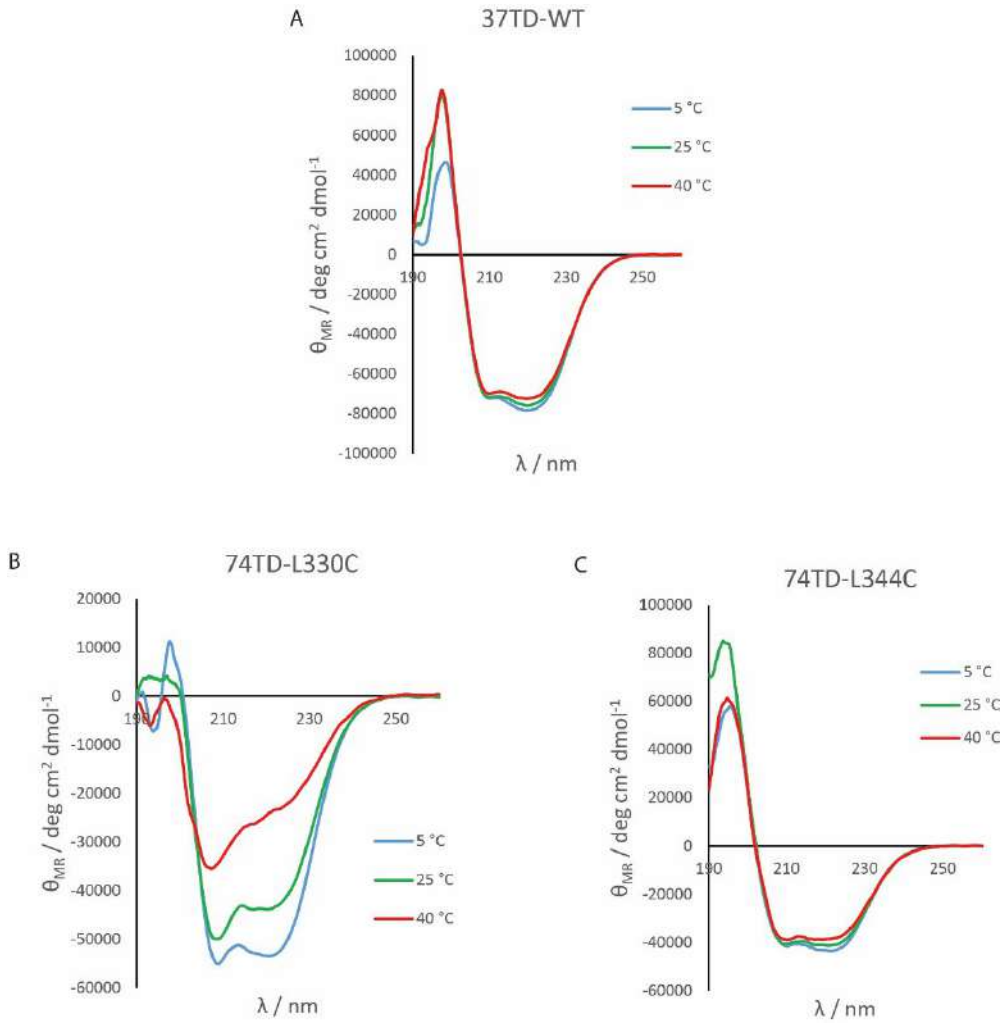

Figure 32. Circular dichroism spectra of the 74TDs (B, C) compared to 37TD-WT (A). The spectra were acquired at 5, 25 and 40 °C at a monomer concentration of 100 µM of each peptide in water, pH 7. For 37TD-WT, non isotope-labelled peptides was used.

These results are consistent with the interpretation of the NMR experiments, where L330C mutant presented different species in solution, including the tetramer, whose signal was in the region of folded peptides. However, the structure of the peptide was unstable with the increasing of the temperature in CD experiments and this may explain the signal disappearance at 40 °C in the NMR spectrum. Moreover, the different CD profile of 74TD-L330C compared to the WT profile, may explain the coexistence of different dimeric conformations in solution. In fact, the NMR spectra showed different folding of the dimeric peptide, which were interpreted as folded and unfolded dimer. Concerning 74TD-L344C, we can conclude that it is a folded domain, but it adopts different conformations than the WT, most probably a molten

globule. It was helical according to the CD profile and 1D ^{1}H NMR experiments showed that it was partially structured. The reason why the cross-peak in the HSQC spectrum is close to the signal of the 37TD-L344P probably is due to a change in the chemical environment of M340. According to the NMR diffusion experiments, this domain was dimeric. However, this contrasts with the MS results, where the signals of the tetramer were detected even at high voltage.

Determination of the K_d of tetramerisation by thermophoresis

As for the 37TDs, we performed thermophoresis experiments to calculate the dissociation constants of oligomerisation for the 74TDs. The experiments of the 74TDs are reported in the 'Supplementary MST' section (Figure S61-S62) and the values found are shown in Table 6.

Peptide	pH	K_d
37TD-WT	7	380 nM
37TD-R337H	5.3	36.5 µM
	7	959 nM
	8	1.51 µM
37TD-D352H	5.3	186 µM
	7	70.2 µM
	8	4.51 µM
37TD-R342L	7	11.2 µM
37TD-T329I	7	14.7 µM
37TD-L344R	7	87.2 µM
37TD-L344P	7	N/A
74TD-L330C	7	57.9 µM
74TD-L344C	7	N/A

Table 6. Dissociation constants of the tetramerisation of 37TDs and 74TDs found by MST.

The value found for 74TD-L330C was 57.9 µM (Table 6). It is similar to the value found for the dimeric peptide 37TD-L344R and it is higher than the values found for the destabilising mutations among the 37TDs, such as R337H, R342L and T329I. We interpreted our results as a dissociation constant of tetramerisation where two species were involved, namely dimer and tetramer. As for 37TD-L344R, only one equilibrium is present: in the case of 74TD-L330C between dimers and tetramer and in of 37TD-L344R between monomers and dimer. The high value of K_d may be explained by a change in the dimer-dimer interface compared to the WT. Concerning 74TD-L344C, any K_d was found, meaning that the dimer was unable to tetramerise. These results are consistent with the NMR data, where the diffusion NMR suggested

this peptide is dimeric, but they are not with MS results, where the signals of the tetramer were detected even at high voltage.

Molecular Dynamics (MD)

Molecular dynamics (MD) simulations were performed using GROMACS version 2019.6, by Dr. Salvador Guardiola. Three systems were independently studied, *i.e.* the WT and the mutants L330C and L344C. The structure used for the MD analysis consisted of the high-resolution structure of the oligomerisation domain of p53, PDB ID 1OLG[28] (res 319-360), which was adapted in order to obtain the same sequence as the peptides used in the experimental part, *i.e.* 37TD-WT, 74TD-L330C and 74TD-L344C (res 320-356). The starting structures of the mutants were generated by substituting the corresponding residues to cysteine and forming the disulphide bridge between two chains. We ran explicit MD simulations to assess the preferred secondary and quaternary structures in the mutants, and to answer the question if the introduction of the disulphide bridges had a stabilising or destabilising effect on the structure of the domain, compared to the WT. The starting structures were solvated and minimised using the steepest descent method to relax the systems. These were then subjected to two steps of equilibration in the NVT and NPT ensemble, respectively, and from there unrestrained MD trajectories were collected for around 500 ns. The trajectories of each system were analysed by plotting several key parameters, such as the potential energy of the systems, backbone root-mean-square deviations (RMSD), backbone root-mean-square fluctuations (RMSF), as well as by clustering the main conformations explored by each system during the simulation.

By looking at the potential energy of the systems (Figure 33), which takes into account the sum of all the interactions within the system (bonded and non-bonded), we can conclude it was mostly constant during the simulation, meaning that all three systems were stable during the 500-ns simulations. The values of potential energy for the mutants were comparable between each other, having the same number of atoms and the same type of bonds, but it is more difficult to compare them with the value of the WT, due to the aforementioned differences. In any case, the values were similar, and they were maintained almost constant during the simulation. From this first MD analysis, the results suggested that there was not a significant difference in stability among the two mutants.

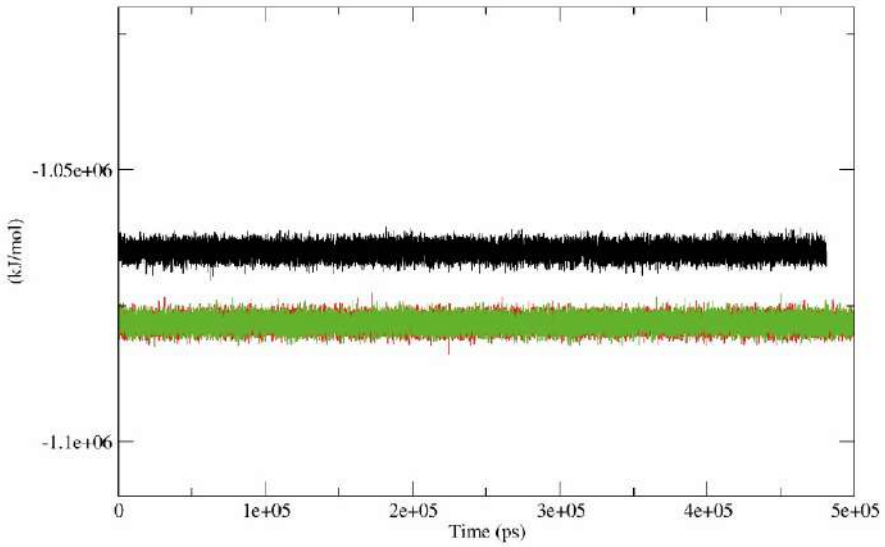

Figure 33. Potential energy of the system along the MD simulation. In black the analysis of 37TD-WT, in red of 74TD-L330C and in green of 74TD-L344C.

In order to gather information about the secondary structure adopted by the constrains during the simulation, the root mean square deviation (RMSD) of the protein backbone was calculated and its RMS distribution was represented for the three systems. Moreover, the gyration radius was calculated to get information on the shape and degree of compactness of the domains (Figure 34). The RMSD (Figure 34 A) gives an indication on the movement of the backbone, using the initial structure as reference for the deviation of each frame. Thus, the larger the RMSD, the further the structure moved from the starting conformation. Looking at the Figure 34 A, we can observe significant fluctuations during the first 100 ns of the simulation, as is expected for unrestrained MD. After this time, the molecules reached a stability plateau and presented less fluctuations. Overall, there were no significant differences between each domain and the fluctuations were small during the second part of the trajectories, between 4 – 7 Å, and almost 3 Å away from the starting position. 74TD-L330C showed the largest fluctuations, suggesting that its structure could be slightly less stable. Looking at the distribution of the RMS (Figure 34 B), the profile of the 74TD-L330C mutant deviated the furthest from a Gaussian profile. The profile of this mutant consisted of a main maximum with a shoulder, thus suggesting that the peptide adopted different conformations, and, in particular, the most populated one was further from the native folding of the WT. Concerning 37TD-WT, it showed the closest profile of a Gaussian distribution, meaning that the WT explored less conformations during the simulation and that the conformations adopted were closer to the starting NMR structure. 74TD-L344C

as well showed a Gaussian-like distribution, although it was wider than the one from the WT. Finally, the compactness of these structures was evaluated by the gyration radius calculation (Figure 34 C). The radius decreased slightly during the simulation, meaning that the structures were getting more compacted during the time. Maybe the gyration radius of 74TD-L330C was fluctuating more than the other domains, although the differences were small.

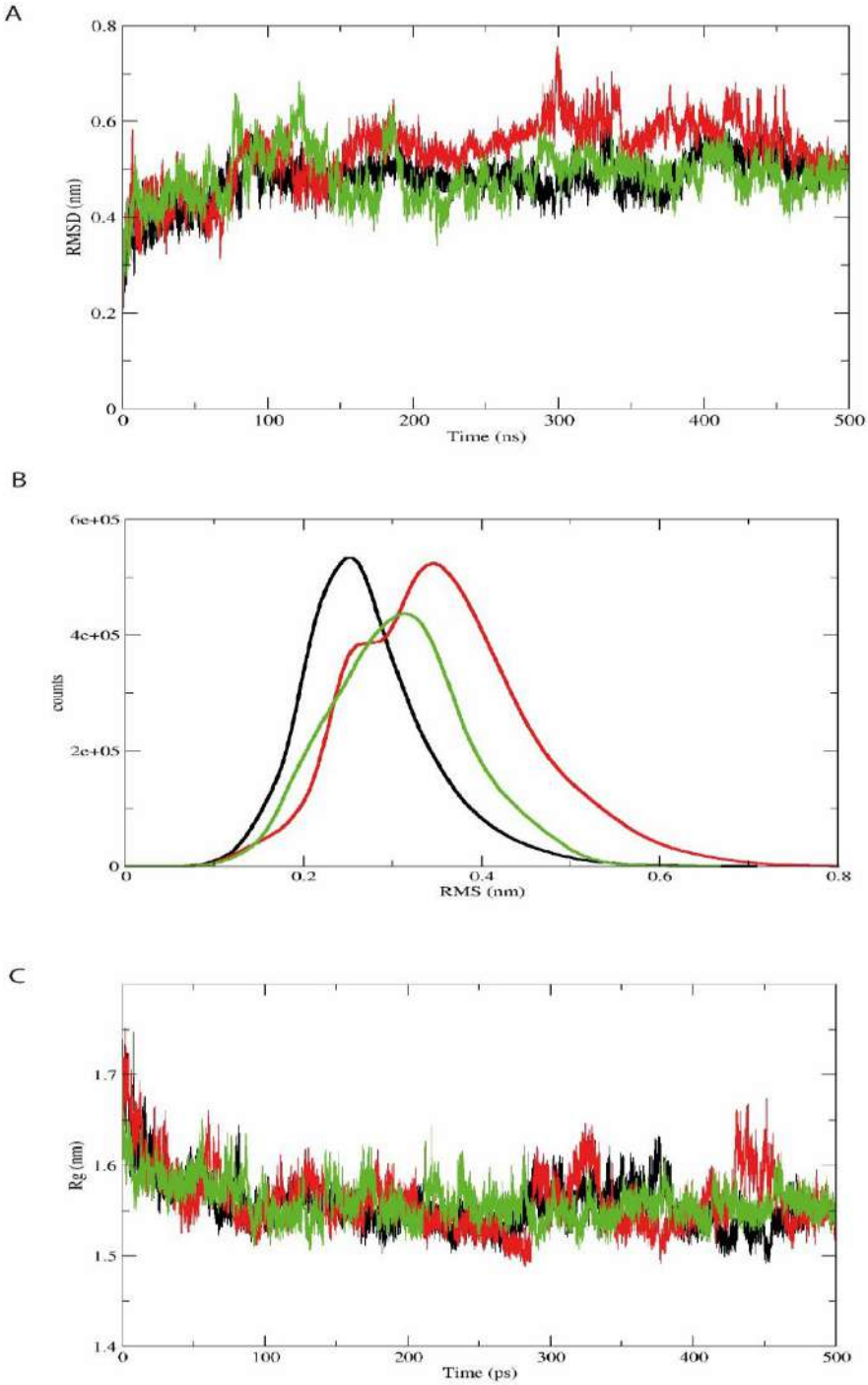

Figure 34. Molecular dynamics analysis of backbone RMSD from initial structure (A), backbone RMS distribution (B) and gyration radius (C). In black the analysis of 37TD-WT, in red of 74TD-L330C and in green of 74TD-L344C.

In order to know if the presence of the disulphide bridge, either in the α-helix or in the β-strand, affected the structure of the helix the RMSD the helical domain was also calculated (Figure 35 A). Its oscillation was quite small during the simulation meaning that the helix was stable, and the introduction of the mutations did not disrupt it. When comparing the two mutants, 74TD-L330C had a less stable helical domain than 74TD-L344C. This means that the presence of the disulphide bridge in the β-strand partially compromises the helical moiety of the domain. Concerning 74TD-L344C, the presence of the disulphide bridge on the helix caused structural modifications of the helix, having a larger RMSD that the WT. However, it stabilised during the simulation. A confirmation of this observation comes from the calculation of the root mean square fluctuations (RMSFs) of the residues, which gives an indication of the per-residue flexibility during the simulation (Figure 35 B). Four lines are present for each construct, corresponding to the four peptide chains. Looking at the RMSF curves, the four green curves (74TD-L344C) almost overlapped with the black ones (37TD-WT), meaning that, although the mutant adopted a different helical conformation, this helix was stable. On the other hand, 74TD-L330C in general fluctuated more and with a less defined pattern as observed by the red curves. This suggests a less stable conformation for this mutant. In general, the extreme parts of the peptides fluctuated more than the central region, as expected, since the terminal parts of the sequence are more flexible and more exposed to the solvent (flanking region). The central region fluctuated less, being better folded and less solvent exposed. Also, we noted a significantly reduced mobility in the hydrophobic residues constituting the α-helix and the β-strand (*i.e.* L330, I332, F338, M340, F341, L344, A347, L348, L350).

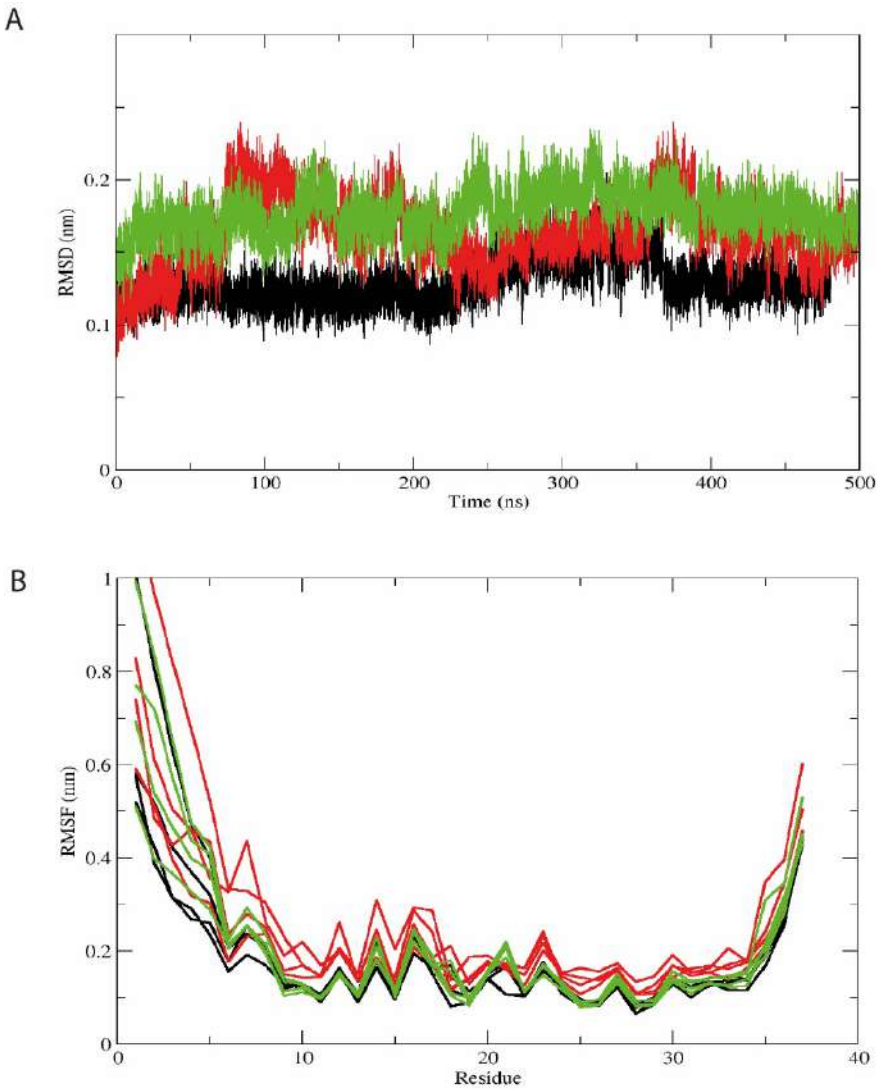

Figure 35. Molecular dynamics analysis of the backbone RMSD of the helical residues to initial structure (A) and RMSFs (B). In black the analysis of the WT, in red of L330C and in green of L344C.

Finally, we clustered by RMSD all the frames explored along the simulations in order to find out which population of conformations was more abundant. Figure 36 shows the structures of the most populated clusters for each system. By comparing the main clusters for each system, we can observe that the mutant 74TD-L330C (main cluster representing 40% of all frames) had a shorter β-strand and the presence of the disulphide bridge caused the α-helix to recede (Figure 36 A and B). This mutant

had a tendency to be more disordered compared to the other domains. On the other hand, 74TD-L344C (main cluster accounting for 54% of all frames) adopted a structure much more similar to the 37TD-WT (main cluster accounting for 80% of all frames), and the presence of the disulphide bridge on the α-helix did not cause any helical distortions and locked the tetramer interface (Figure 36 A and C).

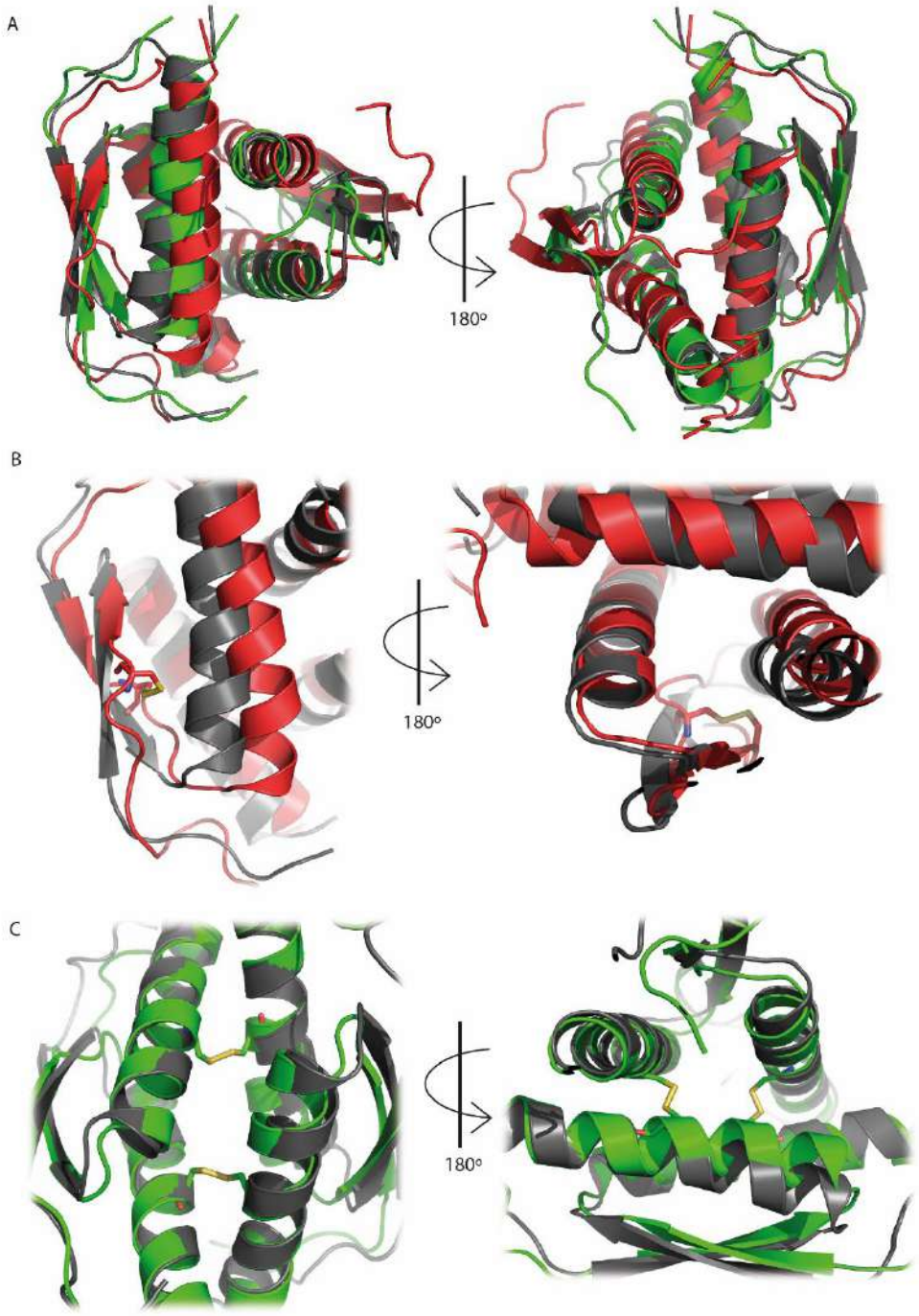

Figure 36. (A) Cluster 1 structures of the WT (black), L330C (red) and L344C (green). (B) Cluster 1 structures of L330C (red) compared to the WT (black), and (C) L344C (green) compared to the WT (black).

In summary, we applied different techniques to prove if the design of these mutants was done correctly, so if the presence of disulphide bridges either in the α-helix or in the β-strand was compatible with the structure of these domains and to study the oligomerisation of 74TDs mutants. Concerning 74TD-L330C, we can conclude that the majority of the results suggested it is mainly dimeric but it is able to tetramerise. Most probably, the structure that the peptide adopts is different from the native folding of the WT. The MD simulation results suggested that the presence of the disulphide bridge in the β-strand affected this moiety making it shorter and it has an impact as well on the α-helix, causing it to recede. These structural changes may destabilise the domain, having a lower thermal stability and resulting in a more fluctuating domain in the MD simulation, although the difference with the other peptides was not big. Concerning 74TD-L344C, overall, from both the experimental and theoretical results, it has a more similar structure to the native folding of the WT compared to the other mutant. This means that the disulphide bridge on the α-helix does not disrupt it and apparently, it has no effect on the β-strand. This peptide is tetrameric in the gas phase and it is stable to the increasing voltage in the native MS experiments. Nevertheless, the NMR results, in particular X-STE NMR experiments, suggested that it is dimeric in solution and any K_d was found by MST, consistent with the fact that the peptide does not oligomerise in solution.

DESIGN OF LIGANDS AND STUDY OF THE INTERACTION BETWEEN THESE LIGANDS AND P53TD

In this chapter, we want to design peptides as ligands able to interact with p53TD with the aim to rescue the stability of mutated tetramers. Several studies about small molecules inhibiting protein-protein interactions (PPIs) are reported, whereas the opposite approach of stabilising a PPI is still underexplored.[114] From the best of our knowledge, only few examples of small molecules able to interact and stabilise p53TD are reported in the literature. Among them, Gordo *et al.*[80] reported the study of a calix[4]arene molecule, designed to fit in the hydrophobic pocket of p53TD, able to bind the protein domain and to stabilise the mutated form of R337H. Based on these promising results, Kamada *et al*.[81] developed another ligand, a calix[6]arene molecule that has 6 arene groups forming the 'crown' of the molecule, able as well to bind and stabilise the mutant R337H. Some years before these studies, Martinell *et al.*[115] reported a library of linear peptides that interacted with p53TD. In this case, they did not study any mutations in the TD, thus the aim of stabilising the mutated protein domain was beyond their objectives. Based on these few examples of molecules that binds p53TD, we designed peptides as potential ligands for p53TD, the WT and R337H mutant. A first generation of ligands originated from the study of Gordo *et al.*[80]; we designed peptides that maintained some structural characteristics of calix[4]arene important for the binding with p53TD. A second generation of ligands derived from the peptide library described by Martinell *et al.*[115] Some peptides were selected and modified to favour their binding to Glu residues on the top of the hydrophobic pocket of p53TD where we believe the ligands bind and stabilise the mutated tetramer. We run molecular docking and molecular dynamics using Schrodinger (Maestro software) to select the best candidates. Afterwards, the selected peptides from both generations were synthesised and their ability to bind p53TD and to stabilise its mutated forms was determined by a variety of biophysical techniques, such as thermal stability circular dichroism, NMR, fluorescence, native MS, and thermophoresis. Finally, after these studies, two ligands were selected as binder of p53TD and potential stabiliser of the mutated tetramer. These peptides were further characterised in terms of conformational structure by NMR and some biological properties, such as their stability in human serum and their cytotoxicity, were determined.

Design of the ligands: 1st generation

The design of the 1st generation of ligands was based on the study of Gordo *et al.*[80] They studied the binding of the calix[4]arene (**8**, Figure 37 A) with the p53TD. Calix[4]arene is composed by a 'calix' of four aromatic rings with ethylene glycol rings in the lower rim and four guanidinium groups in the upper rim. The ligand was designed to fit the hydrophobic pocket of p53TD with its hydrophobic part, consisting in the lower rim, and to interact with glutamate residues of the protein domain with the guanidinium groups in the upper rim (Figure 37 B). Experimental data of HSQC NMR revealed that the designed orientation of the ligand in the protein pocket was favourable and the data were consistent with the *in silico* design. Moreover, the thermal stability was determined by CD unfolding curves, founding that the stability of p53R337H was increased of roughly 10 degrees upon addition of 20 µM of ligand **8**.

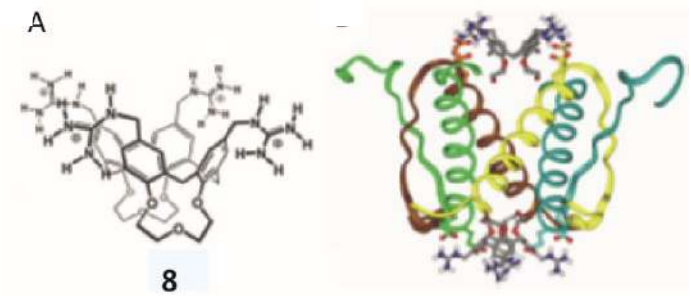

Figure 37. (A) Structure of calix[4]arene (compound **8**). (B) Cartoon representation of the tetramerisation domain interacting with two molecules of compound **8**. Image adapted from Gordo *et al.*[80]

Based on these relevant results, we designed cyclic peptides that maintained the same size of the calix[4]arene ring, *i.e.* 16 atoms, and the four positively charged guanidinium groups. The peptides obtained in this way were cyclo-tetra-β-arginine, consisting in head-to-tail cyclic peptides composed by four β-arginine residues, where the backbone is one methylene group longer than the arginine residue. The side chain of the β-arginine residue can be thus linked to the Cα (β-2) or Cβ (β-3) of the backbone, and for each position, both enantiomers were studied *in silico*, resulting in 4 cyclic peptides, shown in Figure 38. They were evaluated first by docking to determine which isomer was more prone to bind to p53TD.

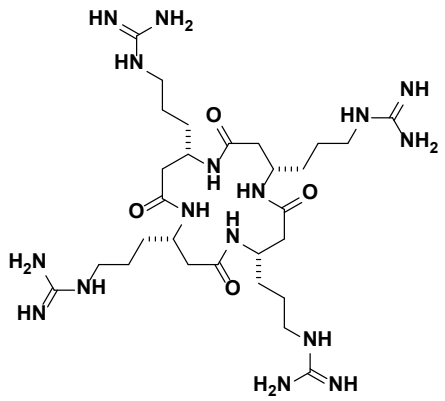

Cyclo-tetra-β-3-arginine *S*

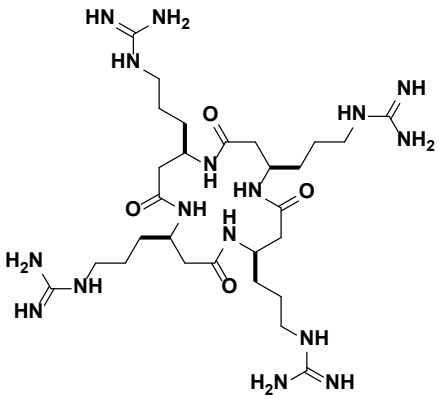

Cyclo-tetra-β-3-arginine *R*

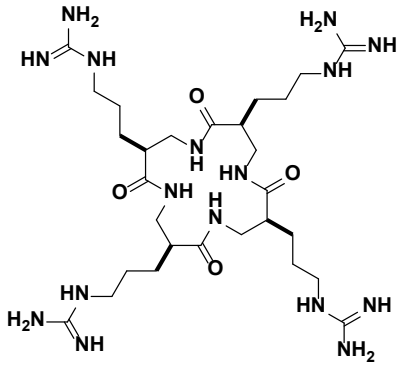

Cyclo-tetra-β-2-arginine *S*

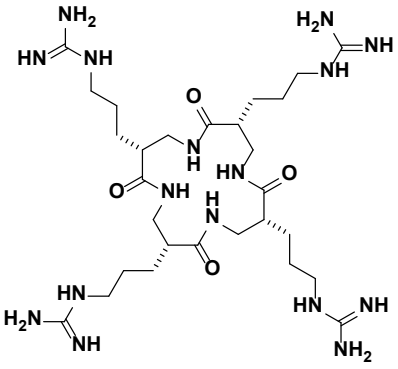

Cyclo-tetra-β-2-arginine *R*

Figure 38. Structures of the four isomers of cyclo-tetra-β-arginine.

In the docking analysis these compounds are named β-2*S*, β-2*R*, β-3*S*, and β-3*R*, referring to the position of the side chain and to the stereochemistry of the residues. We ran molecular docking simulations using Maestro Schrödinger, release 2017,[116] to get information on the orientation and position of the ligand in the protein pocket. The starting structure of the tetramerisation domain used for the docking derived from its NMR structure (PDB ID 1OLG[28]). Concerning the ligands, the structures were built using Maestro and they were adjusted to the docking analysis using 'LigPrep' function that aims to generate their 3D structures. Several conformations of the ligands were generated by the 'CSearch' function, which produces diverse, low-energy, 3D structures of compounds. These conformations were then inserted in the binding pocket of the protein domain (Grid) (Figure 30 A) and docking analysis were performed with Glide.[117] Glide docking considers the receptor as a rigid molecule, whereas several conformations of the ligand are

explored inside the protein pocket to find the poses that best fit and bind the protein domain. The properties of the receptor are represented on a grid by different sets of fields that progressively give more accurate scorings of the ligand pose. New conformations of the ligand are generated by torsions and they are examined during the docking process. After an initial screening, the selected ligand poses are refined in torsional space in the field of the receptor using OPLS3.[118] Finally, a few ligand poses are minimised in the receptor field with full ligand flexibility in a process named post-docking minimisation.[119] The final ligand poses consisting of the output of the docking process are scored by a Glide-Score function. The docking score takes into account several energy contributions of the system, deriving from different type of interactions, such as lipophilic-lipophilic interactions, H-bonds between neutral groups, H-bonds between neutral and charged groups and between charged groups, hydrophilic interactions and Van Der Waals interactions, among others.[120,121] We applied two forms of Glide-Score, the Standard Precision (SP) Glide and the Extra-Precision (XP) Glide. The first one is a function that seeks to identify ligands that reasonably could bind the target protein and it aims to minimise false negative results. The second one, on the contrary, strongly penalises poses that do not take into account physical chemical properties, such as charged parts of the molecule to be solvent exposed. This function aims to minimise false positive results.[120] The results concerning the first generation are reported in Table 7.

Compound	SP Glide	XP Glide
Calix[4]arene (**8**)	-9.809	-7.341
β-2*S*	-8.4	-7.112
β-2*R*	-8.765	-7.485
β-3*S*	-8.725	-7.674
β-3*R*	-8.438	-6.521

Table 7. Docking scores of the first poses of calix[4]arene (**8**), used as reference, and ligands of the first generation, using SP and XP Glide (Maestro).

It is accurate and appropriate comparing the docking scores of different poses of the same ligand because, being the same molecule all the structures have the same number of atoms, chemical bonds, torsional space, etc. Although comparing docking scores of different ligands is not very accurate, we used the calix[4]arene anyway as indicative value for the scores of the 1st generation ligands. Considering the four cyclic peptides, although they are different molecules they are chemically similar. From our results, the compounds β-2*R* and β-3*S* gave the best docking scores considering both the SP and XP Glide functions. Concerning the XP Glide, which is more reliable and more prone to avoid false positive poses, the compound β-3*S* gave the best result (Figure 39 B), comparable in value to the reference molecule of calix[4]arene.

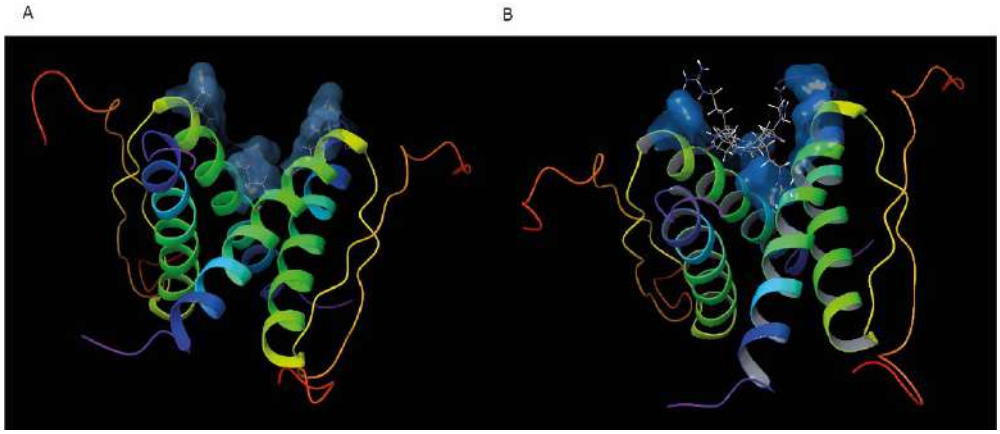

Figure 39. (A) Binding pocket of p53TD showing in blue the surface of Glu residues. (B) First pose of β-3*S* in the binding pocket, obtained with XP Glide function.

In order to study the nature of the interactions between the ligand and the protein domain more in depth, we ran molecular dynamics (MD) simulations using Desmond Schrödinger, release 2017.[122] Four independent systems were studied, one for each isomer of the ligand. The starting structures of the complexes used for the MD consisted of the first poses of the docking simulation outputs. We ran explicit MD simulations to assess the preferred orientation of the ligand in the binding pocket and to study more in depth the type of interactions stabilising the complexes. The starting structures were solvated with predefined water molecule TIP3P box and positive charges were neutralised by adding chlorine ions. The MD simulations in Schrodinger were run using Desmond program and they consist of few main steps, *i.e.* minimisation of the system, simulation and output analysis. The complexes were minimised using the steepest descent method, and then they were subjected to a step of equilibration in the NPT ensemble. From there unrestrained MD trajectories were collected for 10 ns.[123] The trajectories of each system were analysed by plotting several key parameters, such as the backbone root-mean-square deviations (protein RMSD), protein-ligand RMSD, and protein-ligand contacts.

In Figure 40 are shown the protein and the ligand RMSDs concerning the studies of β-3*S* and β-2*R*, whereas the same analysis of the others isomers is shown in the 'Supplementary MD' section at the end of this thesis (Figure S63). To determine the protein RMSD, the conformation of each frame was aligned to the starting structure of the protein and the RMSD was calculated considering the α-carbon of the backbone (left Y-axis). Therefore, larger is the RMSD, further the protein has moved from the starting conformation. In the first nanoseconds of the simulation, the protein of all the complexes fluctuated more, as expected for unrestrained MD. Then they reached a plateau meaning that the system has reached a stable

conformation and fluctuated less. The values of protein RMSDs were around 3 – 6 Å which are inside of an acceptable range for globular proteins. The ligand RMSD (right Y-axis) is a value that indicate how stable the ligand is in the protein pocket. This value was obtained for each frame aligning the protein backbone to the reference position and the RMSD was calculated considering the heavy atoms of the ligand. The values of the ligand RMSDs in our complexes were comparable to the protein RMSDs, meaning that the ligand has not diffused away from the original position.

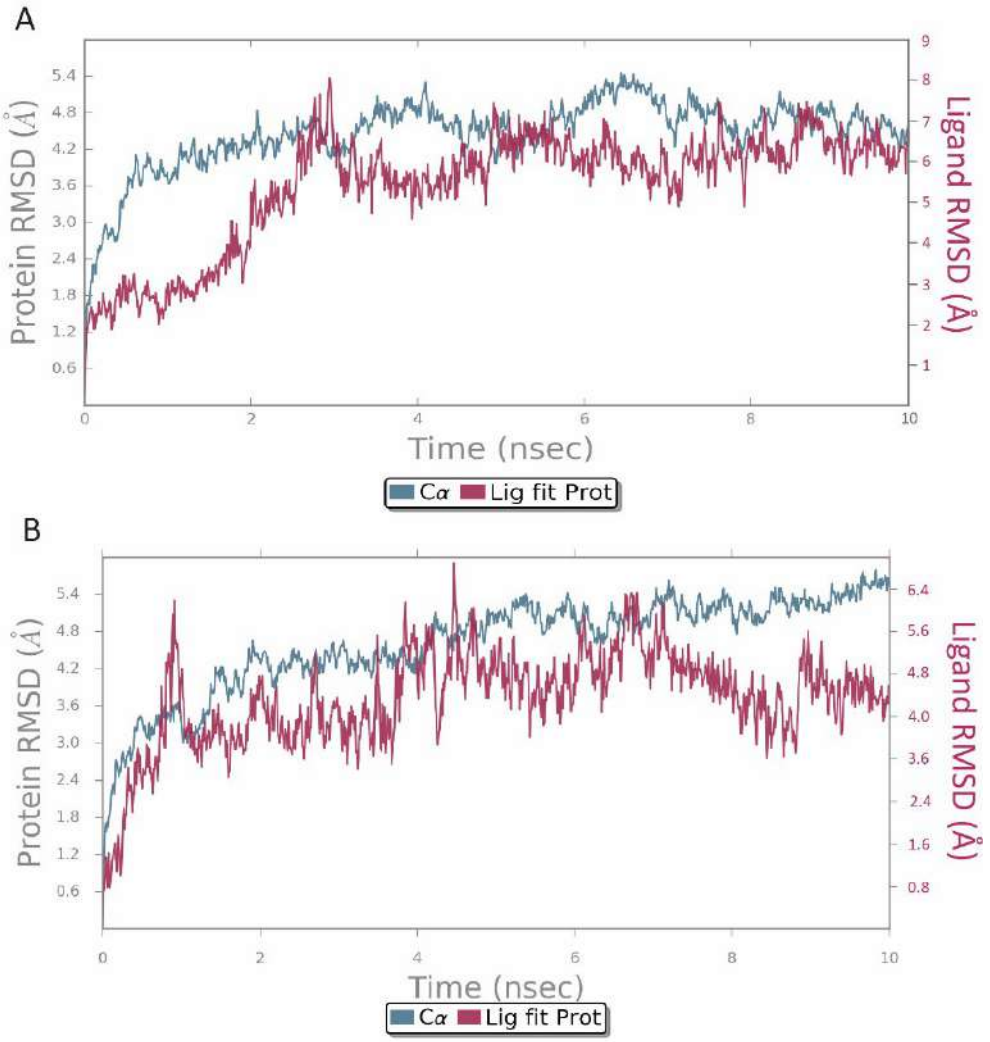

Figure 40. Molecular dynamics analysis of backbone RMSD to initial structure (blue line) and of ligand RMSD to initial pose (purple line). Analysis of the complexes p53WT @ β-3*S* (A) and p53WT @ β-2*R* (B) trajectories.

The protein-ligand contacts for the β-3*S* and β-2*R* isomers along the simulations are shown in Figure 41. The same analysis of the other isomers is reported in the 'Supplementary MD' section at the end of the thesis (Figure S64). As expected, the majority of the interactions involved hydrogen bonds, water bridges or ionic interactions. All the H-bonds counted in this panel referred to H-bonds where the distance between the donor and the acceptor is equal or inferior to 2.5 Å. In the water bridges interactions are considered all the H-bonds between the ligand and the protein mediated by a water molecule. In this type of interaction the geometry between the donor and the acceptor is more relaxed compared to the H-bonds type. The ionic interactions consider all the opposite charges interactions where any H-bond is involved. As the results suggested, our complexes were stabilised mainly by electrostatic or polar interactions which involved polar residues of the protein chains, in particular glutamate, arginine and aspartate residues.

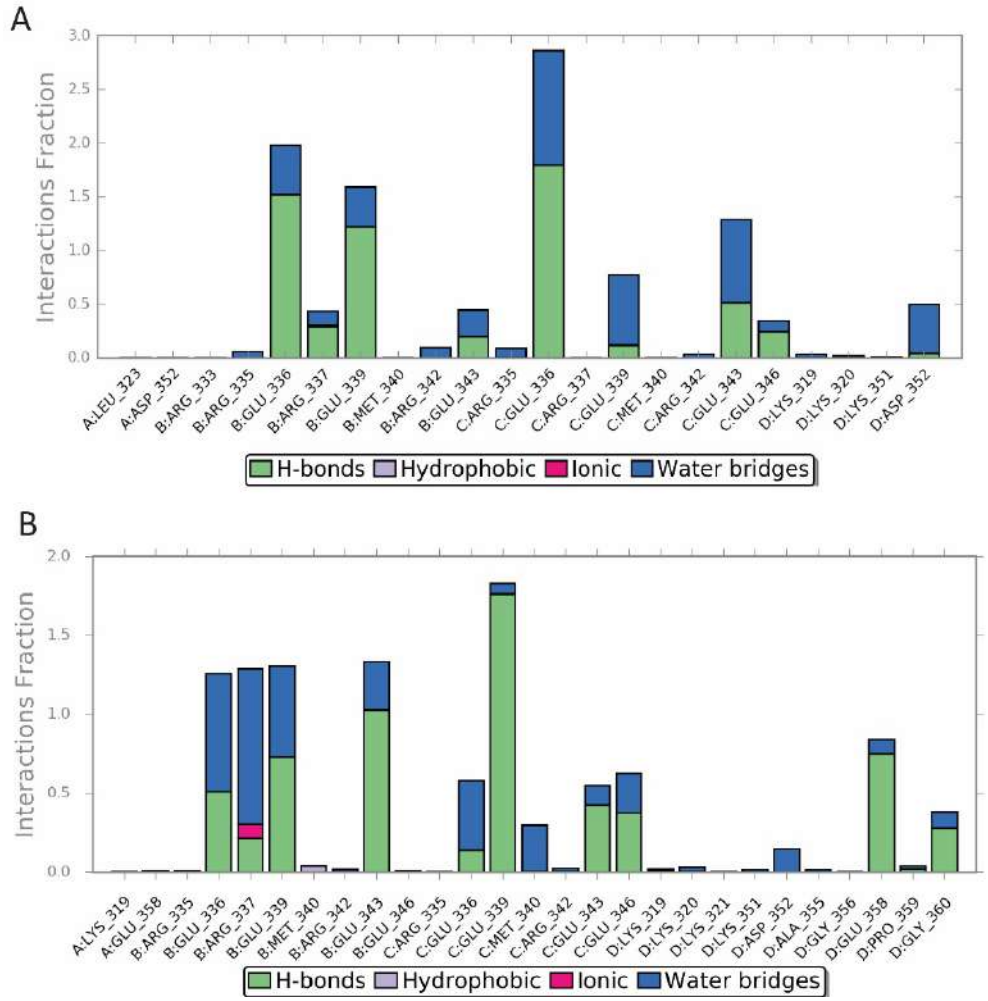

Figure 41. Molecular dynamics analysis of protein-ligand contacts. Analysis of the complexes p53WT @ β-3*S* (A), and p53WT @ β-2*R* (B) trajectories.

After having performed the *in silico* simulations, we selected the isomer β-3*S* as best candidate. It gave the best docking score using XP Glide-Score and from the MD analysis its complex with p53WT looked stable. We decided thus to synthesise this ligand and to study its interaction with our p53TD. Moreover, the residue with the side chain on the β-carbon and with the S stereochemistry was the only one commercially available among the β-arginine residues studied in this project. Therefore, the cyclic peptide β-3*S* was manually synthesised using 2-chlorotrityl resin, oxyma and DIC as coupling reagents. The linear peptide was cleft from the resin, purified and cyclised in solution using PyBOP, HOAt and DIPEA in 1% DMF in DCM. Finally, the guanidiunium groups of the β-arginine residues were deprotected to give the desired product. The detail of the synthesis and the characterisation of the compound are reported in the 'Product characterisation' section at the end of this thesis (Figure S8). We decided to synthesise also calix[4]arene (compound **8**) to have a positive control in our binding experiments. In order to achieve this compound, we performed the synthetic pathway shown in Scheme 1 in the 'Material and methods' section, as previously described by Martos[124] and Gordo *et al*.[80] The characterisation of the desired compound, as well as the intermediates, is reported in the 'Product characterisation' section (Figure S10-S16).

Thermal stability circular dichroism

We performed thermal stability circular dichroism experiments to investigate into the thermal stability of the p53TD WT and R337H mutant, and to gather more details into how they unfold with the increasing of the temperature and how the addition of the ligand changes these curves. In this experiment, a beam of circular polarised light at a constant wavelength of 220 nm passed through the sample and a ramp of temperature was applied to unfold the peptide. From the denaturation curve obtained, the temperature of melting (T_m) was calculated and it corresponds to the temperature at which 50% of the peptide is unfolded. By adding the ligand to the solution, if it is able to bind the tetramerisation domain of p53 and to stabilise it, a shift of the T_m towards higher temperatures is expected. The results concerning 37TD-WT and 37TD-R337H, both peptides used in their unlabelled version, are shown in Figure 42 (panel A). Afterwards, the cyclo-tetra-β-3-arginine *S* ligand was added to study its binding to p53TD and to see how the stability of the TD changes (panel B and C). We found a big difference in stability between the TDs, as expected, with a T_m value of 76 °C in the case of the WT and 48 °C in the case of the mutant (Figure 33 A). Two equivalents of ligand were added to the TDs solutions, reaching

a concentration of 40 µM of ligand. Basically, any difference in the T_m was observed in the case of the WT (Figure 42 B), whereas a shift of roughly 3 °C was detected with R337H mutant (Figure 42 C). Nevertheless, this shift is accompanied by a change in the shape of the melting curve and this fact makes the interpretation of the result more difficult.

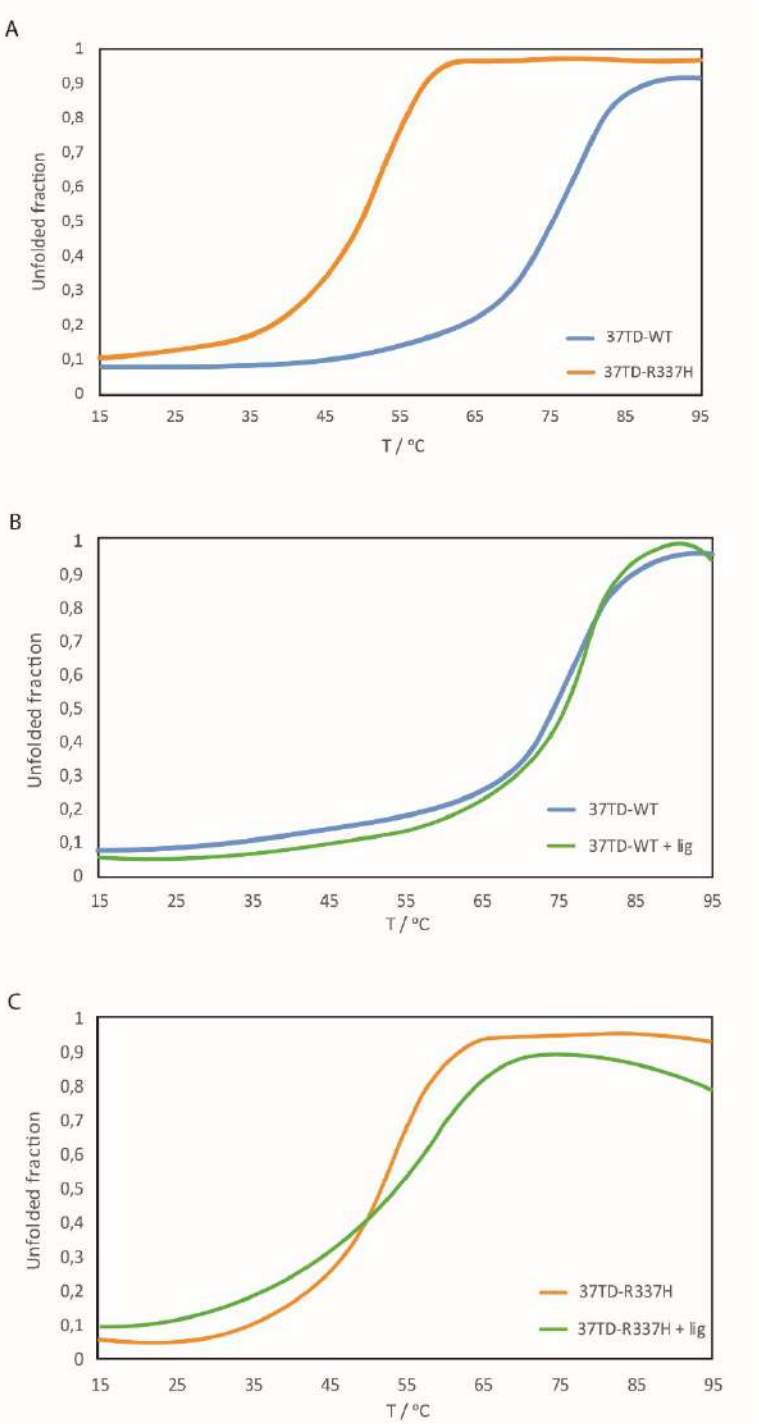

Figure 42. Unfolded curves of thermal denaturation of 37TD-WT and 37TD-R337H at a monomer concentration of 20 µM (A). Two equivalents of ligand (cyclo-tetra-β-3-arginine *S*) were added to 37TD-WT (B) and to 37TD-R337H (C) solutions.

Study of the binding by NMR

After these promising results on complex formation and stabilisation of the mutant tetramer, we performed NMR binding experiments to further investigate on the nature of the interaction between cyclo-tetra-β-3-arginine *S* and p53 TDs (37TD-WT and 37TD-R337H). We acquired thus ^{1}H ^{13}C HSQC spectra of the TDs, at a monomer concentration of 20 µM, 25 °C and pH 7, and we titrated the protein domain with an increasing amount of the ligand. In the case of the WT, only one peak was present in the spectra corresponding to the tetramer (^{1}H 1.50 ppm, ^{13}C 13.54 ppm) (Figure 43 A and B). When the ligand was added (2 and 4 eq) the spectrum did not change significantly, meaning that most probably the two species were not interacting, or the complex formed after the binding of the ligand was not stable enough (Figure 43 A and B). In the case of the mutant, after the addition of 4 equivalents of ligand, the peak corresponding to the tetramer (^{1}H 1.64 ppm, ^{13}C 13.68 ppm) changed significantly its intensity and shape (Figure 43 C and D). In particular starting from a sharped signal of the tetramer, in the presence of 4 eq of ligand, the signal became broad, indicating that the size and the solvent exposed area of the species changed. This is, normally, an indication of binding between the two species. Moreover, the peak slightly shifted upfield in the ^{1}H and ^{13}C axes, again a sign that interaction was taking place. On the other hand, the monomer peak (^{1}H 2.02 ppm, ^{13}C 14.20 ppm) did not change significantly by adding the ligand, suggesting that most probably the ligand was interacting with the tetramer.

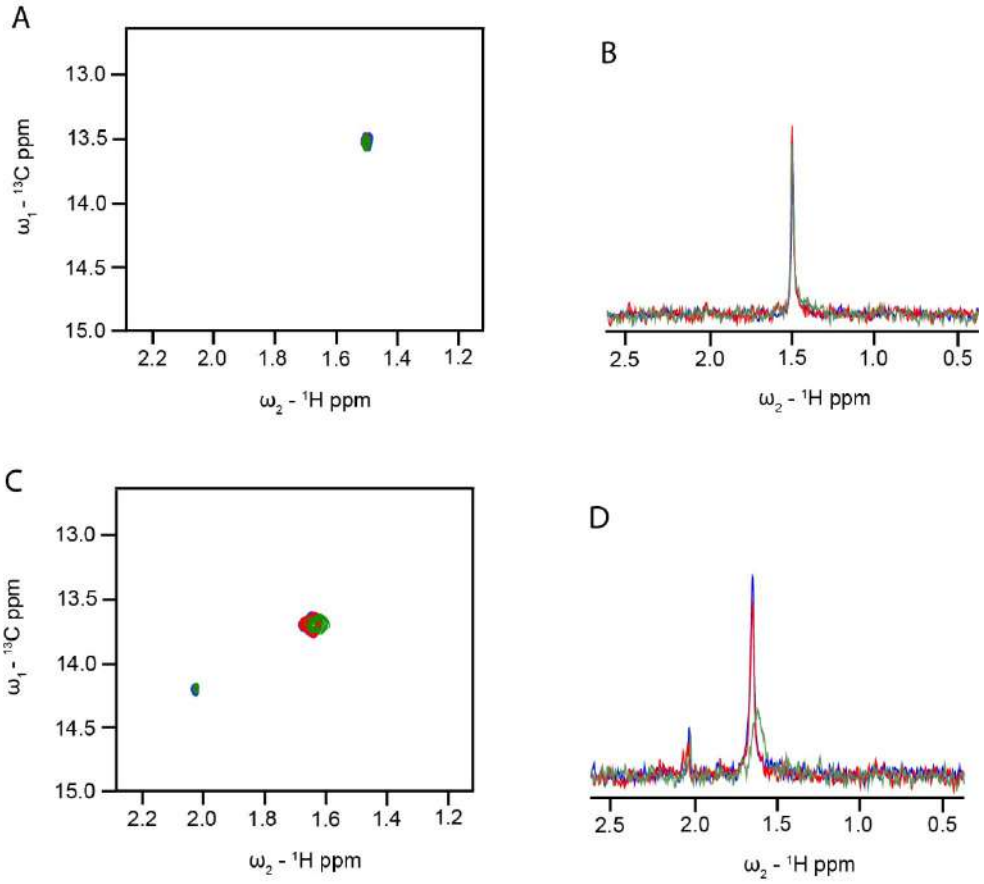

Figure 43. 2D $^{1}H,^{13}C$ HSQC spectra at 25 °C of 37TD-WT (A, blue) and 37TD-R337H (C, blue) which were titrated with 2 eq (red) and 4 eq (green) of cyclo-tetra-β-3-arginine *S*. ^{1}H projections of $^{1}H,^{13}C$ HSQC spectra are represented in (B) for 37TD-WT and in (D) for 37TD-R337H.

Design of the ligands: 2nd generation

The design of the second generation was based on the study of Martinell *et al.*[115] They designed and studied a family of linear peptides able to bind p53 tetramerisation domain. These peptides were designed by molecular mechanics and molecular dynamics simulations based on a polyguanidinium molecule (ligand 1, Figure 44 B) able to interact with p53 TD by polar interactions between positive charges on the guanidinium groups with the negative charges on the glutamate residues of the protein domain (Figure 44 A). From ligand 1, by molecular mechanics and molecular dynamics, they designed a linear peptide (CAN4, Figure 44 C) which contained four arginine residues at a distance that mimicked the distances between

the guanidinium groups in ligand 1. Moreover, CAN4 contained a tryptophan residue to study its interaction with p53TD by fluorescence and alanine residues in the *N*-terminus to act as spacer in order to immobilise the peptide on the surface of a SPR sensor chip.

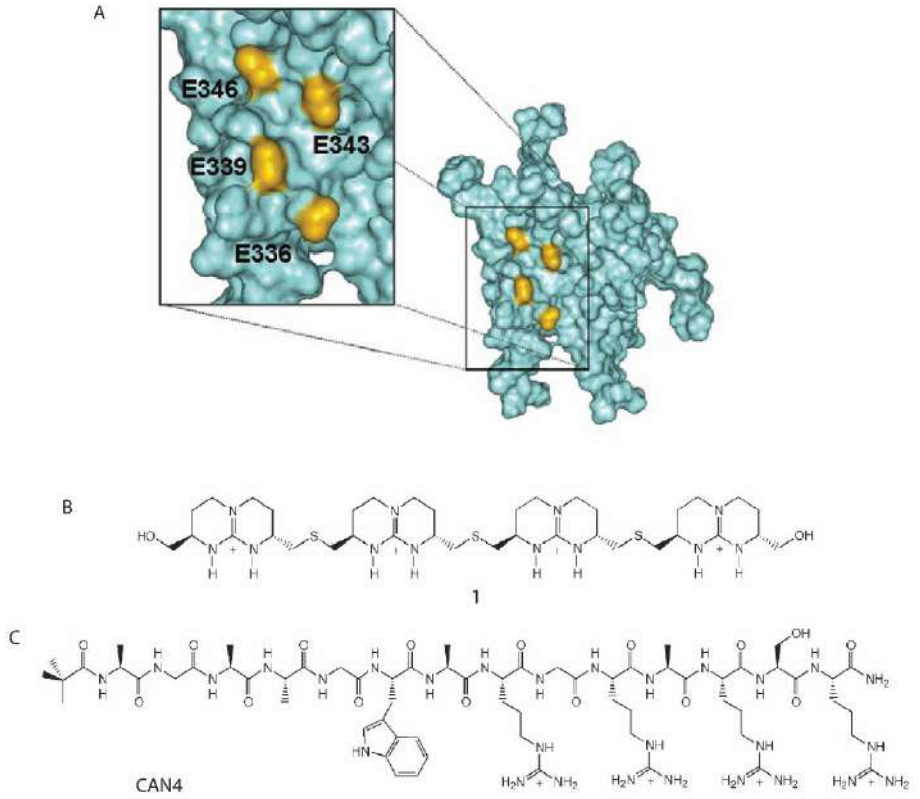

Figure 44. (A) Cartoon representation of p53TD showing the glutamate residues, only in one monomer, involved in the interaction with ligand 1. (B) Polyguanidinium molecule (ligand 1) able to interact with p53TD. (C) Linear peptide (CAN4). Image adapted from Martinell *et al.*[115]

From CAN4, they obtained a library of linear peptides and they studied the interaction of this library with p53TD (Figure 45). The library was composed by the retro version of CAN4 (named RRRR or R4) and other linear peptides obtained by substituting the arginine residues with different residues, modifying the side chains of the arginine residues, as well as increasing or decreasing the distance between the arginine residues (Figure 45). They studied the binding with the protein domain by fluorescence spectroscopy and they found that all these peptides were able to bind p53TD (Figure 45). From this library, we selected three linear peptides, *i.e.* RRRR (or R4), K3R and Rab4 to be synthesised and studied by different biophysical techniques, such as NMR, native MS, and thermophoresis. We chose Rab4 because it gave the best result in terms of K_D by fluorescence. Moreover, we selected RRRR

because it was the parent peptide in this study and K3R because it gave the best result among the peptides composed only by natural amino acids.

Peptide	K_D [μM]	χ^2	Peptide	K_D [μM]	χ^2
RRRR	6.3±1.5	0.13	2xaa	15±6.0	1.91
KR3	24±15	0.38	0xaa	34±12	1.59
K2R2	6.3±2.6	1.28	random	40±9.0	0.18
K3R	5.1±2.1	0.92	TmgR3	9.9±1.3	0.15
KKKK	12±5.0	0.88	Tmg2R2	2.4±0.7	0.29
RKRR	6.6±3.0	1.51	Tmg4	2.7±0.6	0.08
KRKR	12±3.2	0.29	RabR3	11±3.5	1.69
KRRK	84±54	0.47	Rab2R2	18±8.0	0.91
KKRK	6.9±3.4	1.68	Rab4	0.84±0.22	0.17
NvaR3	17±7.1	1.39	RysR3	6.8±2.3	1.43
SR3	42±22	2.92	Rys2R2	2.1±0.4	0.15
S2R2	56±23	2.92	Rys4	9.6±3.5	0.17
S3R	520±330	0.14			

Figure 45. K_D values obtained by fluorescence titration of p53TD. Image adapted from Martinell *et al.*[115]

We selected then six peptides, R4, Rab4, Rys4, Tmg4, Tmg2R2, and Rys2R2, the parent peptide and the ligands that gave the strongest binding with p53TD in terms of K_D by fluorescence, to be modified and studied by molecular docking and molecular dynamics. In this study, we designed cyclic peptides composed by the *N*-terminal part of the original linear peptides, which contains positively charged guanidinium groups that are supposed to interact with p53TD (Figure 46). We cyclised the peptides head-to-tail including 7 or 8 residues and we ran molecular docking and molecular dynamics simulations to select the best candidates to be then synthesised and experimentally studied.

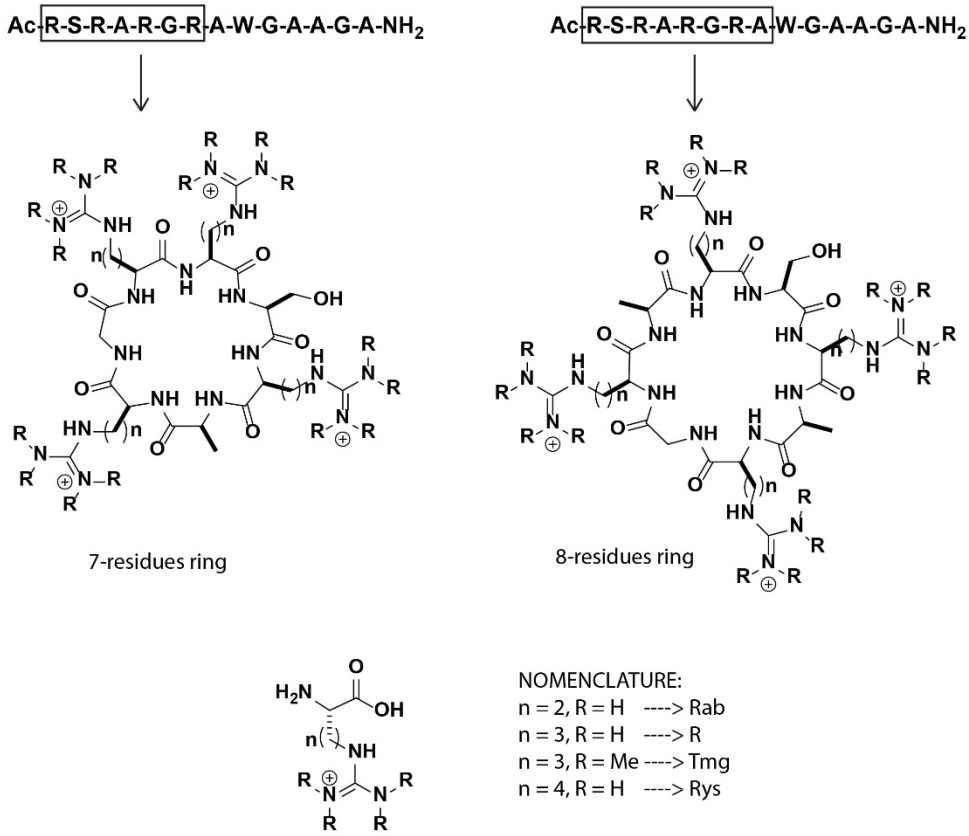

Figure 46. Structures of the cyclic peptides belonging to the 2nd generation of ligands.

The cyclic ligands of the second generation are named, as the linear ones, considering the four residues positively charged preceded by a 'c' (cyclic). For the 8-residue ring peptides that include also the alanine residue the letter 'A' (alanine) is added at the end of the name (Table 8). We run molecular docking, inserting the cyclic peptides in the binding pocket of the tetramerisation domain, as already described for the computational study of the first generation of ligands. Only the XP Glide Score was used in this study of the 2nd generation of ligands and the results are reported in Table 8.

Compound	XP Glide	Compound	XP Glide
Calix[4]arene (**8**)	-7.341	cRys2R2A	-7.646
β-3*S*	-7.674	cRys4	-7.301
cR4	-7.849	cRys4A	-7.765
cR4A	-6.992	cTmg2R2	-7.205
cRab4	-8.078	cTmg2R2A	-6.307
cRab4A	-7.079	cTmg4	-6.02
cRys2R2	-7.719	cTmg4A	-6.449

Table 8. Docking scores of calix[4]arene (**8**) and β-3*S*, used as reference, and cyclic ligands of the second generation, using XP Glide (Maestro).

From our results, four cyclic peptides, *i.e.* cR4, cRab4, cRys2R2, and cRys4A, looked promising giving a better docking score than the two molecules of reference (**8** and β-3*S*). In general, the 7-residues peptides gave better results than their 8-residues analogues. As for the first generation peptides, we ran molecular dynamics simulations using Maestro. The analysis of the dynamics are reported at the end of this thesis (Supplementary MD, Figure S65-S76). Overall, the simulations were promising, as any ligand showed a large RMSD but they fitted nicely in the protein pocket. The main stabilising interactions of the complexes were polar interactions or water bridges involving the glutamate residues of the p53TD. Some ligands, such as cR4 or cRys2R2, showed ionic interactions with R337 of p53TD and hydrophobic ones with M340; the ligand cRab4 showed a smaller RMSD than the other peptides.

From the design of the second generation peptides and the *in silico* simulations, we selected and synthesised three linear peptides (R4, K3R, and Rab4) and four cyclic peptides (cR4, cRab4, cRys2R2, and cRys4A) (Figure 47). The linear peptides were synthesised using ChemMatrix resin, as described for 37TDs. The cyclic peptides were synthesised on 2-chlorotrytil resin, as described for the cyclic peptide of the first generation of ligands. After the cleavage from the resin and the purification of the linear peptides, they were cyclised in solution using MW to speed up the reaction. The details of the synthesis and the characterisation of the final products are reported at the end of the thesis in the 'Product characterisation' section (Figure S8-S9).

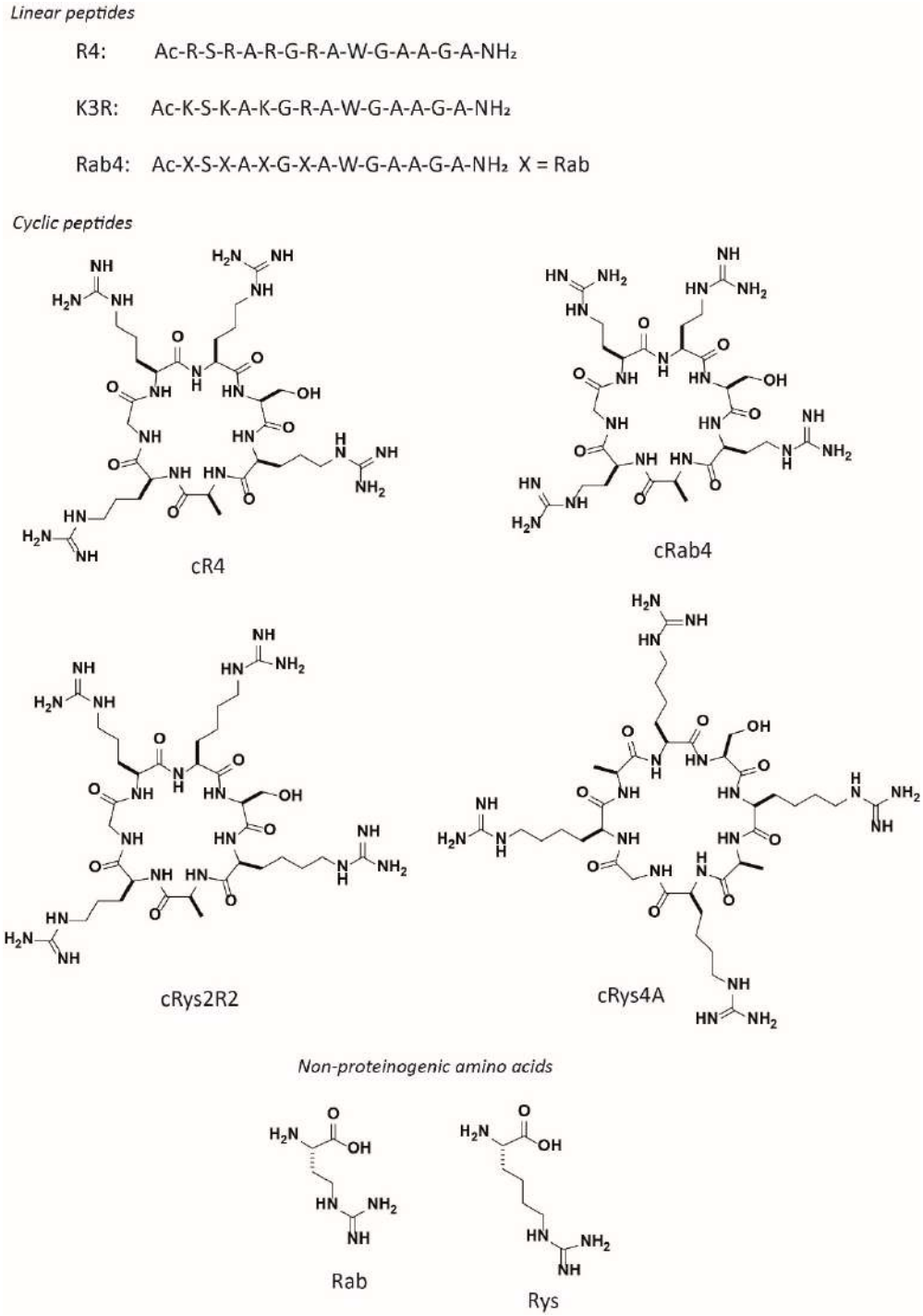

Figure 47. Linear and cyclic peptides belonging to the 2nd generation of ligands.

Taking advantage of the fact that the linear peptides of the second generation contained a tryptophan residue, we studied the binding of these peptides with p53TD by fluorescence spectroscopy and NMR chemical-shift-perturbation looking at the ligand signals, in particular at the indole group signals.

Study of the binding by fluorescence spectroscopy

We studied the interaction between the linear peptides with p53TD, the WT and R337H mutant, where both the TD peptides were used in their unlabelled versions. This experiment is based on the fluorescence of the tryptophan residue, present only in the ligand and not in p53TDs. Therefore, during the experiment the concentration of the ligand (R4, K3R, and Rab4) was maintained constant. The tryptophan was excited with a light beam at a wavelength of 295 nm (λ_{ex} tryptophan ≈ 280 nm)[125] and the spectrum was acquired including the highest intensity of the tryptophan emission (350 nm).[125] By titration of the ligand with an increasing amount of p53TD, if the complex is formed, the protein domain should quench the tryptophan fluorescence decreasing its emission band intensity, as shown by Martinell *et al*.[115]

We studied this system starting from the conditions described by Martinell *et al*.[115] consisting in a constant ligand concentration of 3 µM at which the fluorescence band was intense enough to detect changes in case of binding. The ligands then were titrated with an increasing amount of p53TDs, where the equivalents used referred to the monomer. In our experiments, we got different results from what is described by Martinell *et al*.[115] We detected a change in the fluorescence band intensity upon addition of the protein domain, however, these changes were not consistent with the amount of the protein added (Figure 48). In some cases, the intensity of the band decreased, suggesting a quenching from the protein domain, but in other cases, on the contrary, the band intensity increased. There may be several reasons why the fluorescence intensity of the tryptophan changes upon addition of a binding partner. One reason can be the collisional quenching and in this case the effect increases by increasing the temperature. Another reason can be binding phenomena, thus formation of a complex. In this scenario, the quenching can occur in the ground-state or in the excited-state of the molecules. Conformational changes in the local microenvironment of the tryptophan, due to the binding and formation of a complex, can influence the quantum yield of the tryptophan and these structural changes can provoke both an increase or a decrease of the fluorescence. Moreover, quenching due to ground-state complex formation may occur when the ligand binds directly to the fluorophore.[126] Therefore, a local change in the structure of the peptides close to the tryptophan, probably due to the binding with p53TDs,

might explain the changes in the fluorescence observed in our experiments. Nevertheless, in case of binding, a consistent behaviour with the increasing amount of the quencher (p53TDs) is expected. Although we tried different conditions to reproduced the curves described by Martinell *et al*.,[115] we did not find the experimental conditions to detect a change consistent with the p53TD concentrations. We decided thus to study our system by other techniques, such as NMR.

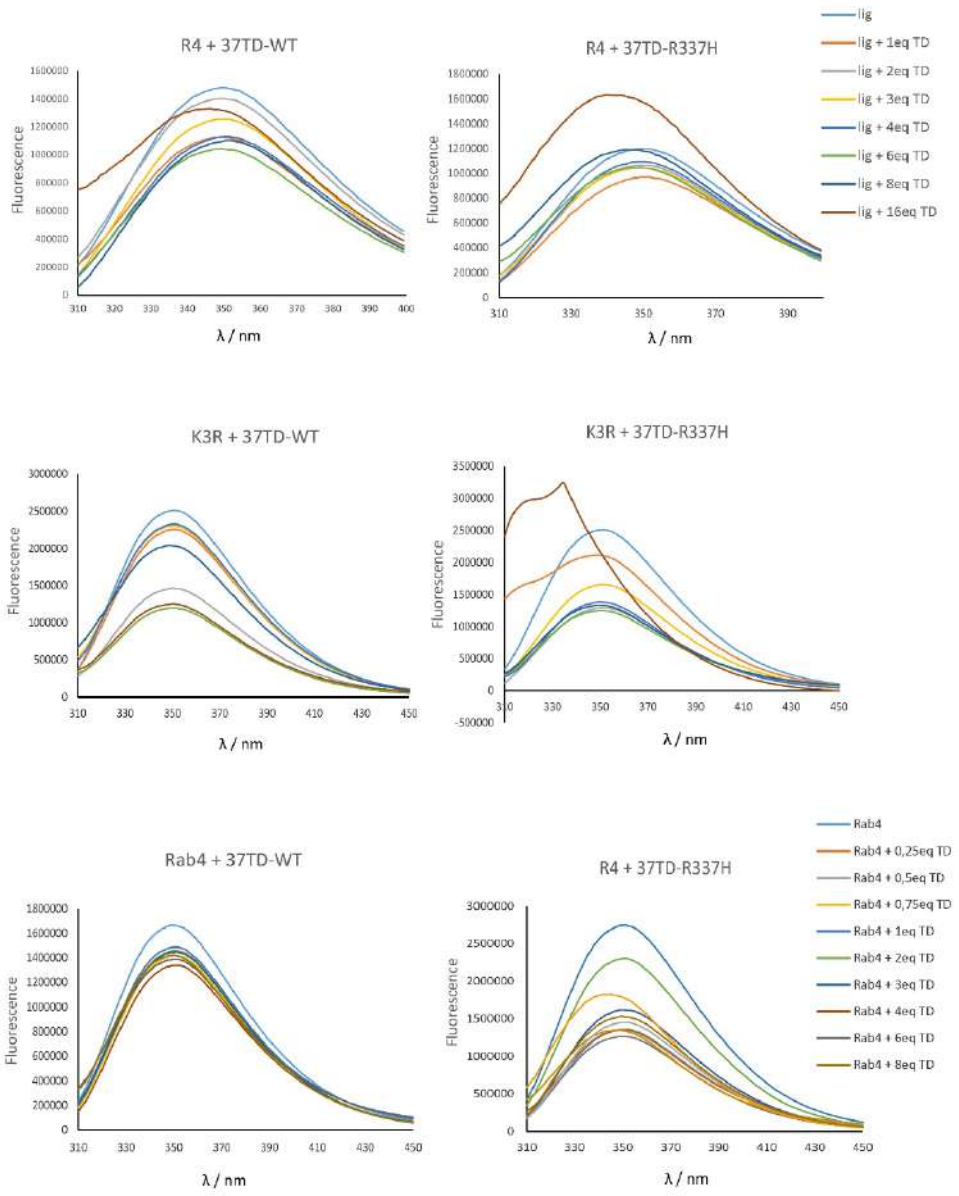

Figure 48. Fluorescence spectroscopy binding experiments between linear ligands (R4, K3R, and Rab4) and 37TD-WT and 37TD-R337H.

Study of the binding by NMR (linear ligands)

We studied the binding between the linear ligands belonging to the second generation and 37TD-R337H by NMR. We performed two types of NMR experiments. The first one consisted in the NMR chemical-shift-perturbation looking at the aromatic signals of the indole group of the tryptophan residue, thus the concentration of the ligand was maintained constant and it was titrated with an increasing amount of p53TD to see how the aromatic signals of the indole group were perturbed by the addition of the protein domain. The second type of NMR experiments consisted in ^{1}H ^{13}C HSQC experiments, as described for cyclo-tetra-β-3-arginine *S,* where, on the contrary, the concentration of 37TD-R337H was maintained constant and it was titrated with an increasing amount of the ligand.

NMR chemical-shift-perturbation

In order to perform these experiments, we chose to monitor the aromatic signals of the indole group because they are in the aromatic region of the spectrum, quite easy to identify as they do not overlap with other signals, so they facilitate a way to detect their perturbation after the addition of the protein domain if binding is occurring. Tryptophan residue is present only in the linear ligands and not in the protein domain, so the signals detected in the ^{1}H NMR belong unequivocally to the ligand. We acquired the spectra using 20 μM of the linear ligands (R4, K3R, and Rab4) and they were titrated with 10, 20, and 40 μM of 37TD-R337H, where these concentrations referred to the monomer. The experiments were performed at 5 and 37 °C, pH 7.5. The results concerning K3R are reported in Figure 49, whereas the spectra of the other ligands are shown in the 'Supplementary NMR' section at the end of this thesis (Figure S48-S49). Looking at the signals of the indole group, they shifted upfield by increasing the amount of 37TD-R337H. At 5 °C the signal of the NH of the indole group was detectable as well (Figure 49 B) and its intensity decreased upon addition of the protein domain. At 37 °C (Figure 49 C) the aromatic signals shifted more than at low temperature (Figure 49 A), as expected. These results suggested interaction between the species in solution and analogous results were observed for the other linear ligands, meaning that all of them were able to interact with 37TD-R337H and maybe they interacted in a similar way as the shift of the peaks was comparable for all the ligands.

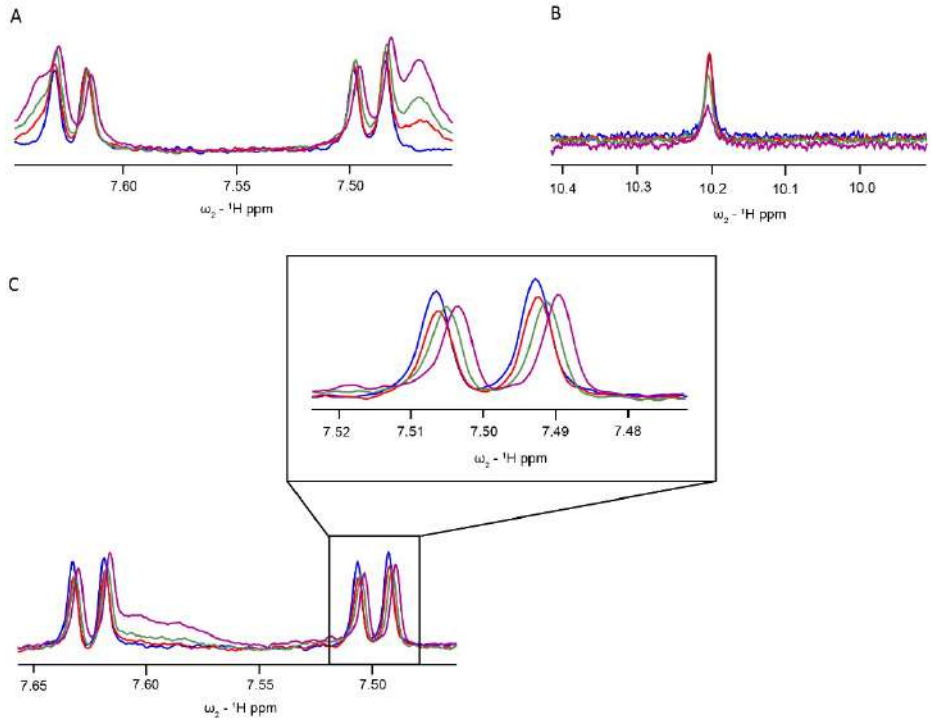

Figure 49. ^{1}H NMR chemical-shift-perturbation experiments of K3R at a concentration of 20 µM (blue) which was titrated with 10 (red), 20 (green), and 40 µM (purple) of 37TD-R337H. The spectra were acquired at 5 °C (A, B) and 37 °C (C), pH 7.5. Only the aromatic region is shown in panel A and C and the indole NH signal is shown in panel B.

^{1}H ^{13}C HSQC binding experiments

To further investigate on the binding between the linear ligands and 37TD-R337H, we performed ^{1}H ^{13}C HSQC binding experiments starting from a monomer concentration of 10 µM of 37TD-R337H, which was then titrated with the linear peptides. The spectra were acquired at 37 °C and pH 7.5 to reproduce physiological conditions and to start from a ratio of 37TD-R337H population of roughly 50% tetramer and 50% monomer in order to be able to detect a change in the p53 species population after the binding with ligand. If the complex is formed and the ligand is able to stabilise the p53 tetramer, we expected to see a reduced monomer population, meaning that part of the monomers oligomerised. From our results, the linear ligands behaved differently from each other and in some cases, although a clear change in the spectrum was observed, the interpretation of these results was not easy and straightforward. In the case of ligand Rab4 for example, the peak corresponding to the tetramer disappeared when 8 eq of ligand were added. One possible explanation could be that the complex was formed and since it was bigger than the tetramer p53, it may have different relaxation time, which could cause its

disappearance in the spectrum. On the contrary, the peak corresponding to the monomer did not significantly change upon addition of the ligand (Figure 50 C). In the case of R4, a third cross-peak (^{1}H 1.36 ppm, ^{13}C 13.28 ppm) appeared at higher field compared to the tetramer signal. Again, this behaviour may be explained by a complex formation and the binding with the ligand changed the chemical environment of the methionine residue resonating at a different chemical shift compared to the tetramer (Figure 50 A). Finally, in the case of K3R, any big change was observed in the spectra. The relative intensities of the two main cross-peak did not vary much suggesting that probably any complex was formed (Figure 50 B). The cross-peaks below the signal of the tetramer (^{1}H 1.67 ppm, ^{13}C 14.32 ppm) belong to the ligand, most probably to the side chain of the lysine residues, and they increased their intensity consistently with the increasing amount of the ligand added. Overall, in any of these studied cases we detected a decreased in the monomer 37TD-R337H signal. Possible scenarios that may explain this behaviour could be that the ligands did not interact with the monomeric protein domain, but with its tetrameric form. Probably they were not able to stabilise the tetramer or the binding was not strong enough to shift the population of 37TD-R337H from its monomeric to its tetrameric form.

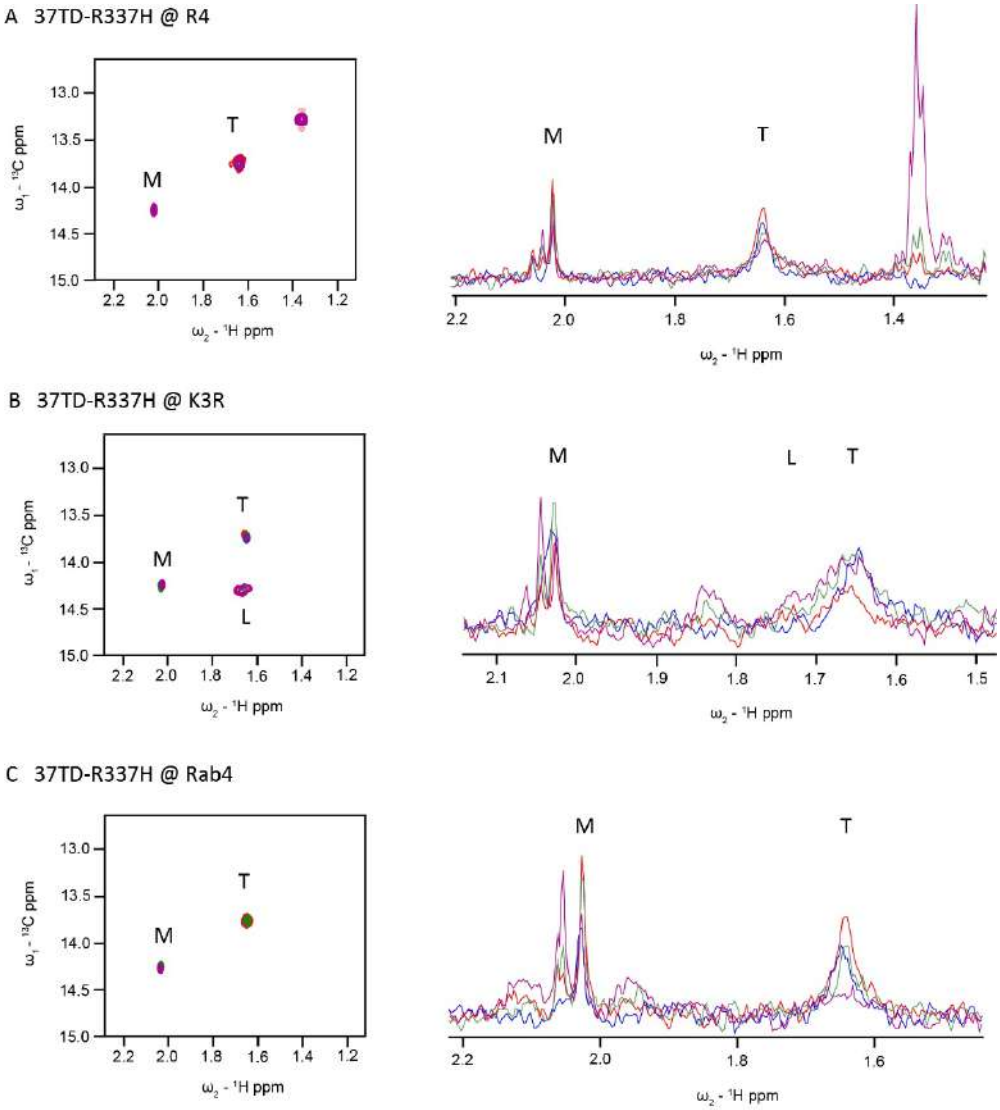

Figure 50. ^{1}H ^{13}C HSQC NMR binding experiments between 37TD-R337H with R4 (A), K3R (B), and Rab4 (C). The experiments were performed starting from a monomer concentration of 37TD-R337H of 10 µM (blue) which was titrated with 20 (red), 40 (green), and 80 µM (purple) of ligands. ^{1}H projections of ^{1}H,^{13}C HSQC spectra are represented on the right. The spectra were acquired at 37 °C, pH 7.5. M: monomer; T: tetramer; L: ligand.

To further study the binding between our ligands and p53TD, we performed NMR, thermophoresis, and native MS experiments using the calix[4]arene (**8**) as positive control to detect the binding.

Study of the binding by NMR (calix[4]arene)

As for the linear peptides, we started from physiological conditions at which 37TD-R337H were roughly half monomeric and half tetrameric (monomer concentration of 10 µM, 37 °C, pH 7.5). The protein domain was then titrated with an increasing amount of the ligand. Gordo *et al.*[80] studied the binding of calix[4]arene with p53TD WT and R337H mutant, both obtained as recombinant peptides with a slightly longer sequence than our 37TDs. Their p53 peptides were ^{15}N labelled and they monitored the chemical-shift-perturbation of the protein residues after the addition of the ligand. They found that the ligand was able to bind both the p53 peptides, although with a different mechanism. In particular, in the case of the mutant, by titrating the protein domain some residue signals disappeared and they appeared back after further addition of the ligand. This behaviour could be explained considering two sequential events, probably corresponding to the binding of two ligand molecules in the binding pockets of the tetramerisation domain.[80] We titrated our protein domain monitoring the methyl signal of M340. The signal corresponding to the tetramer disappeared immediately after the addition of 2 eq of ligand (Figure 51 A), whereas the signal of the monomer shifted upfield both in the ^{1}H and ^{13}C axis. We increased the amount of ligand to see if in our case as well the signal of the protein domain appeared back. By increasing the concentration of compound **8** up to 250 µM or 1 mM, both the signal of monomer and tetramer disappeared and any of them appeared back (Figure 51 B). The cross-peak above the monomer signal (^{1}H 2.04 ppm, ^{13}C 12.86 ppm) is a 'folding' ligand signal meaning that its real resonance is out from the working range of chemical shift, but since it is intense due to the high concentration of **8**, it can reappeared in the working range.[127,128] As for the linear peptide Rab4, where the signal of the tetramer disappeared with high concentration of the ligand, in this case as well the disappearance of the tetramer signal may be due to complex formation. The signal of monomer as well was modified by the addition of the ligand and it shifted towards the tetramer, indicating that probably the relative population between tetramer and monomer changed. It decreased its intensity and this may be an indication that the ligand was stabilising the tetramer. Nevertheless, the signal of the tetramer did not appear back increasing the concentration of the ligand and the interpretation of the results was not easy since the peaks disappeared. Due to these difficulties related to the NMR binding experiments, we decided to further explore our system and complement NMR results using different biophysical techniques, such as thermophoresis.

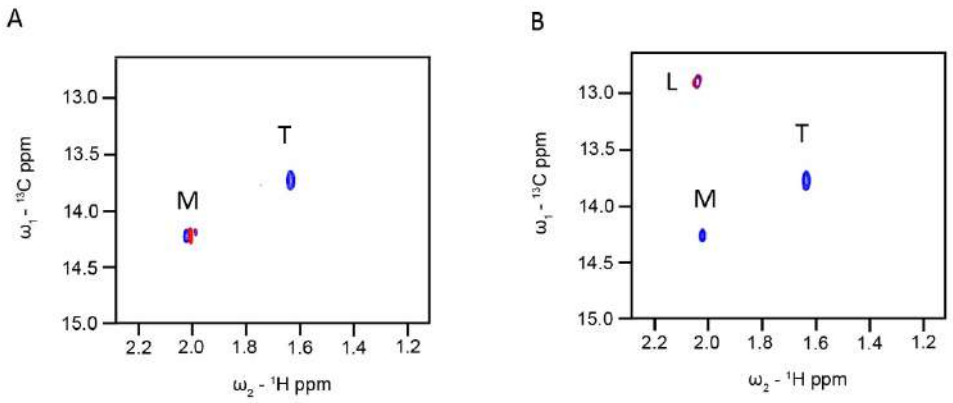

Figure 51. ^{1}H ^{13}C HSQC NMR binding experiments between 37TD-R337H with calix[4]arene (**8**). The experiments were performed starting from a monomer concentration of 37TD-R337H of 10 µM (A and B, blue) which was titrated with 20 (A, red), 40 (A, purple), 250 µM (B, red), and 1 mM (B, purple) of ligand. The spectra were acquired at 37 °C, pH 7.5. M: monomer; T: tetramer; L: ligand.

Study of the binding by thermophoresis (calix[4]arene)

We studied the binding between calix[4]arene and 37TD-WT and 37TD-R337H by thermophoresis. Gordo *et al.*[80] reported apparent K_d of *ca*. 130 and 65 µM for the first and the second ligand binding, respectively, calculated from NMR experiments with the R337H mutant. We performed the thermophoresis experiments in two different ways. In the first case, we studied the binding of the ligand to the monomer of either 37TD-WT or 37TD-R337H. The TDs were fluorescently labelled as described in the first chapter of 'Results and discussion'. The experiment was performed at TDs monomer concentration of 15 nM to detect a sharp fluorescence signal. At this concentration, we expect that both the WT and the mutant are monomeric. To these solutions, an increasing amount of the ligand was added to calculate the K_d of binding (Figure 52). Any K_d was found meaning that the ligand most probably was unable to bind the monomeric TDs.

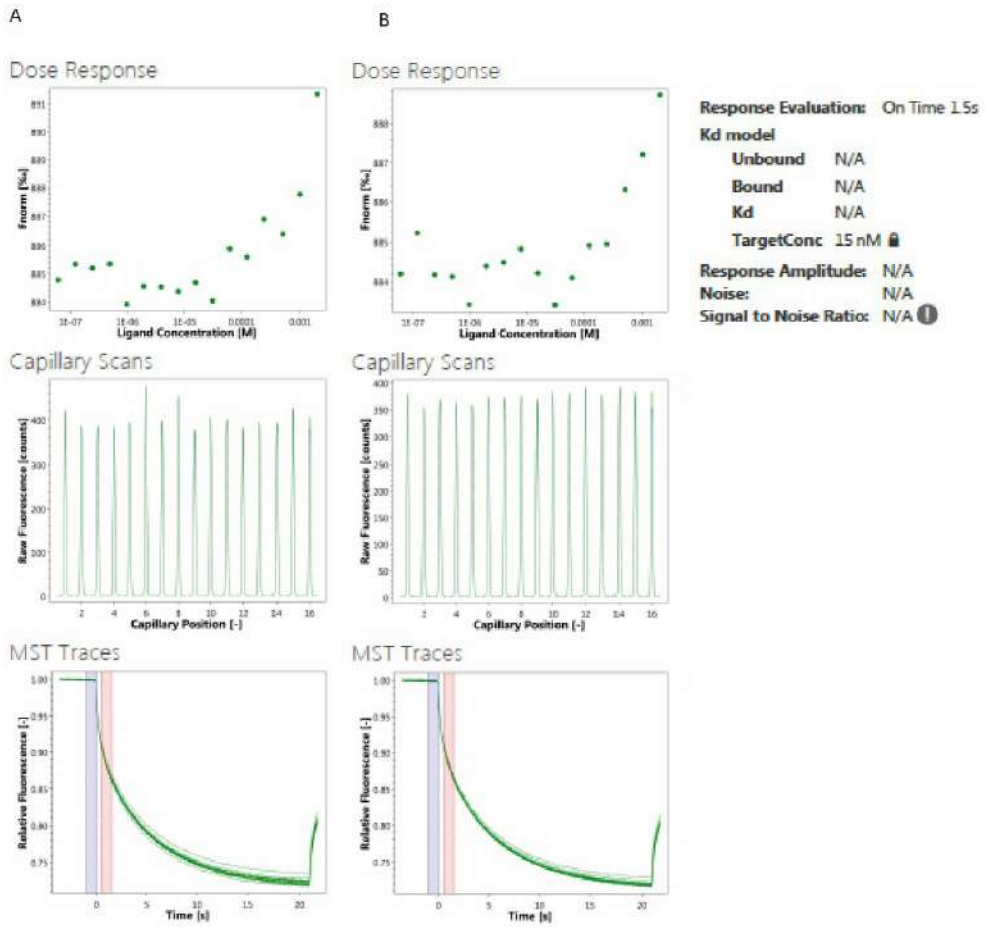

Figure 52. MST binding experiment of calix[4]arene with monomeric 37TD-WT (A) and 37TD-R337H (B). The concentration of 37TD-WT* and 37TD-R337H* (targets) was 15 nM and the highest concentration of calix[4]arene (ligand) was 2 mM.

Therefore, we performed the experiment in a different way, forming first the tetramer of the TDs and studying the binding of the ligand to the tetramers. To do so, a solution of labelled peptide (target) at a concentration of 15 nM was mixed with 'cold' peptide, either 37TD-WT or 37TD-R337H, which were not fluorescently labelled. The amount of 'cold' peptide added was *ca*. 10 times the K_d found in the experiments described in the first chapter of 'Results and discussion'. In this way, we ensured the peptides tetramerised before being titrated with the ligand. The MST curves found in these experiments are shown in Figure 53 and in this case also, any K_d was found. Probably, the affinity of the ligand to these TDs was not strong enough to be detected by MST. We decided thus to apply another biophysical technique, the native MS.

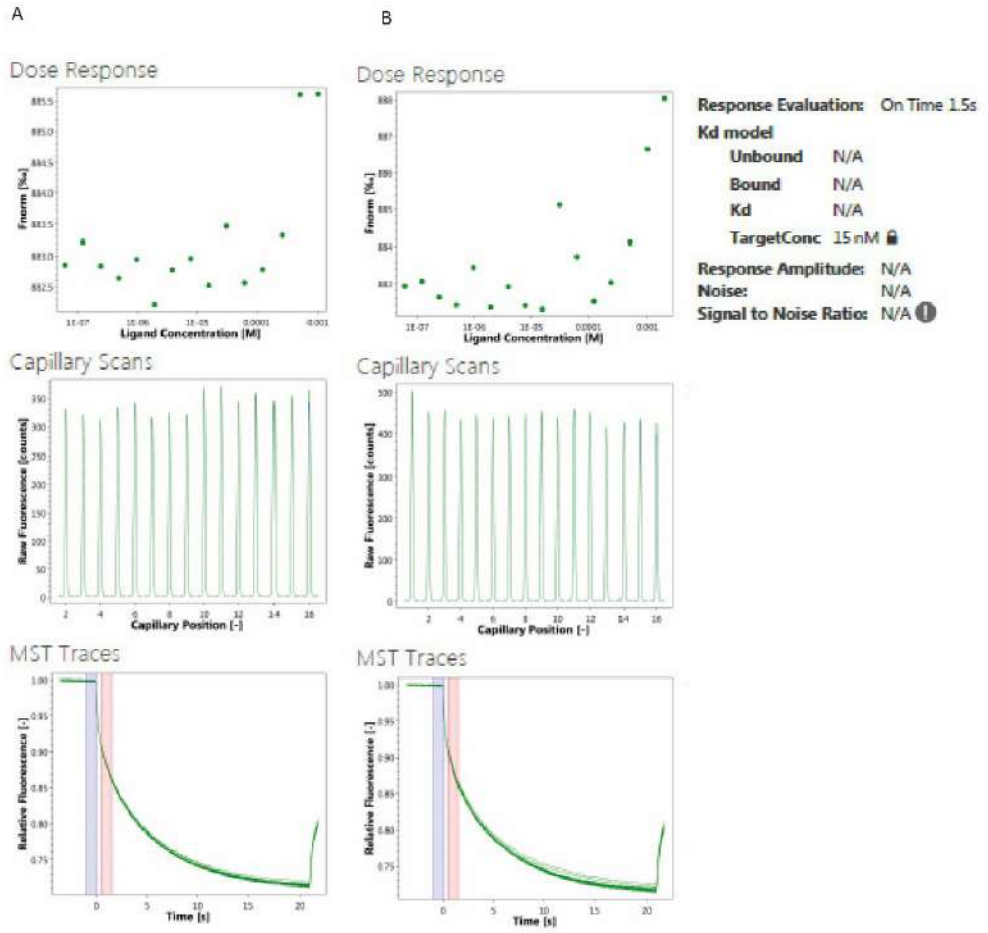

Figure 53. MST binding experiment of calix[4]arene with tetrameric 37TD-WT (A) and 37TD-R337H (B). The concentration of 37TD-WT* and 37TD-R337H* (targets) was 15 nM, 37TD-WT was 4 µM, 37TD-R337H was 10 µM, and the highest concentration of calix[4]arene (ligand) was 2 mM.

Study of the binding by native MS

We decided to perform native MS experiments to detect the binding between p53TD and calix[4]arene. Having found the experimental conditions to detect the complex formation, they were applied to study the binding with the second generation ligands. Several experimental conditions were explored, in particular the source temperature was decreased from 40 °C, as used in the experiments of the TDs, to 29 °C. The trap and transfer voltages were increased to 10 and 8 V, respectively, as described by Gordo *et al.*[80,82] to detect the complex formed by the tetramer and two molecules of ligand. In our case, applying these voltages, the

tetramer disrupted, therefore we reduced the voltages to 6 and 4 V, as already described for the study of the TDs. At these conditions, we detected the tetramer of 37TD-WT and 37TD-R337H and the complexes formed by the TDs tetramer and one molecule of ligand (Figure 54 and 55). We applied thus these conditions to study the interaction of the TDs with the second generation ligands (Figure 54 and 55).

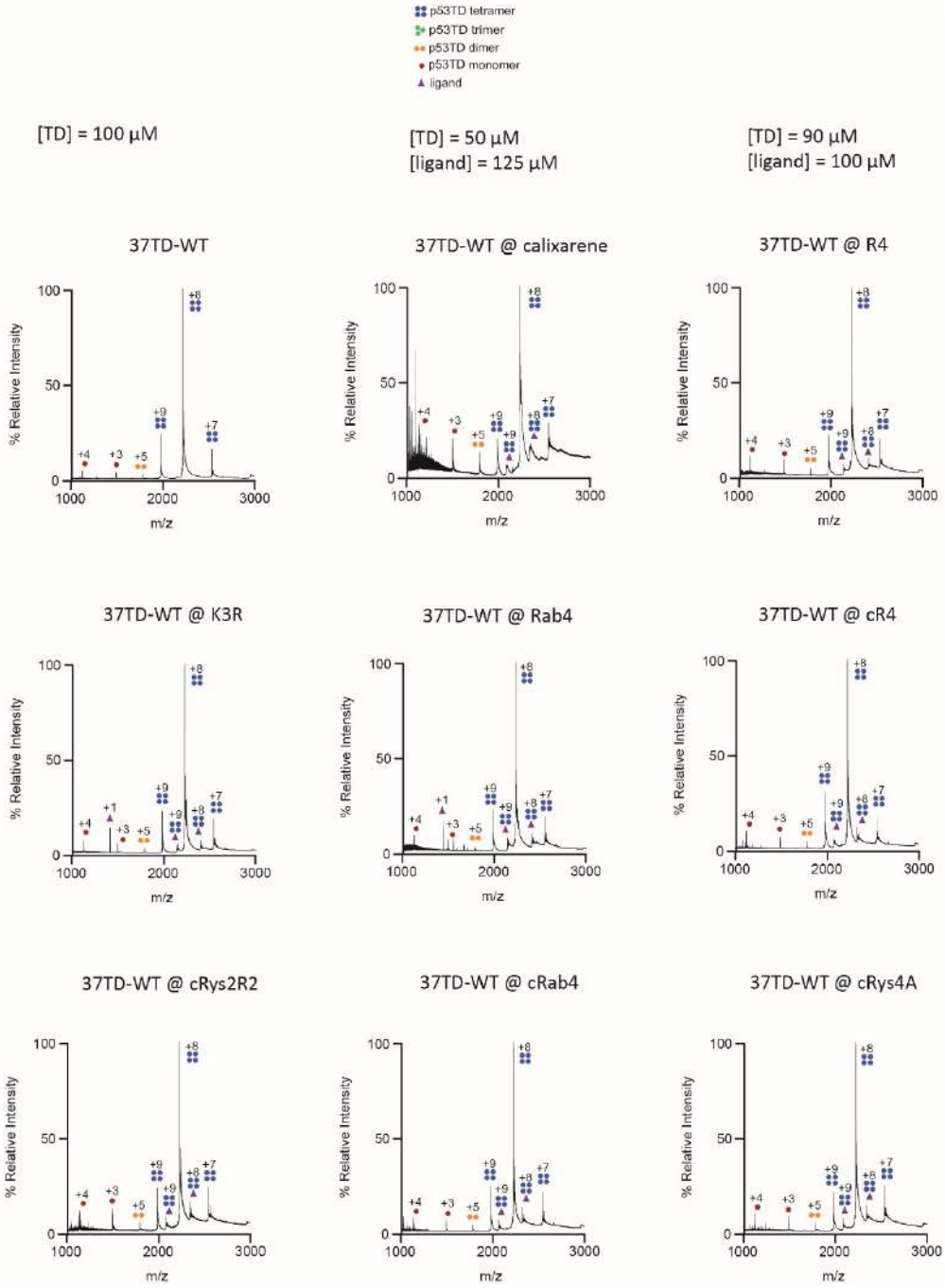

Figure 54. Native MS spectra of 37TD-WT forming complexes with calix[4]arene and 2nd generation ligands. The concentrations of 37TD-WT and calix[4]arene were 50 and 125 µM, respectively, whereas with the other ligands were 90 and 100 µM, respectively. For 37TD-WT, a non-isotope-labelled sequence was used and the concentrations reported refer to the monomer. The samples were dissolved in 200 mM ammonium acetate buffer, pH 7.

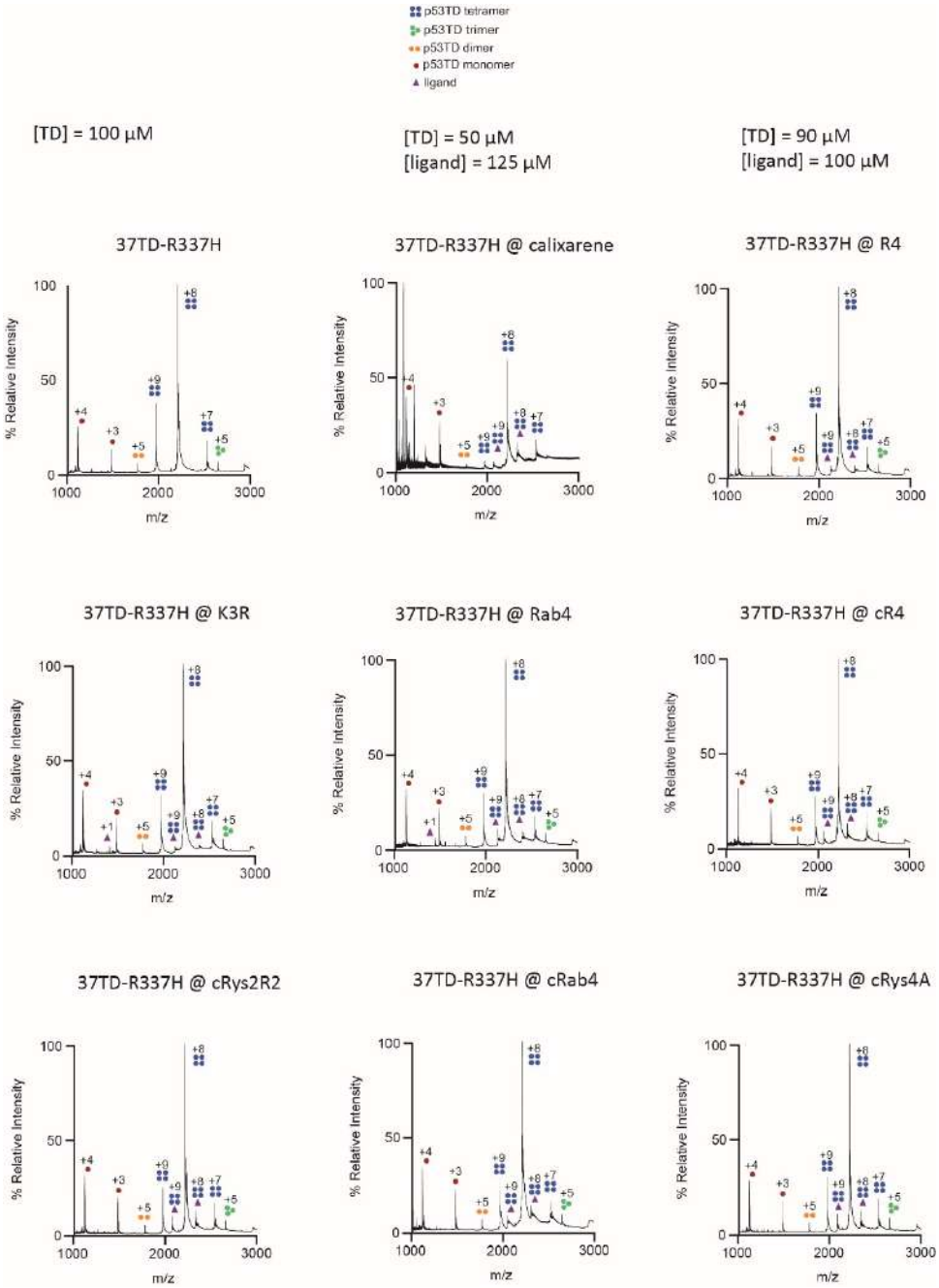

Figure 55. Native MS spectra of 37TD-R337H forming complexes with calix[4]arene and 2nd generation ligands. The concentrations of 37TD-R337H and calix[4]arene were 50 and 125 µM, respectively, whereas with the other ligands were 90 and 100 µM, respectively. For 37TD-R337H, a non-isotope-labelled sequence was used and the concentrations reported refer to the monomer. The samples were dissolved in 200 mM ammonium acetate buffer, pH 7.

From this study, we conclude that all the ligand studied, the calix[4]arene and the 2nd generation ligands are able to bind p53TDs. Although the results were similar for all the ligands studied, we selected the compounds that gave the most intense complex signals, indicating a stronger binding to the TDs. In order to determine which compounds gave the most intense signals, we measured the ratio I / I_0 considering the +8 and +9 charges peaks, which were the peaks detected for the complexes. I corresponds to the intensity of the complex peak and I_0 to the relative charge peak of the tetramer. We did this analysis for the spectra of both 37TDs and we selected in this way two ligands, a linear and a cyclic one that gave the best results, corresponding to Rab4 and cRys2R2. With these two compounds, we further analysed the complexes formed with the TDs by native MS. In particular, the cone voltage was increased to study the complexes stability at high voltages. Moreover, we studied by NMR the conformational structures that the two selected ligands adopted in solution, and, finally, we determined their stability in human serum and their cytotoxicity in HeLa cells.

Stability of the complexes studied by native MS

With the aim to further study the stability of the complexes formed by p53TDs and the two selected ligands, we performed native MS experiments increasing the cone voltage up to 80 and 120 V. Similarly as for 37TDs, we wanted to check if the complexes survived increasing the voltage, therefore to prove if the ligands were able to stabilise the tetramers. We performed the experiments with 37TD-WT (Figure 56) and 37TD-R337H (Figure 57) at a monomer concentration of 100 µM (Figure 56 A and 57 A). To form the complexes, the TDs were mixed with ligands at final concentrations of 90 and 100 µM, respectively. The source temperature was set to 29 °C, and the trap and transfer voltages at 6 and 4 V, respectively.

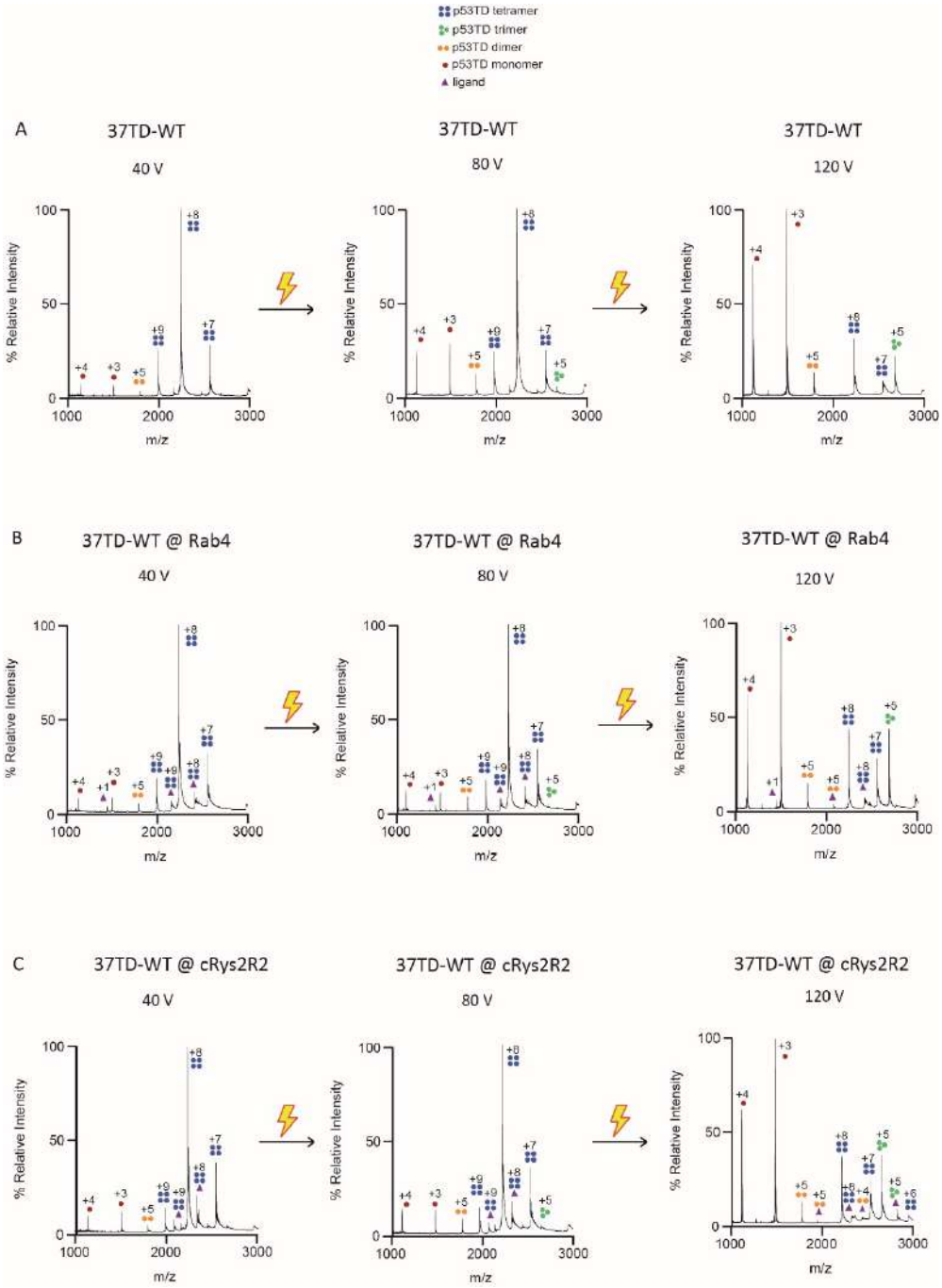

Figure 56. Native MS spectra of 37TD-WT (A) and 37TD-WT forming complexes with Rab4 (B) and cRys2R2 (C) at cone voltages of 40, 80, and 120 V. For 37TD-WT, non-isotope-labelled peptide was used and the concentrations reported refer to the monomer. The samples were dissolved in 200 mM ammonium acetate buffer, pH 7.

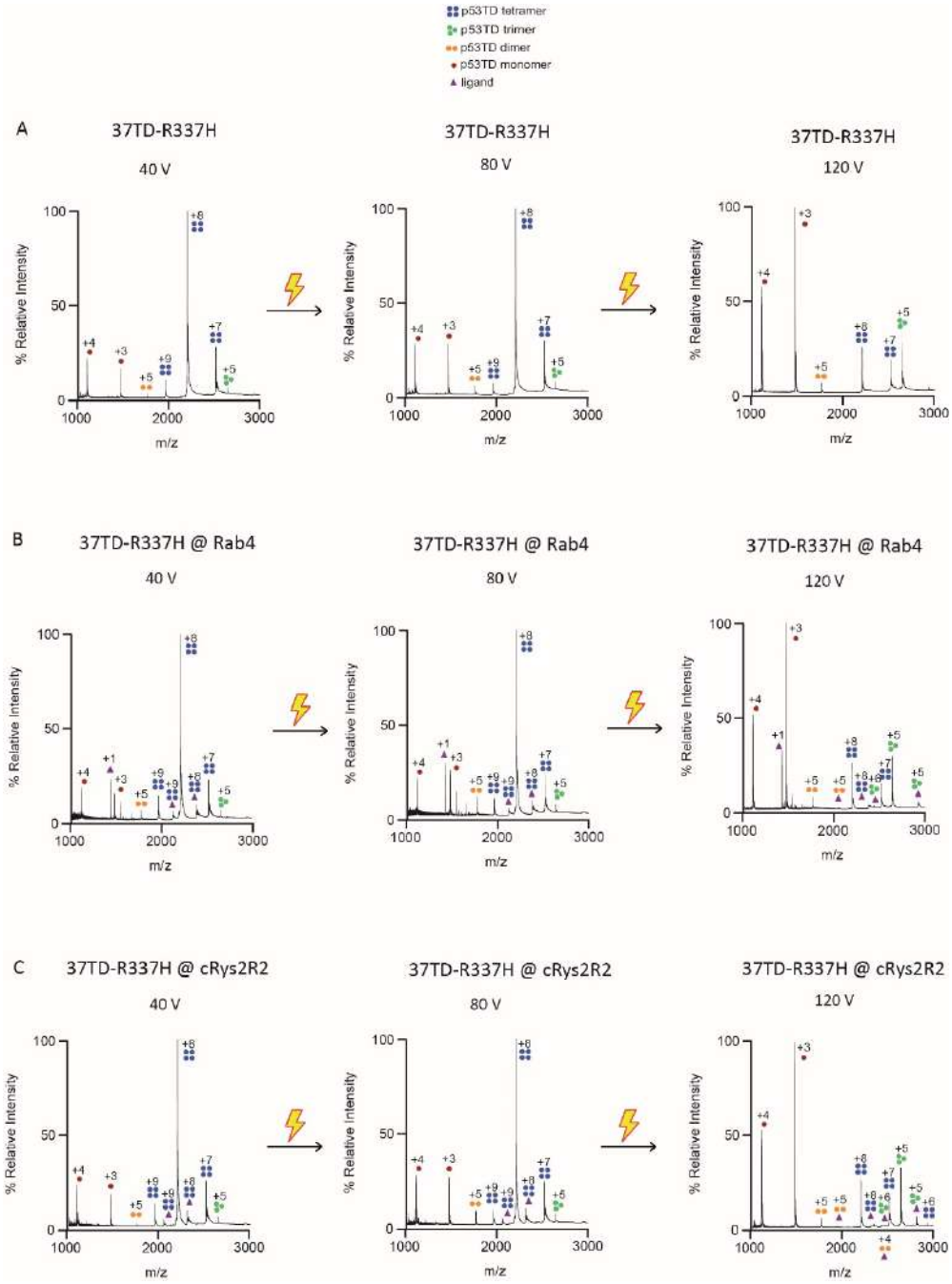

Figure 57. Native MS spectra of 37TD-R337H (A) and 37TD- R337H forming complexes with Rab4 (B) and cRys2R2 (C) at cone voltages of 40, 80, and 120 V. For 37TD-R337H, non-isotope-labelled peptide was used and the concentrations reported refer to the monomer. The samples were dissolved in 200 mM ammonium acetate buffer, pH 7.

From these experiments, we conclude that the complexes were stable at high voltages, as their signals were detected also at 120 V with all the ligands studied. The tetramers disrupted by increasing the voltage since their signals decreased their intensity. Concerning the complexes with the ligands, their behaviour at high voltage is more difficult to evaluate since the intensity of the peaks was much smaller. However, in comparison to the tetramers, it decreased less by increasing the voltage. Although it is not easy to conclude if the ligands were able or not to stabilise the tetramers, the presence of the complexes signals at high voltage may be indicative of the formation of quite stable complexes and a relatively strong interaction in the gas phase.

Conformational study of Rab4 and cRys2R2 by NMR

With the aim to further characterised the selected ligands and study their conformation in solution, we performed NOESY, TOCSY, and ^{1}H ^{13}C HSQC NMR experiments at natural isotopes abundances. In the TOCSY spectrum, the signals correspond to the coupling between the NH of the backbone with the protons of the side chain of the residues. In the NOESY spectrum, based on the nuclear Overhauser effect (NOE), the signals correspond to the coupling of protons closed in space. In this experiment, normally the NOE between the H^N of the *i* residue is stronger with the α-proton of the *i-1* residue compared to *i+1*. Nevertheless, it is possible to detect both of them. We were able to assign the signals of the two ligands by these spectra and the assignation is reported in Tables 9-12, whereas the spectra are shown in the 'Supplementary NMR' section (Figure S50) at the end of the thesis.

Ac-Rab-S-Rab-A-Rab-G-Rab-A-W-G-A-A-G-A-NH_2

Residue	NH	H^{α}	H^{β}	H^{γ}
Rab1		4.43		
S2		4.41	3.86 3.90	-
Rab3	8.59	4.38	1.94 2.08	3.30
A4	8.44	4.26	1.36	-
Rab5	8.68	4.38	1.98 2.08	3.24 3.38
G6	8.59	3.96 3.98	-	-
Rab7	8.45	4.33	1.87	3.13
A8	8.53	4.30	1.33	-

W9	8.36	4.62	3.24 3.29	-
G10	8.29	3.76 3.81	-	-
A11	8.18	4.24	1.37	-
A12	8.49	4.28	1.40	-
G13	8.39	3.90	-	-
A14	8.23	4.20	1.35	-

Table 9. ^{1}H chemical shift of Rab4 peptide.

Residue	C^{α}	C^{β}	C^{γ}
Rab1	53.88		
S2	58.58	63.6	-
Rab3	54.14	32.65	40.38
A4	52.71	19.01	-
Rab5	54.14	24.49	40.40
G6	45.12	-	-
Rab7	53.92	32.82	40.22
A8	52.48	19.08	-
W9	57.52	29.80	-
G10	45.08	-	-
A11	52.63	19.14	-
A12	52.67	18.99	-
G13	45.12	-	-
A14	52.36	19.50	-

Table 10. ^{13}C chemical shift of Rab4 peptide.

&(Rys-S-Rys-A-R-G-R)

Residue	NH	H^{α}	H^{β}	H^{γ}	H^{δ}	H^{ε}
Rys1	7.95	4.43	2.08	1.65	1.59	3.17
S2	7.83	4.63	3.99 3.91	-	-	-
Rys3	8.52	4.15	1.85	1.61	1.45 1.39	3.17
A4	8.30	4.32	1.39	-	-	-
R5	8.12	4.36	1.74 1.86	1.54	3.17	
G6	8.67	3.80 4.10	-	-	-	-
R7		4.13				-

Table 11. ^{1}H chemical shift of cRys2R2 peptide.

Residue	C^{α}	C^{β}	C^{γ}	C^{δ}	C^{ε}
Rys1	57.96	31.20	27.19	27.05	43.49
S2	59.06	64.03	-	-	-
Rys3	57.66	32.42	25.14	25.13	43.49
A4	52.88	19.54	-	-	-
R5	56.05	30.41	27.03	43.49	
G6	45.66	-	-	-	-
R7	58.11				-

Table 12. ^{13}C chemical shift of cRys2R2 peptide.

Based on these assignations of the signals, we used the software δ2D (https://www-cohsoftware.ch.cam.ac.uk/), developed by Camilloni *et al*.[129] to calculate secondary structure populations based on the chemical shifts of the residues. From this analysis, the results suggested that both peptides are mainly disordered, as shown in Figure 58.

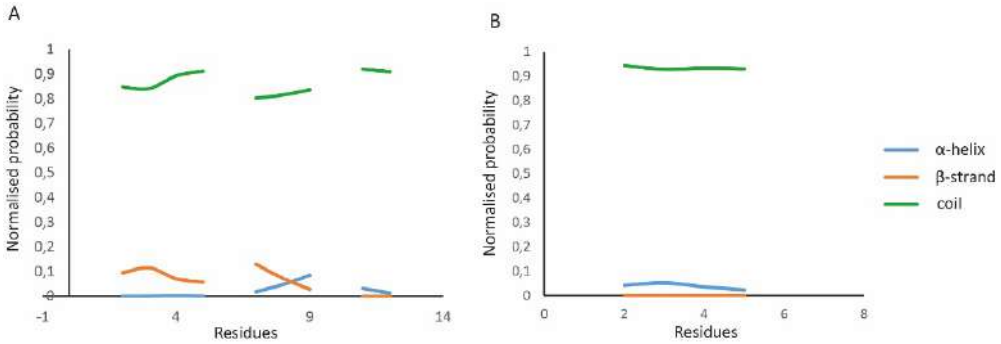

Figure 58. Calculation of the secondary structure populations of Rab4 (A) and cRys2R2 (B) peptides based on their residue chemical shifts, using the software δ2D.

Stability in human serum

In order to further study the selected peptides from their biological properties, we performed serum stability and cytotoxicity assays. To study their stability in human serum, we mixed the peptides, dissolved in Hank's balanced salt solution (HBSS), with 50% human serum in HBSS and the mixture was incubated at 37 °C for 24 h. At different time points we took an aliquot and the serum proteins were precipitated using 15% TFA in water. The suspension was centrifuged and the supernatant collected to be analysed by HPLC, as schematically shown in Figure 59.

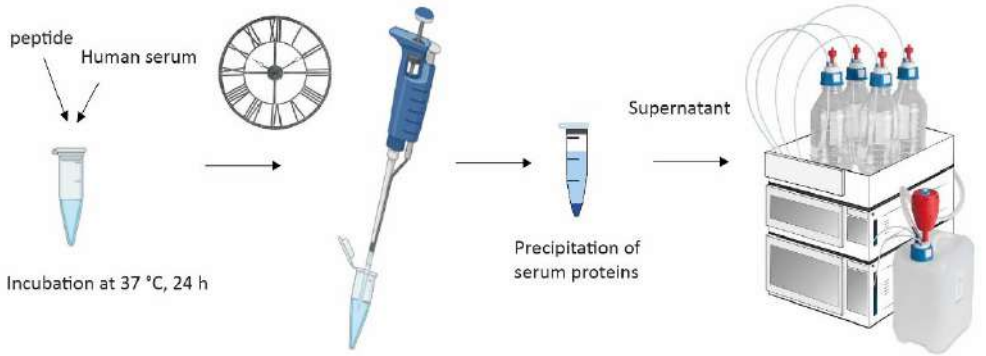

Figure 59. Schematic procedure of serum stability assay.

Starting from time zero (t_0) when the peptides were not yet in contact with serum proteins, the peaks of the peptides were detected in the chromatogram and their areas were calculated to check how they decreased during time. The area of the peak is correlated to the amount of the peptide in solution and several gradients were tried to ensure that peaks corresponding to the fragmented peptides during the experiment did not overlap to the initial peptide signals. Therefore, by calculating the area of the peptides signals of each aliquot, it is possible to determine the half life time of the peptide in the presence of human serum. The results concerning Rab4 and cRys2R2 peptides are reported in Figure 60.

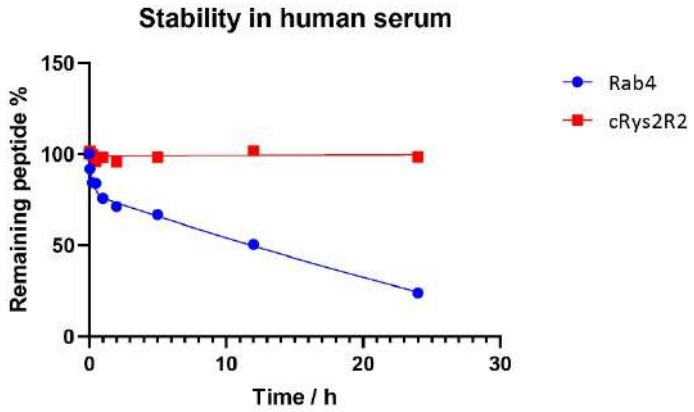

Figure 60. Stability of Rab4 and cRys2R2 peptides in human serum over 24 h.

From our results, we conclude that both peptides are quite stable in human serum over 24 h. The cyclic peptide cRys2R2 was more stable, as expected, with an half-life time > 24 h, whereas the linear peptide Rab4 had an half-life time of ≈ 12 h, meaning that it lasted relatively long considering a linear peptide. The reasons of this observation most probably are related to the fact that, although it is a linear peptide, it is capped at *N*- and *C*-terminus with acetate and amide group, respectively,

decreasing the degradation rate from the proteases of the serum.[130] Moreover, it is composed also by non-natural residues (Rab) that may contribute to increase its half-life time in human serum.[131–133]

Cytotoxicity assay (XTT)

We performed cytotoxicity assay XTT using HeLa cell line to determine the cytotoxicity of the selected peptides and we compared their values to the calix[4]arene (**8**). After the incubation of the studied compound with the cell line at 37 °C, the mitochondrial activity of the cells is determined by adding tetrazolium salt XTT, which is a yellow compound and it is turned to orange formazan compound by metabolic active cells. The dye formed is water soluble and its intensity can be read with a spectrophotometer at 485 nm. Two reads were done, after 4 and 24 h incubation (Figure 61).

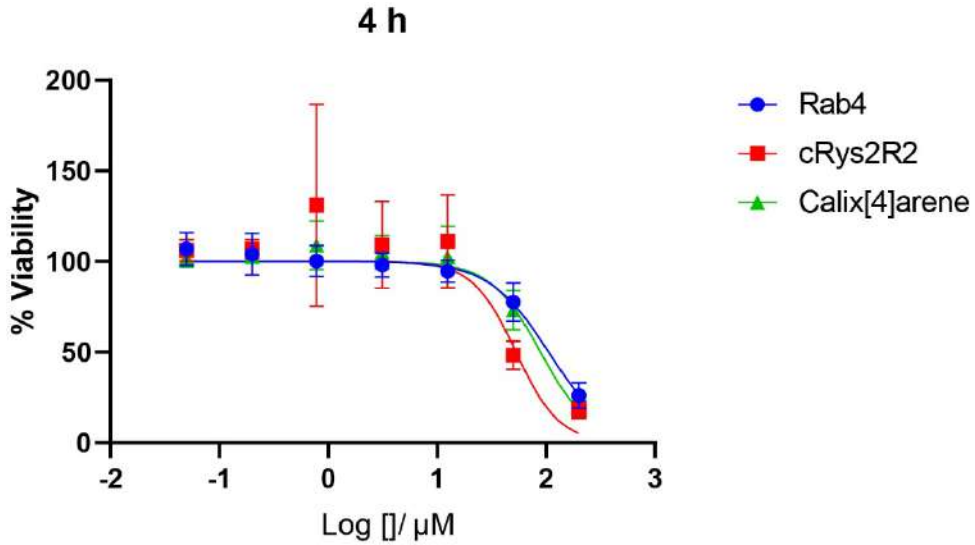

	Rab4	cRys2R2	Calix[4]arene
IC50	105	53.0	89.0

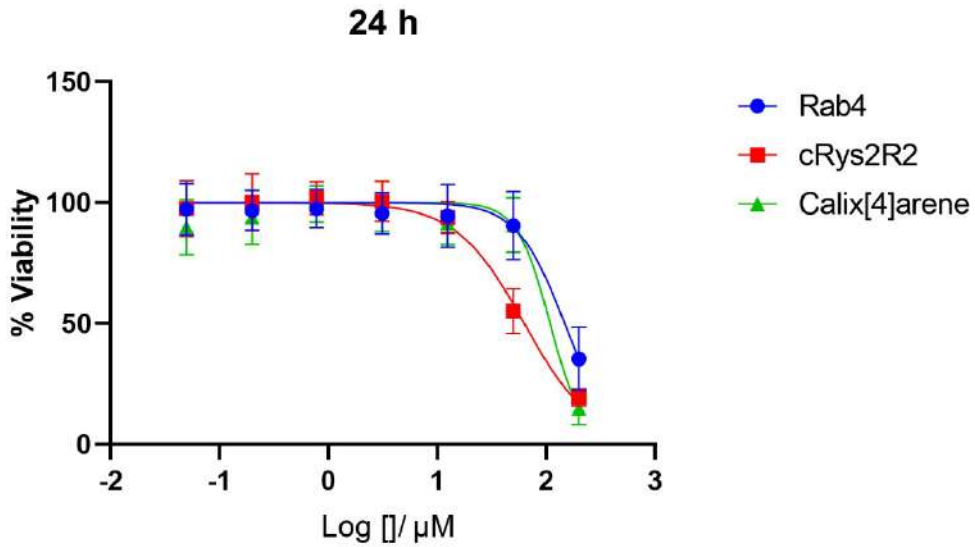

	Rab4	cRys2R2	Calix[4]arene
IC50	148	63.0	109

Figure 61. Cytotoxicity assay using XTT reagent in HeLa cells. The reading was done after 4 and 24 h incubation of Rab4, cRys2R2 and calix[4]arene with the cells.

From our results, we conclude that none of the studied compounds were cytotoxic for HeLa cells. Moreover, there was not a significant difference between the analysis after 4 or 24 h incubation. Although similar, from this experiment, the cyclic peptide looked to be slightly more toxic than the other compounds, whereas the linear peptide and the calix[4]arene behaved very similarly. Surprisingly, the values of IC50 found at 4 h incubation were slightly smaller than the corresponding values at 24 h incubation. The data were analysed and normalised using HeLa cells alone for the 100% of viability and cells incubated with SDS or wells without cells for the 0% viability. All the data were adjusted between these values. There is not significant difference between the analysis considering the two different 0%, in Figure 61 the data adjusted on the values of cells incubated with SDS are reported, whereas the other set is shown in the 'Supplementary XTT' section at the end of the thesis (Figure S77).

In summary, we designed two generations of peptides as potential ligands for p53TD. We run docking simulations and molecular dynamics using Schrodinger (Maestro) and we selected the most promising peptides to be synthesised and experimentally studied. We synthesised also the calix[4]arene as positive control in the binding experiments. Several biophysics techniques were applied to detect the binding between the ligands and p53TD. Concerning the first generation of ligands, NMR and thermal stability CD suggested binding of cyclo-tetra-β-3-arginine *S* with the mutated TD and the ligand was able to increase the T_m of the protein domain. Concerning the second generation of ligands, the binding of the linear peptides was studied by NMR and fluorescence. Both techniques suggested binding, although the fluorescence changes were not consistent with the TD concentration. We decided to explore the interactions between our ligands and the TDs using the calix[4]arene as positive control and some of these experiments gave promising results. For example, ^{1}H ^{13}C HSQC NMR showed a shift upfield of the monomer peak, whereas the tetramer peak disappeared after the addition of the ligand, suggesting binding between the molecules. Native MS also showed the signals of the complexes with all the ligands studied. From these experiments, we selected the peptides that gave the best results in terms of signals intensities. Therefore, two peptides, Rab4 and cRys2R2 were further investigated. The complexes stability was checked increasing the cone voltage. At high voltages the signals of the complexes were still present, nevertheless it was difficult to define if the ligands stabilised the mutated tetramer because the signals were quite weak. The secondary structure of selected ligands was explored by conformational NMR studies, which suggested that both peptides were disordered. Finally, some biological properties were evaluated, such as their stability in human serum and their cytotoxicity in HeLa cells. The cyclic peptide was stable in human serum having a half-life > 24 h and the linear peptide was slowly

degraded, with a half-life of *ca*. 12 h. None of the studied compounds were significantly cytotoxic over 24 h in HeLa cells, with IC50 values between 50 – 150 µM The cyclic peptide looked to be slightly more toxic that the linear one and the calix[4]arene.

MATERIALS AND METHODS

SYNTHESIS

Peptide synthesis and characterisation

Synthesis of the 37TDs

The peptides of interest were synthesised in their acetylated (at *N*-terminus) and amidated forms (at *C*-terminus) by Fmoc/*t*Bu solid-phase peptide synthesis (SPPS). The peptides consist of L-amino acids, and the isotope-labelled sequences were obtained using ^{13}C-methyl methionine provided by Cambridge Isotope Laboratories (Massachusetts, USA).

37TD-WT and 37TD-R337H were synthesised manually on H-Rink Amide ChemMatrix resin at 0.1 mmol scale. The resin was conditioned by washing with MeOH (5 X 30s), DMF (5 X 30s), DCM + 1% TFA (2 X 10 min), DCM (5 X 30s), DMF (5 X 30s), DCM (5 X 30s), DCM + 5% DIPEA (2 X 10 min), DCM (5 X 30s), and DMF (5 X 30s) using 10 ml per gram of resin each time. The first amino acid was attached twice using distinct coupling conditions. The first time, the protected amino acid (3 eq.) was activated using diisopropylcarbodimide (DIC, 3eq.) and Oxyma Pure (3 eq.) and the second time using HATU (3 eq.) and DIPEA (6 eq.). The mixture was allowed to react in an orbital shaker at room temperature (RT) for 1 h and 40 min, respectively. The yield of this reaction was calculated by UV absorption of the dibenzofulvane, the leaving group of Fmoc, at 301 nm.[134,135] The remaining active sites on the resin that did not react with the first amino acid (free NH_2 groups) were capped through acetylation with a solution of 5% acetic anhydride, 8.5% DIPEA, and 86.5% DMF, by stirring at RT for 15 min. The chain up to the 11th residue was elongated using HATU/DIPEA as coupling reagents, followed by DIC/Oxyma Pure until the end of the synthesis. The efficiency of each coupling step was followed by the Kaiser (for primary amines)[136] and chloranil (for secondary amines) tests.[137] The Fmoc group was removed using two solutions of 40% and 20% (v/v) of piperidine in DMF until deprotection of the G325 was achieved (Figure 2 A), and then using a solution of 10% (w/v) piperazine in 90: 10 NMP in EtOH with 0.1 M Oxyma Pure in order to prevent the formation of the aspartimide, which is particularly prone after the DG sequence.[138] 37TD-WT and 37TD-R337H were synthesised twice, using a Fmoc-methionine or ^{13}C-methyl methionine, respectively.

The other 37TDs (37TD-D352H, 37TD-R342L, 37TD-T329I, 37TD-L344R, and 37TD-L344P) were synthesised using a Liberty Blue CEM microwave-assisted peptide synthesiser (Matthews, NC). All these sequences were obtained using a ^{13}C-methyl methionine and were synthesised on Rink Amide ProTide LL resin, on a reaction scale of 0.05 mmol. The resin was conditioned with DCM for 15 min and afterwards placed in the synthesiser without preloading of the first amino acid. Each coupling

was performed using 4 eq. of the Fmoc-amino acid and DIC (4 eq.)/Oxyma Pure (4 eq.) in DMF. All the couplings were programmed as double coupling, apart from the introduction of R, K, E, and M, which were set up as triple coupling. The Fmoc group was removed with a solution of 10% (w/v) piperazine in 90:10 NMP in EtOH containing 0.1 M Oxyma Pure.

All synthesised peptides were acetylated at their *N*-terminus using a solution of 5% acetic anhydride, 8.5% DIPEA, and 86.5% DMF in an orbital oscillator at RT for 15 min.

Cleavage from the resin and side-chain deprotection

The 37TDs that were manually synthesised were cleaved from the resin and deprotected with a cocktail of 92.5% TFA, 2.5% H_2O, 2.5% triisopropylsilane (TIPS) and 2.5% dithiothreitol (DTT), while for the rest of the sequences a cocktail of 92.5% TFA, 2.5% H_2O, 2.5% TIPS and 2.5% 2,2'-(Ethylenedioxy)diethanethiol (EDT) was used. In both cases, the reaction was left for 3 h and the crude peptides were precipitated with cold Et_2O, then solubilised in water and lyophilised.

Peptide purification

37TD-WT and 37TD-R337H were purified by semi-preparative HPLC on a Waters system (Milford, MA, USA) with MassLynx software, a 2545 binary gradient module, a 2767 manager collector, and a 2998 photodiode array detector, using Aeris C_{18} column (250 X 10 mm, 5 µm, 100 Å, Phenomenex, Torrance, CA, USA). The lyophilised peptides were dissolved in 5% acetonitrile in water and 9 ml of the solution was injected. The flow rate was 6.6 ml/min, solvent A=0.1% TFA in water, solvent B=0.1% TFA in acetonitrile. Elution was carried out with linear 10-45% gradients of solvent B into A over 30 min, with UV detection at 220 nm.

The other 37TDs were purified by semi-preparative HPLC on a Shimadzu LC-8A system (Kyoto, Japan) with UV detection at 220 nm and an Aeris C_{18} column (250 X 10 mm, 5 µm, 100 Å, Phenomenex, Torrance, CA, USA). The lyophilised peptides were dissolved in 5% acetonitrile in water and 9 ml of solution was injected. The flow rate was 5 ml/min, solvent A=0.1% TFA in water and solvent B=0.1% TFA in acetonitrile. Elution was carried out with linear 5-60% gradients of solvent B into A over 30 min, with UV detection at 220 nm.

Fractions corresponding to the pure peptides (> 85%) were collected, combined, lyophilised and stored at -20 °C.

Characterisation

The manually synthesised and purified peptides (37TD-WT and 37TD-R337H) were characterised by UPLC and UPLC-MS. UPLC analysis was performed on a Waters Acquity equipped with Acquity photodiode array detector, using flow rate of 0.610 ml/min, Acquity UPLC BEH C_{18} column, 130 Å, 1.7 µm, 2.1 mm x 100 mm, solvents A=0.045% TFA in water, and B=0.036% TFA in acetonitrile. Elution was carried out with linear 0-70% gradients of solvent B into A over 40 min. UPLC-MS analysis was performed on a Waters Acquity UPLC System equipped with ESI-SQ Detector2, using a flow rate of 0.610 ml/min, Acquity UPLC BEH C_{18} column, 130 Å, 1.7 µm, 2.1 mm x 100 mm, solvents A=0.1% formic acid in water, and B=0.07% formic acid in acetonitrile. Elution was carried out with linear 0-70% gradients of solvent B into A over 40 min.

The other 37TDs were characterised by HPLC and HPLC-MS. HPLC analysis was performed on a C_{18} column, 4.6 mm x 50 mm, 3 µm, Phenomenex, Torrance, CA, USA in a LC-2010A system (Shimadzu, Kyoto, Japan), solvents A=0.045% TFA in water, and B=0.036% TFA in acetonitrile. Elution was carried out with linear 5-60% gradients of solvent B into A over 15 min. HPLC-MS analysis was performed on C_{18} column, 4.6 mm x 150 mm, 3.5 µm, Phenomenex, Torrance, CA, USA in a Shimadzu LC-MS 2010EV instrument, solvents A=0.1% formic acid in water, and B=0.08% formic acid in acetonitrile. Elution was carried out with linear 5-60% gradients of solvent B into A over 15 min.

All the final products were further characterised by LTQ-FT MS and quantified by amino acid analysis.

LTQ-FT MS

A high-resolution mass spectrometer was used to determine the exact mass of the peptides. The samples were diluted in H_2O/ACN (1:1) with 1% formic acid and analysed with a LTQ-FT Ultra (Thermo Scientific). They were introduced by automated nanoelectrospray. A NanoMate (Advion Biosciences, Ithaca, NY) infused the samples through the nanoESI Chip (which consisted of 400 noozles in a 20 x 20 array). The spray voltage was 1.70 kV, and the delivery pressure was 0.5 psi. MS conditions were as follow: nanoESI, positive ionisation, capillary temperature 200 °C, tube lens 100 V, ion spray voltage 2 kV, and *m/z* 200-2000 a.m.u.

Amino acid analysis

The content and ratio of amino acids present in a peptide sample were determined by ion exchange chromatography analysis after acid hydrolysis. The hydrolysis was performed with 6 M HCl at 110 °C for 16 h. After that time, the sample was

evaporated to dryness at reduced pressure. The residue was dissolved in 20 mM acqueous HCl, derivatised using the AccQ-Tag protocol from Waters, which uses 6-aminoquinolyl-N-hydroxysuccinimidyl carbamate as a derivatisation reagent, and finally analysed by ion exchange HPLC.

Synthesis of the 74TDs

The monomer sequences of 74TDs were synthesised using a Liberty Blue CEM microwave-assisted peptide synthesiser as 37TD-D352H, 37TD-R342L, 37TD-T329I, 37TD-L344R, and 37TD-L344P. After monomer purification, the disulphide bridge was formed in solution using BisNPys as activator reagent. The monomer with the free cysteine (5 mg, 1.17 µmol, 1 eq) was dissolved in 2 ml of 0.1 M sodium phosphate buffer, pH 7.8 and it was activated with BisNPys (0.4 mg, 1.36 µmol, 1.2 eq), previously dissolved in DMF (50 µl). The solution was stirred at RT and the reaction was monitored by HPLC-MS. When the free cysteine disappeared and it was converted in the activated peptide, the suspension was centrifuged for 5 min to remove the excess of the activator reagent and the supernatant was collected. The monomer with free cysteine (5 mg, 1.17 µmol, 1 eq) was added to form the covalent dimer. The reaction was monitored by HPLC-MS and stopped when any monomer was detected. The solution was stirred for 5 days to complete the reaction. Afterwards, it was lyophilised and purified by semi-preparative HPLC on a Shimadzu LC-8A system, with a linear gradient of 5-60% of ACN in water, as for the other 37TDs.

Fractions corresponding to the pure peptides (> 85%) were collected, combined, lyophilised and stored at -20 °C. The final products were characterised by HPLC-MS, HPLC, and LTQ-FT MS and they were quantified by amino acids analysis, as described for the 37TDs.

Synthesis of the ligands

Linear ligands (R4, K3R, and Rab4)

The linear peptides R4, K3R, and Rab4 were synthesised manually, as described for 37TD-WT and 37TD-R337H. HATU and DIPEA were used as coupling reagents and the Fmoc deprotection was achieved with solutions of 20% and 40% of piperidine in DMF. The peptides were cleaved from the resin, purified, characterised, and quantified as described for 37TD-WT and 37TD-R337H.

Cyclic ligands (cyclo-tetra-β-3-arginine *S*, cR4, cRab4, cRys2R2, and cRys4A)

The cyclic peptides were manually synthesised on 2-chlorotrityl resin at 0.1 mmol scale. The resin was swelled with dry DCM for 20 min and the first amino acid (0,1

mmol, 1 eq) was attached using DIPEA (6 eq) in dry DCM. The mixture was allowed to react in an orbital shaker at room temperature (RT) for 40 min. The yield of this reaction was calculated by UV absorption of the dibenzofulvane, the leaving group of Fmoc, at 301 nm.[134,135] The remaining active sites on the resin that did not react with the first amino acid (free Cl groups) were capped through methylation with a solution of 80% dry DCM, 15% MeOH, and 5% DIPEA, by stirring at RT for 15 min. The chain was elongated using DIC (1.5 eq) and Oxyma Pure (1.5 eq) as coupling reagents in DCM. The mixture was allowed to react in an orbital shaker at room temperature (RT) for 1 h and the efficiency of each coupling step was followed by the Kaiser test for primary amines.[136] The Fmoc group was removed using two solutions of 40% and 20% (v/v) of piperidine in DMF. Having reached the desired sequence, the linear peptide was cleaved from the resin with 1% TFA in DCM to maintain the protective groups on the side-chains of the residues. The reaction was left for 1.5 h and the crude peptides were precipitated with cold Et_2O, then solubilised in water and lyophilised.

The linear peptides were purified by semi-preparative HPLC on a Waters system, as described for 37TD-WT and 37TD-R337H. The lyophilised peptide (tetra-β-3-arginine *S*) was dissolved in 30% acetonitrile in water and 9 ml of the solution was injected. The flow rate was 6.6 ml/min, solvent A=0.1% TFA in water, solvent B=0.1% TFA in acetonitrile. Elution was carried out with linear 30-70% gradients of solvent B into A over 40 min, with UV detection at 220 nm. The peptides of the 2nd generation were purified with linear 50-100% gradients of solvent B into A over 35 min.

Cyclisation in solution

The purified linear peptides were cyclised head-to-tail in solution using PyBOP (3 eq), HOAt and DIPEA in 1% DMF in DCM. The concentration of the linear peptide was 1 mM and the reaction was speed up using microwaves (MW) for 30 min. The cyclic peptides were purified by semi-preparative HPLC with the same gradient as for their corresponding linear peptides (30-70% gradients of solvent B into A over 40 min for cyclo-tetra-β-3-arginine *S*; 50-100% gradients of solvent B into A over 35 min for the other cyclic peptides).

Side-chain deprotection and purification

The side chain deprotection was achieved using a cocktail of 95% TFA, 2.5% H_2O, 2.5% TIPS. The reaction occurred at RT for 3 h. The final peptides were purified by semi-preparative HPLC in isocratic gradient of 100% of water.

Fractions corresponding to the pure peptides (> 85%) were collected, combined, lyophilised and stored at -20 ºC. The final products were characterised by UPLC-MS,

UPLC, and LTQ-FT MS and they were quantified by amino acids analysis, as described for the 37TDs.

Calix[4]arene synthesis and characterisation

Synthesis. All the reactions were carried out under N_2 atmosphere with dry solvents. All commercially available reagents were used without further purification.

Chromatography. Reactions were monitored by thin layer chromatography (TLC) performed on DC-Fertigplatten SIL UV_{254} (MACHEREY-NAGEL GmbH) or by analytical ultra high performance liquid chromatography (UPLC) with RP-C_{18} column Symmetry300^{TM} C_{18} 5 µm 4.6 x 150 mm, UV210-220, 1µl inj., 1 ml/min flux.

Analysis. Yields refer to chromatographically pure compounds. ^{1}H NMR and ^{13}C NMR spectra were recorded on a Brucker Avance 400 MHz UltraShield spectrometer (^{1}H: 400 MHz, ^{13}C: 100 MHz) and are reported in part per millions (ppm) relative to the residual solvent peak. Data for ^{1}H are reported as follow: chemical shift (δ ppm), multiplicity (s = singlet, bs = broad singlet, d = doublet, dd = double doublet, t = triplet, q = quartet, m = multiplet), coupling constants (Hz), and integration. Exact masses were measured on a Waters LCQ-FT MS.

For the synthesis of calix[4]arenes we followed the synthetic approach previously reported by Martos[124] and Gordo *et al*.[80] with minor modifications (Scheme 1).

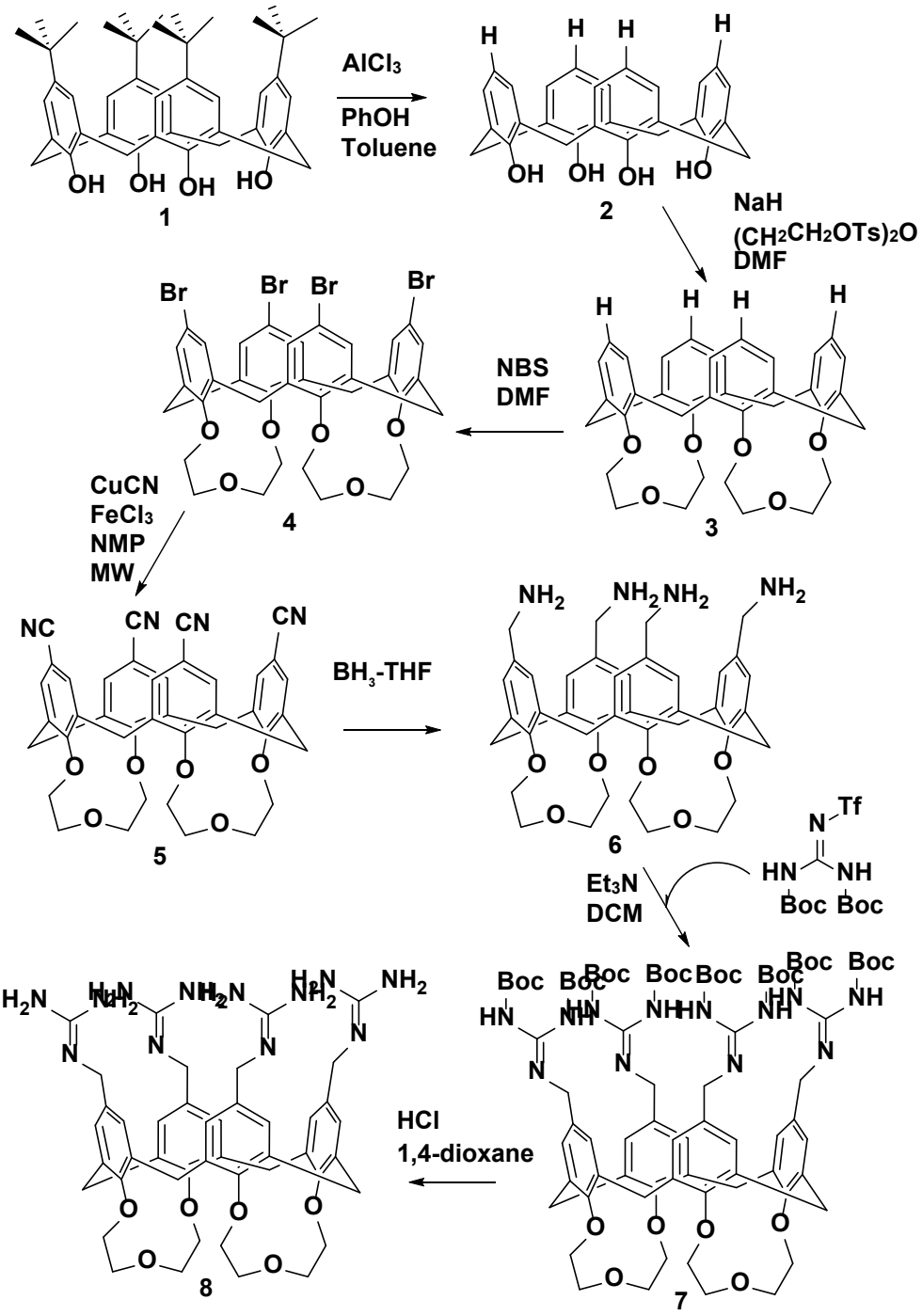

Scheme 1. Synthesis pathway to obtain 5,11,17,23-Tetraguanidiniummethyl-25,26,27,28-biscrown-3-calix[4]arene (**8**).

Step 1: dealkylation

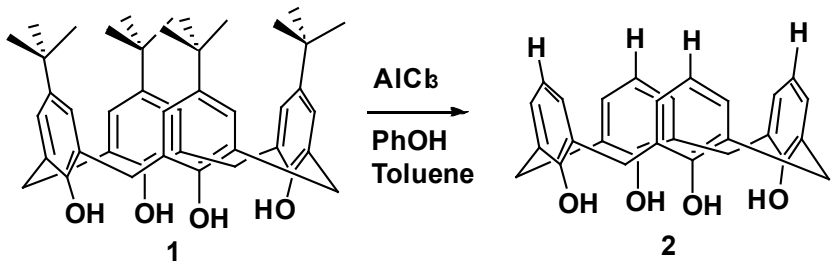

To a suspension of the t-butyl calixarene (6 g, 9.24 mmol) in dry toluene (90 ml), phenol (921 mg, 9.79 mmol) and $AlCl_3$ (6.16 g, 46.2 mmol) were added sequentially. The mixture turned to red after the addition of $AlCl_3$ and to brownish after 15-20 minutes. The mixture was stirred at RT under N_2 atmosphere for 18 h. Afterwards the reaction was quenched with 50 ml of HCl 1M and it was stirred an additional hour at RT. The mixture turned to yellow. DCM was added to the mixture and the aqueous phase was extracted with DCM (3 x 50 ml). The combined organic layers were washed with H_2O and brine, dried over $MgSO_4$ and filtered. The crude material was obtained removing the solvent under reduced pressure, resulting in a suspension with yellow solid, most probably due to the presence of *tert*-butoxybenzene. The product was triturated with 10-15 ml of cold Et_2O (3 times).[139] The mixture was sonicated and the supernatant was removed. The product was obtained as a white solid (3.324 g, Y=85%).

The product was analysed and characterised by TLC, eluent 9:1 hexane, EtOAc (R_f = 0,14), UPLC-MS G0100 retention time 1.57 min, 425.48 m/z (M+1). ^{1}H NMR ($CDCl_3$): δ 10.19 (s, 4H, OH), 7.05 (d, *J* = 7.6 Hz, 8H, ArH_m), 6.72 (t, *J* = 7.6 Hz, 4H, ArH_p), 4.26 (bs, 4H, Ar-C*H*$_2$-Ar), 3.54 (bs, 4H, Ar-C*H*$_2$-Ar).

^{13}C NMR (101 MHz, $CDCl_3$) δ 148.92 (CAr), 129.12 (CHAr), 128.38 (CAr), 122.39 (CHAr), 31.86 (CH_2).

Exact Mass: 425.17489 $[M+H]^+$, 442.20128 $[M+NH_4]^+$.

Step 2: bridges lower rim

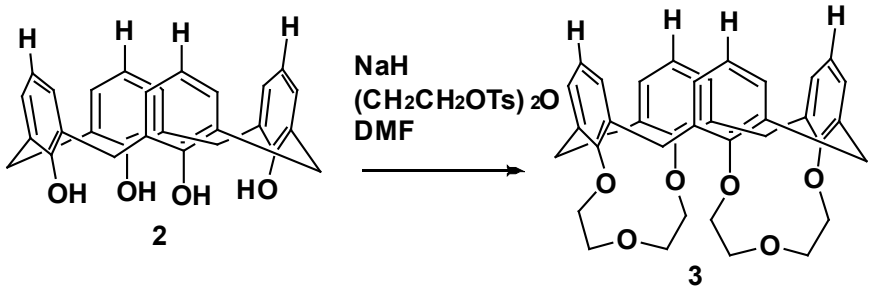

The starting material (1.6 g, 3.8 mmol) was dissolved in dry DMF (400 ml) and NaH (1.2 g 60% dispersion in oil, 30.8 mmol) was added. The solution was warmed up to 80 °C and it was stirred under N_2 atmosphere. By warming the solution became opalescent and whitish. The ditosylate (3.9 g, 9.5 mmol) previously dissolved in dry DMF was added and the reaction was stirred under inert atmosphere at 80 °C overnight. The following day, NaH was quenched with H_2O, added dropwise until any bubbles were detected.[140] The mixture was concentrated at rotary evaporator and the crude material was extracted with EtOAc and an aqueous solution of HCl 2M. The crude material was a yellow/orange oil. The crude material was purified by flash chromatography, eluent 5:1 hexane EtOAc. The product obtained was a white solid (700 mg, Y=33%).

The product was analysed by UPLC-MS, G6080, retention time 1.25 min, m/z 565 (M+1). ^{1}H NMR ($CDCl_3$) δ 7.04 – 6.96 (m, 8H, ArH), 6.73 (t, *J* = 7.5 Hz, 4H, ArH), 5.03 (d, *J* = 12.1 Hz, 2H, ArCH*Hax*Ar), 4.50 (d, *J* = 12.1 Hz, 2H, ArCH*Hax*Ar), 4.30 – 4.23 (m, 12H, CH_2O), 3.88 (ddd, *J* = 11.5, 9.3, 3.5 Hz, 4H, CH_2O), 3.26 (d, *J* = 12.1 Hz, 2H, ArCH*Heq*Ar), 3.22 (d, *J* = 12.1 Hz, 2H, ArCH*Heq*Ar).

^{13}C NMR (101 MHz, $CDCl_3$) δ 155.21 (CAr), 135.69 (CAr), 135.51 (CAr), 129.03 (CHAr), 128.08 (CHAr), 123.78 (CHAr), 76.38 (CH_2O), 74.81 (CH_2O), 30.81 ($ArCH_2Ar$), 29.85 ($ArCH_2Ar$).

Exact Mass: 565.25921 $[M+H]^+$, 582.28598 $[M+NH_4]^+$.

Step 3: bromination of the upper rim

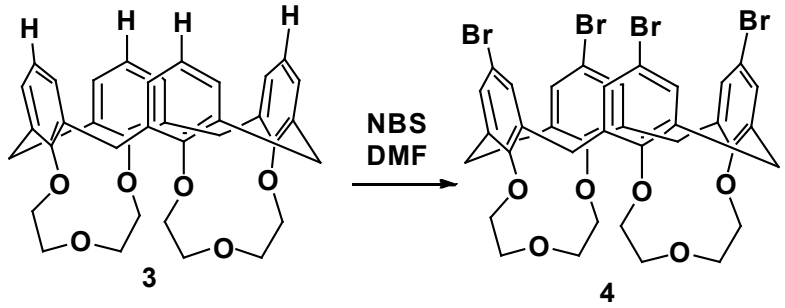

The starting material (700 mg, 1.24 mmol) was dissolved in dry DMF (23 ml) and NBS (1.8 g, 10.2 mmol) was added. The solution turned to yellow and it was stirred at RT under N_2 atmosphere for 24 h. After 5 h the solution turned to orange. The following day 30 ml of HCl 2M were added and the product precipitated. The solid was filtered in a Buchner funnel and it was recrystallized from CH_3OH. The product was obtained as a white solid (900 mg, Y=82%) and it was analysed by UPLC-MS.

UPLC-MS, G6080, retention time 1.80 min, m/z 880 (M+1), 896 (M+18), 901 (M+23).

^{1}H NMR ($CDCl_3$) δ 7.13 (dd, *J* = 8.6, 2.4 Hz, 8H, ArH), 4.96 (d, *J* = 12.2 Hz, 2H, ArCH*Hax*Ar), 4.37 (d, *J* = 12.2 Hz, 2H, ArCH*Hax*Ar), 4.20 (ddd, *J* = 15.9, 12.0, 9.1 Hz, 12H, CH_2O), 3.77 (td, *J* = 10.7, 2.1 Hz, 4H, CH_2O), 3.19 (d, *J* = 12.2 Hz, 2H, ArCH*Heq*Ar), 3.13 (d, *J* = 12.2 Hz, 2H, ArCH*Heq*Ar).

^{13}C NMR (101 MHz, $CDCl_3$) δ 154.58 (CAr), 137.13 (CAr), 136.92 (CAr), 132.19 (CHAr), 131.21 (CHAr), 116.51 (CAr), 76.72 (CH_2O), 74.70 (CH_2O), 30.40 ($ArCH_2Ar$), 29.61 ($ArCH_2Ar$).

Exact Mass: 876.90200 $[M+H]^+$.

Step 4: cyanation of the upper rim

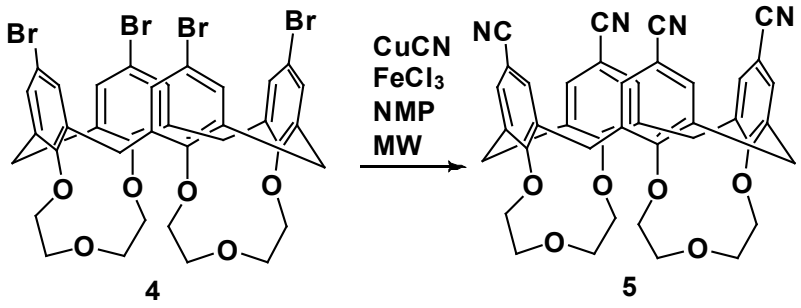

The starting material (517 mg, 0.587 mmol) and CuCN (380 mg, 4.23 mmol) were dissolved in anhydrous NMP (3 ml) in a microwave tube. The solution was yellowish and the mixture was allowed to react at 200 °C with MW for 40 minutes.[124] When the reaction was worked up, the solution was dark red. A solution of $FeCl_3$ (1.075 g, 6.63 mmol) in HCl 1M (20 ml) was added in order to quench the reaction and the mixture was stirred at RT for 30 minutes. The product precipitated and it was filtered in a Buchner funnel. The reaction was worked up when the UPLC-MS did not show any intermediate products. The desired product eluted at 1.10 min with linear gradient 50-100% ACN in water. The crude material was purified by silica gel flash chromatography, eluent 95:5 DCM:EtOAc. The pure product was a white solid (279 mg, Y=72%), which was analysed by UPLC-MS.

UPLC-MS, G50100 retention time 0.83 min, m/z 665.483 (M+1), 683.546 (M+18)

TLC eluent 95:5 DCM EtOAc R_f=0.27

^{1}H NMR ($CDCl_3$) δ 7.74 (m, 8H, ArH), 5.03 (d, *J* = 12.3 Hz, 2H, ArCH*Hax*Ar), 4.40 (d, *J* = 12.3 Hz, 2H, ArCH*Hax*Ar), 4.36 – 4.14 (m, 12H, OCH_2), 3.83 (t, *J* = 10.0 Hz, 4H, OCH_2), 3.33 (d, *J* = 12.4 Hz, 2H, ArCH*Heq*Ar), 3.29 (d, *J* = 12.4 Hz, 2H, ArCH*Heq*Ar).

^{13}C NMR (101 MHz, $CDCl_3$) δ 158.64 (CAr), 136.34 (CAr), 136.11 (CAr), 134.74 (CHAr), 133.49 (CHAr), 119.34 (CN), 108.28 (CAr), 77.13 (CH_2O), 75.05 (CH_2O), 29.60 ($ArCH_2Ar$), 28.87 ($ArCH_2Ar$).

Exact Mass: 665.24038 $[M+H]^+$, 682.26701 $[M+NH_4]^+$.

Step 5: reduction of cyano groups

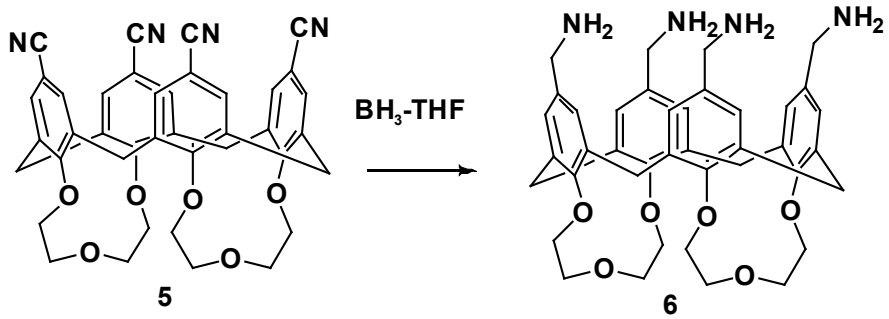

To a two-neck flask, the starting material (149 mg, 0.224 mmol) was added and it was dissolved in a solution of BH_3-THF 1M (7 ml) at 0 °C, under N_2 atmosphere. The reaction was warmed up to 75 °C and the mixture was stirred for 24 h. The following day CH_3OH (1 ml) and HCl 1M (3 ml) were added dropwise to the mixture, which was stirred at 50 °C for 30 minutes. The aqueous phase was extracted with DCM. To the aqueous phase pellet of NaOH were added until the product precipitated.[141] The

suspension was centrifuged and the supernatant was removed. The product was obtained as a white solid (441 mg). Any yield was calculated because the product was achieved in salty form.

UPLC-MS G0100, retention time 0.94 min, m/z 681.586 (M+1), 703.710 (M+23)

^{1}H NMR (CD_3OD) δ 7.12 (s, 8H, ArH), 5.06 (d, *J* = 11.8 Hz, 2H, ArCH*Hax*Ar), 4.55 (d, *J* = 12.0 Hz, 2H, ArCH*Hax*Ar), 4.41 – 4.22 (m, 12H, OCH_2), 3.79 (t, *J* = 10.0 Hz, 4H, OCH_2), 3.61 (s, 8H, CH_2N), 3.31 (d, *J* = 11.4 Hz, 2H, ArCH*Heq*Ar), 3.23 (d, *J* = 11.4 Hz, 2H, ArCH*Heq*Ar).

^{13}C NMR (101 MHz, CD_3OD) δ 156.59 (CAr), 137.37 (CAr), 130.91 (CAr), 130.49 (CHAr), 129.56 (CHAr), 77.71 (CH_2O), 75.90 (CH_2O), 44.65 (CH_2N), 30.74 ($ArCH_2Ar$), 30.55 ($ArCH_2Ar$).

Exact Mass: 681.36536 $[M+H]^+$.

Step 6: guanidinilation of the upper rim

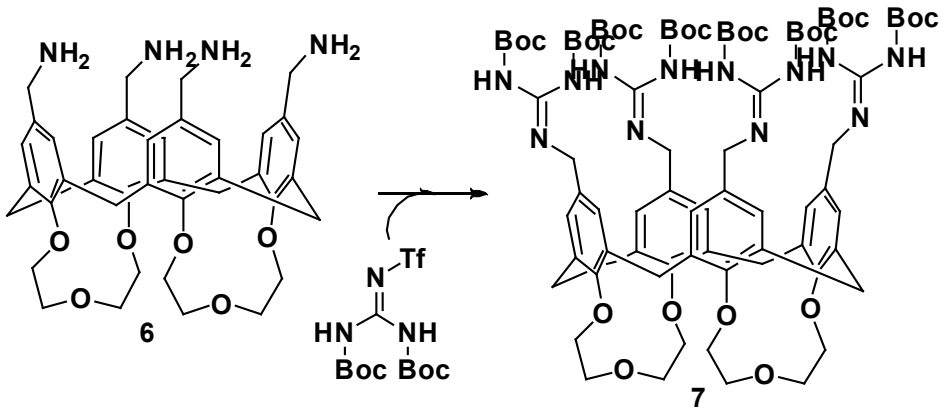

The starting material (**6**, 114 mg) was dissolved in dry DCM (2 ml) and Et_3N (190 µl) was added. The Tf-guanidinium$(Boc)_2$ (263 mg) was dissolved in dry DCM (1 ml) and it was added to the mixture. The mixture was stirred at RT under N_2 atmosphere for 48 h.[142] After 6 h a new aliquot of Et_3N (100 µl) was added again. After 2 days, the mixture was washed with HCl 1M (2 x 5 ml), H_2O (5 ml) and brine (5 ml). The organic layers were combined and dried over Na_2CO_3. The solvent was evaporated in order to get the crude material that was purified by silice gel flash chromatography, eluent from 4:1 hexane EtOAc to 100% EtOAc. The product was obtained as a white solid (82 mg, Y=30%).

UPLC-MS, G0100 any product was found. The compound does not absorb at UV and any mass corresponding to the product was detected.

TLC, eluent 4:1 hexane EtOAc R_f=0. The product was detectable through oxdidation with permanganate.

^{1}H NMR ($CDCl_3$) δ 8.63 (s, 4H, NH), 6.98 – 6.95 (m, 8H, ArH), 4.98 (d, *J* = 12.0 Hz, 2H, ArCH*Hax*Ar), 4.51 – 4.17 (m, 22H, ArCH*Hax*Ar, OCH_2, CH_2N), 3.89 – 3.78 (m, 4H, OCH_2), 3.24 (d, *J* = 12.4 Hz, 2H, ArCH*Heq*Ar), 3.19 (d, *J* = 12.2 Hz, 2H, ArCH*Heq*Ar), 1.48 (2s, 72H, t-Bu).

^{13}C NMR (101 MHz, $CDCl_3$) δ 163.73 (CO), 156.67 (CO), 155.89 (CGuan), 154.92 (CGuan), 153.21 (CAr), 152.00 (CAr), 135.80 (CAr), 135.64 (CAr), 132.20 (CHAr), 128.72 (CHAr), 86.09 ($C(CH_3)_3$), 83.10 ($C(CH_3)_3$), 79.23 (CH_2O), 75.00 (CH_2O), 45.67 (CH_2Guan), 29.84 ($ArCH_2Ar$), 28.45 ($ArCH_2Ar$), 28.22 ($C(CH_3)_3$), 27.99 ($C(CH_3)_3$).

Exact Mass: 1548.81464 M-1Boc; 1448.76217 M-2Boc; 1348.70940 M-3Boc, 1248.65655 M-4Boc, 1148.60385 M-5Boc, 1048.55097 M-6Boc, 948.49806 M-7Boc, 848.44606 M-8Boc.

Step 7: Boc deprotection

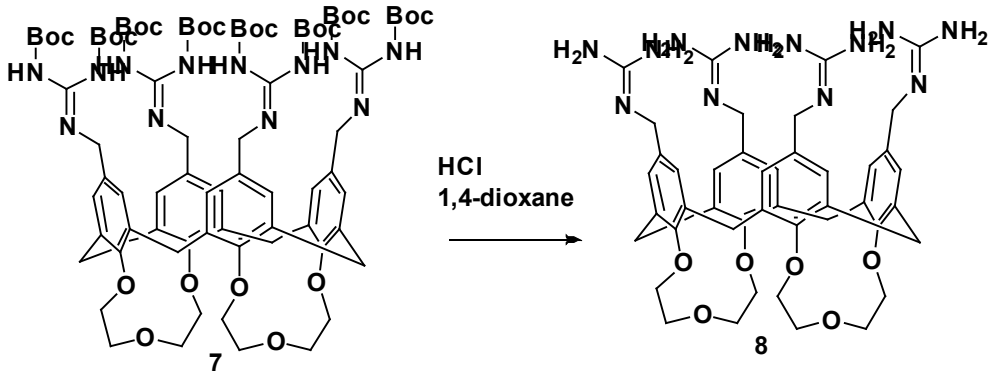

The starting material (70 mg, 0.042 mmol) was dissolved in dry 1,4-dioxane (4 ml) and concentrated HCl (300 µl) was added. The reaction was stirred under N_2 atmosphere at RT for 24 h. The reaction was monitored by UPLC-MS and aliquots of concentrated HCl were added if necessary. After 24 h the solvent was evaporated and the solid was triturated with EtOAc. The crude material was a yellowish solid (30 mg, Y=83 %). The product was purified by semi-preparative HPLC with a linear gradient 10-45% of CH_3CN in H_2O. The product obtained was a white solid.

^{1}H NMR (CD_3CN) δ 8.20 (t, *J* = 6.3 Hz, 4H, Guan), 7.10 (s, 8H, ArH), 6.97 (bs, 12H, Guan), 5.02 (d, *J* = 11.9 Hz, 2H, $ArCH_2Ar$), 4.48 (d, *J* = 12.1 Hz, 2H, $ArCH_2Ar$), 4.26 - 4.22 (m, 12H, OCH_2), 4.15 (d, *J* = 6.5 Hz, 8H, CH_2Guan), 3.76 – 3.67 (m, 4H, OCH_2), 3.27 (d, *J* = 12.1 Hz, 2H, $ArCH_2Ar$), 3.20 (d, *J* = 11.9 Hz, 2H, $ArCH_2Ar$).

^{13}C NMR (101 MHz, CD_3CN) δ 158.60 (CAr), 155.82 (CGuan), 136.97 (CAr), 133.31 (CAr), 128.99 (CHAr), 128.01 (CHAr), 77.68 (CH_2O), 75.49 (CH_2O), 44.60 (CH_2Guan), 30.82 ($ArCH_2Ar$), 30.08 ($ArCH_2Ar$).

Exact Mass: 849.45242 $[M+H]^+$.

BIOPHYSICS

Circular Dichroism (CD)

The lyophilised peptides were dissolved either in 50 mM sodium phosphate buffer, pH 7, or in water, pH 7, to a final monomer concentration of 20 µM. The spectra were recorded in a Jasco J-810 spectropolarimeter equipped with a Jasco-CDF-426S Peltier thermostated cell holder and a Julabo external bath. Each CD spectrum was obtained by averaging three scans, recorded at 10 nm/min, DIT of 4 s, band width 1 nm, T = 25 °C, and λ 190-260 nm, using a 1 mm path length quartz cell. Experimental data were smoothed using the software package provided by Jasco (Spectra Manager software).

CD unfolding curves

CD unfolding curves were recorded measuring CD ellipticity at 220 nm while heating from 15 to 95 °C at 1.5 °C min^{-1} with 4 s response time, 1 nm bandwidth, and 0.1 °C data pitch. CD spectra of the initial temperature were also recorded after having performed the experiment. Recorded data were processed in Spectra Manager software, normalising concentration and smoothing by binomial factor. The initial and final baseline slopes were also corrected by subtraction of a slope straight line. Data were transformed into normalised unfolded fraction in Excell considering a two-state unfolding model. Comparison of the CD spectra before and after running the unfolding experiment was done in Spectra Manager software.

Native Mass Spectrometry

MS samples were prepared by dissolving lyophilised peptides in 200 mM ammonium acetate buffer, pH 7, to a final monomer concentration of 100 µM. The samples were further cleaned from salts by centrifugation in a Viva spin 500 with 3 kDa cut off (11500 rpm, 4 °C, 20 min, three times). The final concentration was estimated by NanoDrop at 280 nm. The samples were stored in ice during the acquisition. Experiments were performed on a Synapt G1 HDMS (Waters) equipped with an Advion TriVersa NanoMate (Advion Biosciences). The positive mode for ESI was used. The source temperature, the voltages, and the parameters are summarised in Table 13. Acquisitions were performed in the m/z range of 800 – 7000 with a 1.5 s

scan time. Spectra were smoothed (smoothing method, mean; smooth window, 3; number of smooths, 2) with MassLynx V4.1 software (Waters). Definitive voltages for the capillary and the cone were tuned according to the threshold values (Table 13). These parameters were optimized to 1.5-1.75 kV and 20 V for the capillary and the cone, respectively. In order to facilitate ion transmission in the trap region, collision energy (CE) and bias were kept at the minimum value (6 V and 15 V, respectively); higher values caused unfolding of gaseous protein ions.[143] Finally, the backing pressure was minimised in order to avoid possible structural interactions of POP gasseous ions;[94] lower values than those recommended by Ruotolo *et al.* were chosen.[144] In addition, all these voltages and pressures were compatible for native calibrating protein ions.

The ion mobilograms were analysed using DriftScope 2.5 software and displayed with m/z versus ms (milliseconds).

Source T	Bias	Trap	Transfer	Backing	Wave velocity (IM)	Wave height (IM)
40 °C	4 V (TOF) 15 V (IM)	6 V	4 V	5.7-5.9 mbar	300 m/s	8V

Table 13. Conditions of native MS experiments.

Nuclear Magnetic Resonance (NMR)

NMR spectra were acquired on a Bruker 600 MHz spectrometer equipped with a TCI cryoprobe. The NMR samples were prepared by dissolving the lyophilised peptides in D_2O at a final monomer concentration of 100 µM. The pD was adjusted using the equation:

pD = pH + 0.4 [145]

Chemical shifts were referenced to internal DSS (4,4-dimethyl-4-silapentane-1-sulfonic acid) at 0,0 ppm. The HSQC of 37TDs and 74TDs, as well as the spectra of the binding experiments were recorded at different temperatures, *i.e.* 25, 5, 37, or 40 °C.

X-STE NMR diffusion experiments

Diffusion NMR experiments of 37TDs (100 µM) were performed at 25 °C using an in-house modified X-STE pulse sequence[100] to measure the diffusion of ^{13}C-attached ^{1}H. Encoding/decoding gradient lengths (δ) of 2.7-3.0 ms and diffusion delays (Δ) of 100-120 ms were used. Diffusion measurements under identical experimental conditions

were carried out for 1,4-dioxane. In this case the PG-SLED sequence[102] was used applying a gradient time (δ) of 1.8 ms and a diffusion time (Δ) of 70 ms. Diffusion coefficients (D^{37TD} and D^{diox}) were obtained fitting the gradient strength-dependent decay in signal intensity to a mono exponential equation using the MestreNova software.

Hydrodynamic radii of 37TDs (R_H^{37TD}) were deduced using the following equation:

$$R_H^{37TD} = (D^{diox}/D^{37TD}) * R_H^{diox}$$

Assuming that R_H^{diox} is 2.12 Å.[102]

Predicted hydrodynamic radii were calculated from empirical equations for folded proteins:[101]

$$R_H = 4.75 * N^{0,29}$$

and for disordered proteins:

$$R_H = (1.24 * P_{Pro} + 0.904) * (0.00759 * |Q| + 0.963) * 2.49* N^{0,509}$$

Where N is the number of residues (37, 74, and 148 for monomer, dimer, and tetramer, respectively), P_{Pro} is the fraction of proline residues, and |Q| the absolute net charge. |Q| was calculated at pH 7 using the Protein Calculator v3.4 software (http://protcalc.sourceforge.net).

NMR chemical-shift-perturbation

^{1}H NMR spectra were acquired at 5 and 37 ºC. The ligands (R4, K3R, and Rab4) were dissolved in 10% D_2O in water at a final concentration of 20 µM. The ligands were titrated with 10, 20, and 40 µM of 37TD-R337H to detect perturbation on the aromatic signals of the indole group. Chemical shifts were referenced to internal DSS at 0,0 ppm.

Conformational study by NOESY and TOCSY NMR experiments

To assess the solution structure of Rab4 and cRys2R2, 2D homo- (NOESY and TOCSY) and natural abundance hetero-nuclear ^{1}H ^{13}C HSQC spectra were acquired at 5 ºC. The TOCSY and NOESY mixing times were 70 and 200 ms, respectively. Suppression of water signal was achieved by exicitation sculpting. The samples were dissolved in 10% D_2O in water at a final concentration of 2 mM. ^{1}H chemical shifts were referenced to internal DSS. After having assigned the signals in the spectra, we used the software δ2D (https://www-cohsoftware.ch.cam.ac.uk/), developed by Camilloni *et al*.[129] to calculate secondary structure populations based on the proton and carbon chemical shifts of the residues.

Microscale Thermophoresis (MST)

MST was used to calculate the binding affinities in solution of our p53TD. To this end, 37TDs were fluorescently labelled by reaction of the Lys side chains with NT-647-NHS (3.5 eq) for 30-45 min at room temperature in the dark. The labelled peptide was purified by Mini G-10 column eluting with PBS buffer. The concentration of the peptide in the elution fraction was estimated using the Pierce colorimetric peptide assay measuring the absorbance at 480 nm. MST binding assays were performed on a Monolith NT.115 instrument (NanoTemper Technologies) with standard capillaries at 25 °C. Nano RED excitation colour, medium MST power and a potency of 20% of the LED were set as experimental parameters in the machine. Fluorescently labelled peptides were diluted to a final concentration of 15-50 nM (Table 14) with HEPES 50 mM + 0.05% Tween 20, pH 7. These solutions were used to prepared a 16-sample dilution series, where the labelled peptide (target) was titrated with increasing amount of 'cold' peptide (ligand, not labelled) (Table 14). The thermophoresis response was baseline-corrected and normalized (ΔFnorm [‰]). The curves were analysed using a standard Langmuir binding model, from which dissociations constants (K_D) were determined. The experiment was performed in triplicate.

p53 domain	[TD*] (target)	Highest [TD] (ligand)
37TD-WT	15 nM	500 µM
37TD-R337H	15 nM	500 µM
37TD-D352H	10 nM	1 mM
37TD-R342L	15 nM	500 µM
37TD-T329I	15 nM	500 µM
37TD-L344R	50 nM	1 mM
37TD-L344P	10 nM	2 mM
74TD-L330C	30 nM	1 mM
74TD-L344C	15 nM	2 mM

Table 14. MST experimental conditions.

Concerning the binding experiments with calix[4]arene (**8**), the conditions are reported in Table 15. Either the monomer of 37TD-WT and 37TD-R337H or the tetramer were titrated with the ligand (**8**). The tetramer was formed in solution by adding the corresponding TD (*ca*. 10 times the K_d of tetramerisation, Table 4) not fluorescently labelled.

p53 domain	[TD*] (target)	[TD] (target)	Highest [8] (ligand)
37TD-WT	15 nM	-	2 mM
37TD-WT	15 nM	4 µM	2 mM
37TD-R337H	15 nM	-	2 mM

37TD-R337H	15 nM	10 µM	2 mM

Table 15. MST experimental conditions with calix[4]arene (**8**).

Fluorescence spectroscopy

Fluorescence data were collected with an Aminco Bowman Series2 fluorescence spectrophotometer with a scan resolution of 1 nm/s. A set of 400 µL solutions of linear ligands (R4, K3R, and Rab4) in water was prepared, and small aliquots of a concentrated 37TD-WT and 37TD-R337H solution were added. The volume of the aliquots was small enough to ensure that dilution was less than the 5%. The mixture in a 1 cm path length fluorescence cuvette was irradiated at 295 nm, to selectively excite tryptophan residues, and fluorescence emission was recorded from 310 to 450 nm. Residual fluorescence from the tyrosine of TDs was subtracted by performing a blank titration. Data were processed with Excell.

Stability in human serum

A solution of peptide in HBSS was mixed with human serum to reach a final peptide concentration of 300 µM in 50% serum. The mixture was incubated at 37 °C for 24 h in an orbital shaker. At various time points (0, 5, 15, and 30 min, and 1, 2, 5, 12, and 24 h), 150 µL were taken and precipitated with 100 µL cold solution of 15% TFA in water. After 15 minutes in ice and 15 minutes centrifugation at 4 °C, 12500 rpm, the supernatant was filter and analysed by HPLC (20 minutes linear gradient of 15-35% ACN in water for Rab4 and 5-25% ACN in water for cRys2R2) to calculate the percentage of intact peptide in the sample. The data were analysed in GraphPad Prism 8.

XTT Citotoxicity assay

HeLa cells were seeded in 96-well plates, 3500 cells per well, 24 h before starting the assay. Solutions of studied compounds (Rab4 and cRys2R2 peptides and calix[4]arene (**8**)) at concentration of 200 µM were prepared in DMEM (4.5 mg/mL glucose) supplemented with 10% serum and they were progressively diluted 1:4 to reach a total of seven solutions per compound. These solutions were added to the cells and they were incubated for 4 and 24 h at 37 °C. Two hours before the reading, XTT reagent at concentration of 0.5 mg/ml was added (50 µl in each well) and incubated for 2 h to be reduced by mitochondrial active cells. After this time, absorbance was measured at 485 and 680 nm, where the latter reading was subtracted from the first one. The data were normalised considering 100% of cell viability the absorbance of the untreated cells and 0% either the absorbance of solution without cells or the absorbance of cells treated with 1% SDS. Each measurement was done in triplicate and the values obtained were processed in GraphPad Prism 8 to calculate the IC50 of each compound.

COMPUTATIONAL STUDIES

Molecular Dynamics (MD, GROMACS)

Unrestrained molecular dynamics (MD) simulations were performed with GROMACS version 2019.6. To generate the starting structures, residues 320 to 356 of p53 were extracted from the Protein Data Bank (PDB) code 1OLG.[28] For the p53 L330C and L344C mutants, the corresponding residues in each of the structures were mutated to Cys and the inter-chain disulphide linkages were manually introduced. The input structures were solvated in a pre-equilibrated dodecahedron box of SPC water molecules with a 2.0 nm distance between the solute and the box. Chlorine or sodium ions were added to obtain an electrostatically neutral system with a physiological concentration of [NaCl] = 150 mM. The initial complex structure was first subjected to a steepest descent minimization protocol until a maximum force of 500 kJ/mol/nm or 20,000 minimization steps were reached. Thermalisation of the system was performed in the NVT ensemble during 100 ps, using a time step of 2 fs and increasing the temperature from 100 to 310 K, during which the LINCS method[146] was applied to restrain the position of the protein atoms. Prior to the production run, a short MD simulation (200 ps) in the NPT ensemble was done in order to equilibrate the system density to 1 bar and 310 K. The Parrinello-Rahman barostat[147] was used for the pressure coupling section. For the production runs, all position restraints on the proteins were removed and trajectories were collected for a total of 500 ns. The particle-mesh Ewald summation method was used to deal with long range electrostatic interactions and a cut-off of 10 Å was applied for non-bonded interactions. Bond lengths will be constrained to their equilibrium values using the LINCS method[146] which allows the use of a 2 fs time step for the integration of the equations of motions. Analysis of the MD trajectories was performed using the *gmx* module implemented in GROMACS. Cluster analysis of the protein structures extracted at regular time intervals of 0.1 ns was performed using the *gromos* algorithm.[148]

Docking (Maestro)

Molecular docking comprises 5 main steps: protein preparation, ligand preparation, receptor grid generation, ligand docking procedure and visual analysis of the docking results. The protein domain (p53TD, PDB ID 1OLG[28]) was subjected to preparation by *Protein Preparation Wizard* in Maestro Schrödinger, release 2017.[149] During preparation, the missing hydrogens were added, and partial charges were assigned using OPLS3 force field. Hydrogens and heavy atoms were optimized by restrained minimization.

Ligand structures were generated in *Build* section of Maestro[116] and they were converted to 3D structure via *Ligprep*[150] module. *Ligprep* corrects the protonation, and ionization states of the compounds, and assigned proper bond orders. Several conformations of the ligands were generated by *Conformational search* module.

The grid box was generated by *Receptor Grid Generation* tool in *Glide*, Maestro.[117] The grid box was defined by selecting the calix[4]arene (**8**) molecule inside the hydrophobic pocket of p53TD in a box of 15 Å. Rigid receptor docking protocol was run in Standard Precision (SP) and Extra-Precision (XP) modes of Glide based on OPLS3 force field. During the process of docking, the protein was fixed, while ligands were flexible.

Molecular Dynamics (MD, Maestro)

Molecular dynamics (MD) simulations study was performed starting from the docking complexes structures of p53TD-ligands by using Desmond as implemented in Schrödinger package.[122] The complexes were first solvated with predefined TIP3P water molecules in orthorhombic box of 10 Å. Counter ions were added to neutralise charges. The MD simulation was performed in the NPT ensemble at temperature of 300 K and 1.01325 bar pressure over 10 ns with recording intervals of 10 ps for trajectory and 1000 frames. Simulations were run with the OPLS3 force field and we used the option for relaxing the model before simulation. Finally, plots and figures were sketched with Desmond simulation interaction diagram tool of Maestro.

PRODUCT CHARACTERISATION AND SUPPLEMENTARY FIGURES

Peptide	Molecular formula	Calc. MW	Found MW[a]	Gradient	t_R UPLC or HPLC min	% Purity[b]
37TD-WT (not labelled)	$C_{197}H_{312}O_{59}N_{56}S$	4438.28559	4438.28981	0 – 70% ACN/H_2O 40 min	16.722	> 95
37TD-WT	$C_{196}{}^{13}CH_{312}O_{59}N_{56}S$	4439.28894	4439.29224	0 – 70% ACN/H_2O 40 min	16.881	> 95
37TD-R337H (not labelled)	$C_{197}H_{307}O_{59}N_{55}S$	4419.24339	4419.24725	0 – 70% ACN/H_2O 40 min	16.625	> 95
37TD-R337H	$C_{196}{}^{13}CH_{307}O_{59}N_{55}S$	4420.24674	4420.25107	0 – 70% ACN/H_2O 40 min	16.656	> 95
37TD-D352H	$C_{198}{}^{13}CH_{314}O_{57}N_{58}S$	4461.32091	4461.32512	5 – 60% ACN/H_2O 15 min	9.210	> 95
37TD-R342L	$C_{196}{}^{13}CH_{311}O_{59}N_{53}S$	4396.27189	4396.27627	5 – 60% ACN/H_2O 15 min	10.036	85
37TD-T329I	$C_{198}{}^{13}CH_{316}O_{58}N_{56}S$	4451.32533	4451.33161	5 – 60% ACN/H_2O 15 min	9.770	90
37TD-L344R	$C_{196}{}^{13}CH_{313}O_{59}N_{59}S$	4482.30599	4482.31032	5 – 60% ACN/H_2O 15 min	8.489	> 95
37TD-L344P	$C_{195}{}^{13}CH_{308}O_{59}N_{56}S$	4423.25764	4423.25888	5 – 60% ACN/H_2O 15 min	8.634	86
74TD-L330C	$C_{386}{}^{13}C_2H_{610}O_{118}N_{112}S_4$	8856.4111	8856.4241	5 – 60% ACN/H_2O 15 min	9.469	> 95
74TD-L344C	$C_{386}{}^{13}C_2H_{610}O_{118}N_{112}S_4$	8856.4111	8856.4179	5 – 60% ACN/H_2O 15 min	9.127	> 95
Cyclo-tetra-β-arginine *S*	$C_{28}H_{56}O_4N_{16}$	680.47	-	0 – 40% ACN/H_2O 20 min	3.160	> 95

R4	C_{61} H_{102} O_{16} N_{28}	1482.80286	1482.80423	0 – 50% ACN/H_2O 15 min	4.467	> 95
K3R	C_{61} H_{102} O_{16} N_{22}	1398.78441	1398.78855	0 – 100% ACN/H_2O 2 min	1.123	> 95
Rab4	C_{57} H_{94} O_{16} N_{28}	1426.74026	1426.74098	0 – 100% ACN/H_2O 2 min	1.173	> 95
cR4	C_{32} H_{62} O_8 N_{19}	840.50233	840.50414	0 – 40% ACN/H_2O 20 min	1.690	> 95
cRys2R2	C_{34} H_{66} O_8 N_{19}	868.53363	868.53594	0 – 40% ACN/H_2O 2 min	1.107	92
cRab4	C_{28} H_{54} O_8 N_{19}	784.43973	784.44134	0 – 40% ACN/H_2O 2 min	0.946	85
cRys4A	C_{39} H_{75} O_9 N_{20}	967.60204	967.60358	0 – 40% ACN/H_2O 2 min	1.279	> 95

Table S1. Molecular weight, chromatography retention times and purity of the synthetic peptides. [a]Measured by LQT-FT MS. [b]Measured by UPLC for 37TD-WT and 37TD-R337H sequences (either labelled or not) and for the ligands; measured by HPLC for the other 37TDs and 74TDs.

PRODUCT CHARACTERISATION

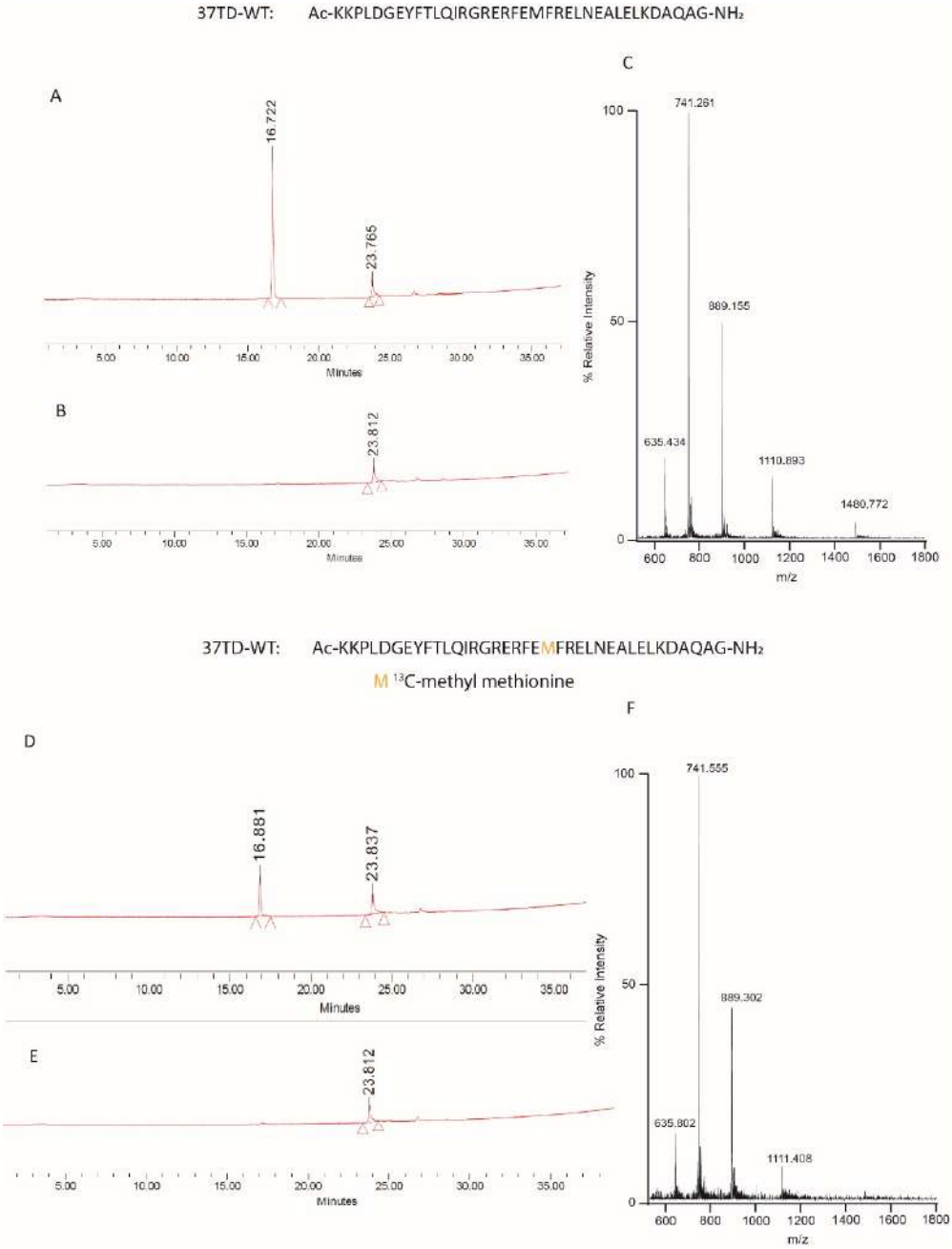

Figure S1. Characterisation of 37TD-WT, labelled and non-labelled peptides. UPLC of the peptides (A, D), UPLC of a blank run (B, E), and UPLC-MS (C, F).

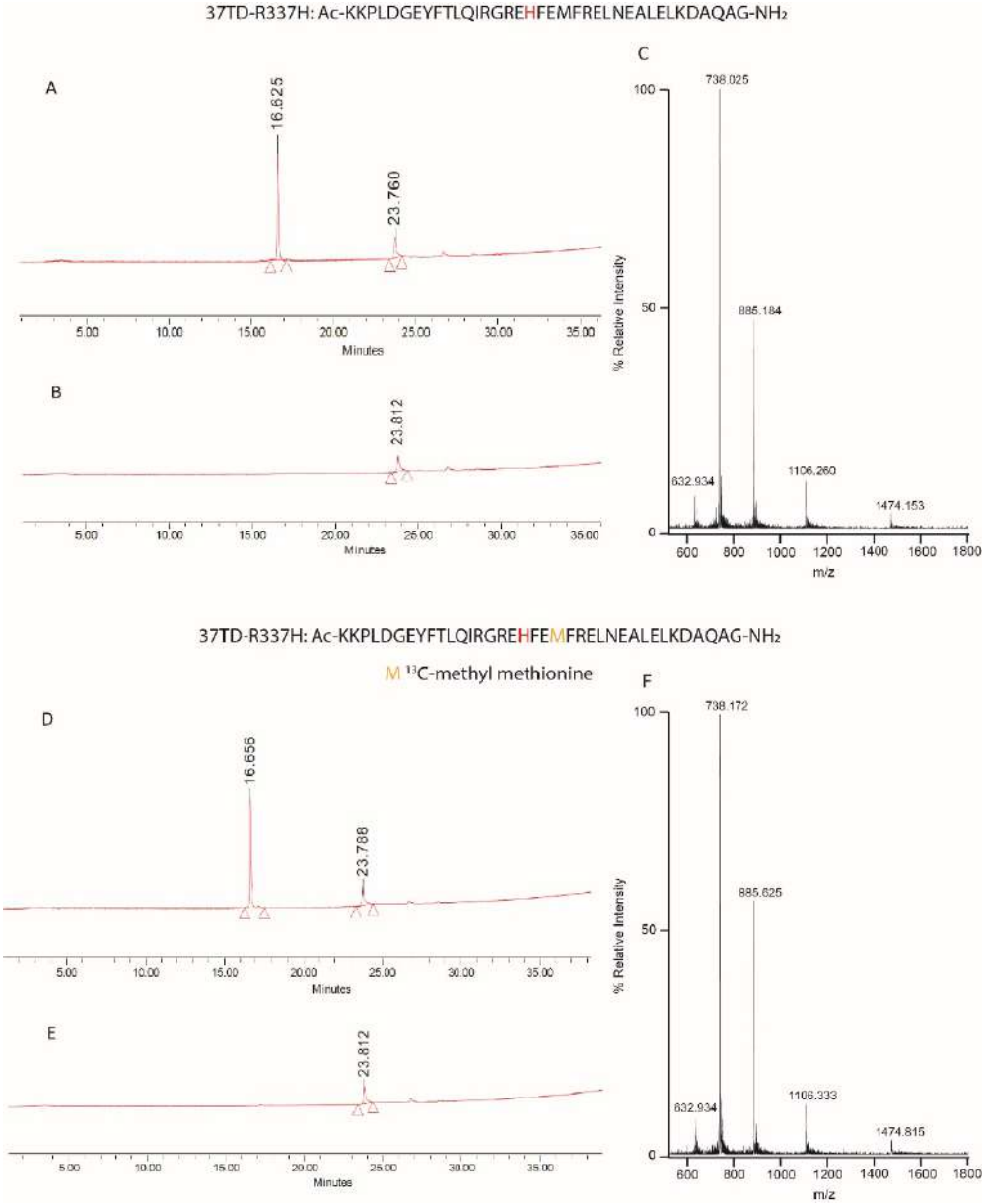

Figure S2. Characterisation of 37TD-R337H, labelled and non-labelled peptides. UPLC of the peptides (A, D), UPLC of a blank run (B, E), and UPLC-MS (C, F).

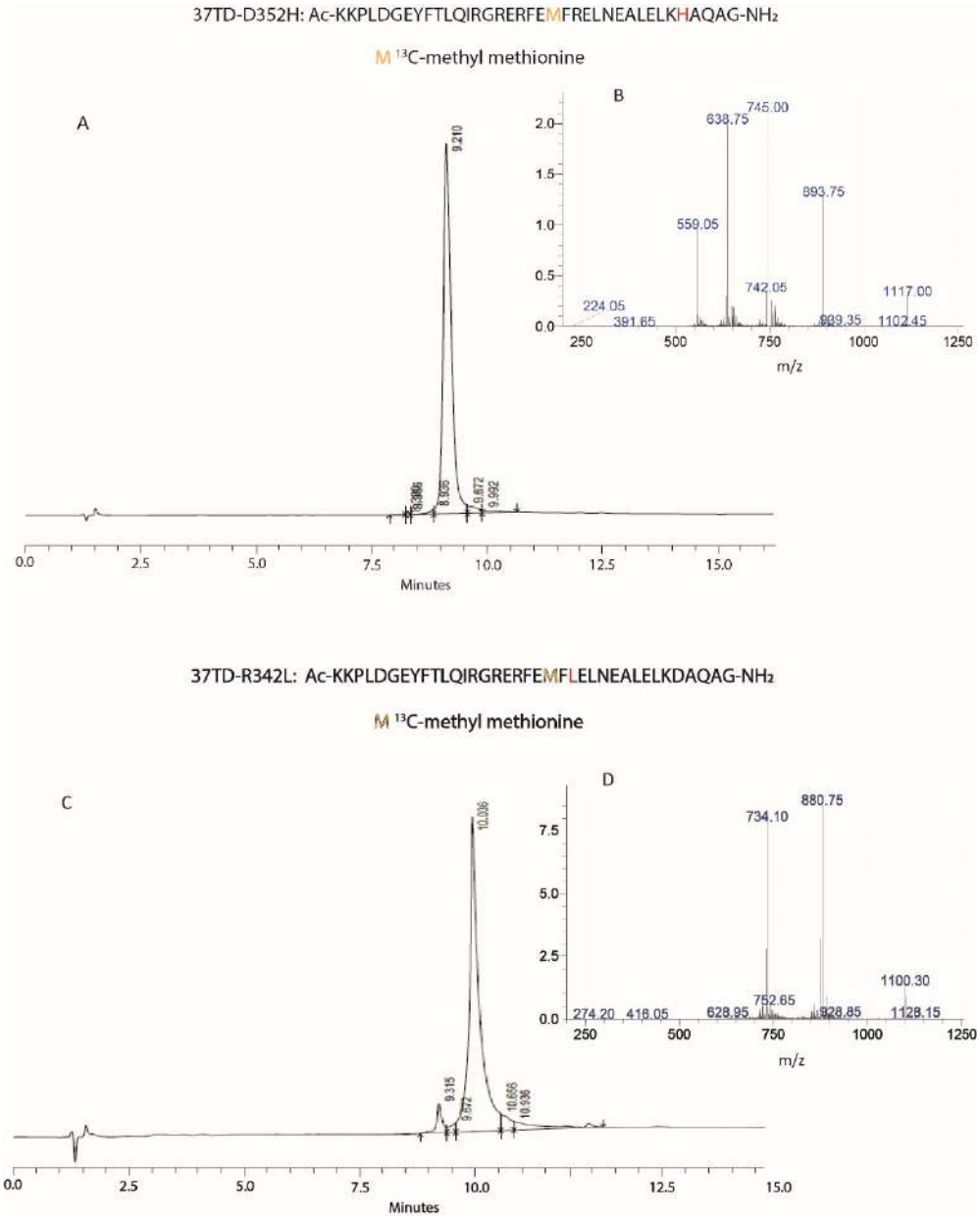

Figure S3. Characterisation of 37TD-D352H (A, B) and 37TD-R342L (C,D). HPLC of the peptides (A, C) and HPLC-MS (B, D).

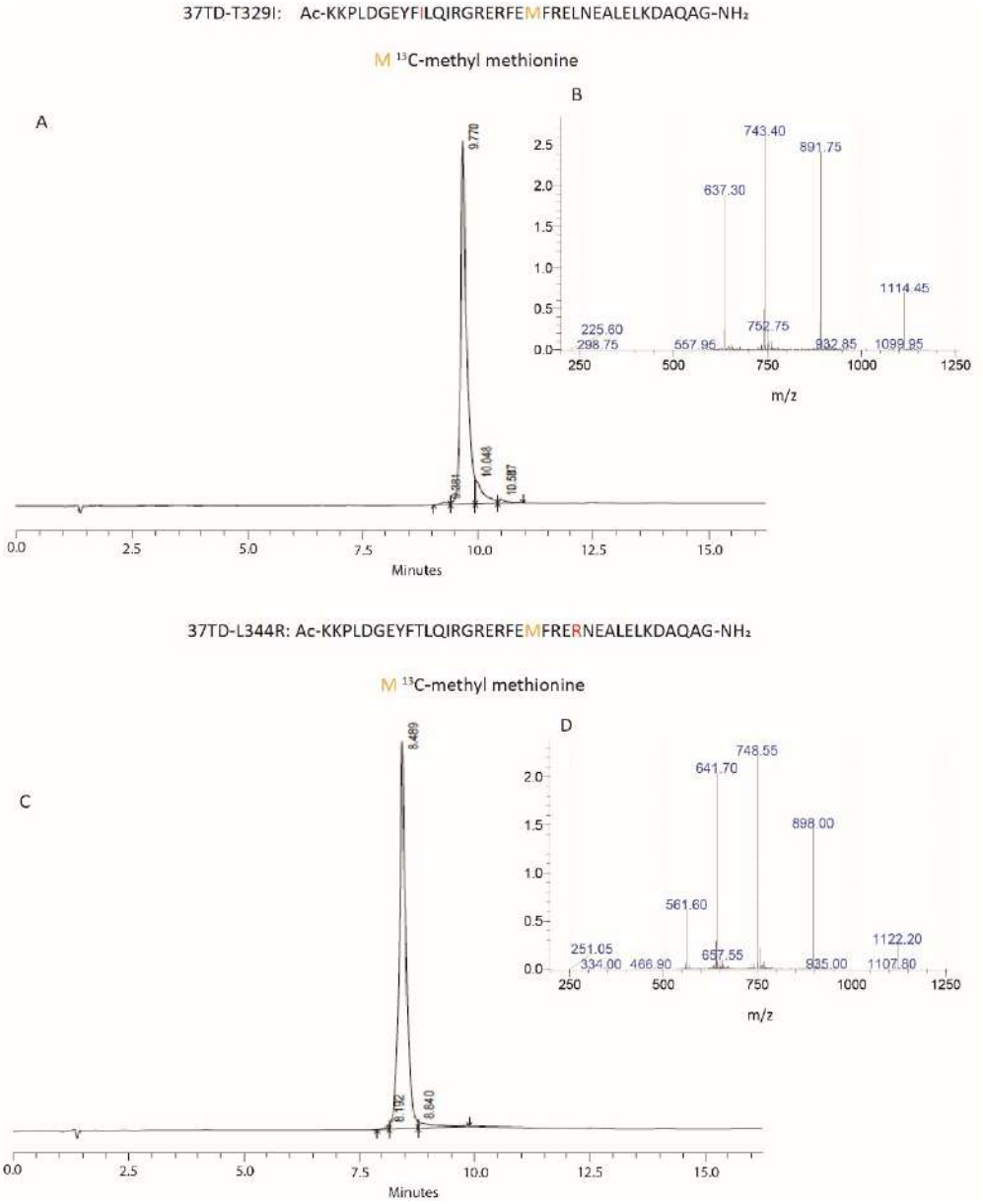

Figure S4. Characterisation of 37TD-T329I (A, B) and 37TD-L344R (C,D). HPLC of the peptides (A, C) and HPLC-MS (B, D).

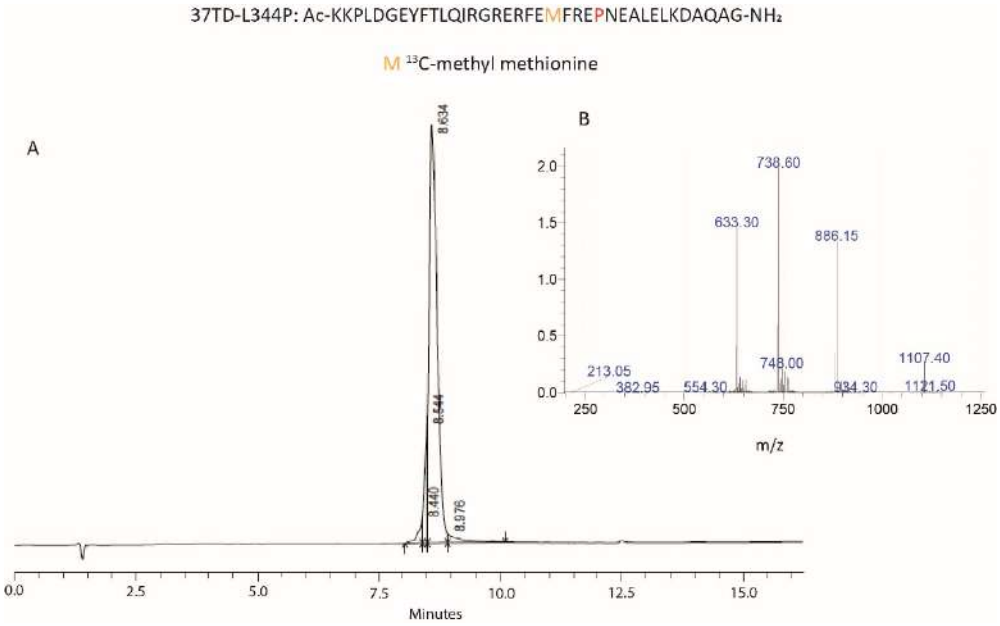

Figure S5. Characterisation of 37TD-L344P. HPLC of the peptide (A) and HPLC-MS (B).

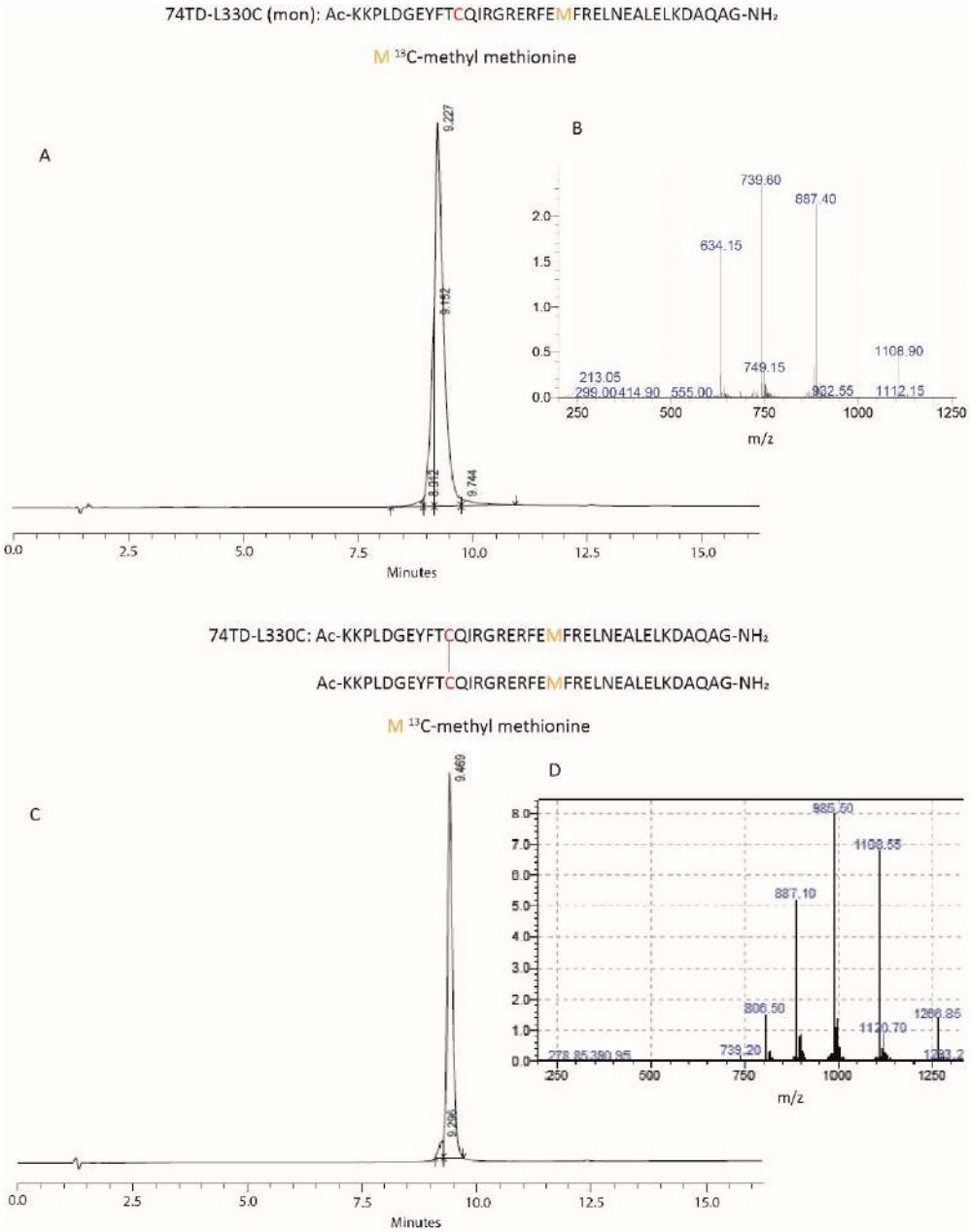

Figure S6. Characterisation of 74TD-L330C: monomeric peptide (A, B) and dimeric peptide (C,D). HPLC of the peptides (A, C) and HPLC-MS (B, D).

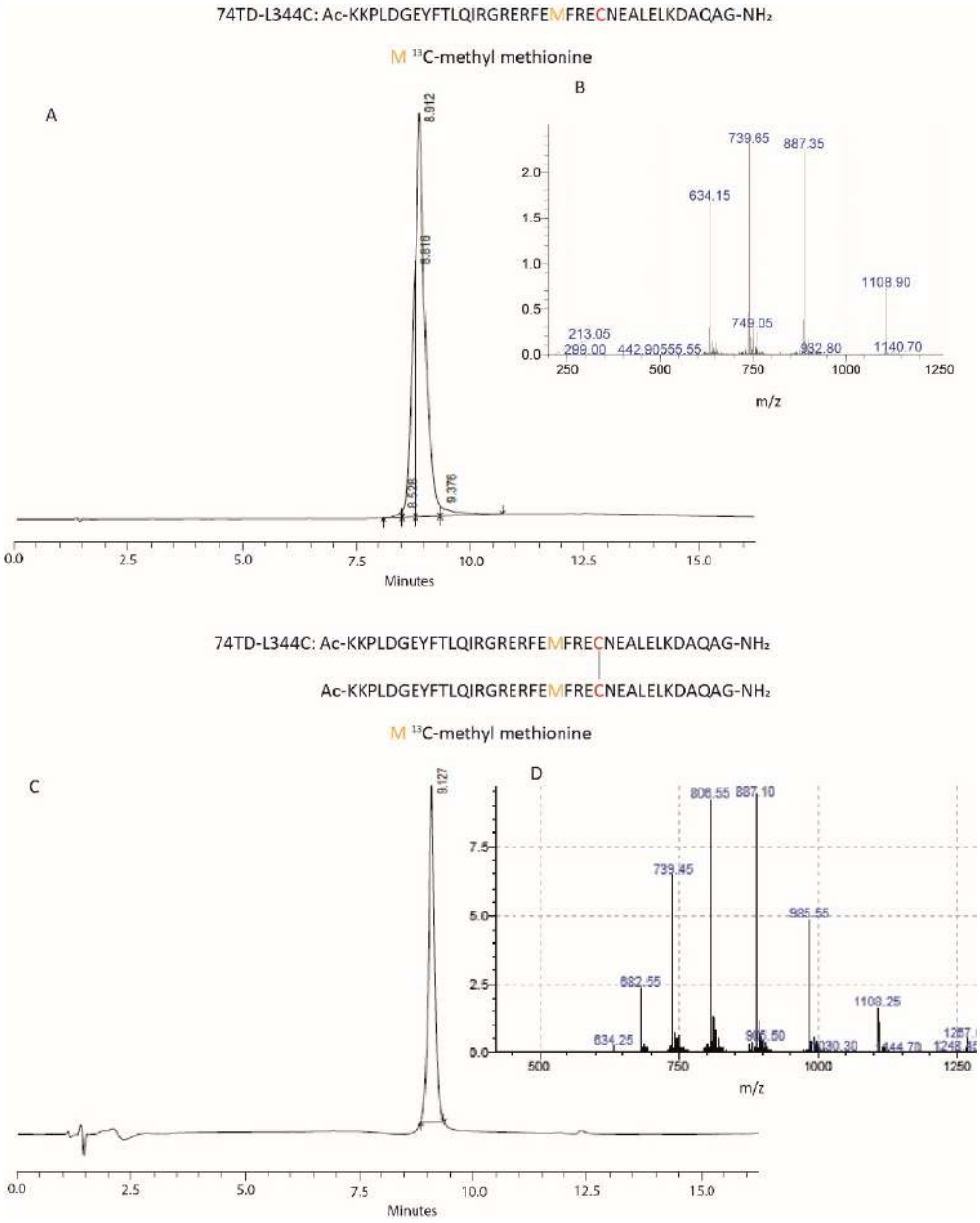

Figure S7. Characterisation of 74TD-L344C: monomeric peptide (A, B) and dimeric peptide (C,D). HPLC of the peptides (A, C) and HPLC-MS (B, D).

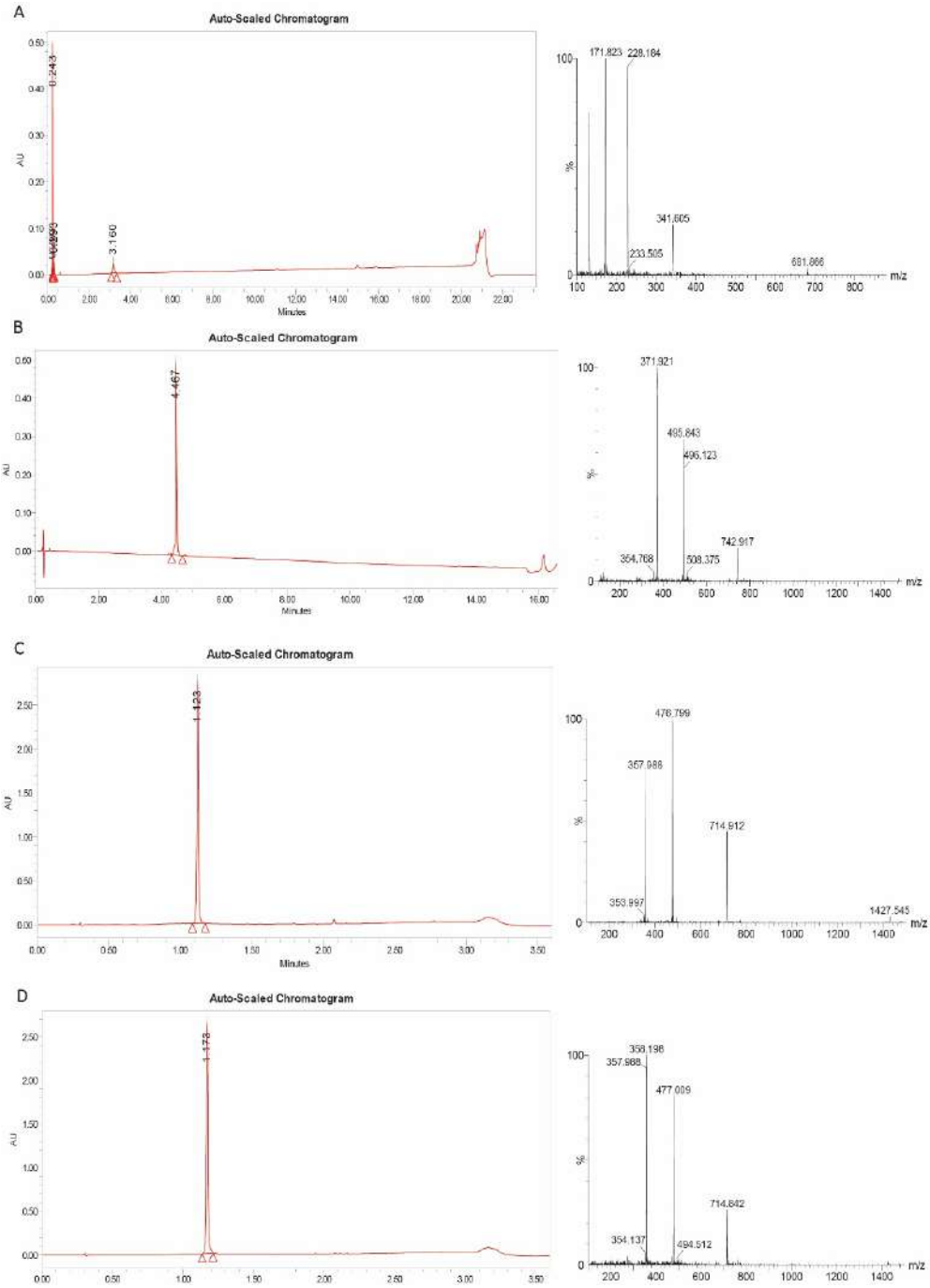

Figure S8. UPLC and UPLC-MS of cyclo-tetra-β-arginine *S* (A), R4 (B), K3R (C), and Rab4 (D).

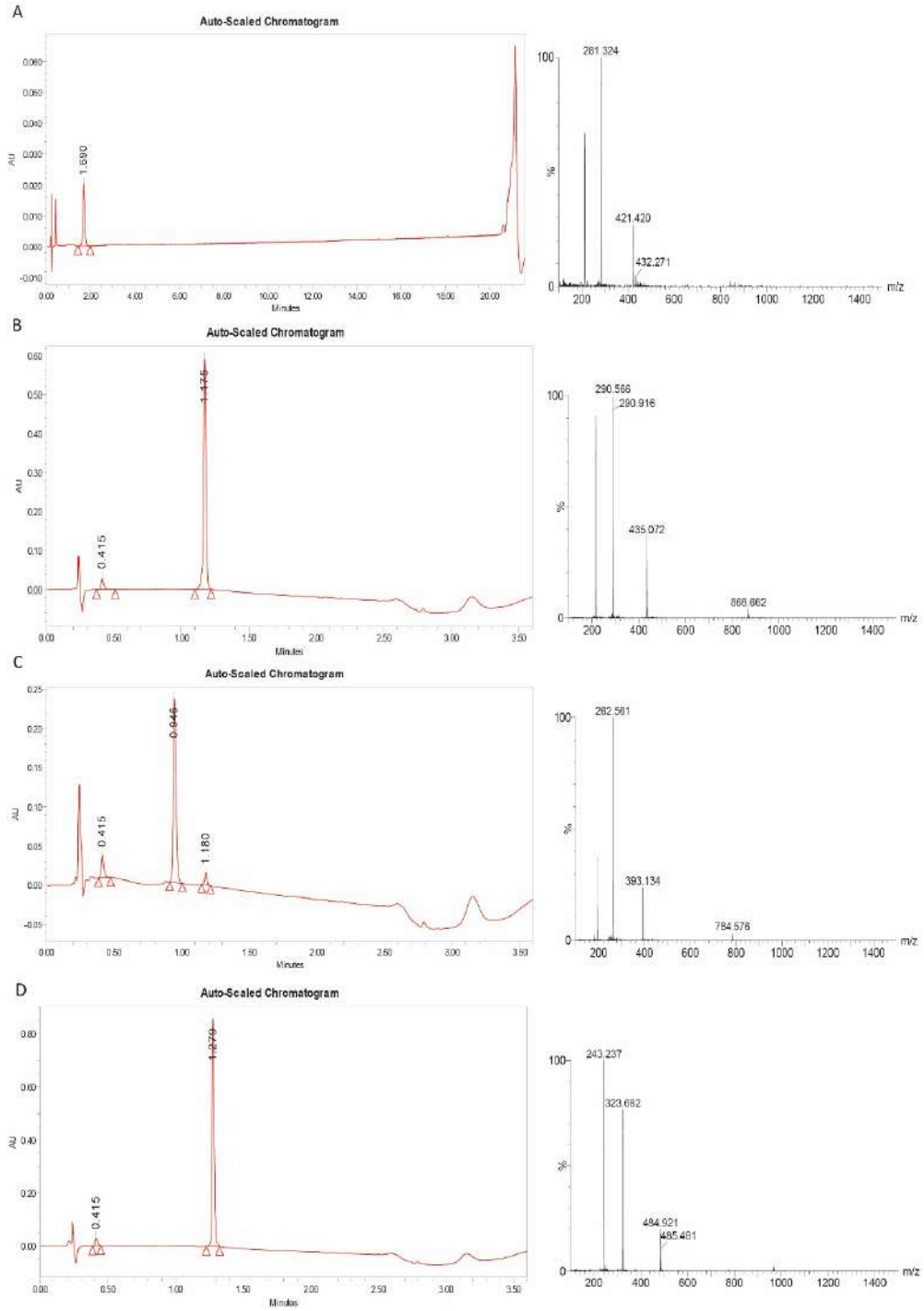

Figure S9. UPLC and UPLC-MS of cR4 (A), cRys2R2 (B), cRab4 (C), and cRys4A (D).

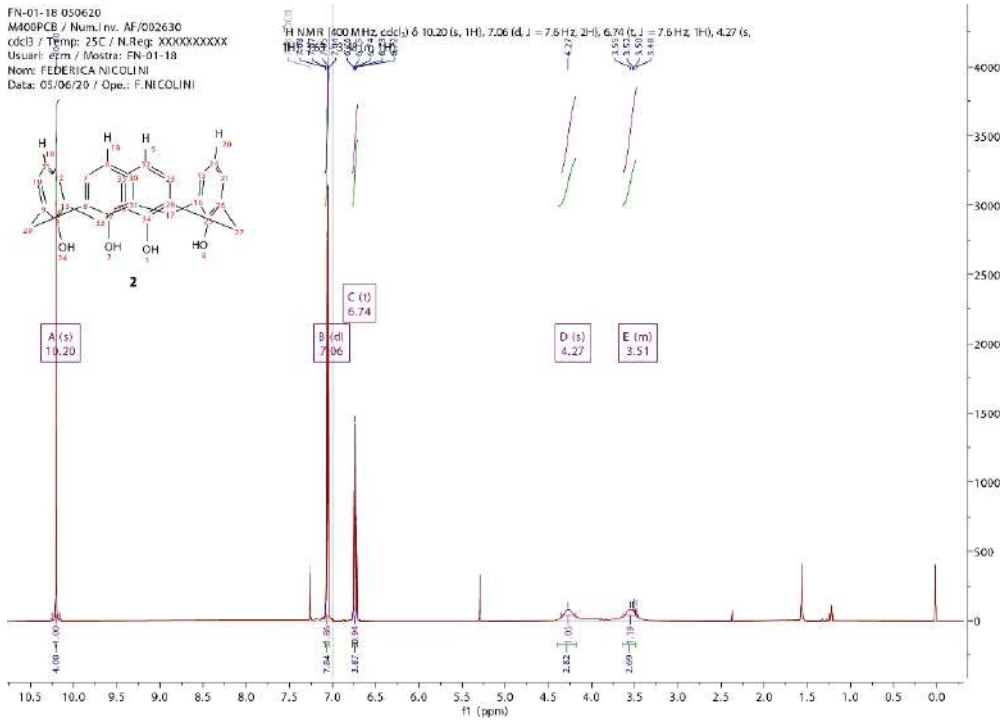

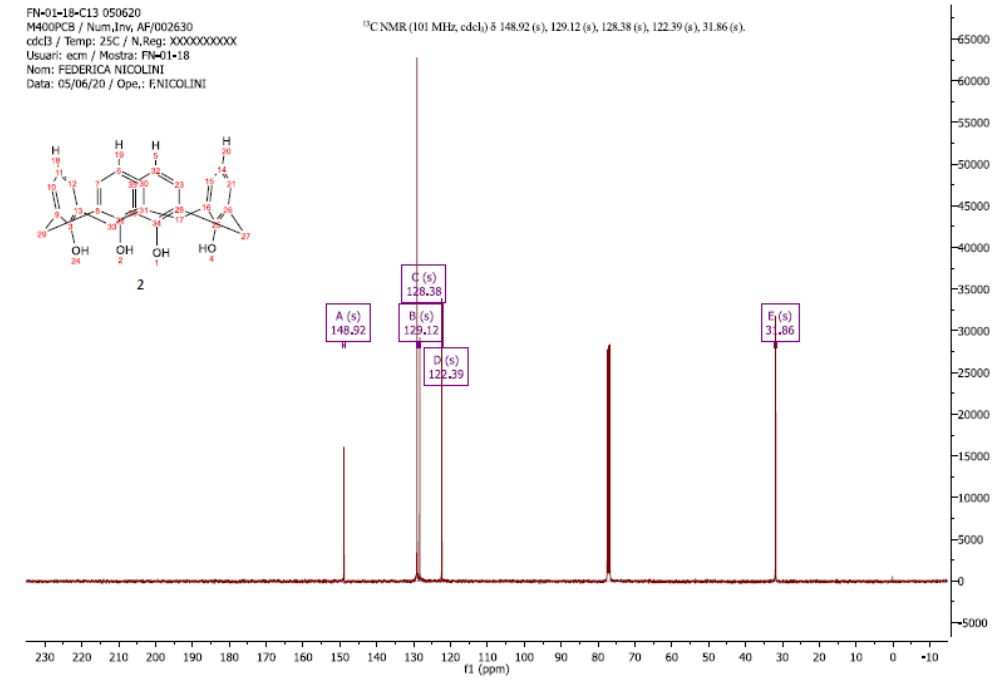

Figure S10. ^{1}H and ^{13}C NMR spectra of calix[4]arene **2**.

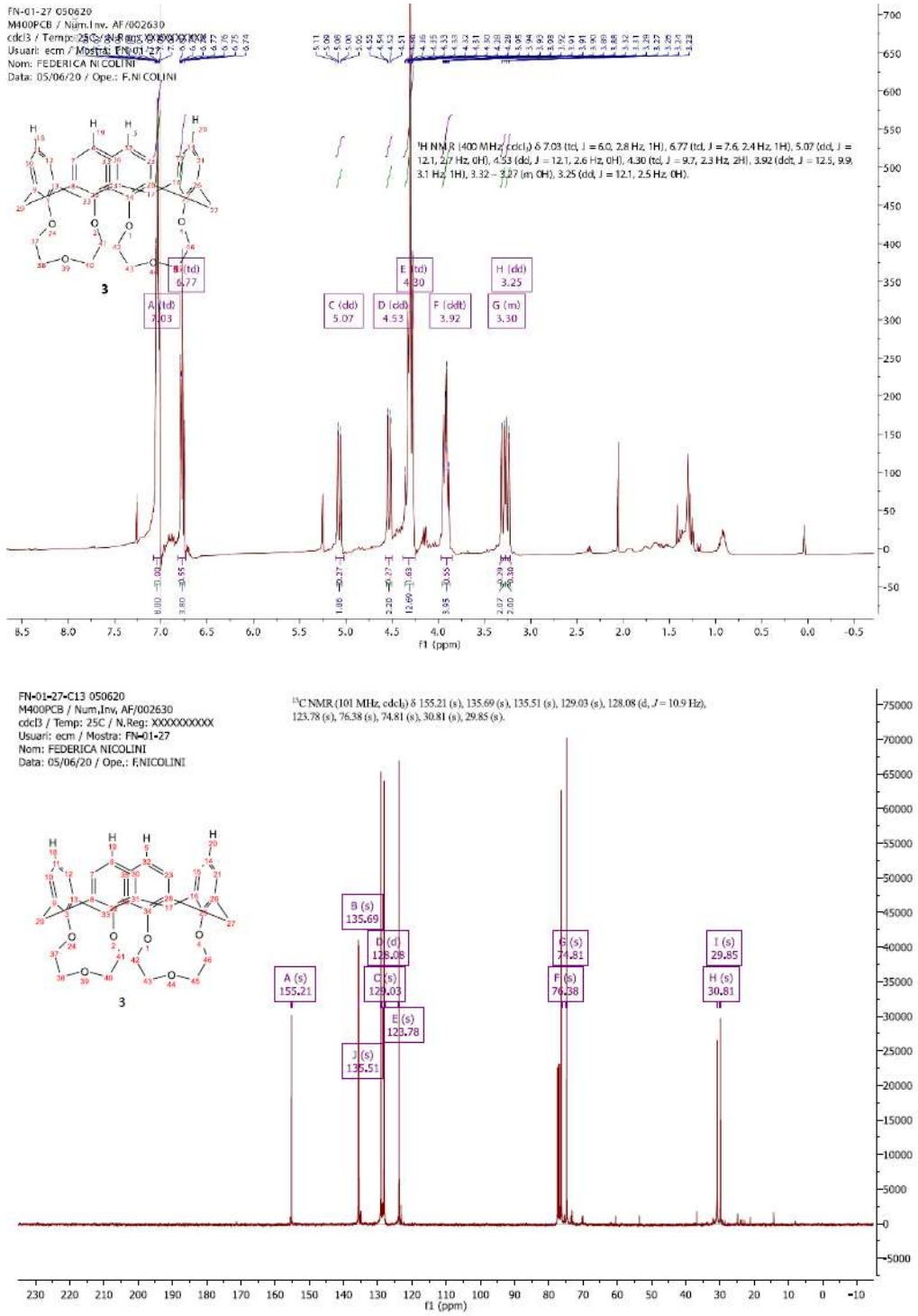

Figure S11. ^{1}H and ^{13}C NMR spectra of calix[4]arene **3**.

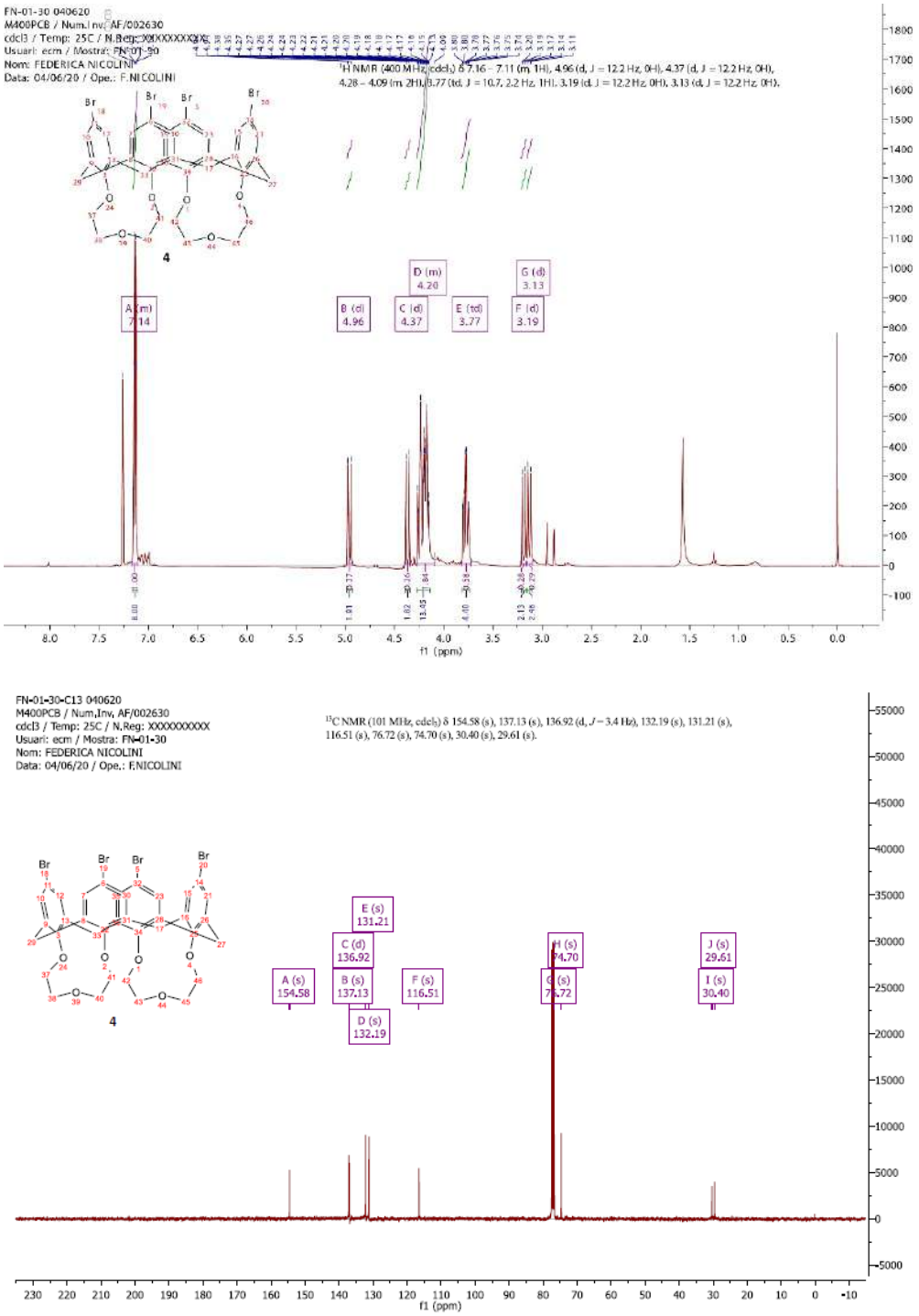

Figure S12. ^{1}H and ^{13}C NMR spectra of calix[4]arene **4**.

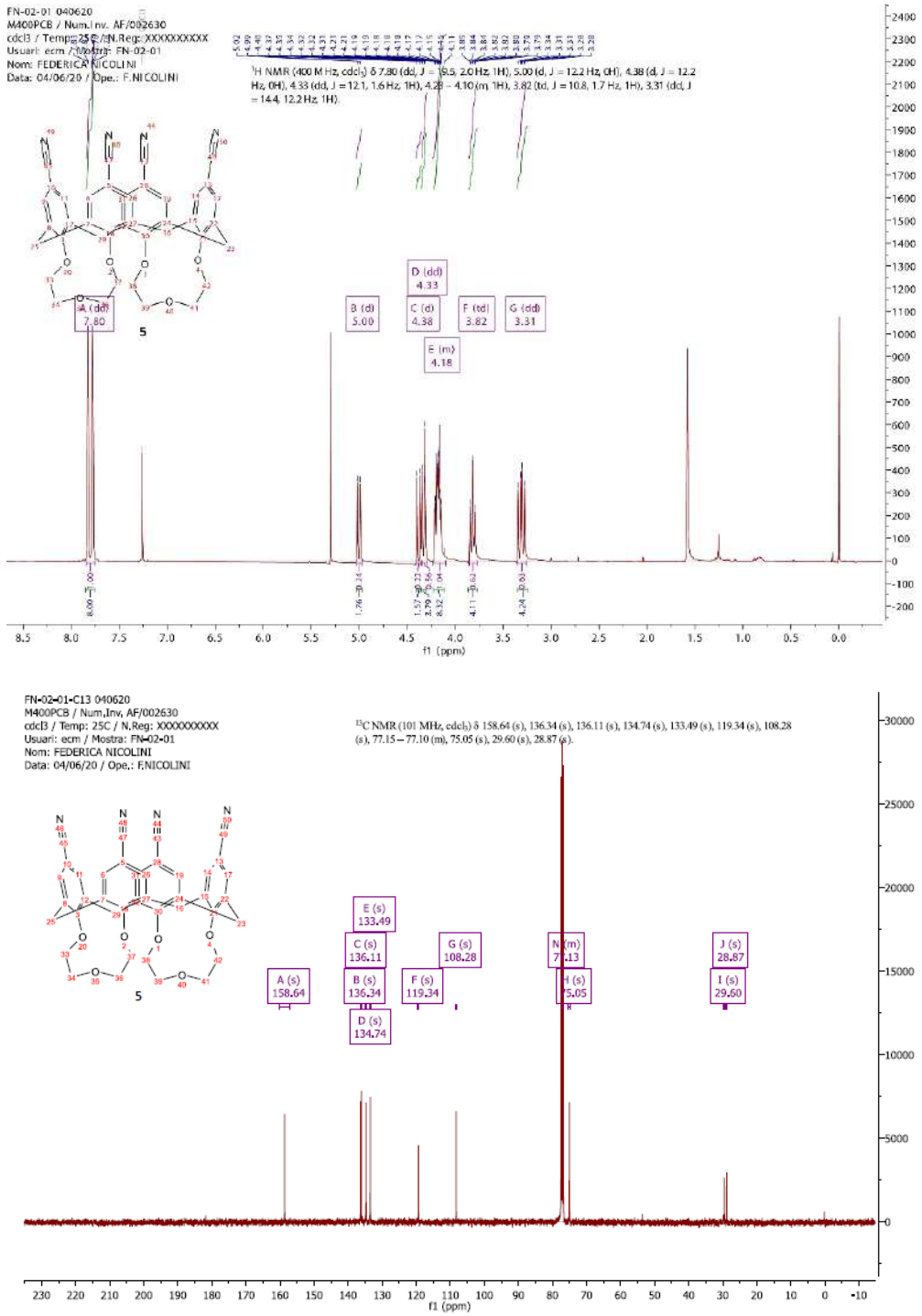

Figure S13. ^{1}H and ^{13}C NMR spectra of calix[4]arene **5**.

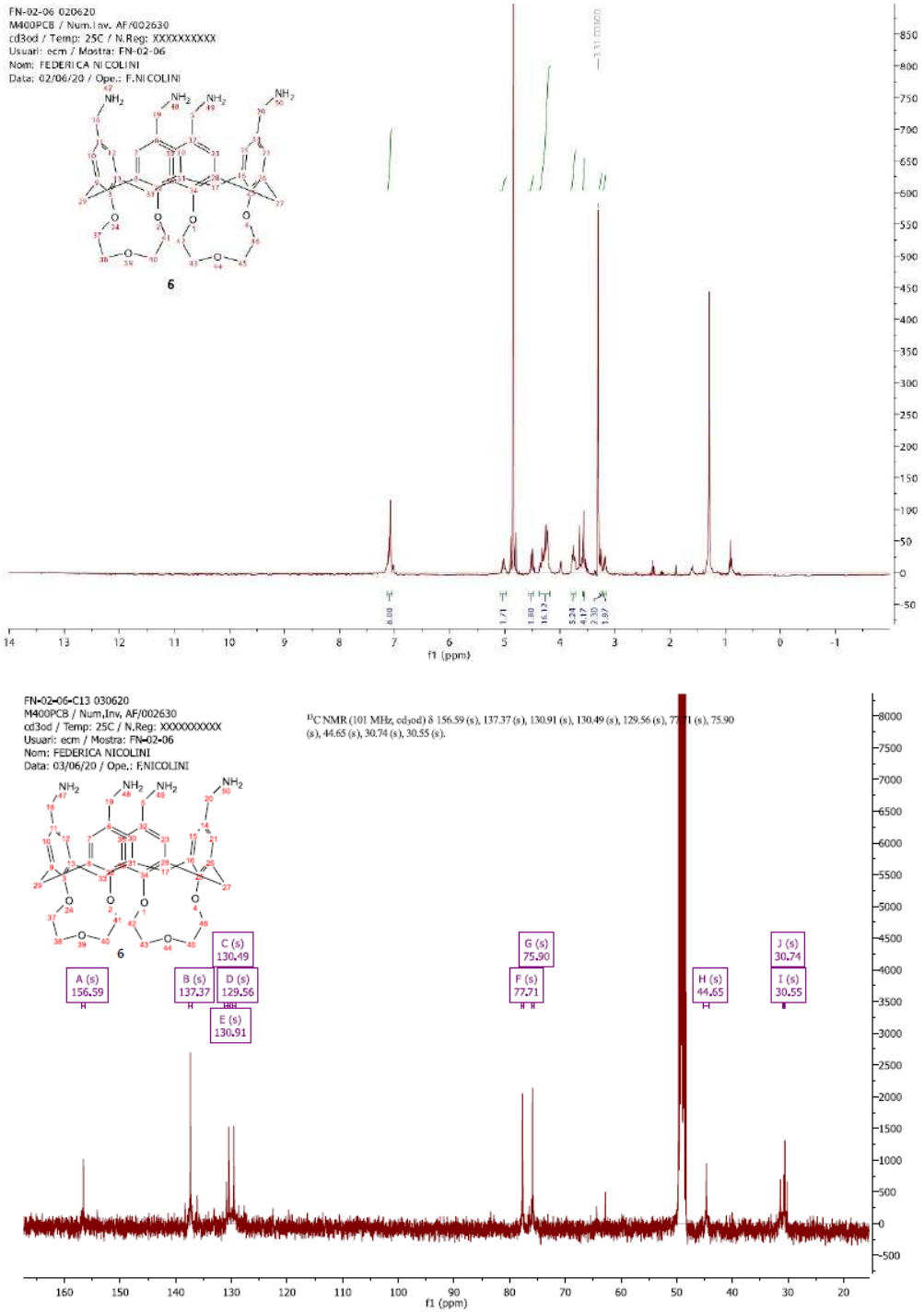

Figure S14. ^{1}H and ^{13}C NMR spectra of calix[4]arene **6**.

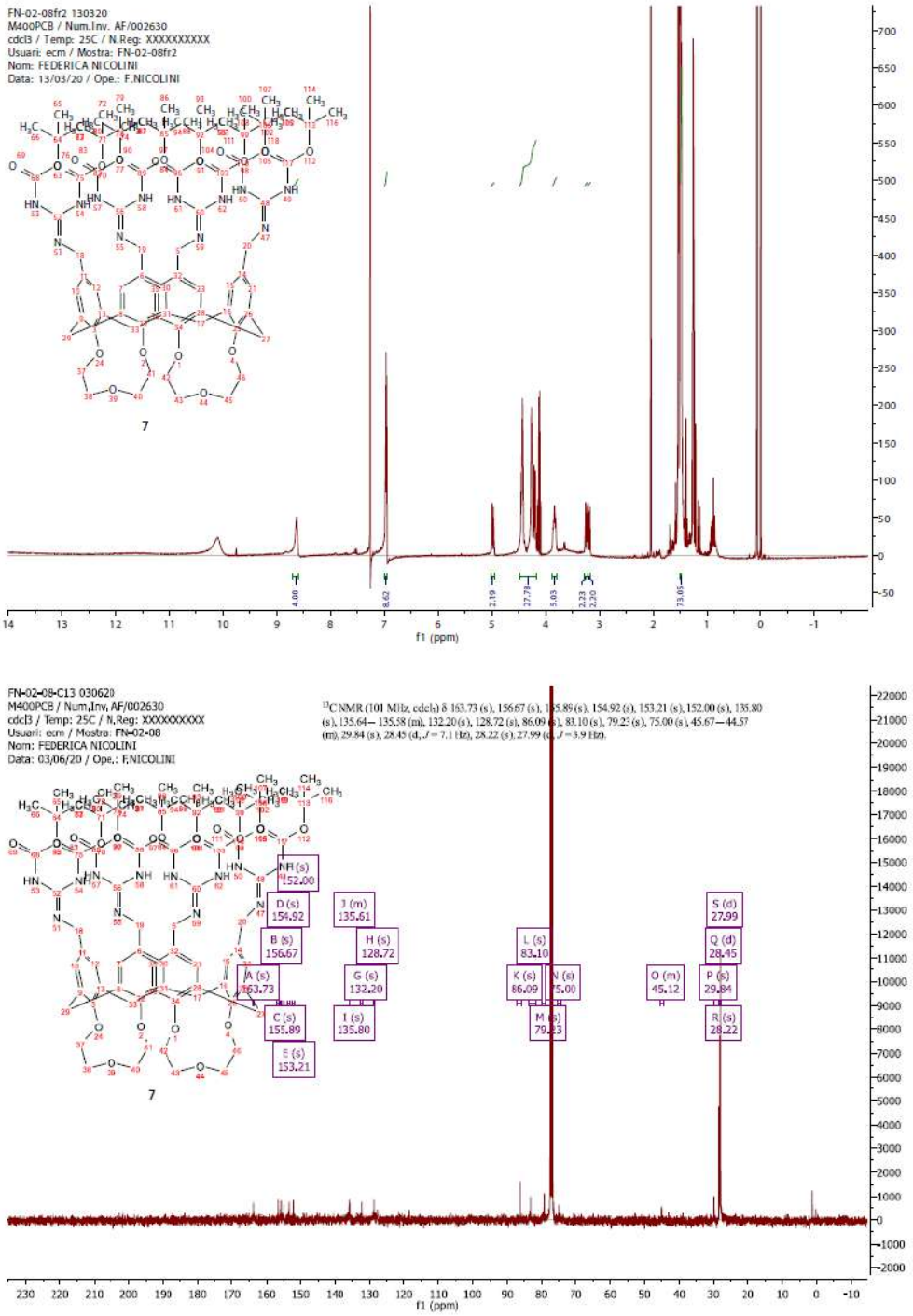

Figure S15. ^{1}H and ^{13}C NMR spectra of calix[4]arene **7**.

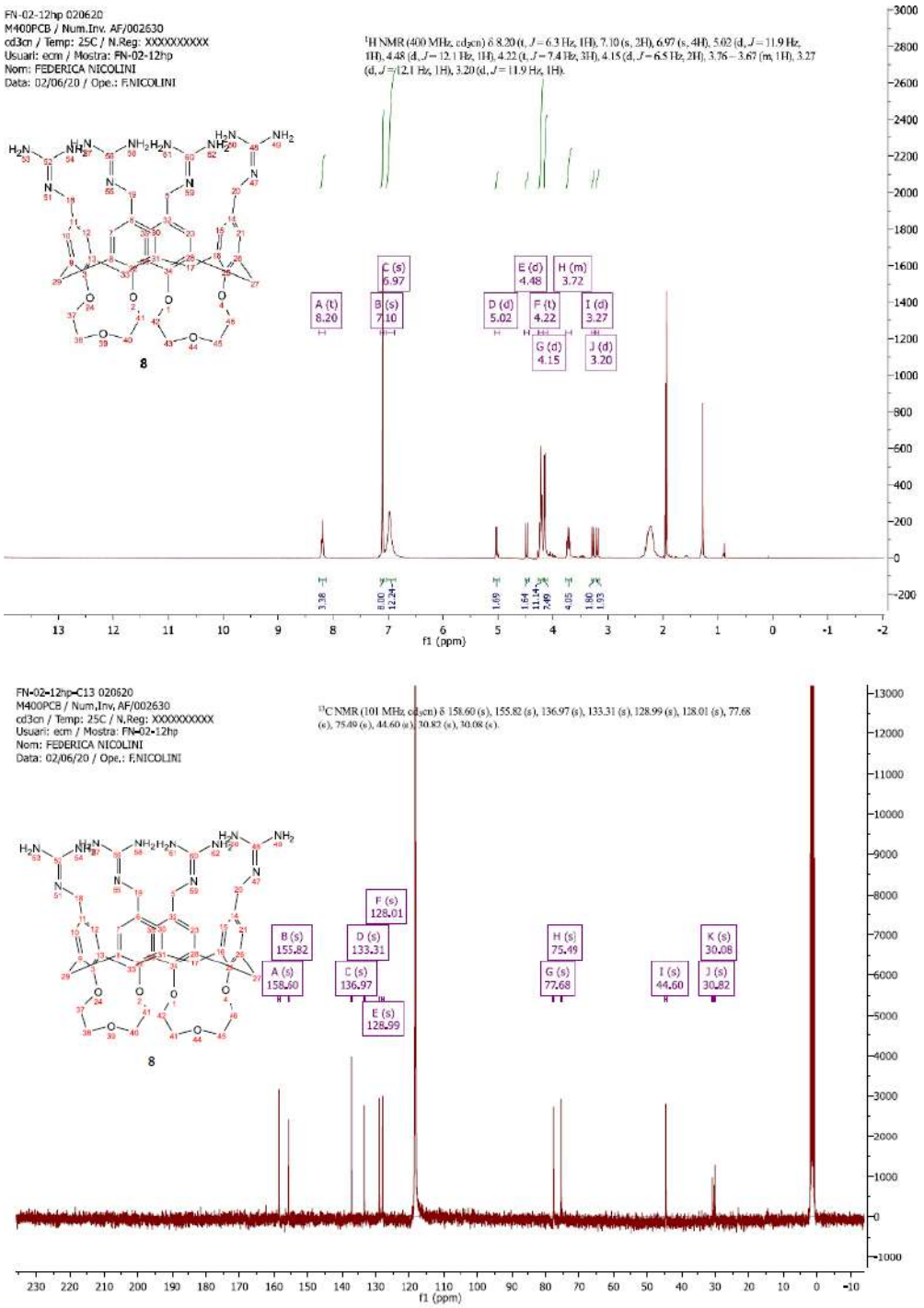

Figure S16. ^{1}H and ^{13}C NMR spectra of calix[4]arene **8**.

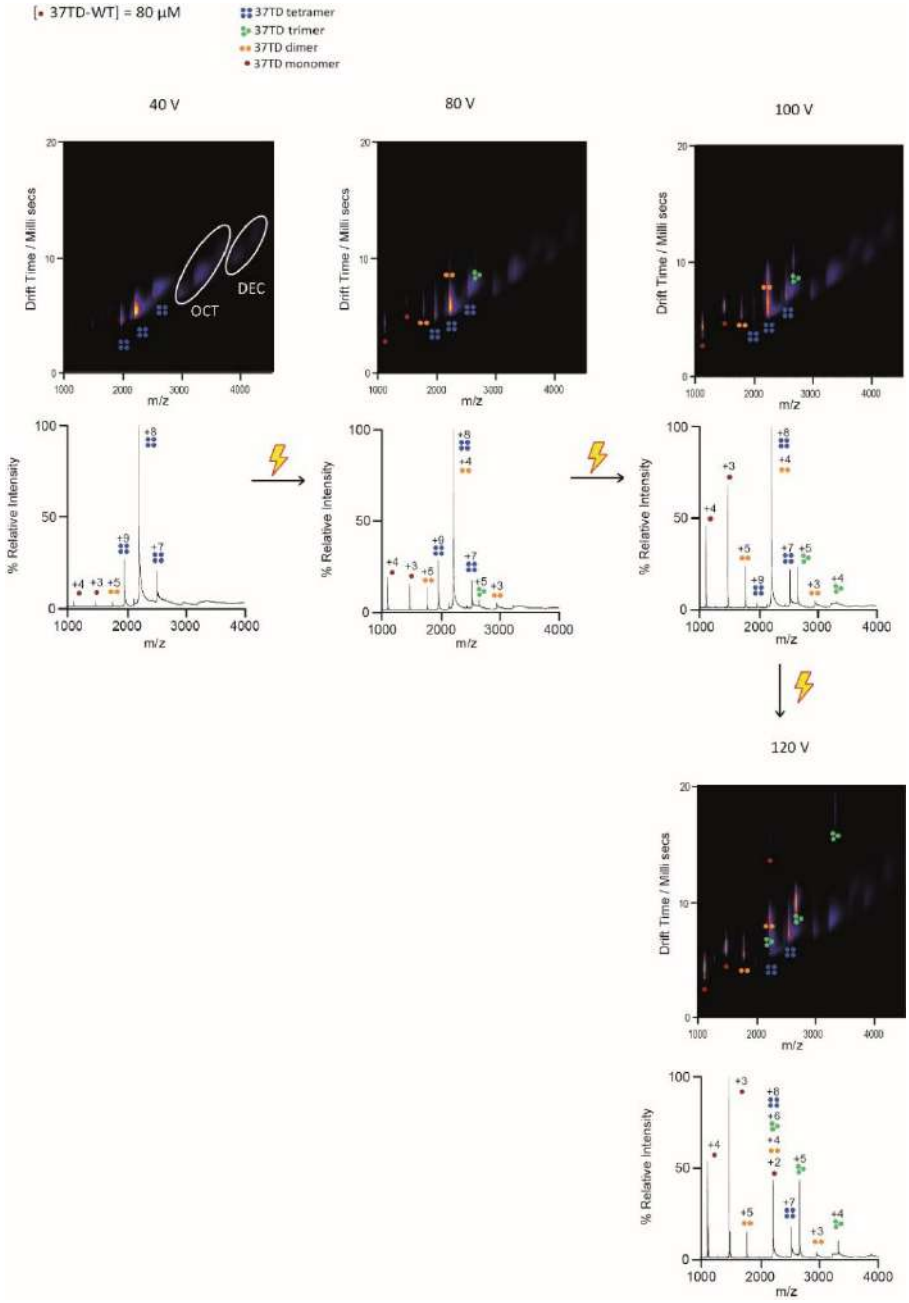

Figure S17. Native Mass Spectrometry and Ion Mobility spectra of 80 µM 37TD-WT at different cone voltages (40, 80, 100, and 120 V). Non isotope-labelled peptide was used. The concentrations reported always refer to the monomer. The sample was dissolved in 200 mM ammonium acetate buffer, pH 7. OCT: octamer; DEC: decahexamer (16 monomers).

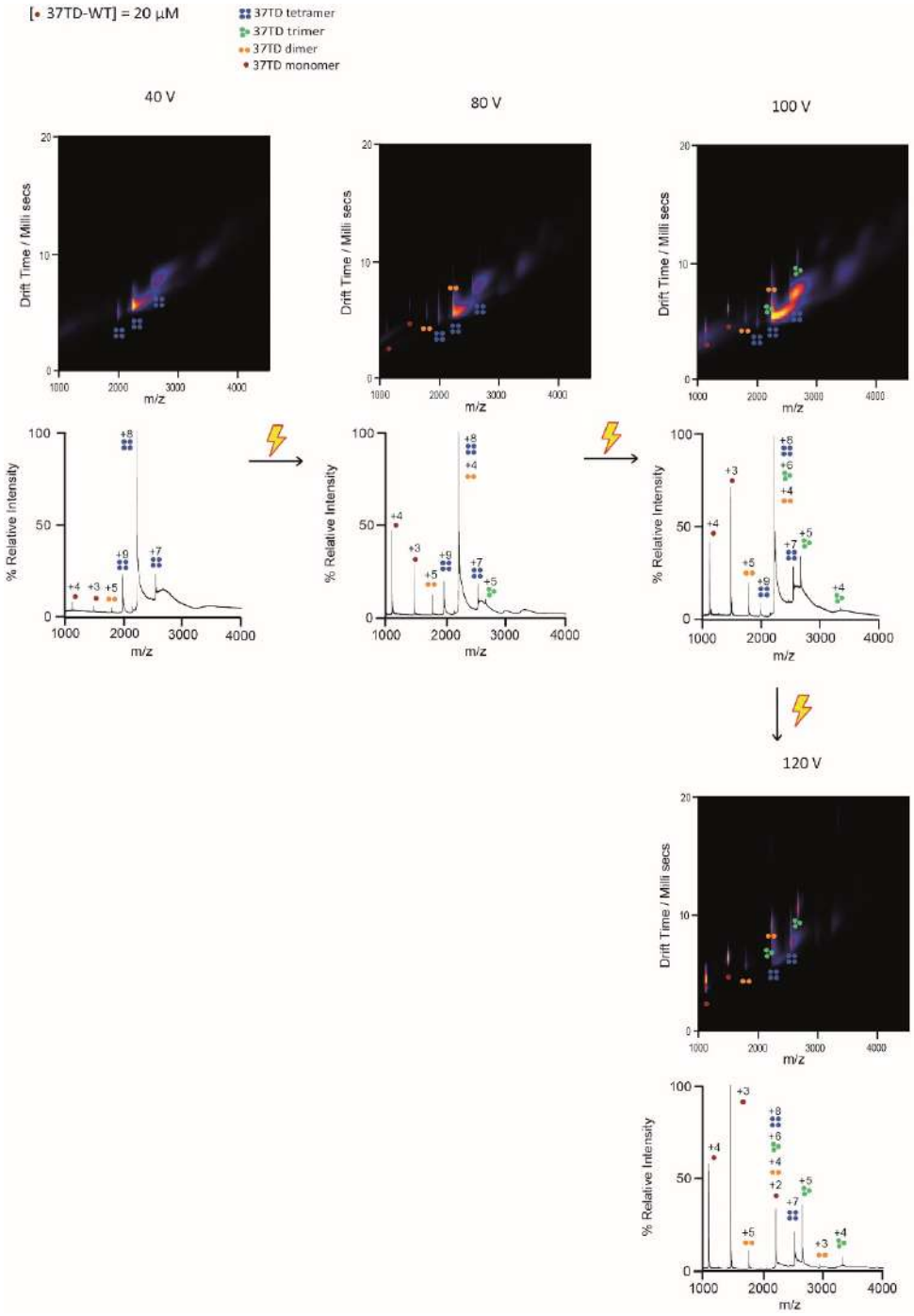

Figure S18. Native Mass Spectrometry and Ion Mobility spectra of 20 µM 37TD-WT at different cone voltages (40, 80, 100, and 120 V). Non isotope-labelled peptide was used. The concentrations reported always refer to the monomer. The sample was dissolved in 200 mM ammonium acetate buffer, pH 7.

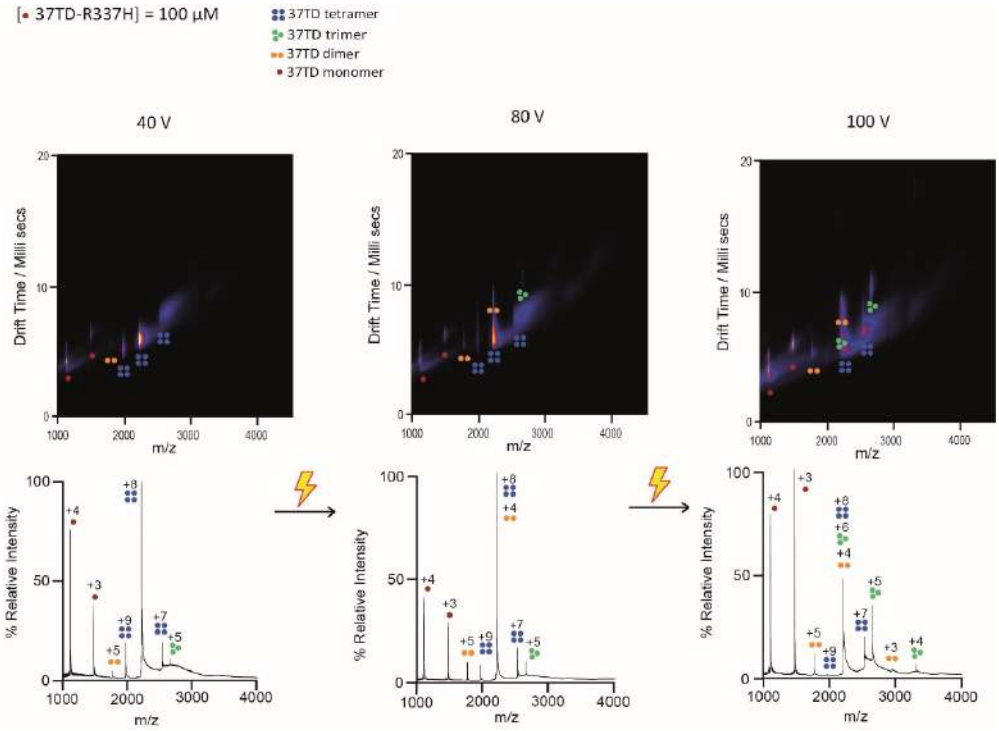

Figure S19. Native Mass Spectrometry and Ion Mobility spectra of 100 µM 37TD-R337H at different cone voltages (40, 80, and 100 V). Non isotope-labelled peptide was used. The concentrations reported refer to the monomer. The sample was dissolved in 200 mM ammonium acetate buffer, pH 7.

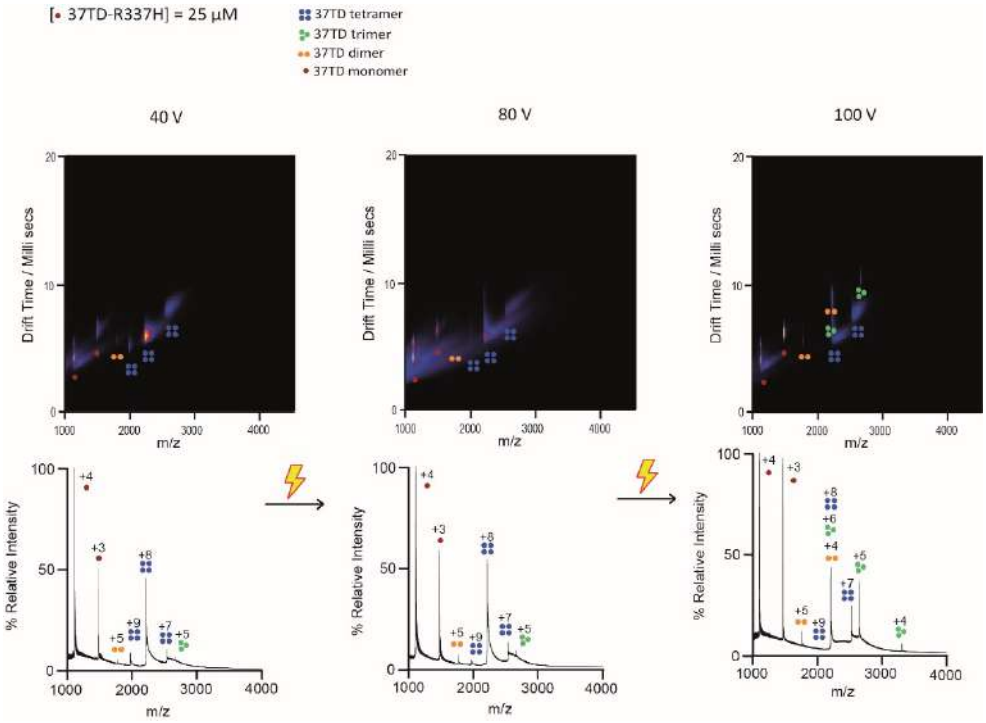

Figure S20. Native Mass Spectrometry and Ion Mobility spectra of 25 µM 37TD-R337H at different cone voltages (40, 80, and 100 V). Non isotope-labelled peptide was used. The concentrations reported refer to the monomer. The sample was dissolved in 200 mM ammonium acetate buffer, pH 7.

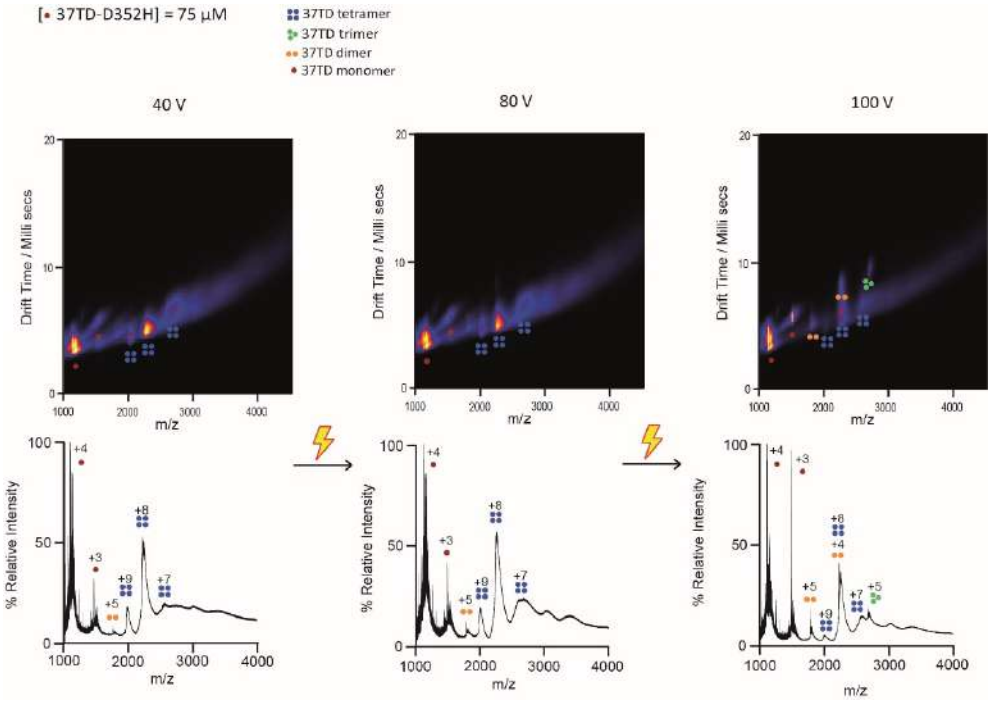

Figure S21. Native Mass Spectrometry and Ion Mobility spectra of 75 µM 37TD-D352H at different cone voltages (40, 80, and 100 V). The concentrations reported refer to the monomer. The sample was dissolved in 200 mM ammonium acetate buffer, pH 7.

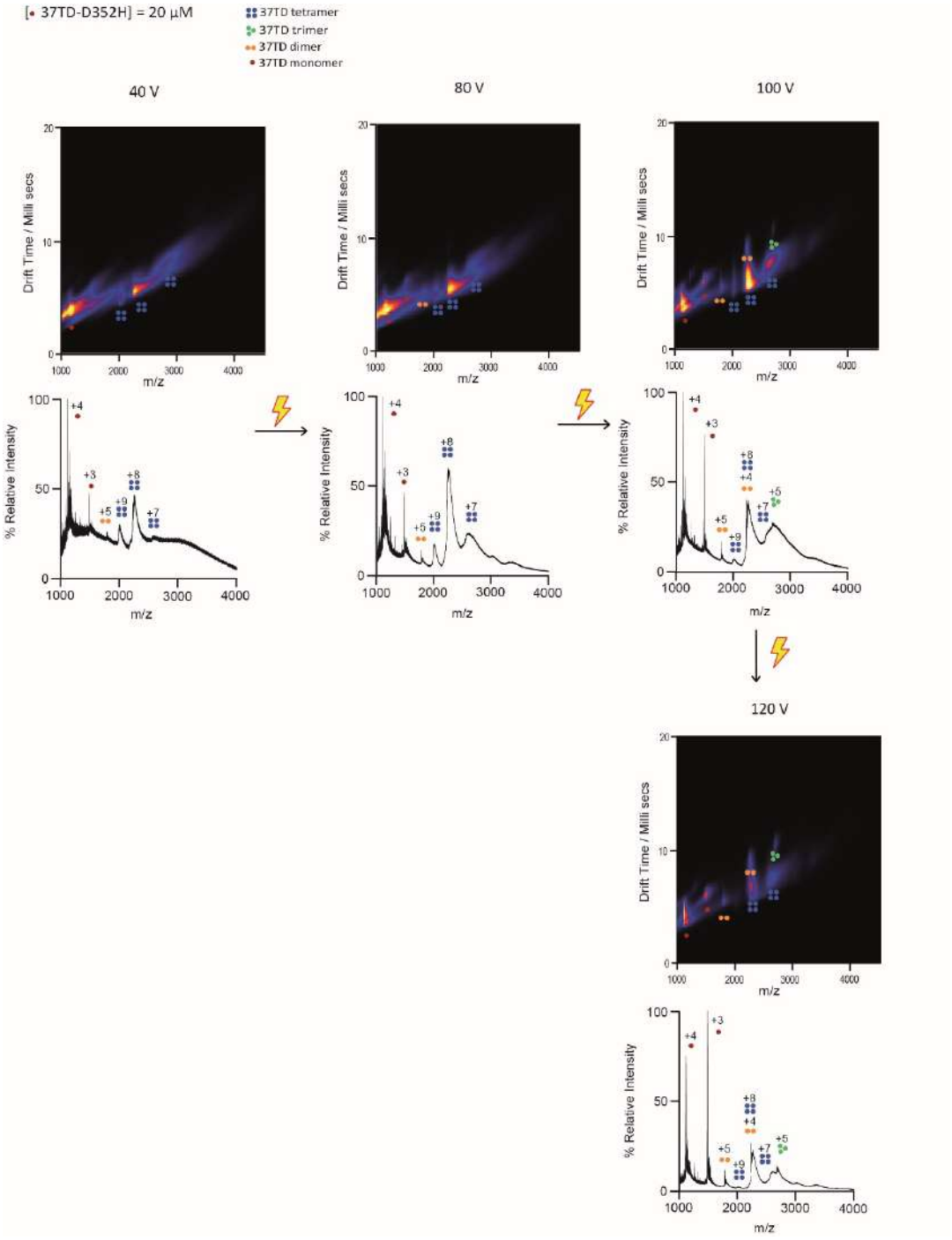

Figure S22. Native Mass Spectrometry and Ion Mobility spectra of 20 µM 37TD-D352H at different cone voltages (40, 80, 100, and 120 V). The concentrations reported refer to the monomer. The sample was dissolved in 200 mM ammonium acetate buffer, pH 7.

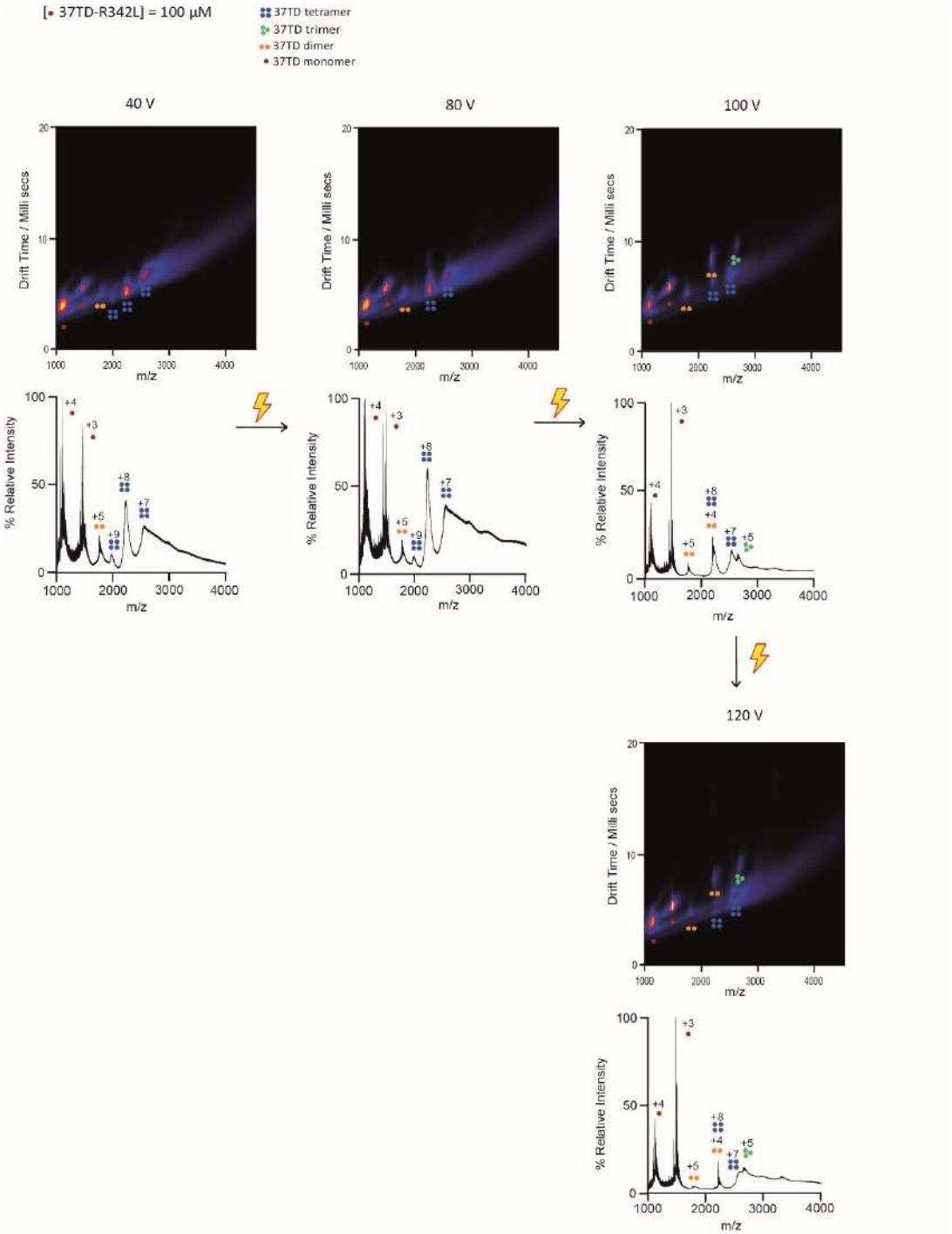

Figure S23. Native Mass Spectrometry and Ion Mobility spectra of 100 µM 37TD-R342L at different cone voltages (40, 80, 100, and 120 V). The concentrations reported refer to the monomer. The sample was dissolved in 200 mM ammonium acetate buffer, pH 7.

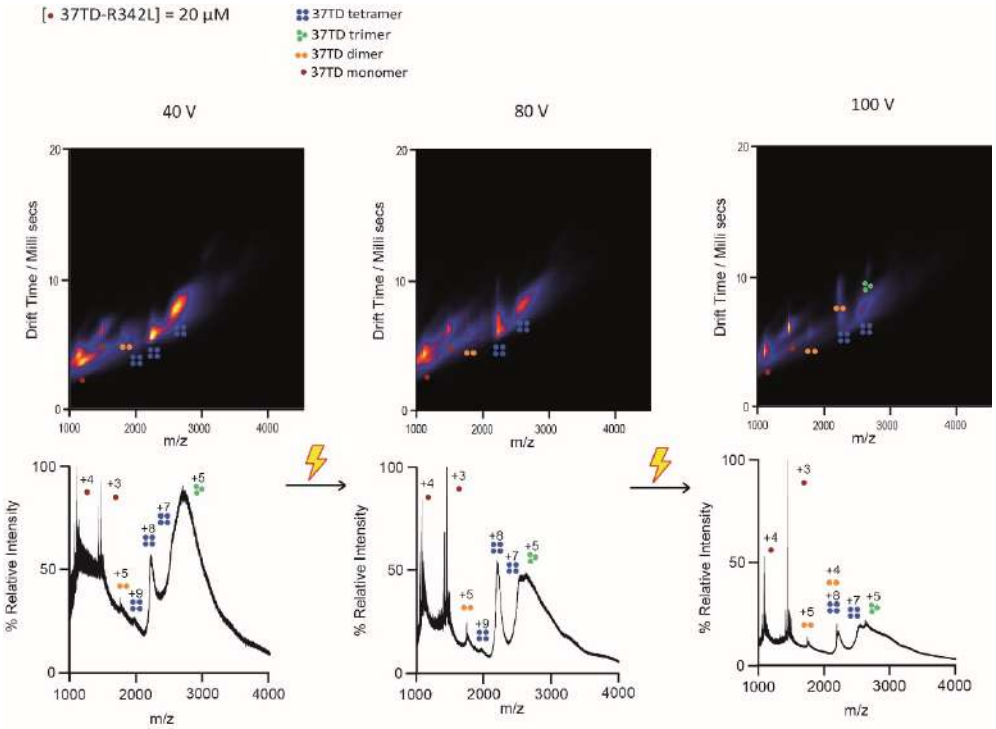

Figure S24. Native Mass Spectrometry and Ion Mobility spectra of 20 µM 37TD-R342L at different cone voltages (40, 80, and 100 V). The concentrations reported refer to the monomer. The sample was dissolved in 200 mM ammonium acetate buffer, pH 7.

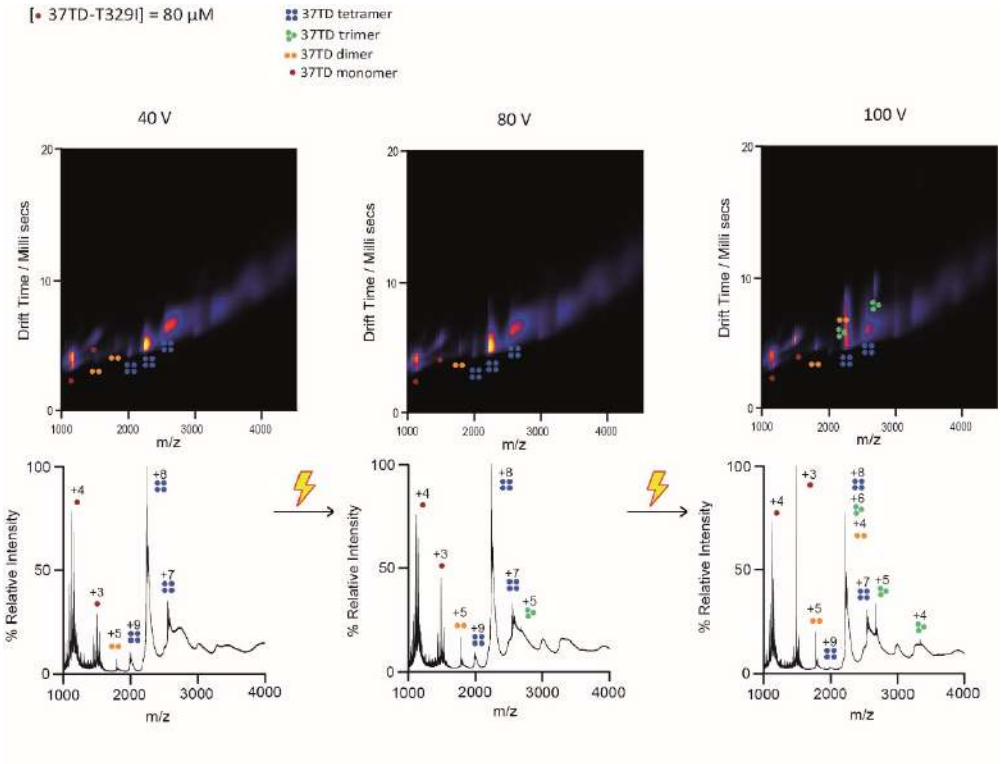

Figure S25. Native Mass Spectrometry and Ion Mobility spectra of 80 µM 37TD-T329I at different cone voltages (40, 80, and 100 V). The concentrations reported refer to the monomer. The sample was dissolved in 200 mM ammonium acetate buffer, pH 7.

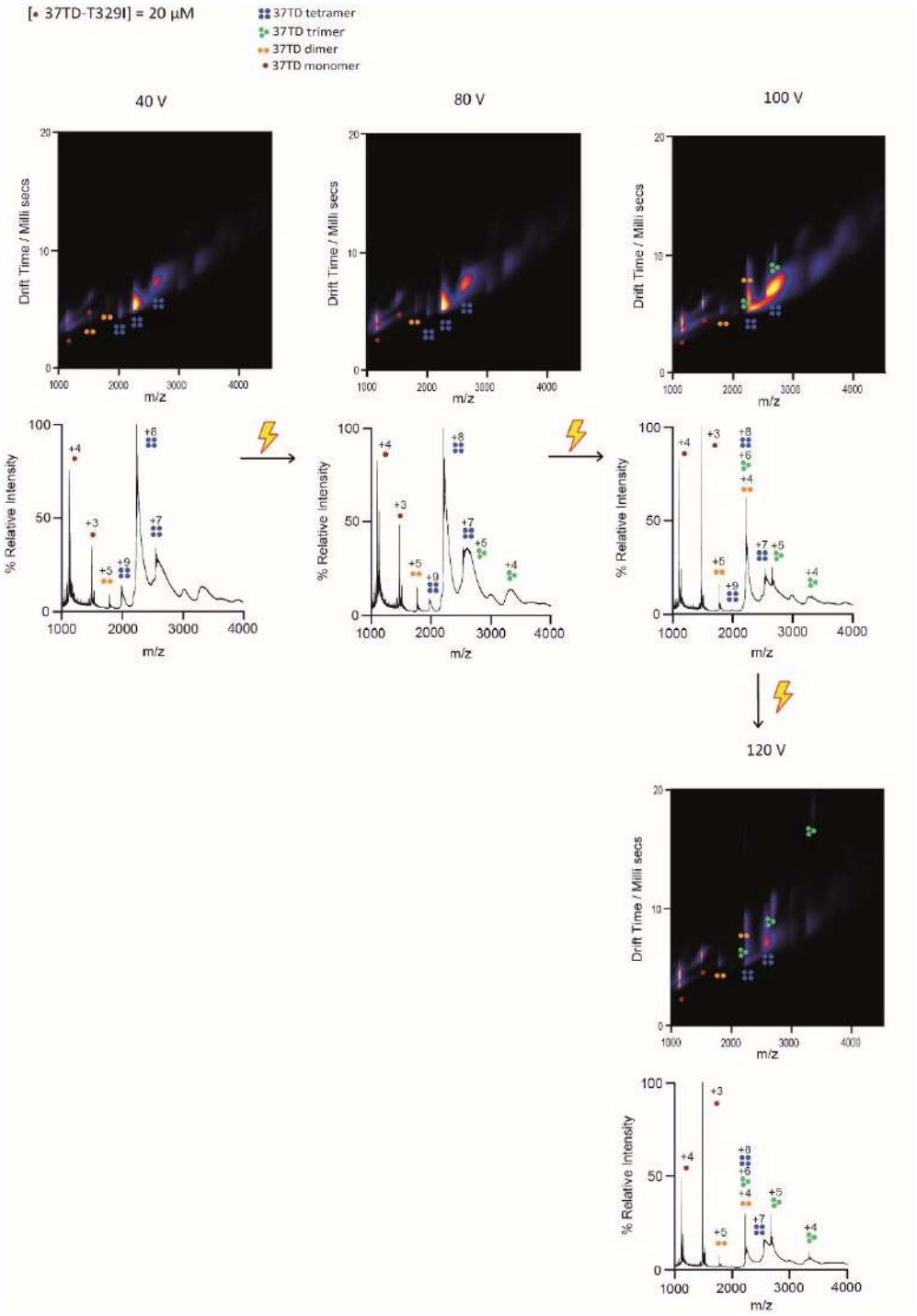

Figure S26. Native Mass Spectrometry and Ion Mobility spectra of 20 µM 37TD-T329I at different cone voltages (40, 80, 100, and 120 V). The concentrations reported refer to the monomer. The sample was dissolved in 200 mM ammonium acetate buffer, pH 7.

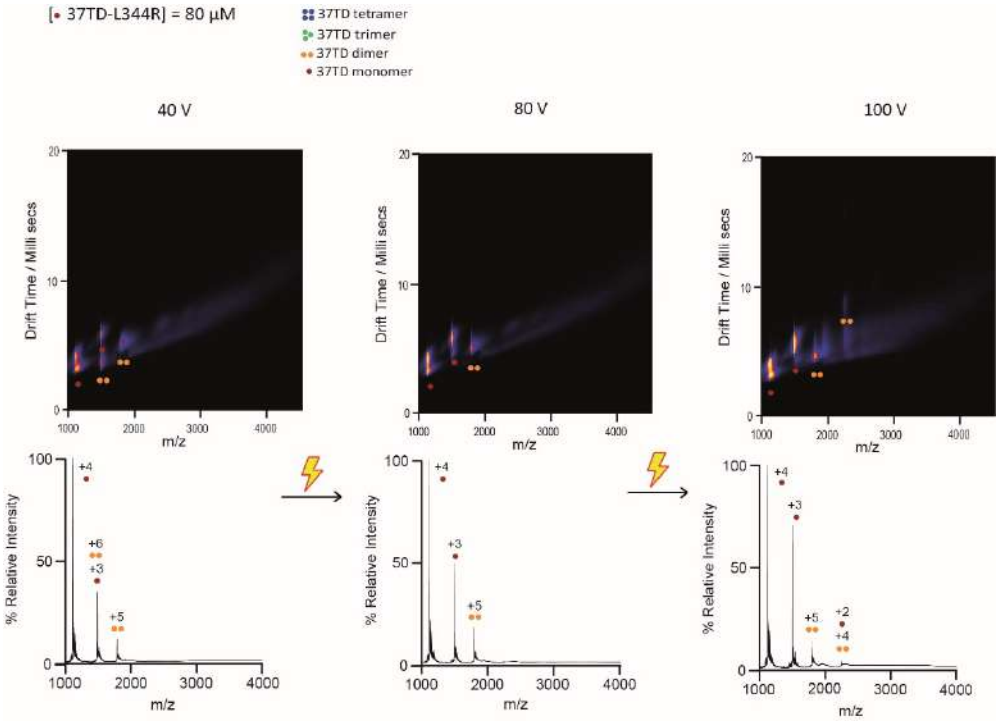

Figure S27. Native Mass Spectrometry and Ion Mobility spectra of 80 µM 37TD-L344R at different cone voltages (40, 80, and 100 V). The concentrations reported refer to the monomer. The sample was dissolved in 200 mM ammonium acetate buffer, pH 7.

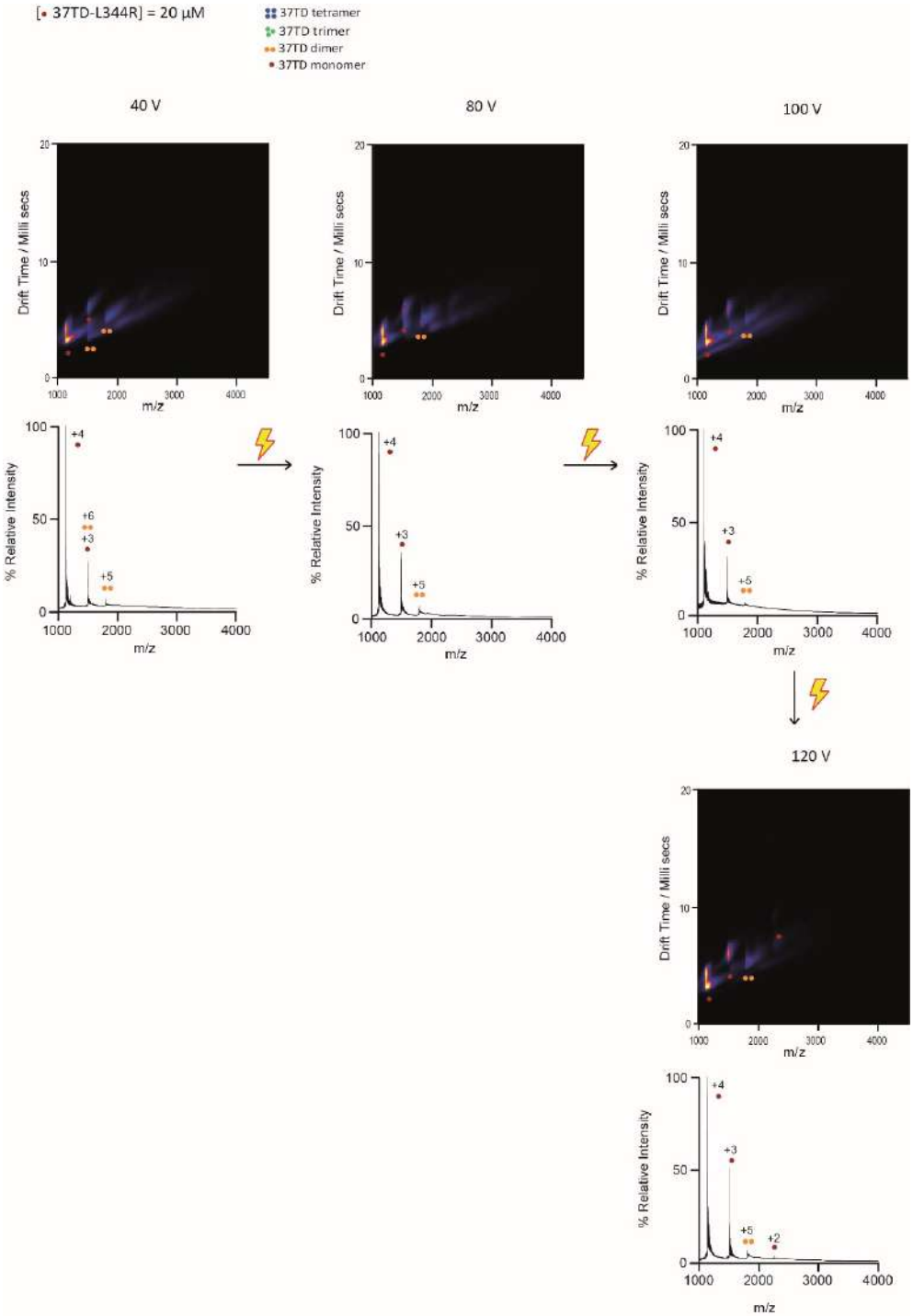

Figure S28. Native Mass Spectrometry and Ion Mobility spectra of 80 µM 37TD-L344R at different cone voltages (40, 80, 100, and 120 V). The concentrations reported refer to the monomer. The sample was dissolved in 200 mM ammonium acetate buffer, pH 7.

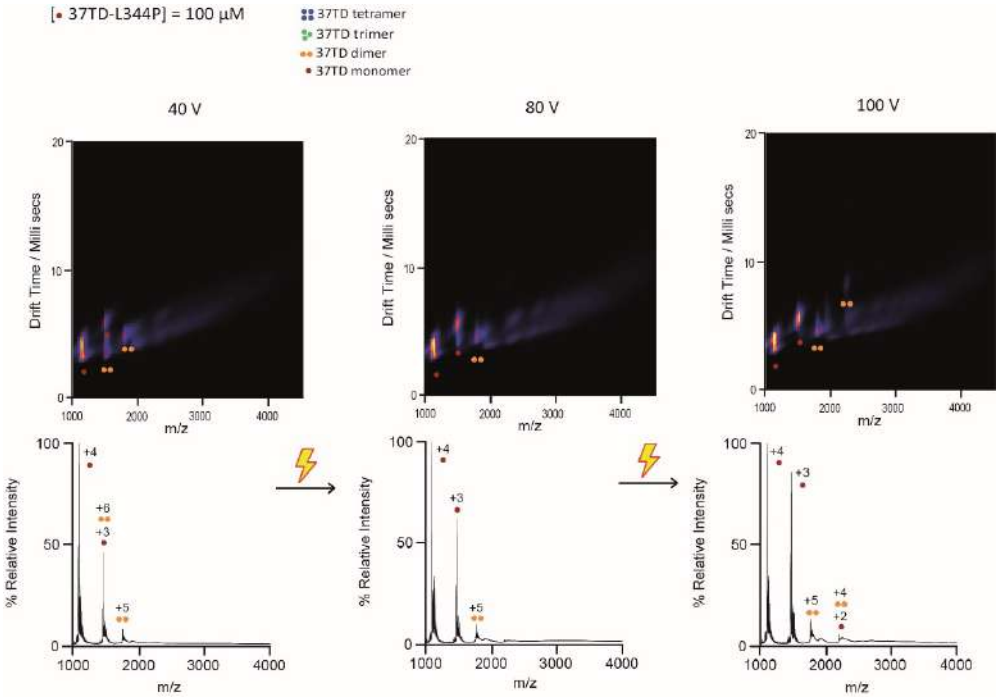

Figure S29. Native Mass Spectrometry and Ion Mobility spectra of 100 µM 37TD-L344P at different cone voltages (40, 80, and 100 V). The concentrations reported refer to the monomer. The sample was dissolved in 200 mM ammonium acetate buffer, pH 7.

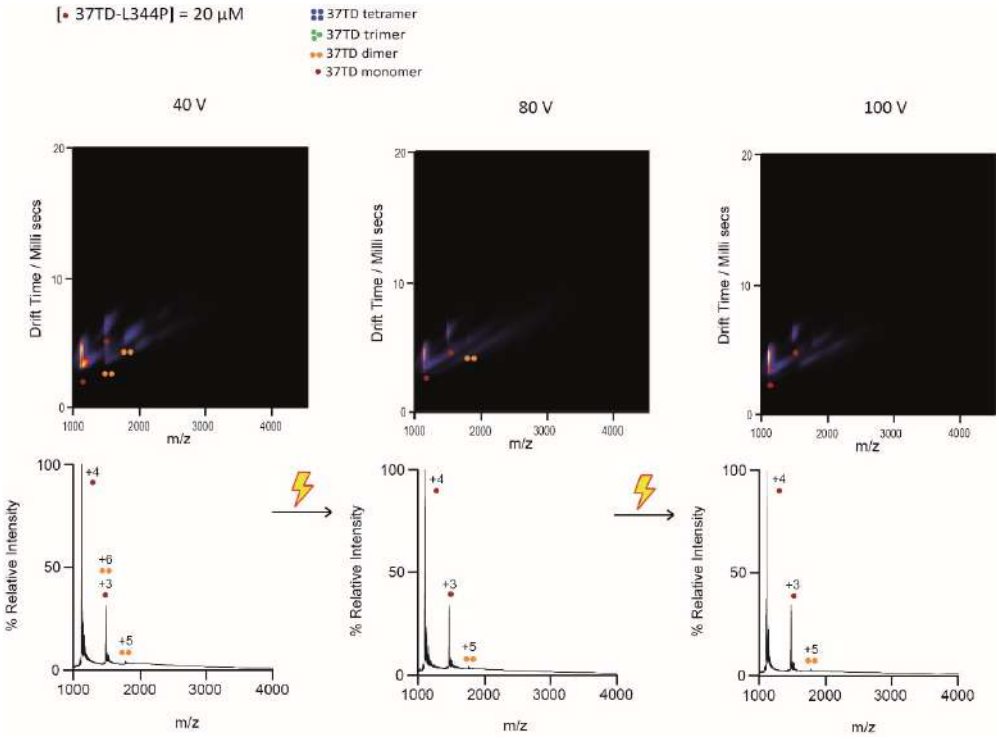

Figure S30. Native Mass Spectrometry and Ion Mobility spectra of 20 µM 37TD-L344P at different cone voltages (40, 80, and 100 V). The concentrations reported refer to the monomer. The sample was dissolved in 200 mM ammonium acetate buffer, pH 7.

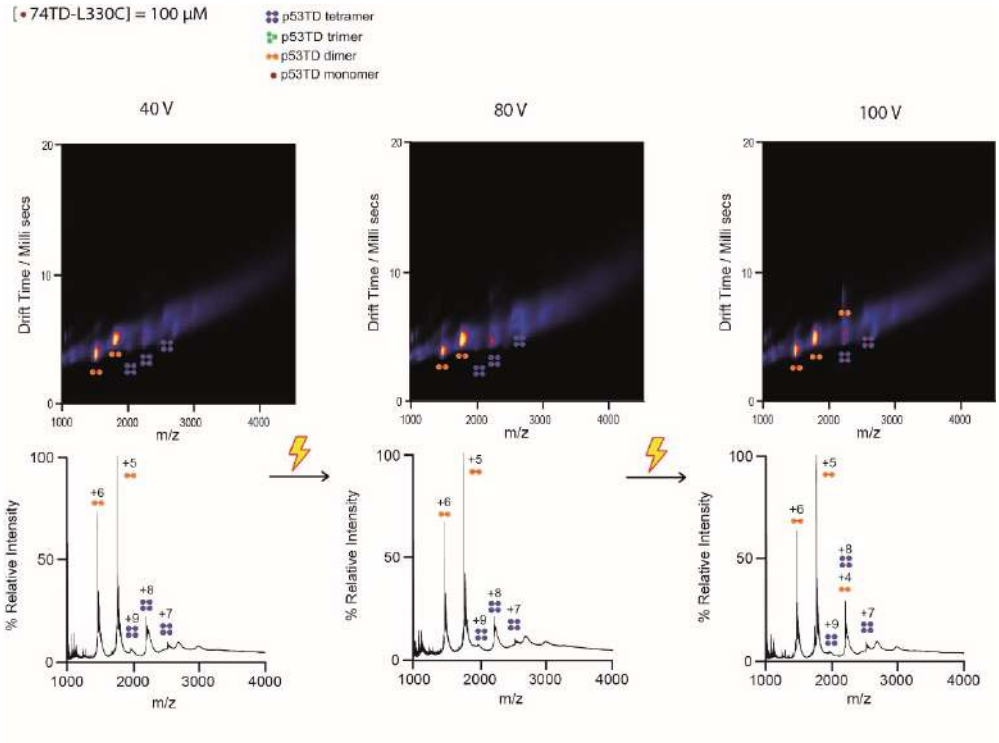

Figure S31. Native Mass Spectrometry and Ion Mobility spectra of 100 µM 74TD-L330C at different cone voltages (40, 80, and 100 V). The concentrations reported refer to the monomer. The sample was dissolved in 200 mM ammonium acetate buffer, pH 7.

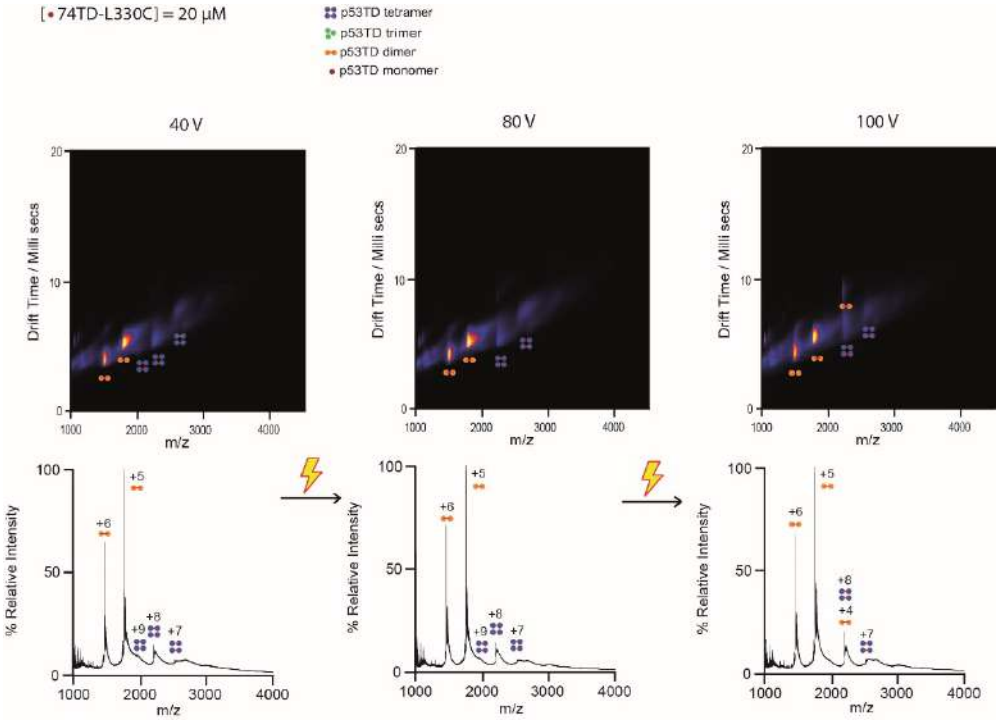

Figure S32. Native Mass Spectrometry and Ion Mobility spectra of 20 µM 74TD-L330C at different cone voltages (40, 80, and 100 V). The concentrations reported refer to the monomer. The sample was dissolved in 200 mM ammonium acetate buffer, pH 7.

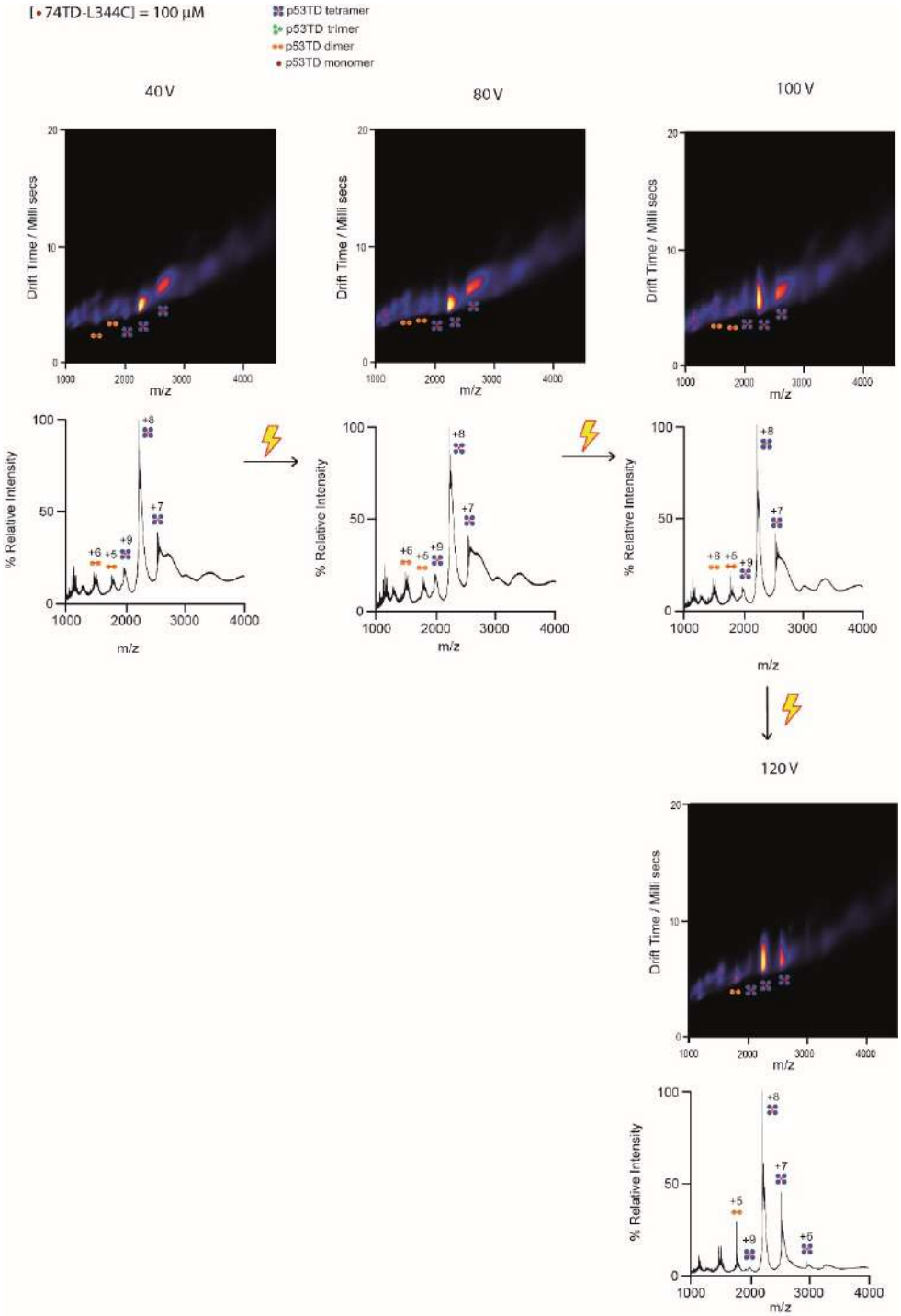

Figure S33. Native Mass Spectrometry and Ion Mobility spectra of 100 µM 74TD-L344C at different cone voltages (40, 80, 100, and 120 V). The concentrations reported refer to the monomer. The sample was dissolved in 200 mM ammonium acetate buffer, pH 7.

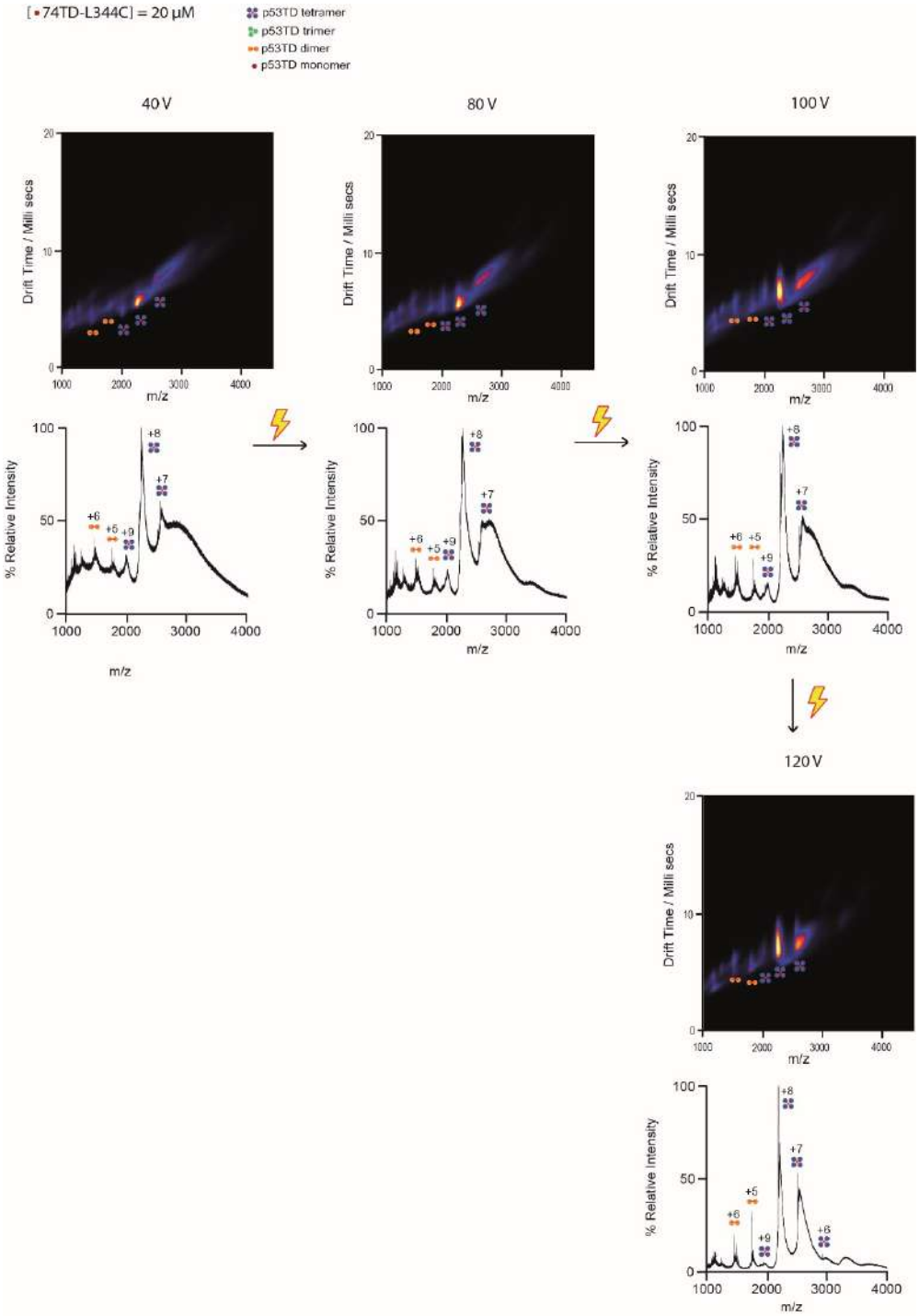

Figure S34. Native Mass Spectrometry and Ion Mobility spectra of 20 µM 74TD-L344C at different cone voltages (40, 80, 100, and 120 V). The concentrations reported refer to the monomer. The sample was dissolved in 200 mM ammonium acetate buffer, pH 7.

37TD-WT

MW 4441,02

		Monomer	Dimer	Trimer	Tetramer	Octamer	Decahexamer
Charge	1	4442,02	8883,04	13324,06	17765,08	35529,16	71057,32
	2	2221,51	4442,02	6662,53	8883,04	17765,08	35529,16
	3	1481,34	2961,68	4442,02	5922,36	11843,72	23686,44
	4	1111,26	2221,51	3331,77	4442,02	8883,04	17765,08
	5	889,20	1777,41	2665,61	3553,82	7106,63	14212,26
	6	741,17	1481,34	2221,51	2961,68	5922,36	11843,72
	7	635,43	1269,86	1904,29	2538,73	5076,45	10151,90
	8	556,13	1111,26	1666,38	2221,51	4442,02	8883,04
	9	494,45	987,89	1481,34	1974,79	3948,57	7896,15
	10	445,10	889,20	1333,31	1777,41	3553,82	7106,63

37TD-R337H

MW 4421,98

		Monomer	Dimer	Trimer	Tetramer
Charge	1	4422,98	8844,96	13266,94	17688,92
	2	2211,99	4422,98	6633,97	8844,96
	3	1474,99	2948,99	4422,98	5896,97
	4	1106,50	2211,99	3317,49	4422,98
	5	885,40	1769,79	2654,19	3538,58
	6	738,00	1474,99	2211,99	2948,99
	7	632,71	1264,42	1896,13	2527,85
	8	553,75	1106,50	1659,24	2211,99
	9	492,33	983,66	1474,99	1966,32
	10	443,20	885,40	1327,59	1769,79

37TD-T329I

MW 4454,077

		Monomer	Dimer	Trimer	Tetramer
Charge	1	4455,08	8909,15	13363,23	17817,31
	2	2228,04	4455,08	6682,12	8909,15
	3	1485,69	2970,38	4455,08	5939,77
	4	1114,52	2228,04	3341,56	4455,08
	5	891,82	1782,63	2673,45	3564,26
	6	743,35	1485,69	2228,04	2970,38
	7	637,30	1273,59	1909,89	2546,19
	8	557,76	1114,52	1671,28	2228,04
	9	495,90	990,79	1485,69	1980,59
	10	446,41	891,82	1337,22	1782,63

37TD-D352H

MW 4464,08

		Monomer	Dimer	Trimer	Tetramer
Charge	1	4465,08	8929,15	13393,23	17857,30
	2	2233,04	4465,08	6697,11	8929,15
	3	1489,03	2977,05	4465,08	5953,10
	4	1117,02	2233,04	3349,06	4465,08
	5	893,82	1786,63	2679,45	3572,26
	6	745,01	1489,03	2233,04	2977,05
	7	638,73	1276,45	1914,18	2551,90
	8	559,01	1117,02	1675,03	2233,04
	9	497,01	993,02	1489,03	1985,03
	10	447,41	893,82	1340,22	1786,63

37TD-L344R

MW 4485,051

		Monomer	Dimer	Trimer	Tetramer
Charge	1	4486,05	8971,10	13456,15	17941,20
	2	2243,53	4486,05	6728,58	8971,10
	3	1496,02	2991,03	4486,05	5981,07
	4	1122,26	2243,53	3364,79	4486,05
	5	898,01	1795,02	2692,03	3589,04
	6	748,51	1496,02	2243,53	2991,03
	7	641,72	1282,44	1923,16	2563,89
	8	561,63	1122,26	1682,89	2243,53
	9	499,34	997,68	1496,02	1994,36
	10	449,51	898,01	1346,52	1795,02

37TD-R342L

MW 4399,00

		Monomer	Dimer	Trimer	Tetramer
Charge	1	4400,00	8798,99	13197,99	17596,98
	2	2200,50	4400,00	6599,49	8798,99
	3	1467,33	2933,66	4400,00	5866,33
	4	1100,75	2200,50	3300,25	4400,00
	5	880,80	1760,60	2640,40	3520,20
	6	734,17	1467,33	2200,50	2933,66
	7	629,43	1257,86	1886,28	2514,71
	8	550,87	1100,75	1650,62	2200,50
	9	489,78	978,55	1467,33	1956,11
	10	440,90	880,80	1320,70	1760,60

37TD-L344P

MW 4425,98

		Monomer	Dimer	Trimer	Tetramer
Charge	1	4426,98	8852,96	13278,94	17704,92
	2	2213,99	4426,98	6639,97	8852,96
	3	1476,33	2951,65	4426,98	5902,31
	4	1107,50	2213,99	3320,49	4426,98
	5	886,20	1771,39	2656,59	3541,78
	6	738,66	1476,33	2213,99	2951,65
	7	633,28	1265,57	1897,85	2530,13
	8	554,25	1107,50	1660,74	2213,99
	9	492,78	984,55	1476,33	1968,10
	10	443,60	886,20	1328,79	1771,39

Table S2. Mass-to-charge ratio (m/z) of the 37TDs in monomeric, dimeric, trimeric, and tetrameric states.

74TD-L330C and 74TD-L344C

MW 4432,01 *(monomer)*

MW 8862,01 *(dimer, disulfide bridge)*

		Monomer	Dimer	Trimer	Tetramer
Charge	1	4433,01	8863,01	13297,02	17725,02
	2	2217,00	4432,01	6649,01	8863,01
	3	1478,34	2955,00	4433,01	5909,01
	4	1109,00	2216,50	3325,00	4432,01
	5	887,40	1773,40	2660,20	3545,80
	6	739,67	1478,00	2217,00	2955,00
	7	634,14	1267,00	1900,43	2533,00
	8	555,00	1108,75	1663,00	2216,50
	9	493,45	985,67	1478,34	1970,34
	10	444,20	887,20	1330,60	1773,40

Table S3. Mass-to-charge ratio (m/z) of the 74TDs in monomeric, dimeric, trimeric, and tetrameric states. Since both mutations replace a leucine to a cysteine, the molecular weight is the same for both the mutants.

SUPPLEMENTARY NMR

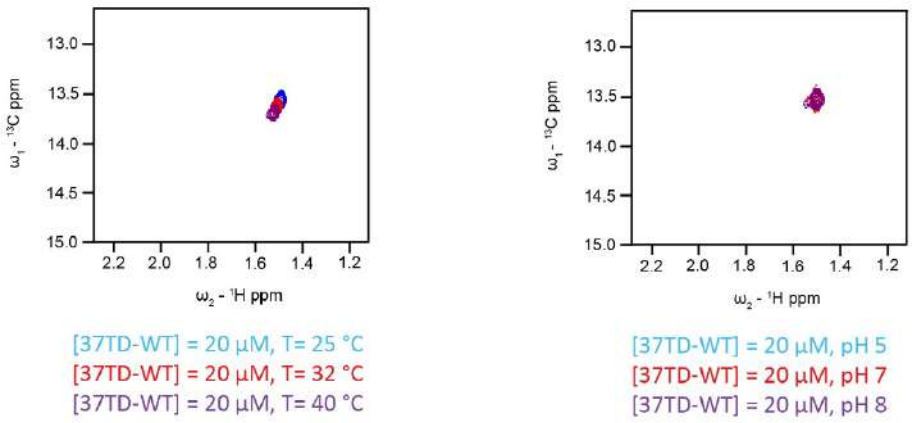

Figure S35. 2D $^{1}H,^{13}C$ HSQC spectra of 37TD-WT at different pH and temperature. The concentrations refer to the monomer. All the samples were dissolved in D_2O, pH 7, and all the spectra recorded at 25 °C unless otherwise indicated.

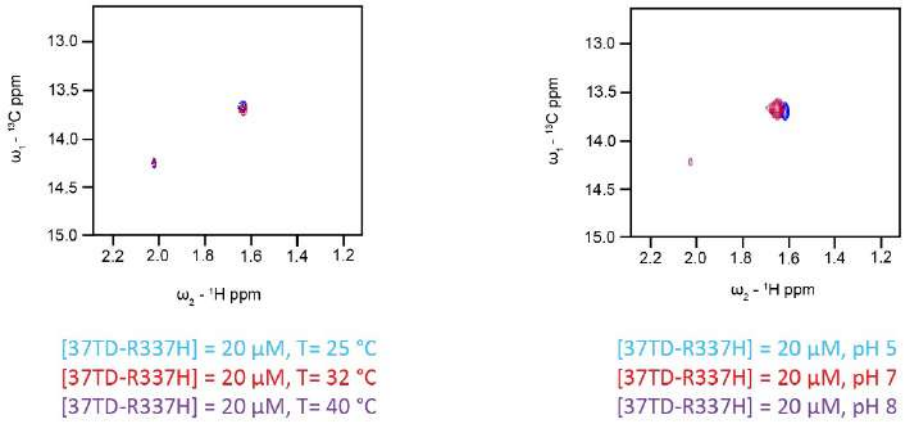

Figure S36. 2D $^{1}H,^{13}C$ HSQC spectra of 37TD-R337H at different pH and temperature. The concentrations refer to the monomer. All the samples were dissolved in D_2O, pH 7, and all the spectra recorded at 25 °C unless otherwise indicated.

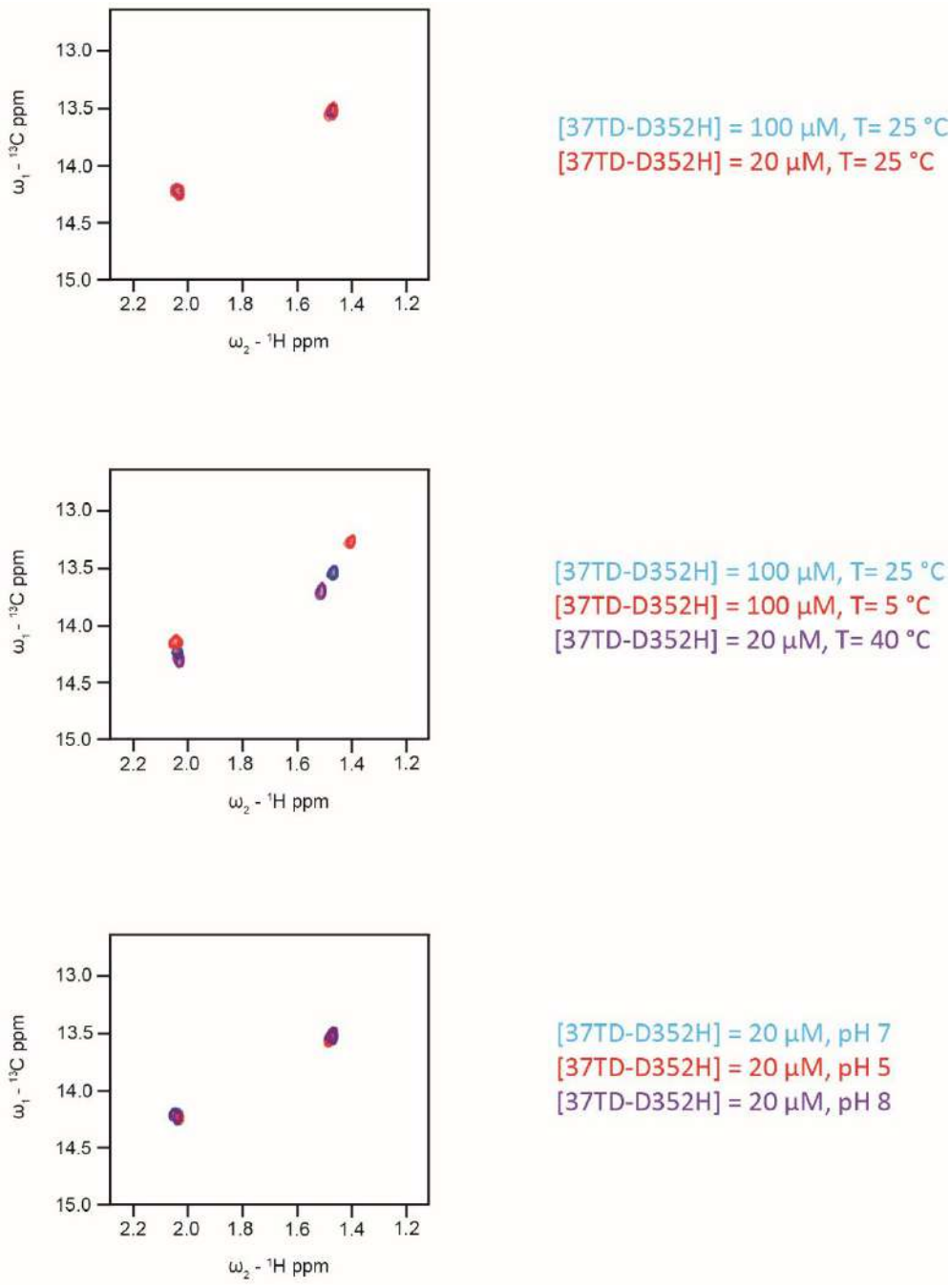

Figure S37. 2D $^{1}H,^{13}C$ HSQC spectra of 37TD-D352H at different sample concentration, temperature and pH. The concentrations refer to the monomer. All the samples were dissolved in D_2O, pH 7, and all the spectra recorded at 25 °C unless otherwise indicated.

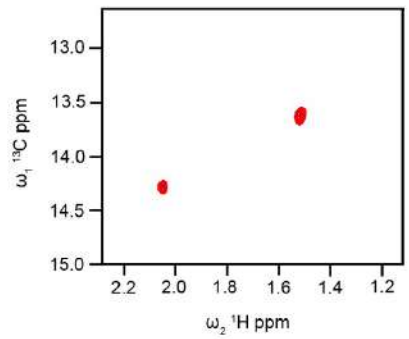

[37TD-R342L]= 75 µM, T = 25 °C
[37TD-R342L]= 20 µM, T = 25 °C

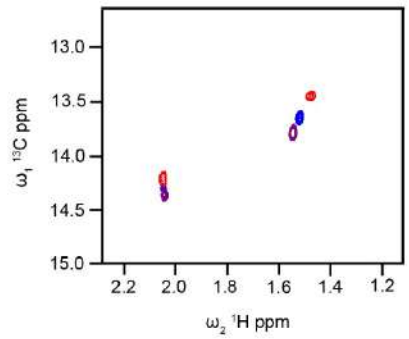

[37TD-R342L]= 75 µM, T = 25 °C
[37TD-R342L]= 75 µM, T = 5 °C
[37TD-R342L]= 20 µM, T = 40 °C

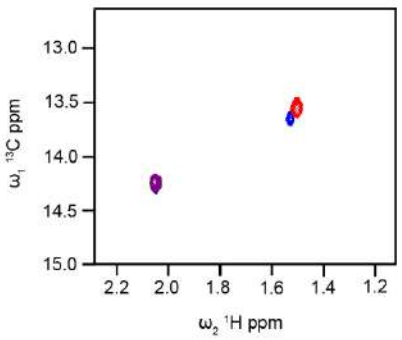

[37TD-R342L]= 75 µM, T = 25 °C
[37TD-WT]= 100 µM, T = 25 °C
[37TD-L344P]= 100 µM, T = 25 °C

Figure S38. 2D $^{1}H,^{13}C$ HSQC spectra of 37TD-R342L at different sample concentration and temperature. The concentrations refer to the monomer. All the samples were dissolved in D_2O, pH 7, and all the spectra recorded at 25 °C unless otherwise indicated.

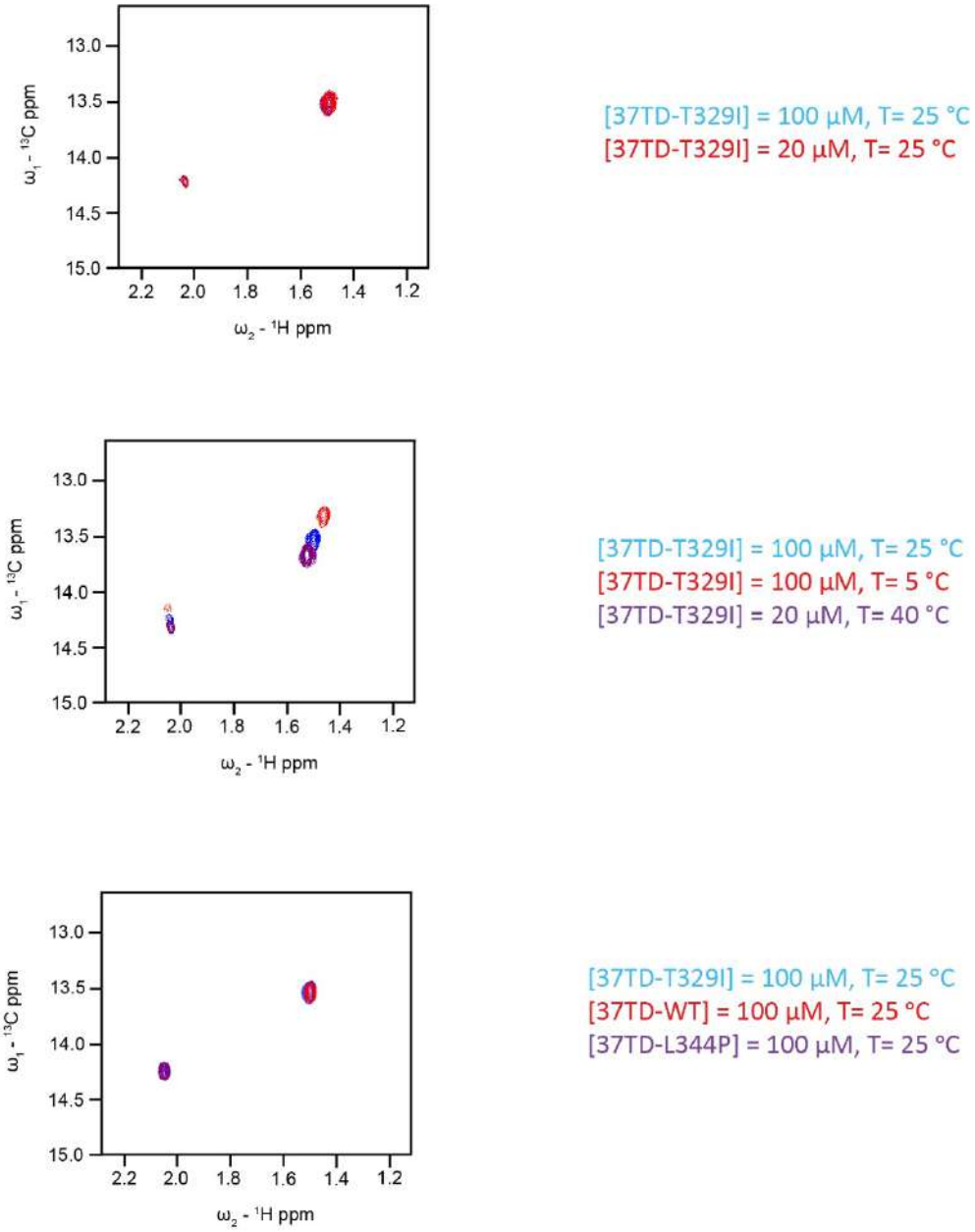

Figure S39. 2D $^{1}H,^{13}C$ HSQC spectra of 37TD-T329I at different sample concentration and temperature. The concentrations refer to the monomer. All the samples were dissolved in D_2O, pH 7, and all the spectra recorded at 25 °C unless otherwise indicated.

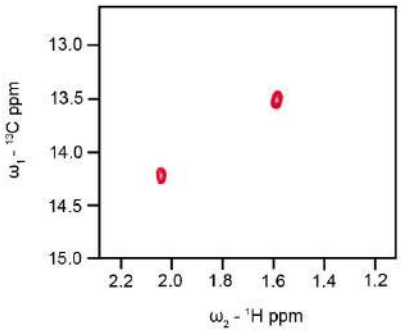

[37TD-L344R] = 100 µM, T= 25 °C
[37TD-L344R] = 20 µM, T= 25 °C

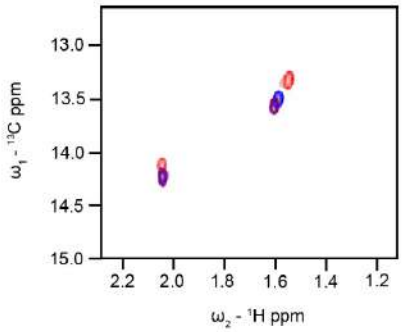

[37TD-L344R] = 100 µM, T= 25 °C
[37TD-L344R] = 100 µM, T= 5 °C
[37TD-L344R] = 20 µM, T= 32 °C

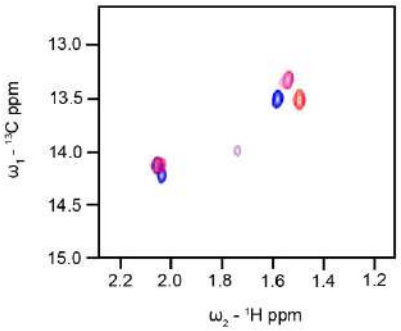

[37TD-L344R] = 100 µM, T= 25 °C
[37TD-WT] = 100 µM, T= 25 °C
[37TD-L344P] = 100 µM, T= 5 °C
[37TD-L344R] = 100 µM, T= 5 °C

Figure S40. 2D $^{1}H,^{13}C$ HSQC spectra of 37TD-L344R at different sample concentration and temperature. The concentrations refer to the monomer. All the samples were dissolved in D_2O, pH 7, and all the spectra recorded at 25 °C unless otherwise indicated.

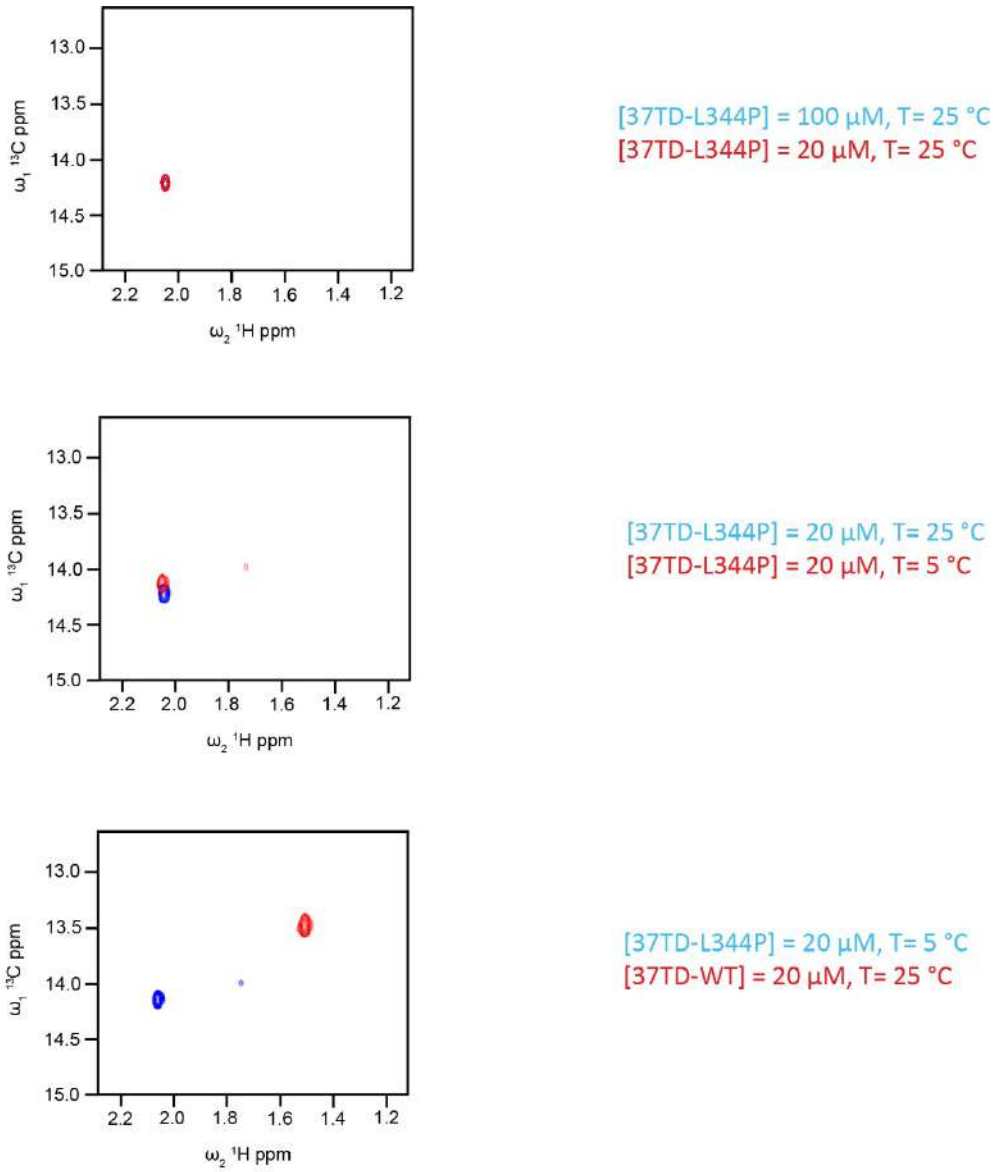

Figure S41. 2D $^{1}H,^{13}C$ HSQC spectra of 37TD-L344P at different sample concentration and temperature. The concentrations refer to the monomer. All the samples were dissolved in D_2O, pH 7, and all the spectra recorded at 25 °C unless otherwise indicated.

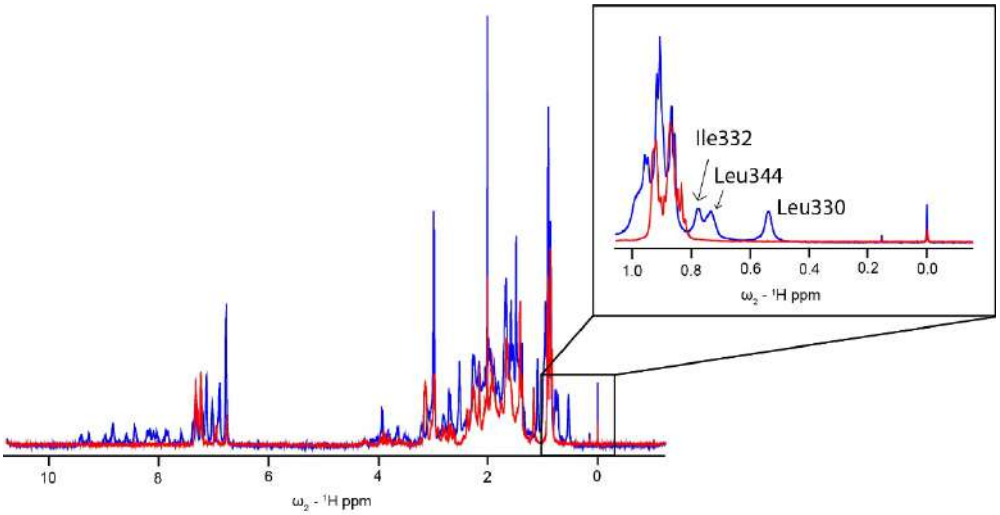

Figure S42. 1D ^{1}H spectra of 37TD-WT (blue) and 37TD-L344P (red) dissolved in D_2O, pH 7, at a monomer concentration of 100 µM. The spectra are recorded at 25 °C.

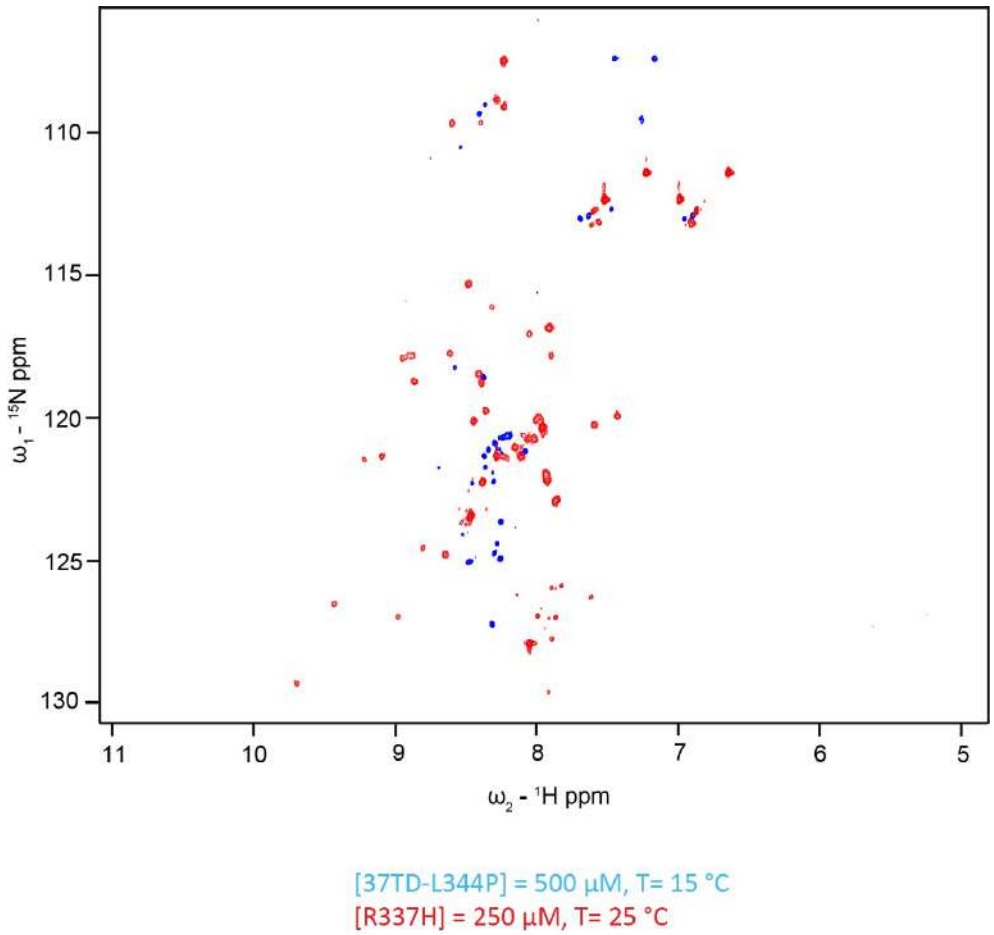

Figure S43. In blue, $^{1}H,^{15}N$ HSQC spectrum of 37TD-L344P dissolved in D_2O, pH 7. The signals of the spectrum are due to the natural abundance of ^{15}N. For comparison, in red, $^{1}H,^{15}N$ HSQC spectrum of a reference R337H, res 311-367, expressed in *E. coli* and enriched in ^{15}N [24] . R337H was dissolved in 10 mM sodium phosphate buffer, pH 7. The concentrations refer to the monomer.

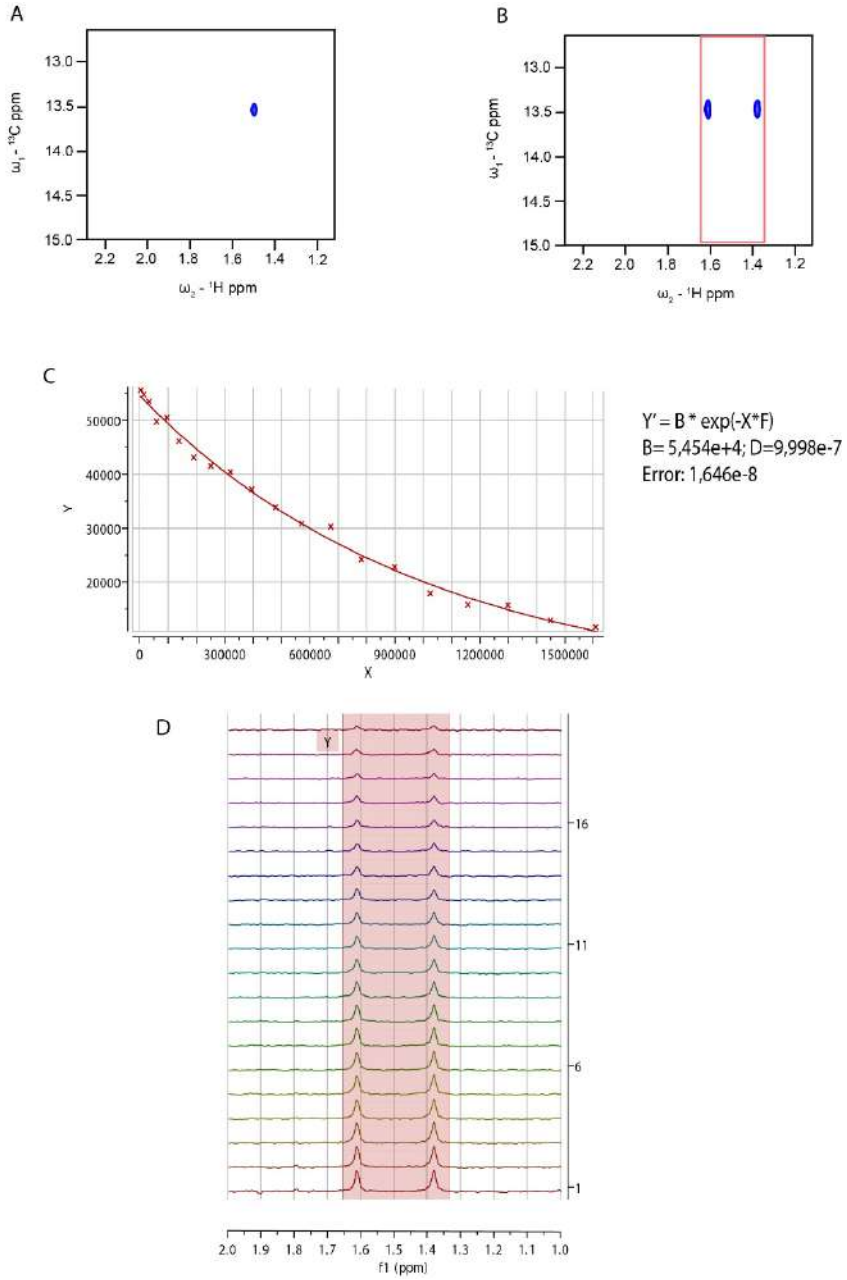

Figure S44. X-STE NMR diffusion of 37TD-WT monitoring the size of the species containing ^{13}C-attached ^{1}H nuclei. (A) 2D ^{1}H,^{13}C-HSQC. (B) ^{13}C-coupled 2D ^{1}H,^{13}C-HSQC illustrating the splitting of the Met340 $^{1}H^{\varepsilon}$ signal ($^{1}J_{HC}$ ≈140 Hz). (C,D)) X-STE NMR diffusion experiments. The decay in signal intensity of the Met340 $^{1}H^{\varepsilon}$ signal (panel D) was fitted to a mono exponential function to obtain the coefficient diffusion. X-STE experiments were acquired without decoupling and the Met340 $^{1}H^{\varepsilon}$ signal splits into a doublet ($^{1}J_{HC}$ ≈140 Hz). The spectra were recorded at 25 °C using a monomer concentration of 100 µM (D_2O, pH 7).

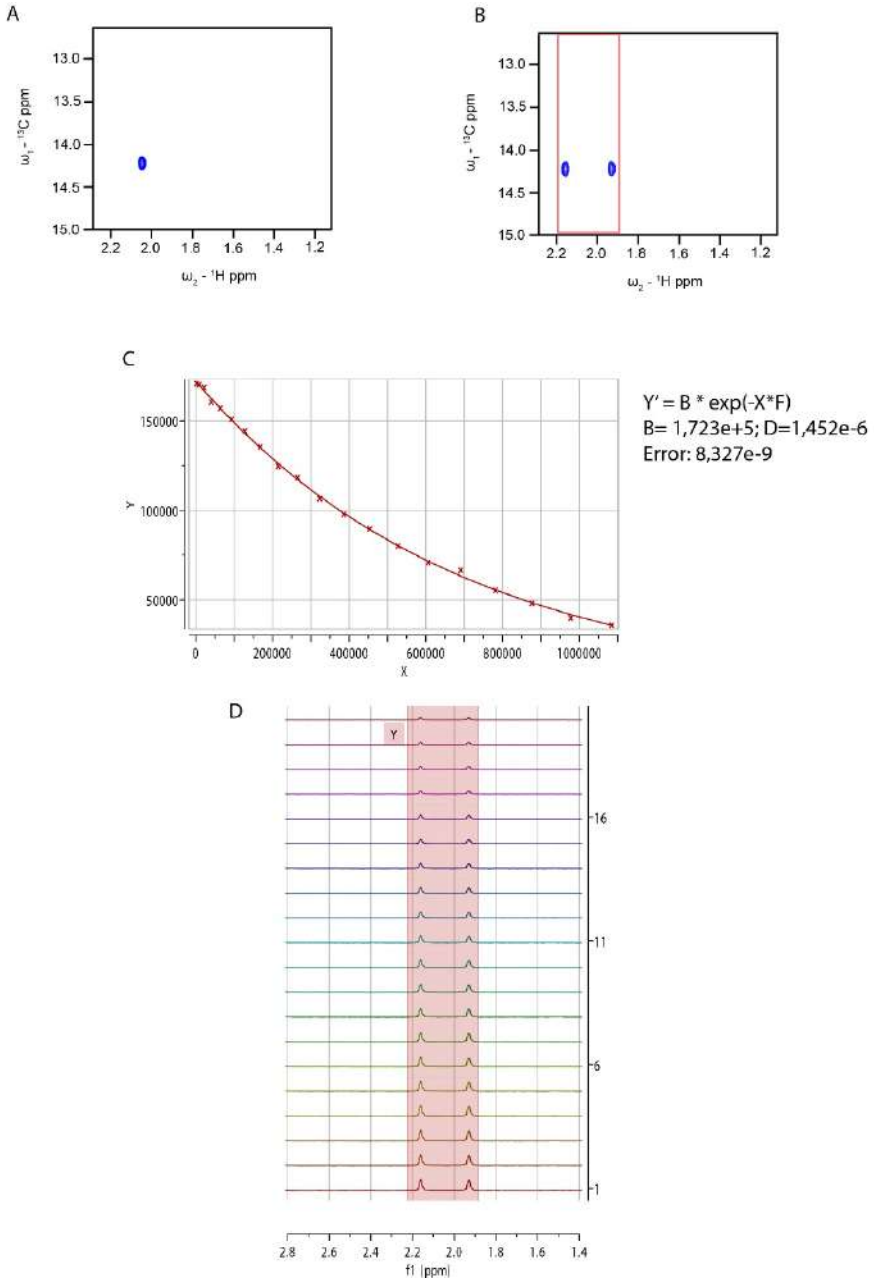

Figure S45. X-STE NMR diffusion of 37TD-L344P monitoring the size of the species containing ^{13}C-attached ^{1}H nuclei. (A) 2D ^{1}H,^{13}C-HSQC. (B) ^{13}C-coupled 2D ^{1}H,^{13}C-HSQC illustrating the splitting of the Met340 $^{1}H^{\varepsilon}$ signal ($^{1}J_{HC}$ ≈140 Hz). (C,D)) X-STE NMR diffusion experiments. The decay in signal intensity of the Met340 $^{1}H^{\varepsilon}$ signal (panel D) was fitted to a mono exponential function to obtain the coefficient diffusion. X-STE experiments were acquired without decoupling and the Met340 $^{1}H^{\varepsilon}$ signal splits into a doublet ($^{1}J_{HC}$ ≈140 Hz). The spectra were recorded at 25 °C using a monomer concentration of 100 µM (D_2O, pH 7).

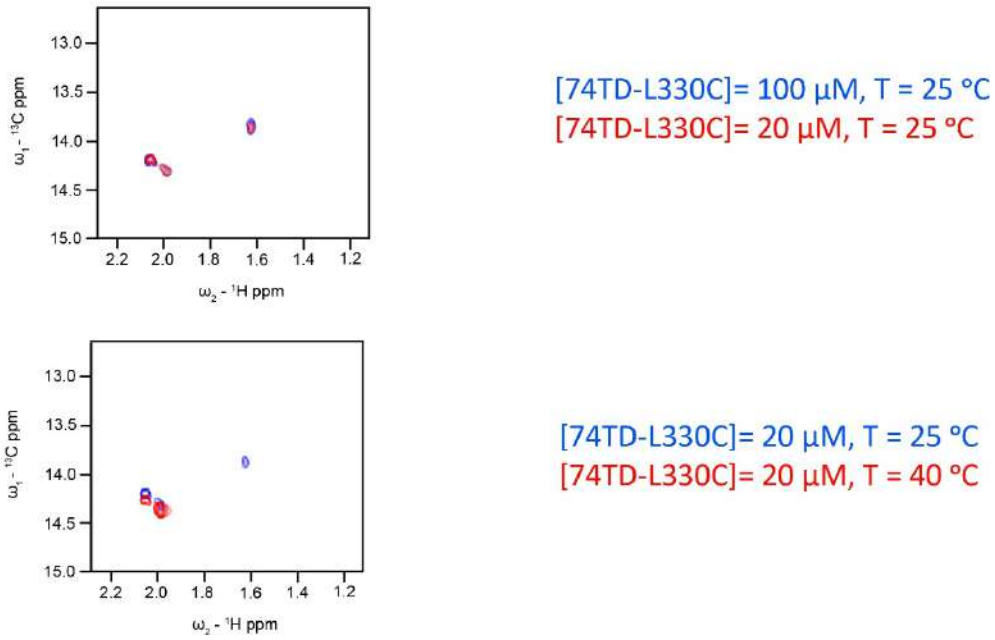

Figure S46. 2D $^{1}H,^{13}C$ HSQC spectra of 74TD-L330C at different sample concentration and temperature. The concentrations refer to the monomer. All the samples were dissolved in D_2O, pH 7, and all the spectra recorded at 25 °C unless otherwise indicated.

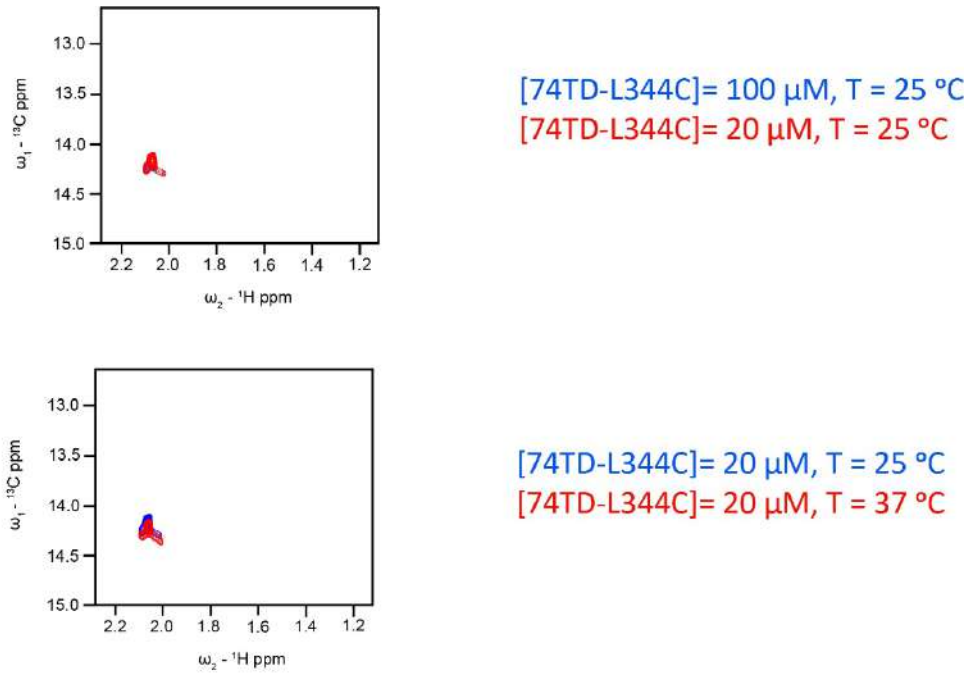

Figure S47. 2D $^{1}H,^{13}C$ HSQC spectra of 74TD-L344C at different sample concentration and temperature. The concentrations refer to the monomer. All the samples were dissolved in D_2O, pH 7, and all the spectra recorded at 25 °C unless otherwise indicated.

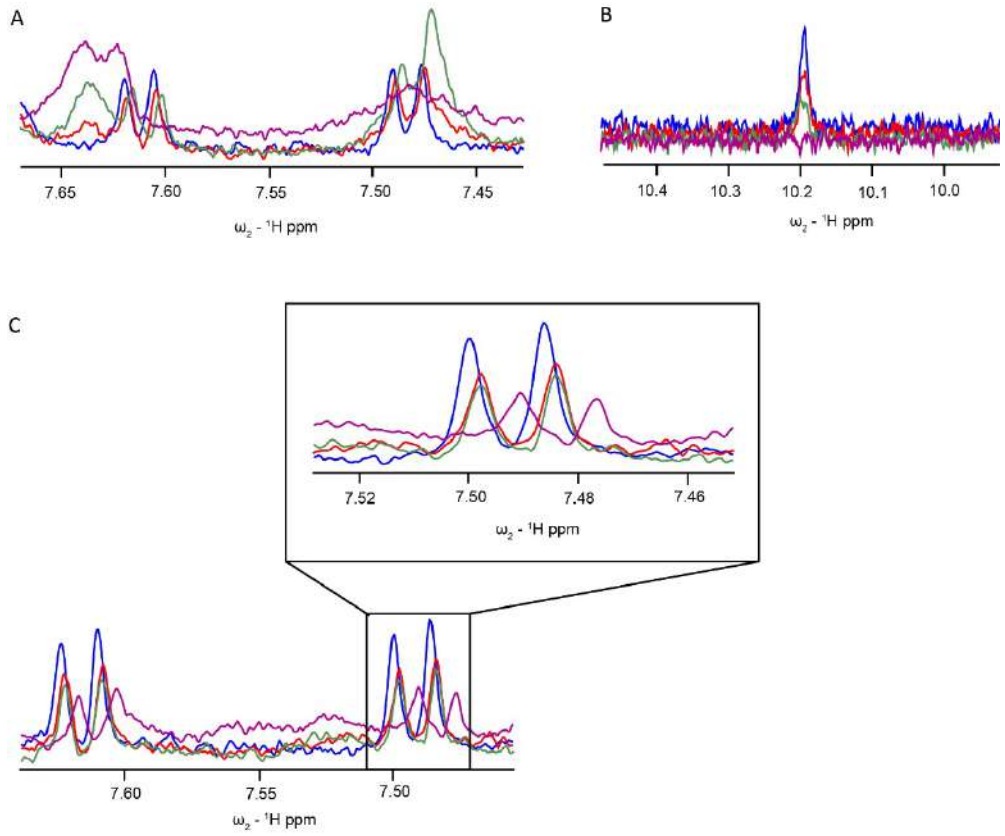

Figure S48. ^{1}H NMR chemical-shift-perturbation experiments of R4 at a concentration of 20 µM (blue) which was titrated with 10 (red), 20 (green), and 40 µM (purple) of 37TD-R337H. The spectra were acquired at 5 °C (A, B) and 37 °C (C), pH 7.5. Only the aromatic region is shown in panel A and C and the indole NH signal is shown in panel B.

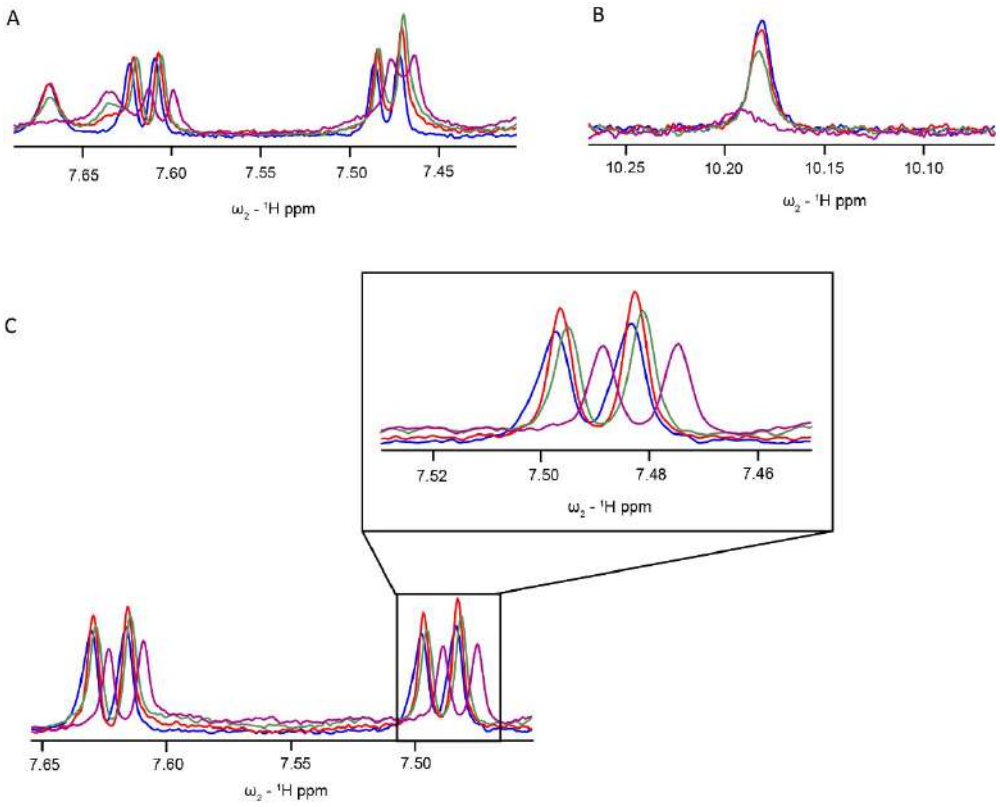

Figure S49. ^{1}H NMR chemical-shift-perturbation experiments of Rab4 at a concentration of 20 µM (blue) which was titrated with 10 (red), 20 (green), and 40 µM (purple) of 37TD-R337H. The spectra were acquired at 5 °C (A, B) and 37 °C (C), pH 7.5. Only the aromatic region is shown in panel A and C and the indole NH signal is shown in panel B.

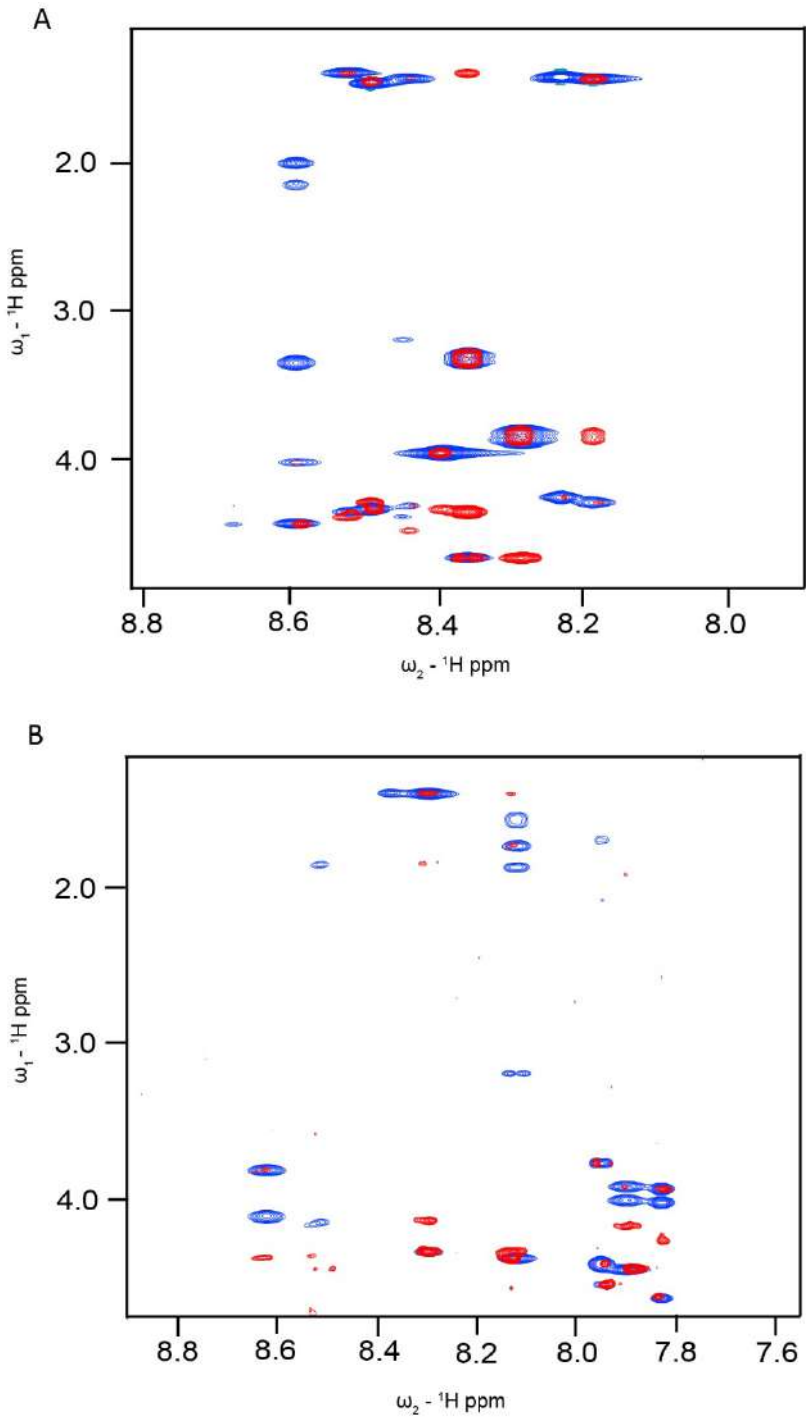

Figure S50. TOCSY (blue) and NOESY (red) 2D ^{1}H ^{1}H NMR experiments of Rab4 (A) and cRys2R2 (B). The spectra were acquired at 5 °C, at peptide concentration of 2 mM in 10% D_2O, pH 7.

SUPPLEMENTARY MST

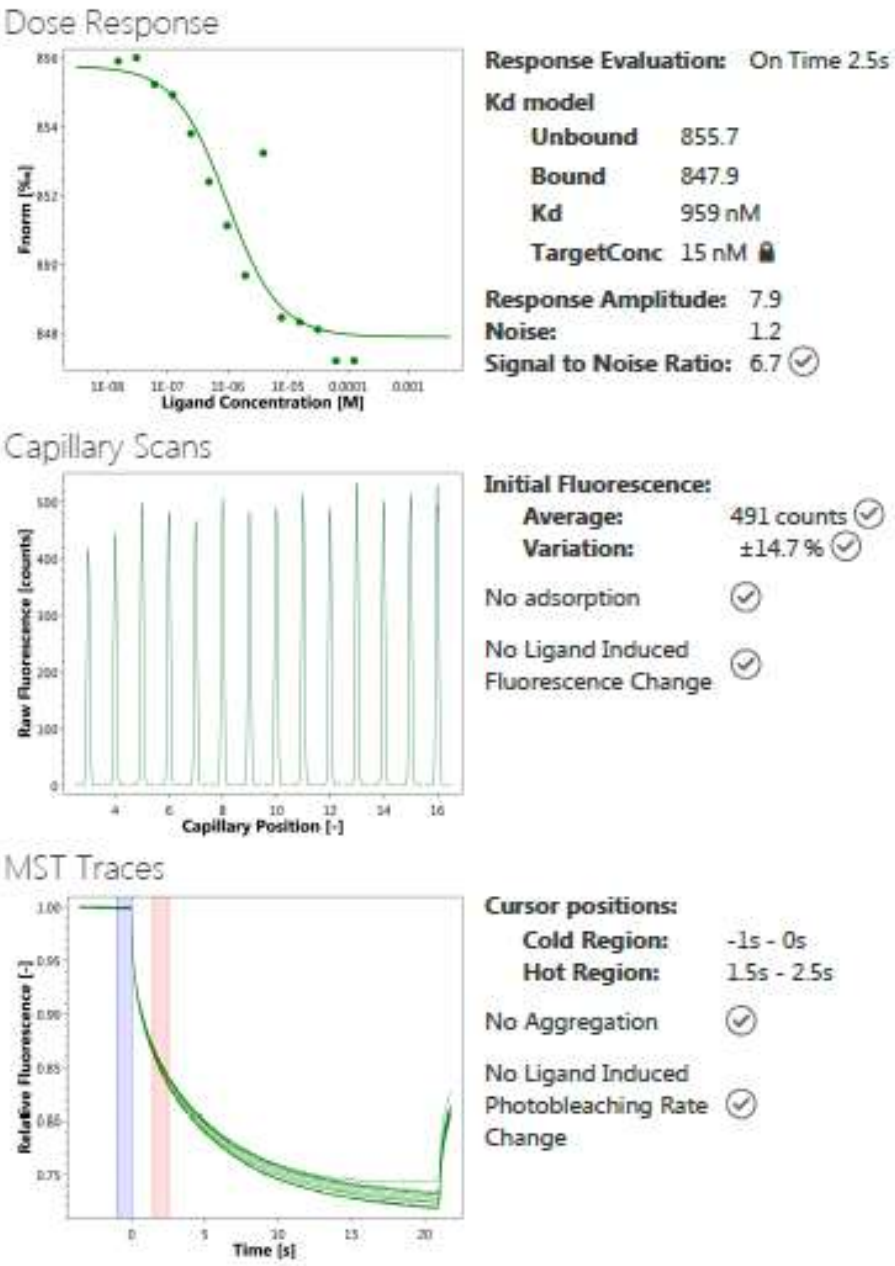

Figure S51. MST experiment of 37TD-R337H at pH 7. The concentration of 37TD-R337H* (target) was 15 nM and the highest concentration of 37TD-R337H (ligand) was 500 µM.

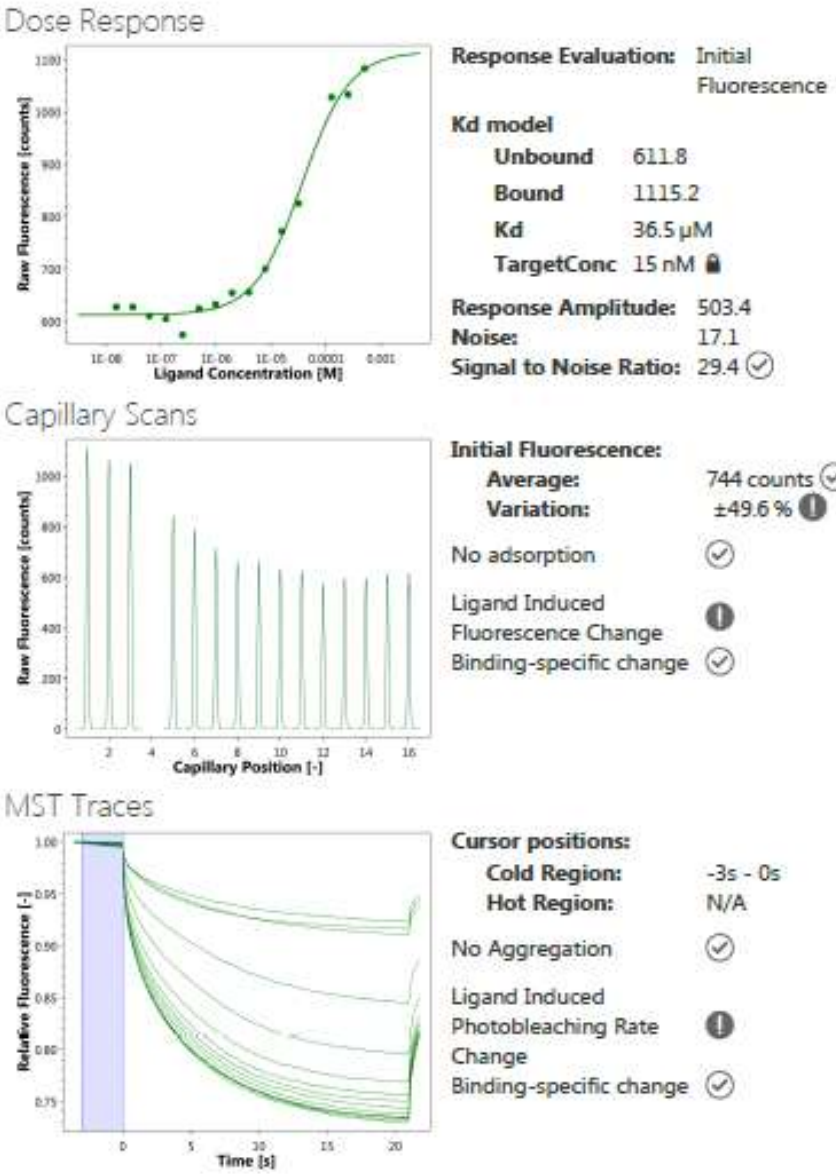

Figure S52. MST experiment of 37TD-R337H at pH 5.3. The concentration of 37TD-R337H* (target) was 15 nM and the highest concentration of 37TD-R337H (ligand) was 500 µM.

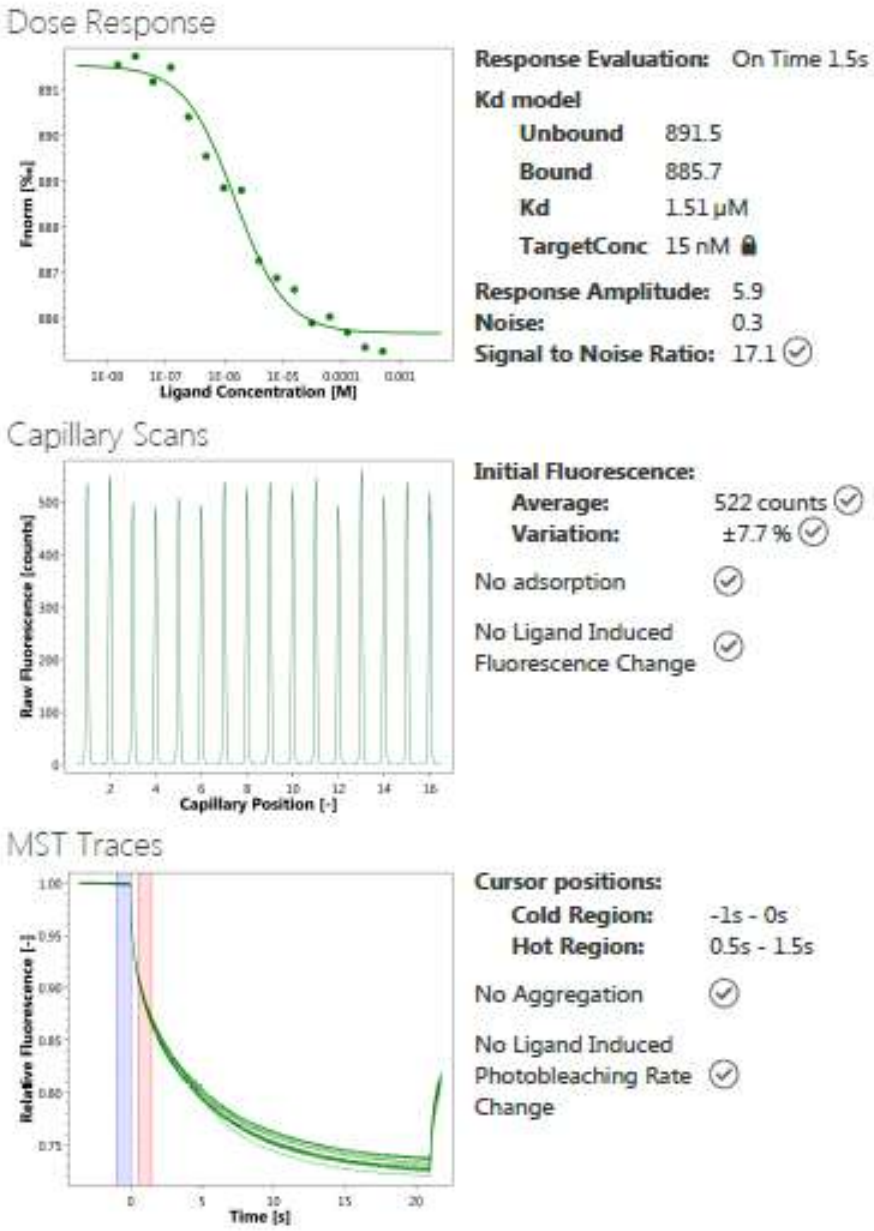

Figure S53. MST experiment of 37TD-R337H at pH 8. The concentration of 37TD-R337H* (target) was 15 nM and the highest concentration of 37TD-R337H (ligand) was 500 µM.

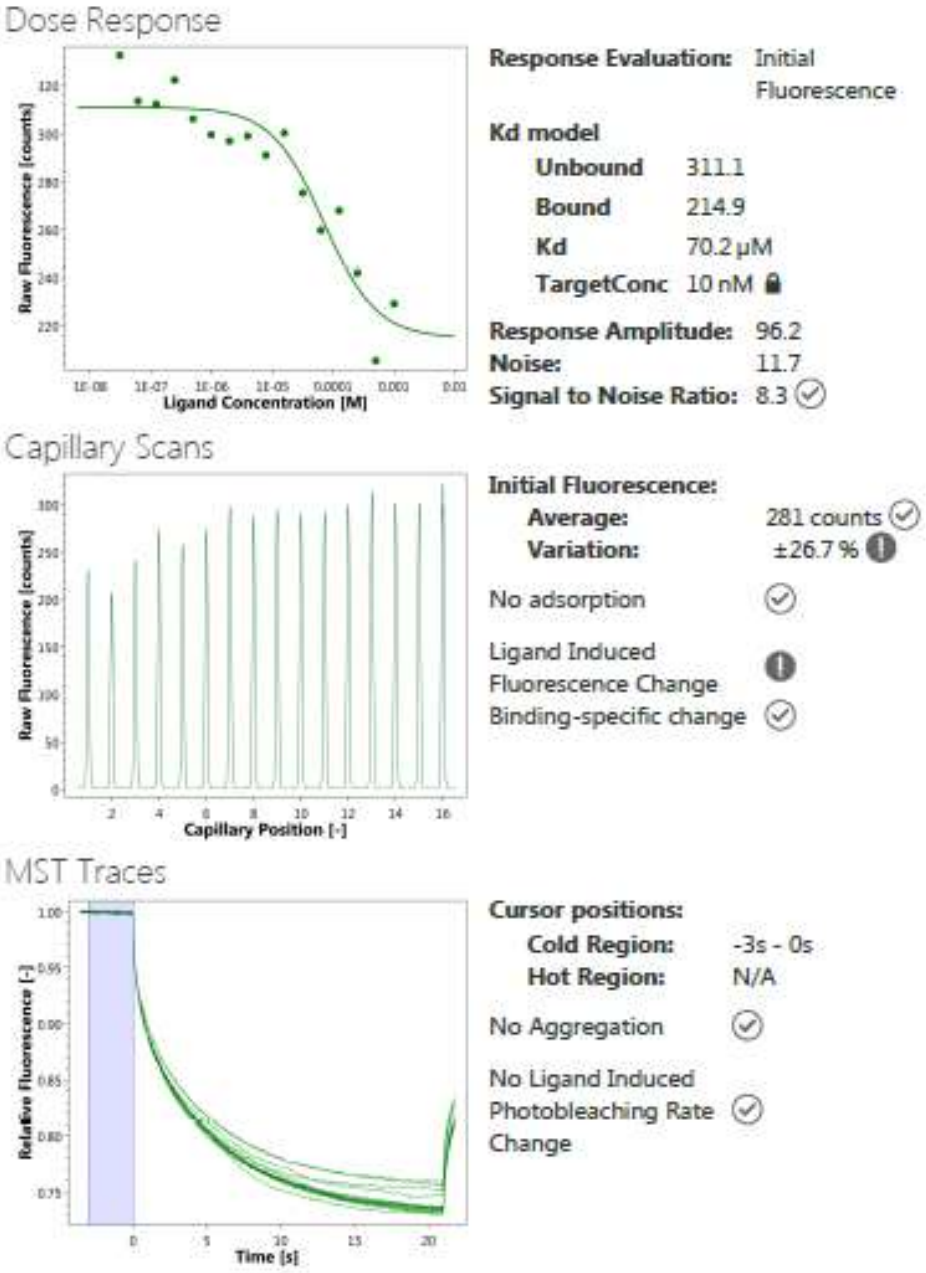

Figure S54. MST experiment of 37TD-D352H at pH 7. The concentration of 37TD-D352H* (target) was 10 nM and the highest concentration of 37TD-D352H (ligand) was 1 mM.

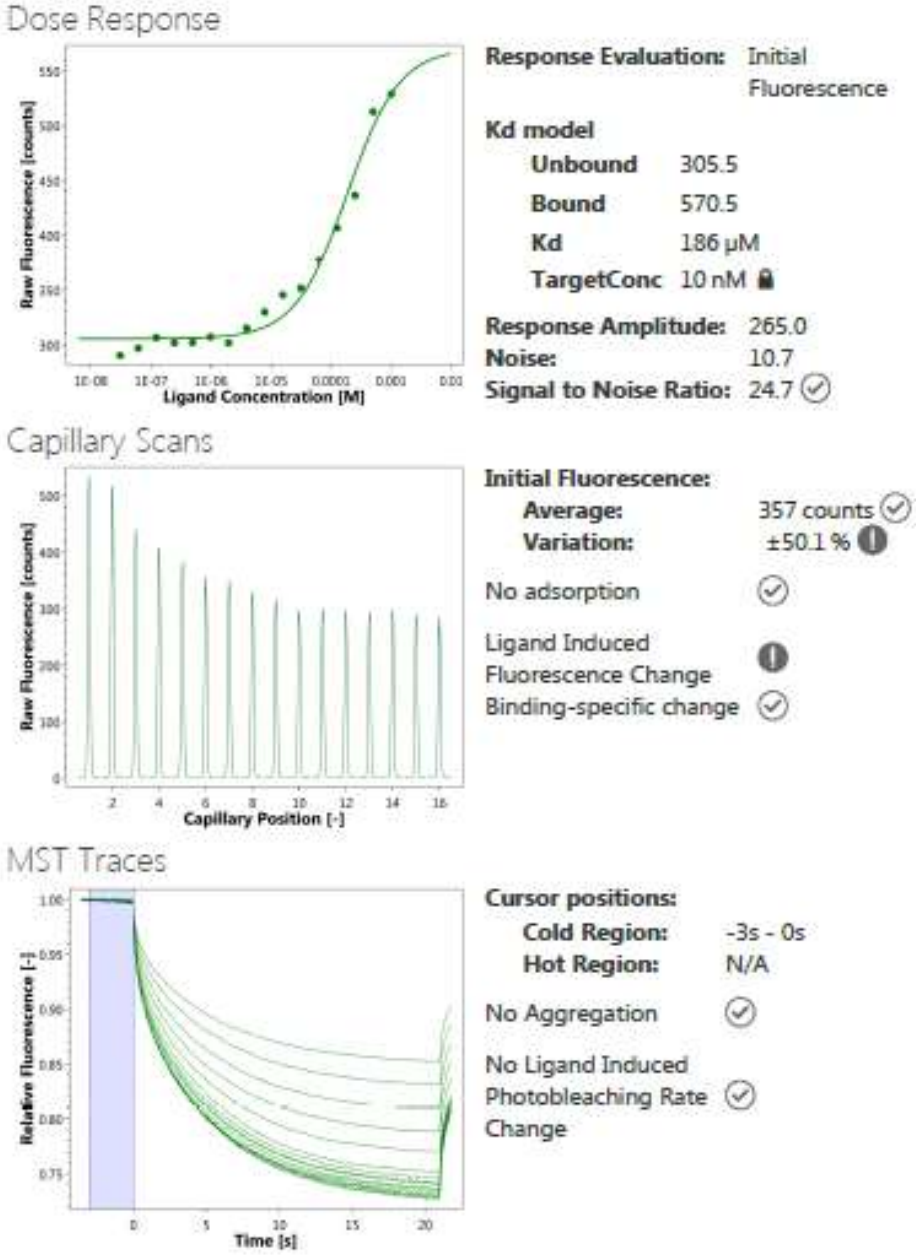

Figure S55. MST experiment of 37TD-D352H at pH 5.3. The concentration of 37TD-D352H* (target) was 10 nM and the highest concentration of 37TD-D352H (ligand) was 1 mM.

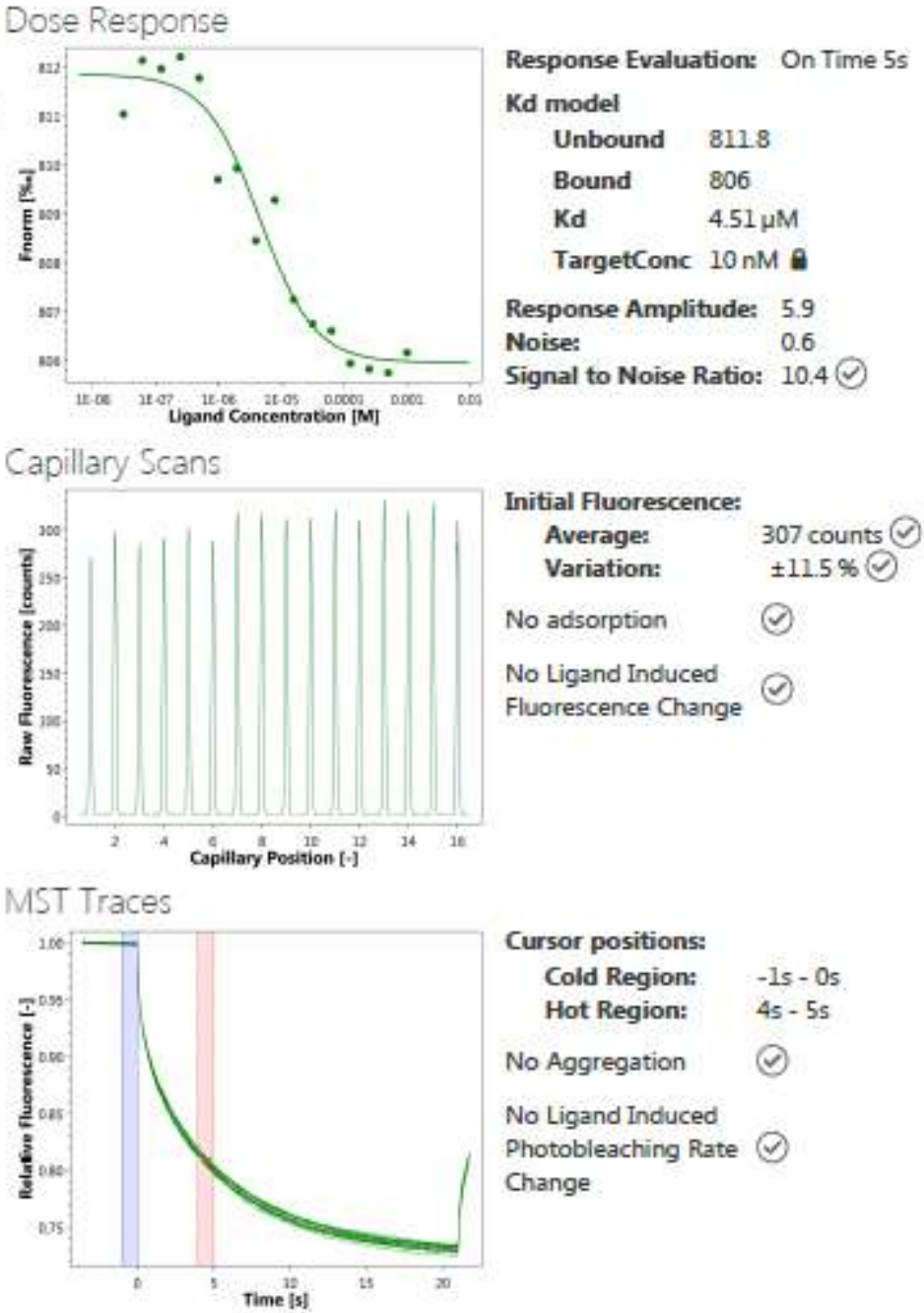

Figure S56. MST experiment of 37TD-D352H at pH 8. The concentration of 37TD-D352H* (target) was 10 nM and the highest concentration of 37TD-D352H (ligand) was 1 mM.

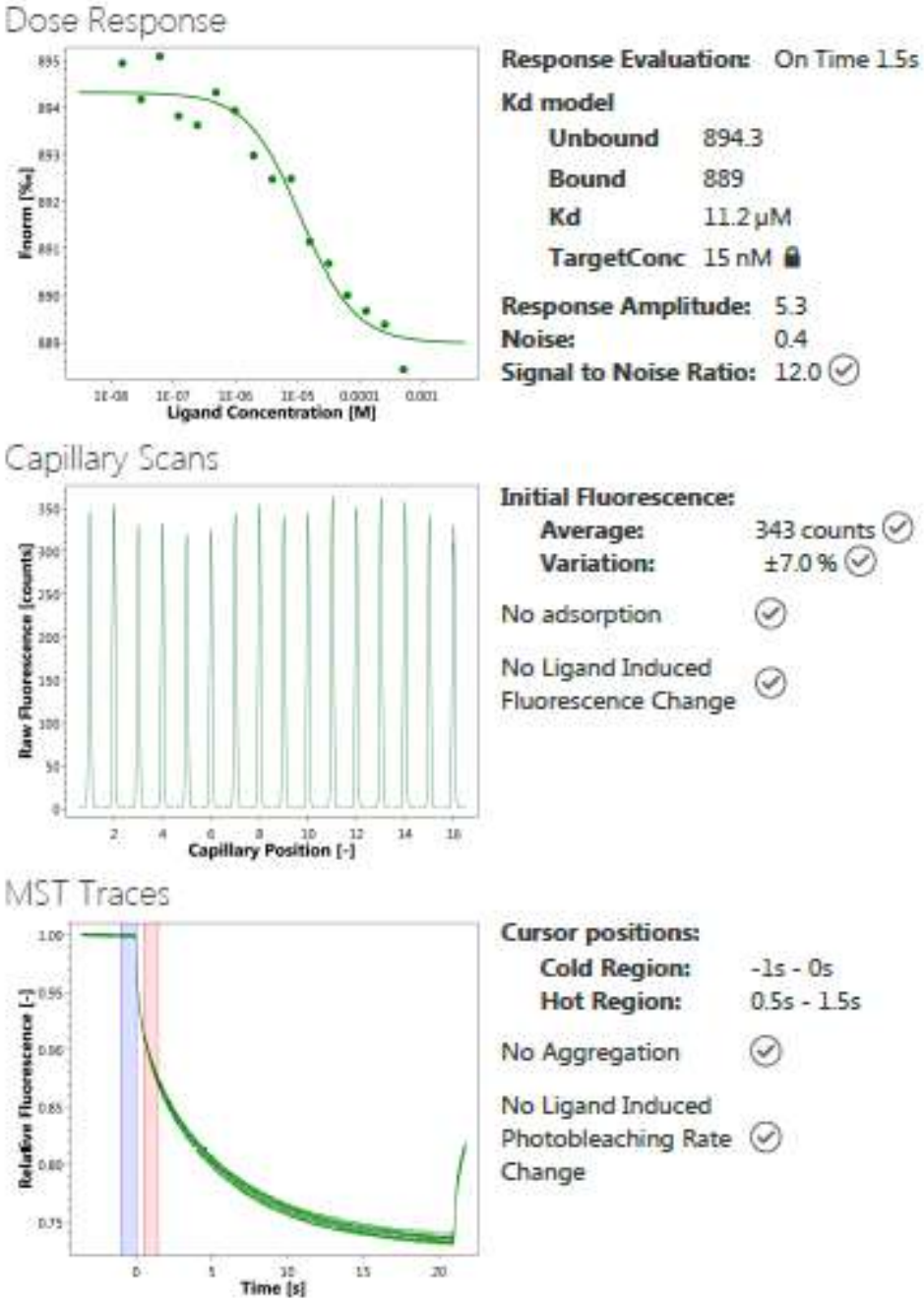

Figure S57. MST experiment of 37TD-R342L. The concentration of 37TD-R342L* (target) was 15 nM and the highest concentration of 37TD-R342L (ligand) was 500 µM.

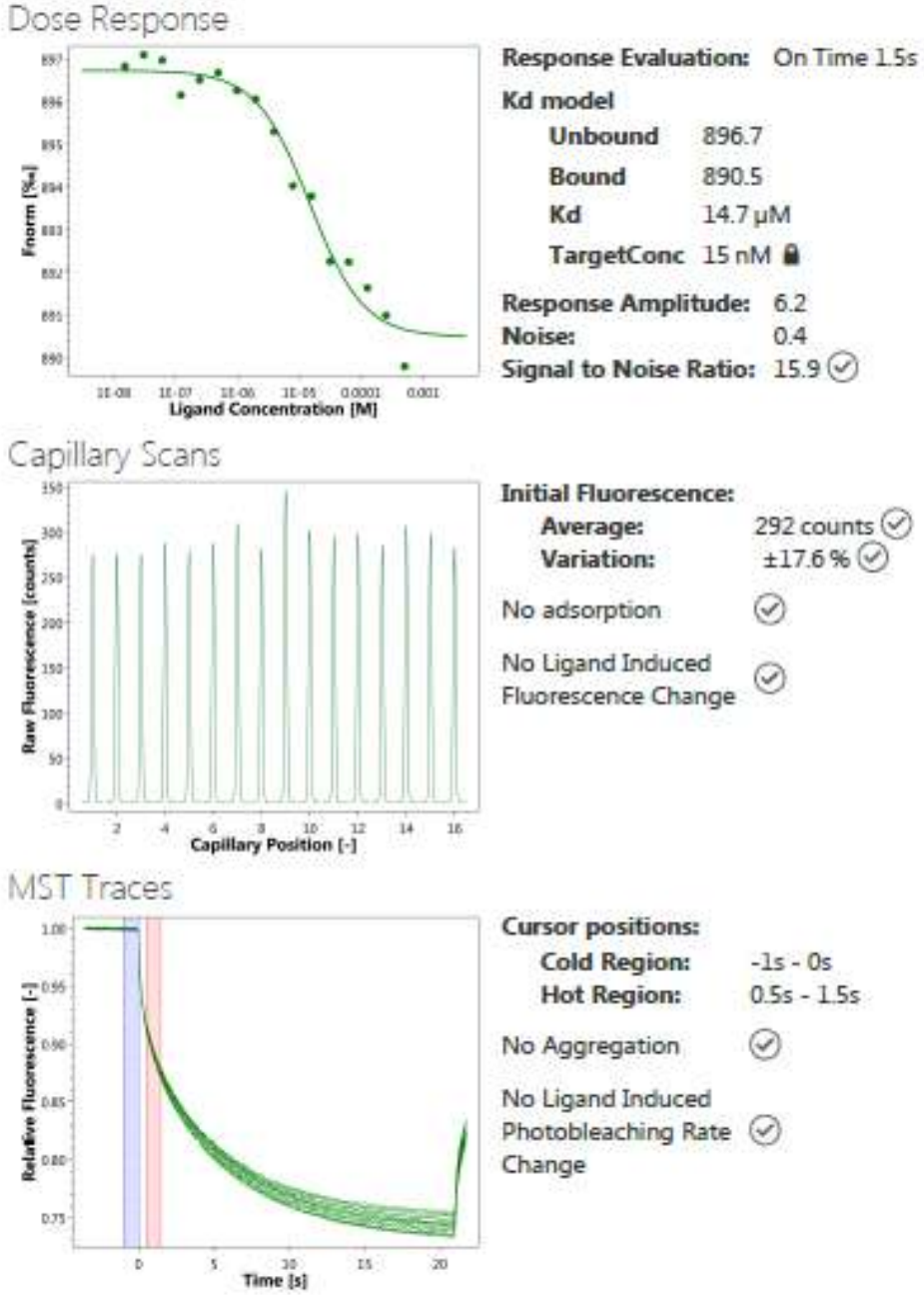

Figure S58. MST experiment of 37TD-T329I. The concentration of 37TD- T329I * (target) was 15 nM and the highest concentration of 37TD- T329I (ligand) was 500 µM.

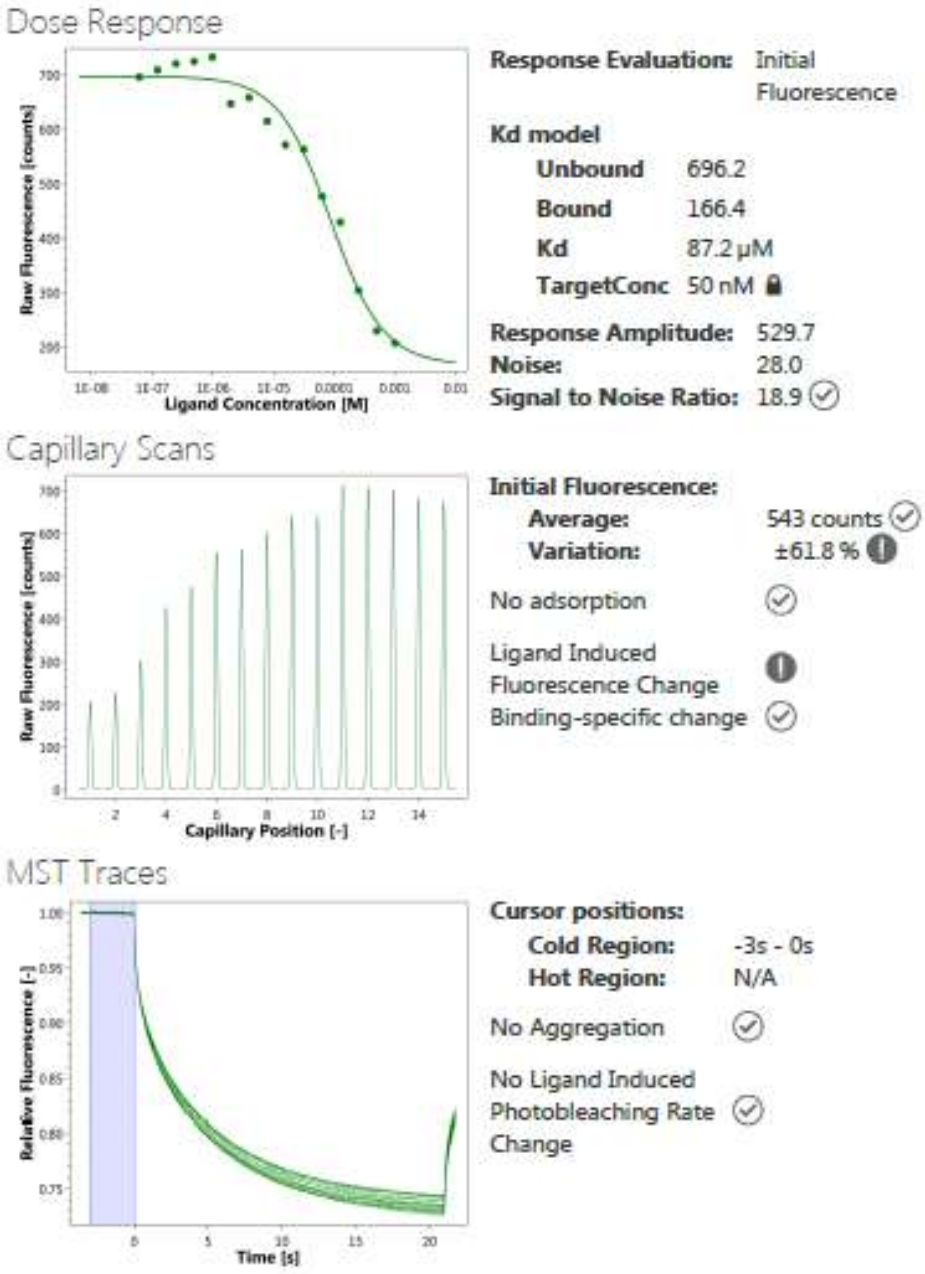

Figure S59. MST experiment of 37TD-L344R. The concentration of 37TD-L344R* (target) was 50 nM and the highest concentration of 37TD-L344R (ligand) was 1 mM.

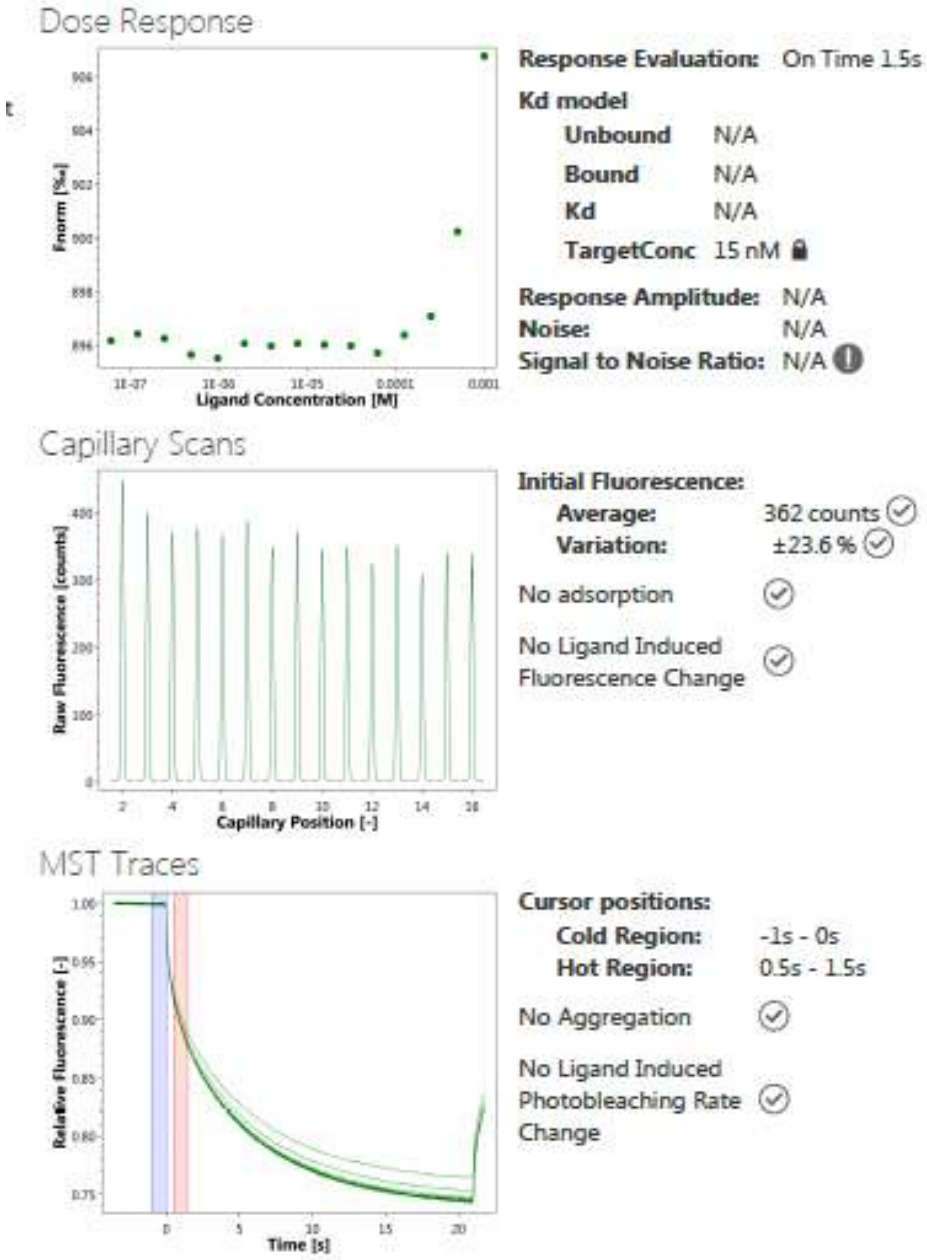

Figure S60. MST experiment of 37TD-L344P. The concentration of 37TD-L344P* (target) was 10 nM and the highest concentration of 37TD-L344P (ligand) was 2 mM.

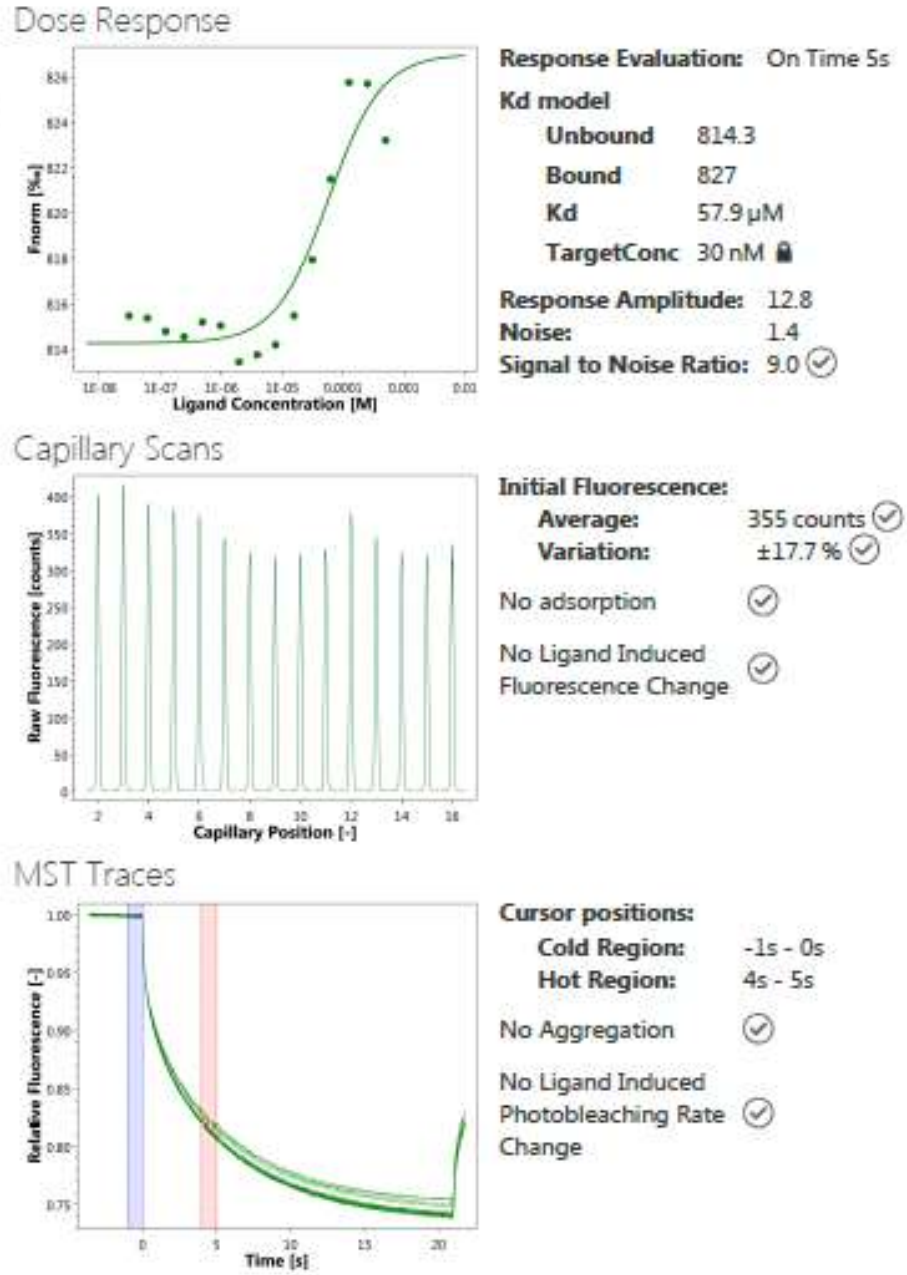

Figure S61. MST experiment of 74TD-L330C. The concentration of 74TD-L330C* (target) was 30 nM and the highest concentration of 74TD-L330C (ligand) was 1 mM.

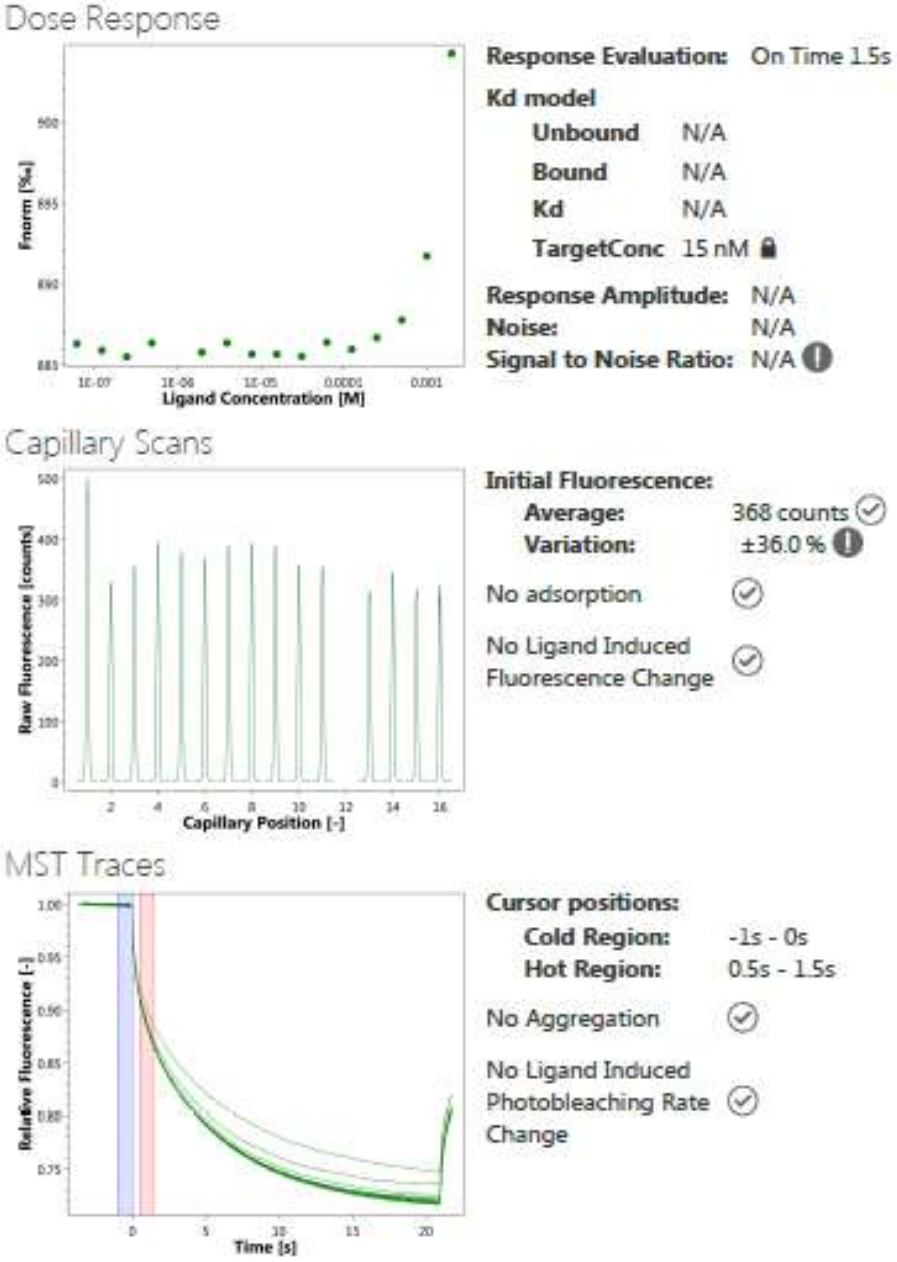

Figure S62. MST experiment of 74TD-L344C. The concentration of 74TD-L344C* (target) was 15 nM and the highest concentration of 74TD-L344C (ligand) was 2 mM.

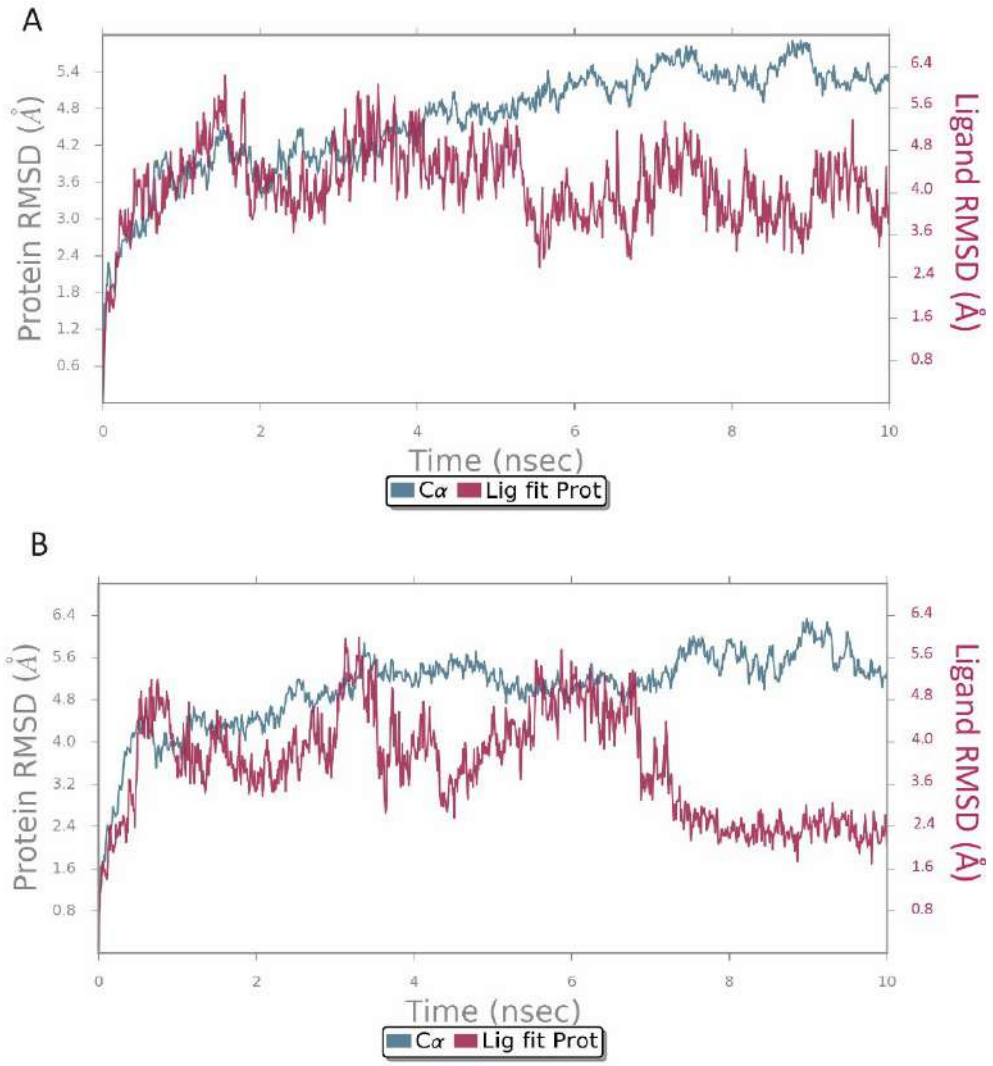

Figure S63. Molecular dynamics analysis of backbone RMSD from initial structure (blue line) and of ligand RMSD to initial pose (purple line). Analysis of the complexes p53WT @ β-3*R* (A) and p53WT @ β-2*S* (B) trajectories.

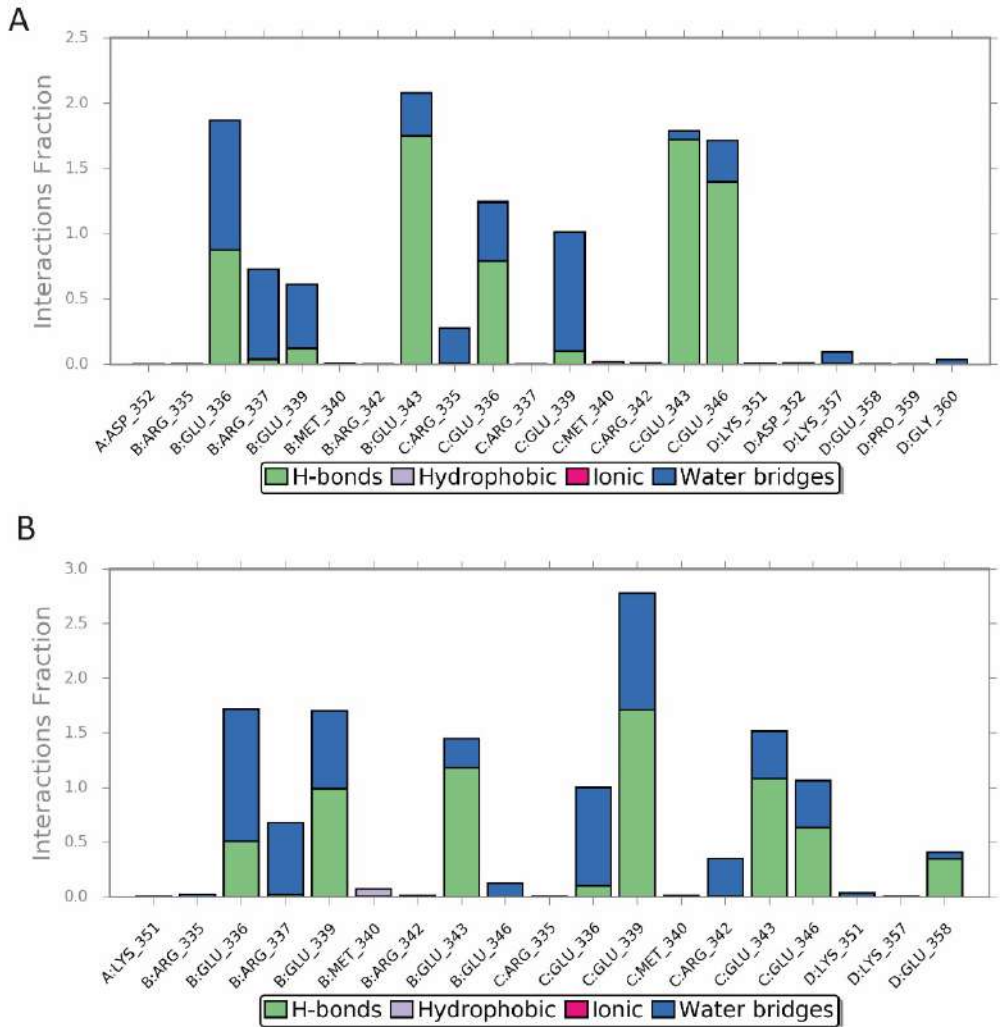

Figure S64. Molecular dynamics analysis of protein-ligand contacts. Analysis of the complexes p53WT @ β-3*R* (A) and p53WT @ β-2*S* (B) trajectories.

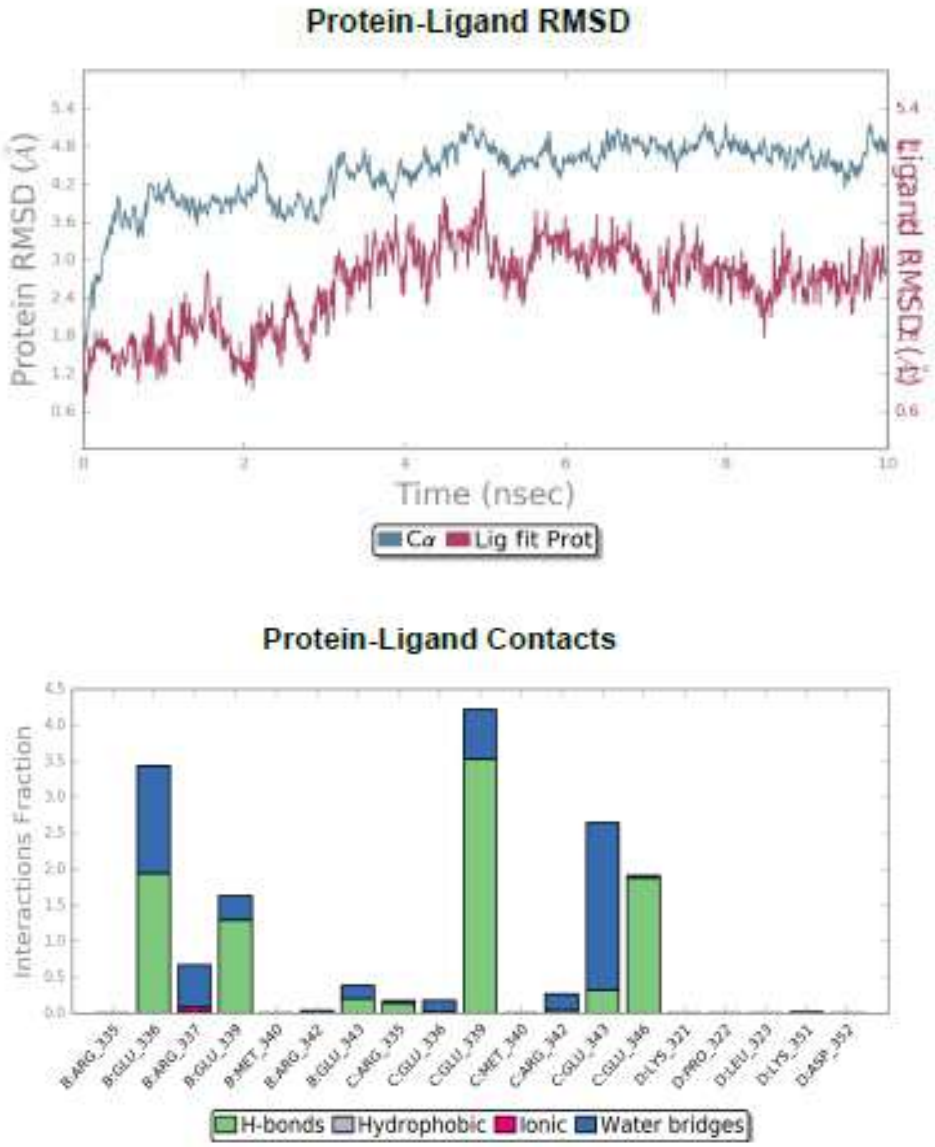

Figure S65. Molecular dynamics analysis of backbone RMSD from initial structure (blue line) and of ligand RMSD to initial pose (purple line). Below, molecular dynamics analysis of protein-ligand contacts. Analysis of the complexes p53WT @ cR4 trajectories.

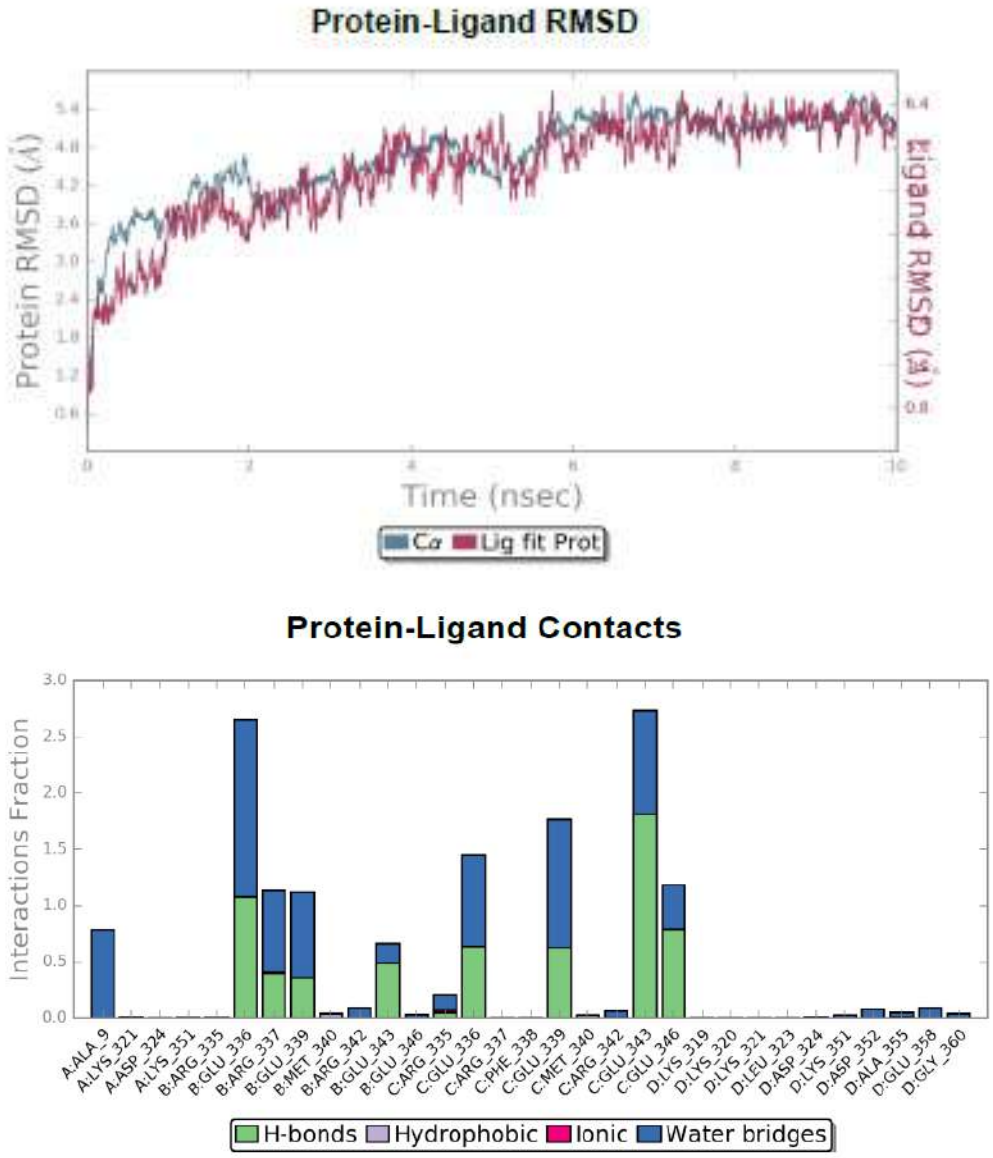

Figure S66. Molecular dynamics analysis of backbone RMSD from initial structure (blue line) and of ligand RMSD to initial pose (purple line). Below, molecular dynamics analysis of protein-ligand contacts. Analysis of the complexes p53WT @ cR4A trajectories.

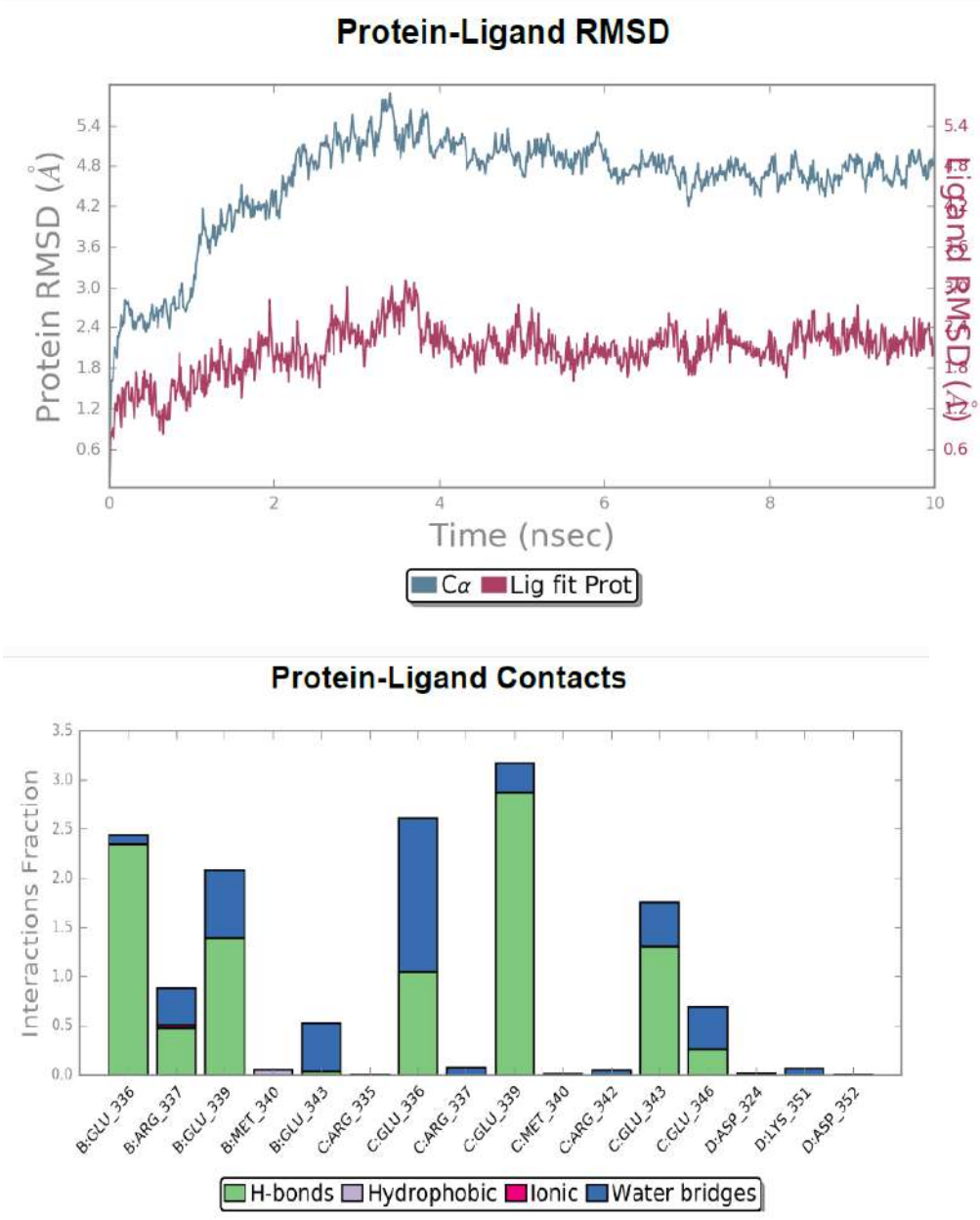

Figure S67. Molecular dynamics analysis of backbone RMSD from initial structure (blue line) and of ligand RMSD to initial pose (purple line). Below, molecular dynamics analysis of protein-ligand contacts. Analysis of the complexes p53WT @ cRab4 trajectories.

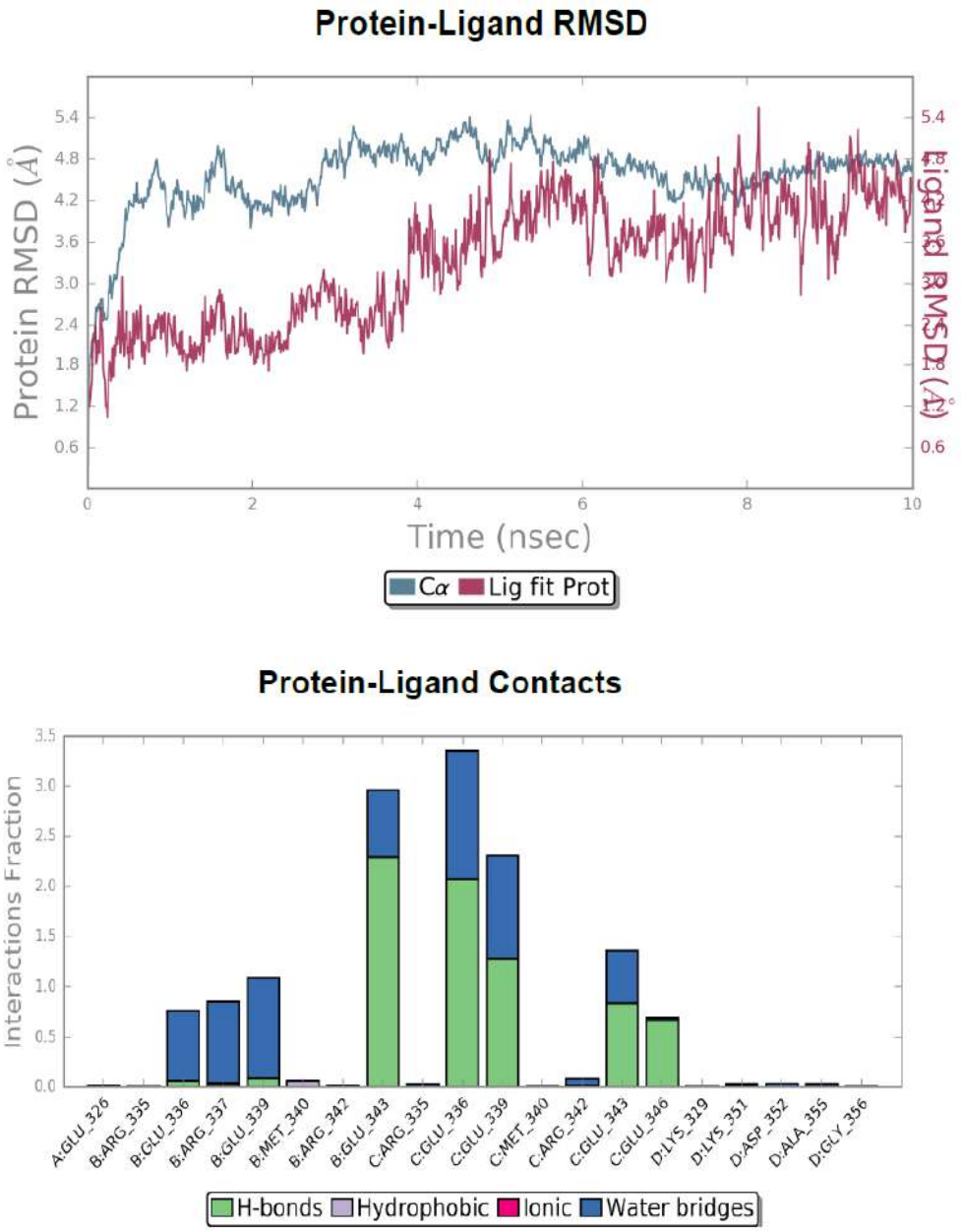

Figure S68. Molecular dynamics analysis of backbone RMSD from initial structure (blue line) and of ligand RMSD to initial pose (purple line). Below, molecular dynamics analysis of protein-ligand contacts. Analysis of the complexes p53WT @ cRab4A trajectories.

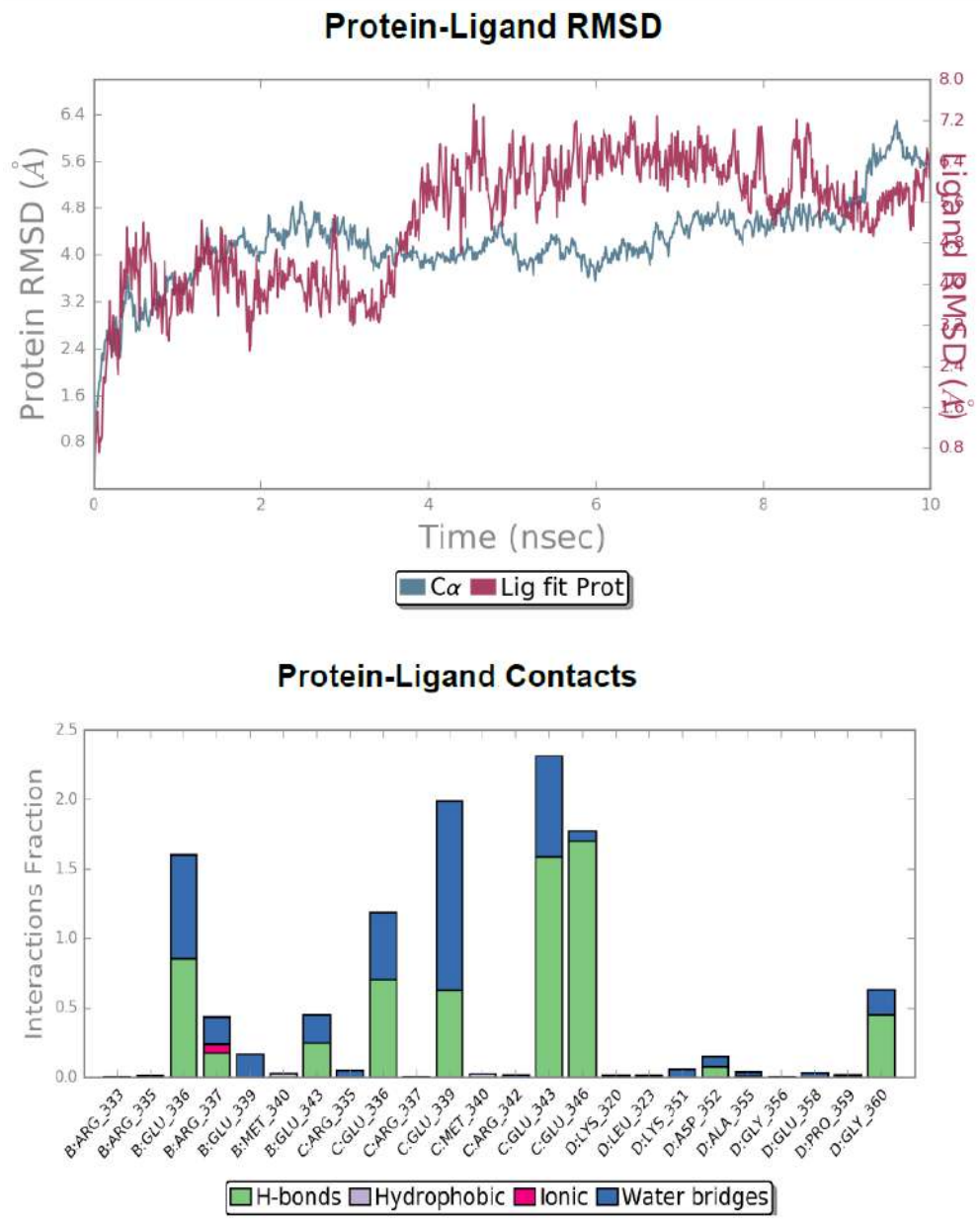

Figure S69. Molecular dynamics analysis of backbone RMSD from initial structure (blue line) and of ligand RMSD to initial pose (purple line). Below, molecular dynamics analysis of protein-ligand contacts. Analysis of the complexes p53WT @ cRys2R2 trajectories.

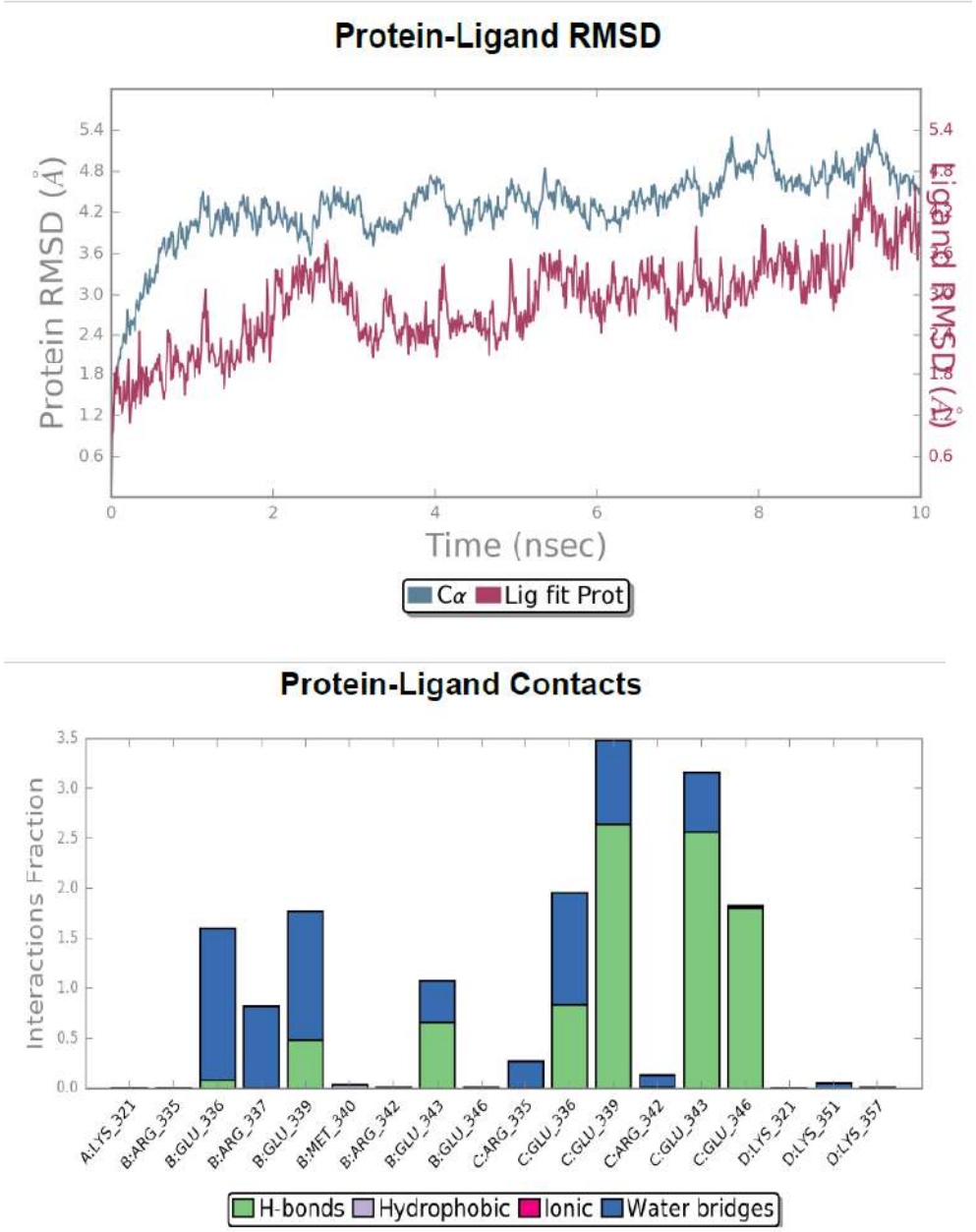

Figure S70. Molecular dynamics analysis of backbone RMSD from initial structure (blue line) and of ligand RMSD to initial pose (purple line). Below, molecular dynamics analysis of protein-ligand contacts. Analysis of the complexes p53WT @ cRys2R2A trajectories.

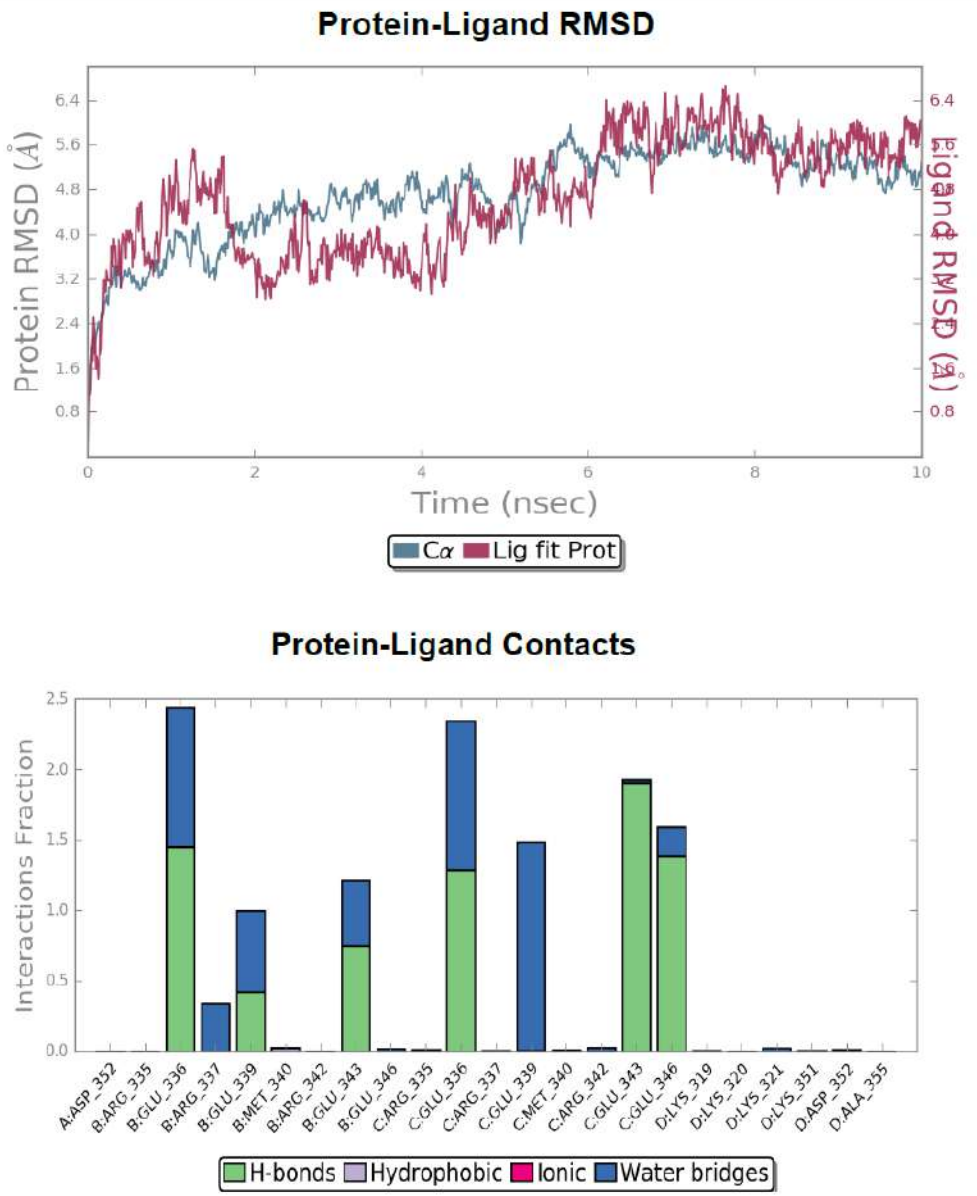

Figure S71. Molecular dynamics analysis of backbone RMSD from initial structure (blue line) and of ligand RMSD to initial pose (purple line). Below, molecular dynamics analysis of protein-ligand contacts. Analysis of the complexes p53WT @ cRys4 trajectories.

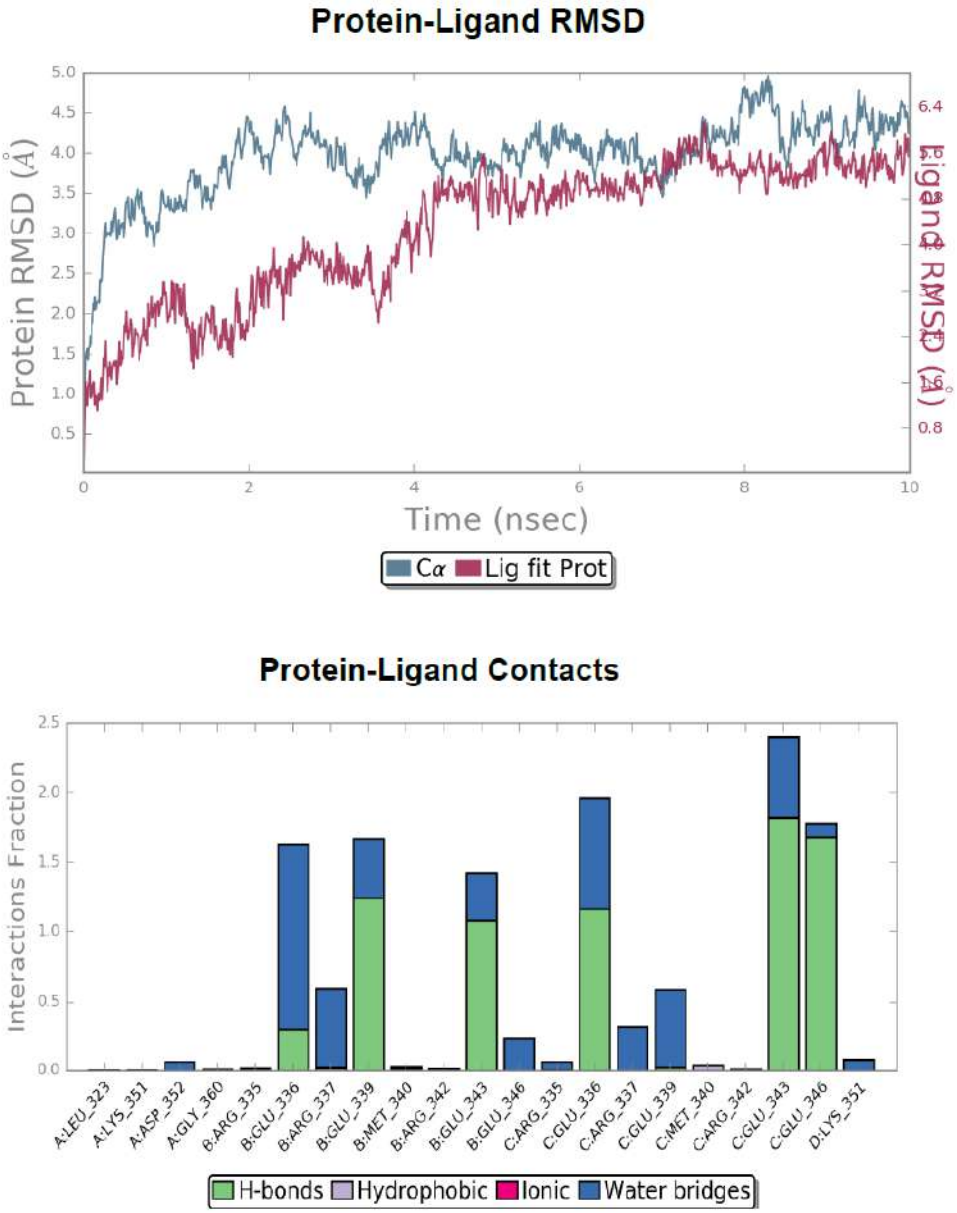

Figure S72. Molecular dynamics analysis of backbone RMSD from initial structure (blue line) and of ligand RMSD to initial pose (purple line). Below, molecular dynamics analysis of protein-ligand contacts. Analysis of the complexes p53WT @ cRys4A trajectories.

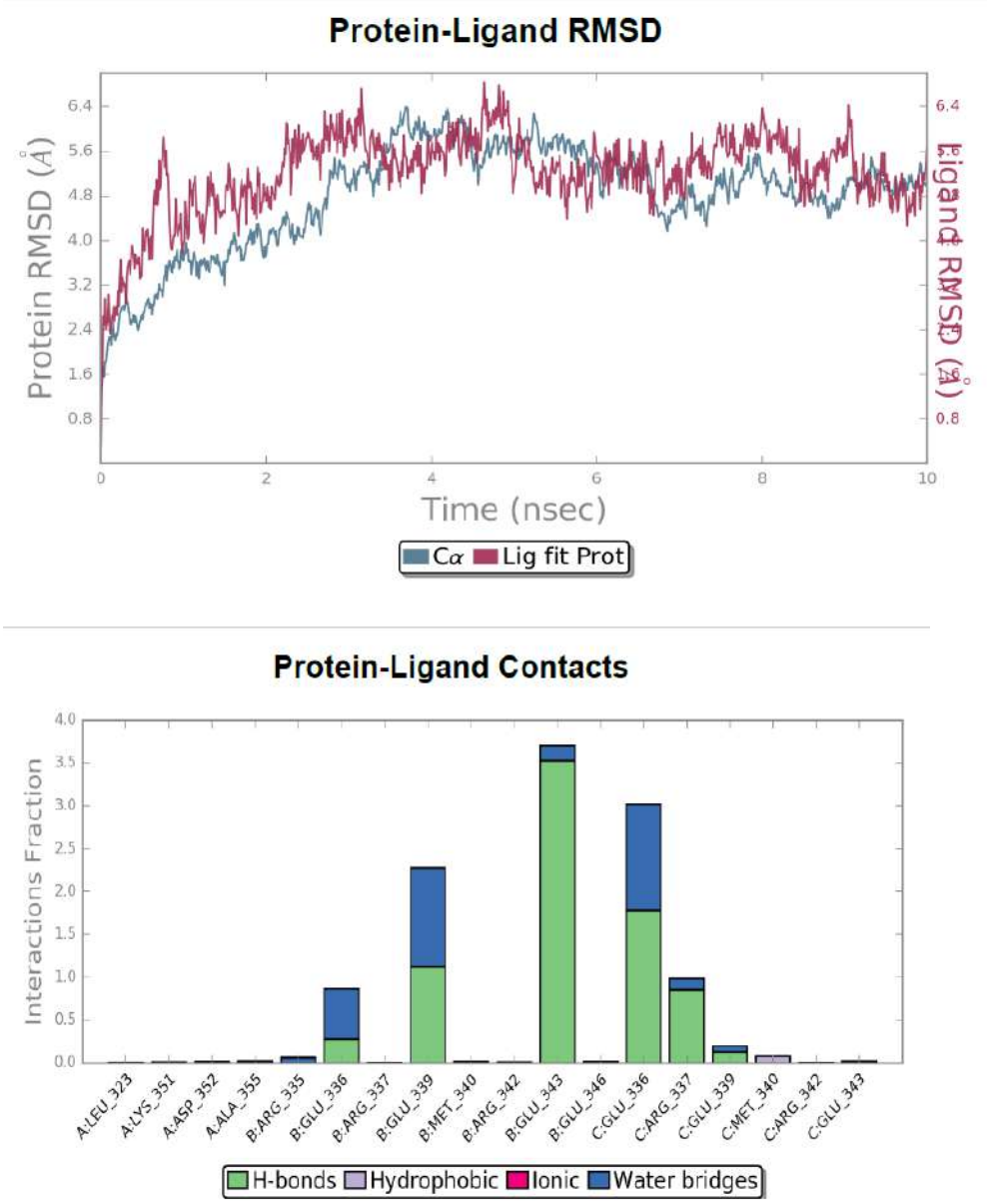

Figure S73. Molecular dynamics analysis of backbone RMSD from initial structure (blue line) and of ligand RMSD to initial pose (purple line). Below, molecular dynamics analysis of protein-ligand contacts. Analysis of the complexes p53WT @ cTmg2R2 trajectories.

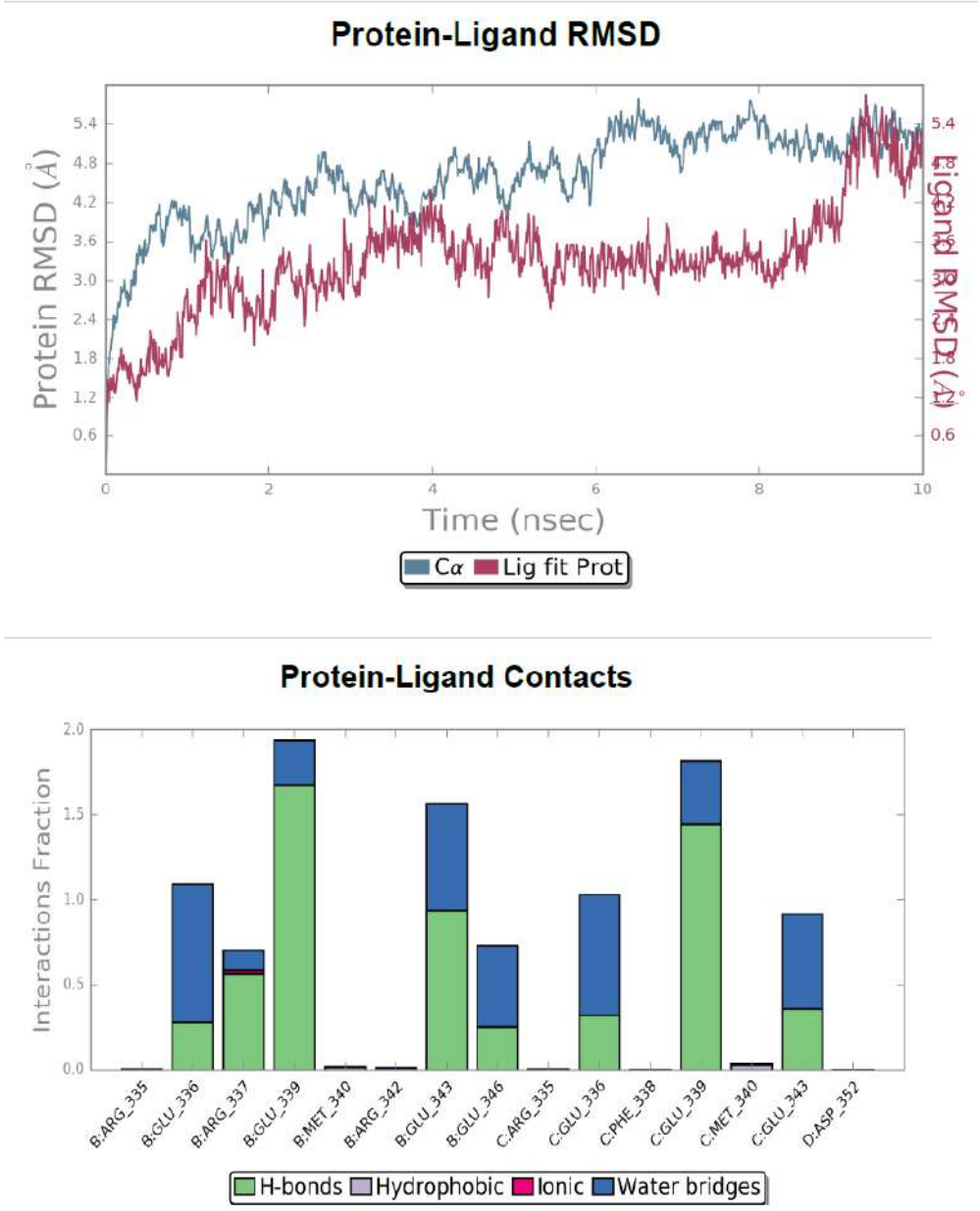

Figure S74. Molecular dynamics analysis of backbone RMSD from initial structure (blue line) and of ligand RMSD to initial pose (purple line). Below, molecular dynamics analysis of protein-ligand contacts. Analysis of the complexes p53WT @ cTmg2R2A trajectories.

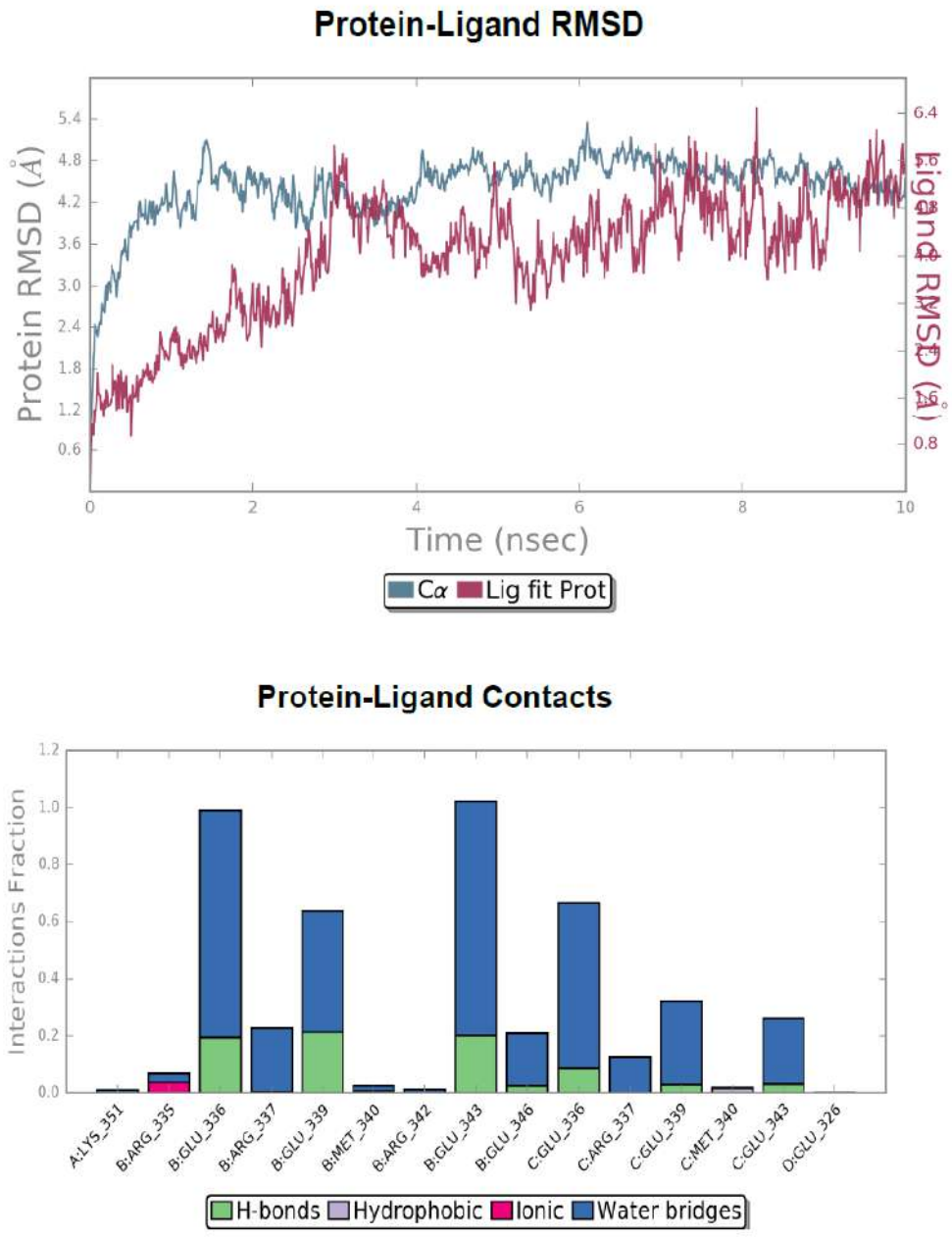

Figure S75. Molecular dynamics analysis of backbone RMSD from initial structure (blue line) and of ligand RMSD to initial pose (purple line). Below, molecular dynamics analysis of protein-ligand contacts. Analysis of the complexes p53WT @ cTmg4 trajectories.

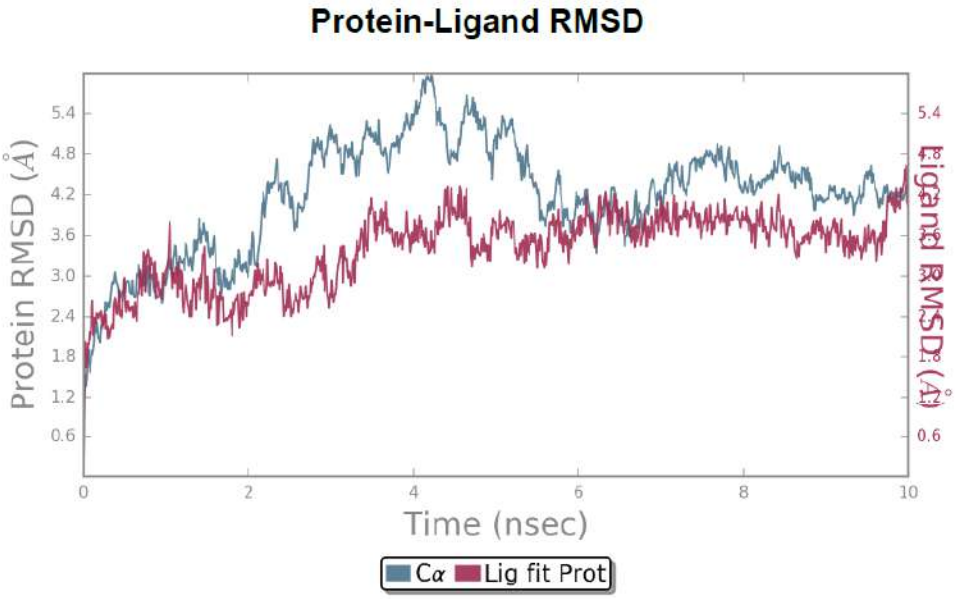

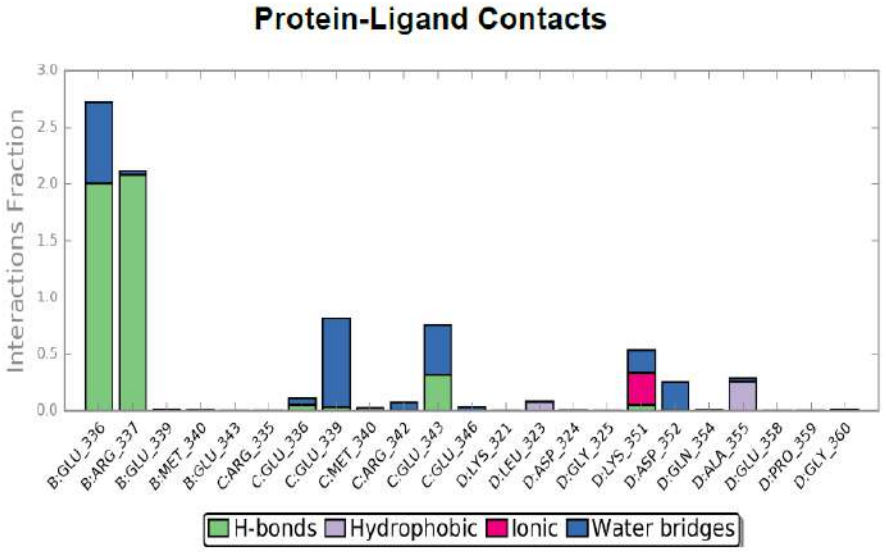

Figure S76. Molecular dynamics analysis of backbone RMSD from initial structure (blue line) and of ligand RMSD to initial pose (purple line). Below, molecular dynamics analysis of protein-ligand contacts. Analysis of the complexes p53WT @ cTmg4A trajectories.

SUPPLEMENTARY XTT

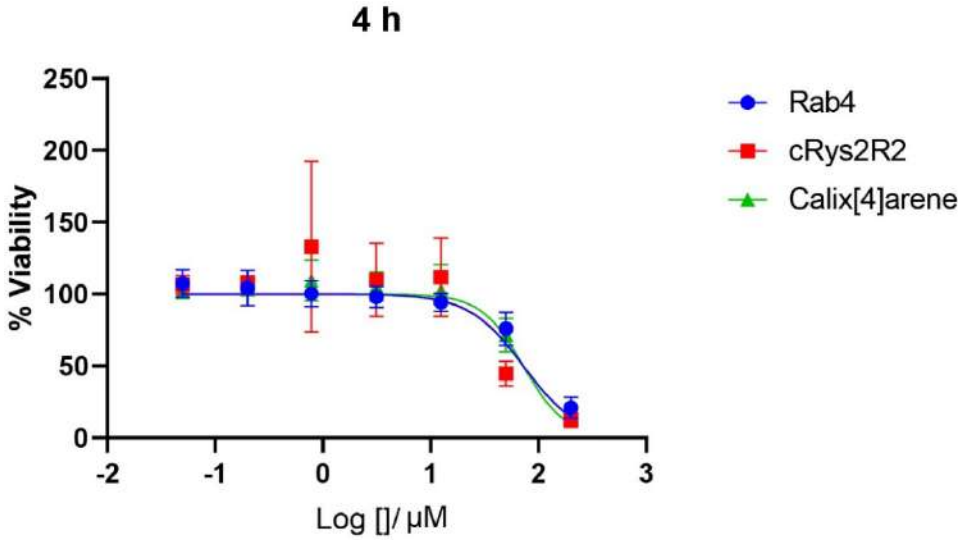

	Rab4	cRys2R2	Calix[4]arene
IC50	94.6	~ 49.0	79.0

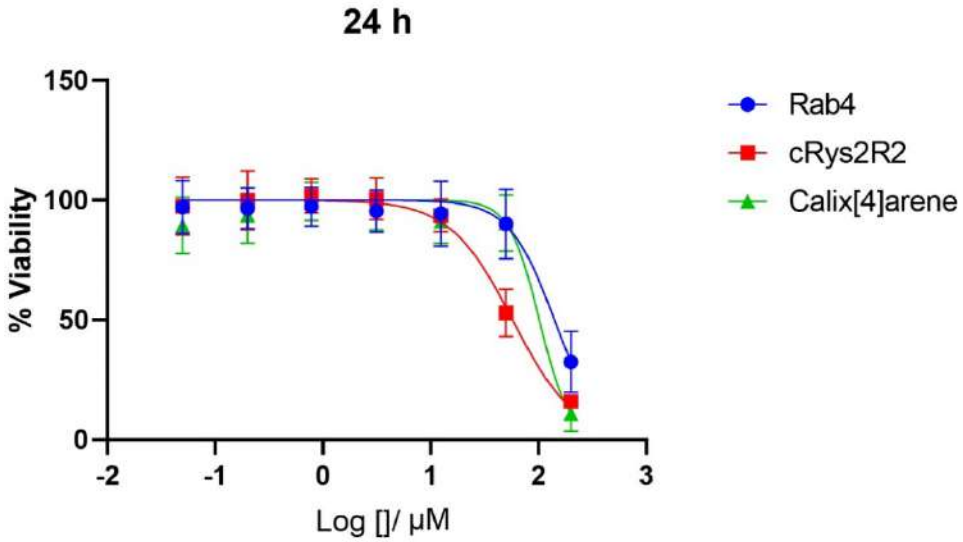

	Rab4	cRys2R2	Calix[4]arene
IC50	141	57.5	102

Figure S77. Cytotoxicity assay using XTT reagent in HeLa cells. The reading was done after 4 and 24 h incubation of Rab4, cRys2R2 and calix[4]arene with the cells.

CONCLUSIONS

In the first chapter of this thesis, we presented the experiments and the results related to the objective 1. The main conclusions are the following:

1. The WT is tetrameric at all the conditions studied and it is the most stable tetramer among our 37TDs. The tetramer dissociation occurs only with the increase of the voltage in the gas phase, and the equilibrium moves straight towards the monomer.
2. R337H, D352H and R342L mutations strongly destabilise the tetramer. 37TD-R337H presents an equilibrium between monomers and tetramers that is dependent on the pH, forming a more stable tetramer at acidic pH in NMR experiments.
3. T329I is the mutation that has the weakest destabilising effect on the tetramer. 37TD-T329I has a similar CD profile to the WT, it is mainly tetrameric both in the gas phase and in solution, but a monomeric population is present as well in the MS and NMR spectra.
4. 37TD-L344R and 37TD-L344P are unable to tetramerise, resulting in dimer and monomer, respectively.

The experiments and the results presented in the second chapter are related to the objective 2 and the following conclusions are drawn:

5. L330C mutation was introduced in the β-strand moiety to cross-link two monomers. 74TD-L330C is mainly dimeric and it is able to tetramerise. Most probably, the secondary structure of the peptide is different from the one resulting from the native folding of the WT.
6. The MD simulation results suggest that the presence of the disulphide bridge in the 74TD-L330C mutant affects both the β-strand, making it shorter, and the α-helix, causing it to recede. These structural changes may destabilise the domain, having a lower thermal stability and resulting in a more fluctuating structure in the MD simulations.
7. Both the experimental and theoretical results suggest that, compared to 74TD-L330C, the 74TD-L344C mutant has a more similar structure to the native folded WT. In particular, the disulphide bridge on the α-helix does not disrupt it and apparently, it has no effect on the β-strand.
8. 74TD-L344C is tetrameric in the gas phase and is stable to the increasing voltage in the native MS experiments. Nevertheless, the NMR results, in particular X-STE NMR experiments, suggested that it is dimeric in solution and any K_d was found by MST, confirming the inability of the peptide to oligomerise in solution.

The design of the ligands (objective 3) and the study of their interactions with p53TD (objective 4) are described in the third chapter. The main conclusions are the following:

9. Two generations of peptides were designed as potential ligands for p53TD. Docking simulations and molecular dynamics suggest that the ligands interact with p53TD mainly through polar and ionic interactions.
10. The first generation of ligands was studied by NMR and thermal stability CD. The results suggest binding of cyclo-tetra-β-3-arginine *S* with the mutated TD and the ligand was able to increase the T_m of the protein domain of *ca.* 3 degrees.
11. The binding of the linear peptides belonging to the second generation ligands was studied by NMR and fluorescence. NMR experiments show a shift of the aromatic protons signals of the indole group when the ligands were titrated with p53TDs. HSQC NMR spectra change after the addition of the ligands, suggesting the formation of a complex. The fluorescence band of the tryptophan changes by titrating the ligands. However, in the conditions of the experiment it is difficult to interpret the behaviour of the fluorescence signal with the changes in TD concentration.
12. The binding of the calix[4]arene with p53TD was studied by several biophysical techniques. ^{1}H ^{13}C HSQC NMR experiments suggest interaction between the molecules as, after the addition of the ligand, they show an upfield shift of the monomer peak, whereas the tetramer peak disappeared.
13. Native MS experiments also show the binding between the protein domain and the ligands (calix[4]arene and 2nd generation of peptides) as signals of the complex formed by the tetramer and one ligand molecule were detected. From these experiments, Rab4 and cRys2R2 were selected as best candidates to bind p53TD.
14. The stability of the complexes was analysed by native MS increasing the cone voltage. The signals of the complexes were still present at high voltage meaning that the complexes are stable in the gas phase.
15. The selected peptides (Rab4 and cRys2R2) were further studied by NMR experiments. The results suggest that both peptides are disordered.
16. Rab4 and cRys2R2 are stable in human serum over 24 h. The cyclic peptide is not degraded during the time of the experiment (half-life > 24 h), whereas the linear peptide has a half-life of *ca*. 12 h.
17. None of the studied compounds (calix[4]arene, Rab4, and cRys2R2) are cytotoxic over 24 h in HeLa cells, having an IC50 value in the range of 50 – 150 μM.

REFERENCES

(1) *Bioorganic Chemistry: Peptides and Proteins*; Hecht, S. M., Ed.; Oxford University Press, 1998.

(2) Luck, K.; Kim, D. K.; Lambourne, L.; Spirohn, K.; Begg, B. E.; Bian, W.; Brignall, R.; Cafarelli, T.; Campos-Laborie, F. J.; Charloteaux, B.; Choi, D.; Coté, A. G.; Daley, M.; Deimling, S.; Desbuleux, A.; Dricot, A.; Gebbia, M.; Hardy, M. F.; Kishore, N.; Knapp, J. J.; Kovács, I. A.; Lemmens, I.; Mee, M. W.; Mellor, J. C.; Pollis, C.; Pons, C.; Richardson, A. D.; Schlabach, S.; Teeking, B.; Yadav, A.; Babor, M.; Balcha, D.; Basha, O.; Bowman-Colin, C.; Chin, S. F.; Choi, S. G.; Colabella, C.; Coppin, G.; D'Amata, C.; De Ridder, D.; De Rouck, S.; Duran-Frigola, M.; Ennajdaoui, H.; Goebels, F.; Goehring, L.; Gopal, A.; Haddad, G.; Hatchi, E.; Helmy, M.; Jacob, Y.; Kassa, Y.; Landini, S.; Li, R.; van Lieshout, N.; MacWilliams, A.; Markey, D.; Paulson, J. N.; Rangarajan, S.; Rasla, J.; Rayhan, A.; Rolland, T.; San-Miguel, A.; Shen, Y.; Sheykhkarimli, D.; Sheynkman, G. M.; Simonovsky, E.; Taşan, M.; Tejeda, A.; Tropepe, V.; Twizere, J. C.; Wang, Y.; Weatheritt, R. J.; Weile, J.; Xia, Y.; Yang, X.; Yeger-Lotem, E.; Zhong, Q.; Aloy, P.; Bader, G. D.; De Las Rivas, J.; Gaudet, S.; Hao, T.; Rak, J.; Tavernier, J.; Hill, D. E.; Vidal, M.; Roth, F. P.; Calderwood, M. A. A Reference Map of the Human Binary Protein Interactome. *Nature* **2020**, *580* (7803), 402–408. https://doi.org/10.1038/s41586-020-2188-x.

(3) Halle, B. Flexibility and Packing in Proteins. *Proc. Natl. Acad. Sci. U. S. A.* **2002**, *99* (3), 1274–1279. https://doi.org/10.1073/pnas.032522499.

(4) Teilum, K.; Olsen, J. G.; Kragelund, B. B. Functional Aspects of Protein Flexibility. *Cell. Mol. Life Sci.* **2009**, *66* (14), 2231–2247. https://doi.org/10.1007/s00018-009-0014-6.

(5) Amaral, M.; Kokh, D. B.; Bomke, J.; Wegener, A.; Buchstaller, H. P.; Eggenweiler, H. M.; Matias, P.; Sirrenberg, C.; Wade, R. C.; Frech, M. Protein Conformational Flexibility Modulates Kinetics and Thermodynamics of Drug Binding. *Nat. Commun.* **2017**, *8* (1). https://doi.org/10.1038/s41467-017-02258-w.

(6) Richard, J. P. Protein Flexibility and Stiffness Enable Efficient Enzymatic Catalysis. *J. Am. Chem. Soc.* **2019**, *141* (8), 3320–3331. https://doi.org/10.1021/jacs.8b10836.

(7) Nevola, L.; Martín-Quirõs, A.; Eckelt, K.; Camarero, N.; Tosi, S.; Llobet, A.; Giralt, E.; Gorostiza, P. Light-Regulated Stapled Peptides to Inhibit Protein-Protein Interactions Involved in Clathrin-Mediated Endocytosis. *Angew. Chemie - Int. Ed.* **2013**, *52* (30), 7704–7708. https://doi.org/10.1002/anie.201303324.

(8) Wójcik, P.; Berlicki, Ł. Peptide-Based Inhibitors of Protein-Protein Interactions. *Bioorganic Med. Chem. Lett.* **2016**, *26* (3), 707–713. https://doi.org/10.1016/j.bmcl.2015.12.084.

(9) De Paola, I.; Pirone, L.; Palmieri, M.; Balasco, N.; Esposito, L.; Russo, L.; Mazzà, D.; Marcotullio, L. Di; Di Gaetano, S.; Malgieri, G.; Vitagliano, L.; Pedone, E.; Zaccaro, L. Cullin3 - BTB Interface:A Novel Target for Stapled Peptides. *PLoS One* **2015**, *10* (4), 1–21. https://doi.org/10.1371/journal.pone.0121149.

(10) Spiegel, J.; Cromm, P. M.; Itzen, A.; Goody, R. S.; Grossmann, T. N.; Waldmann, H.

Direct Targeting of Rab-GTPase-Effector Interactions. *Angew. Chemie - Int. Ed.* **2014**, *53* (9), 2498–2503. https://doi.org/10.1002/anie.201308568.

(11) Misawa, T.; Demizu, Y.; Kawamura, M.; Yamagata, N.; Kurihara, M. Structural Development of Stapled Short Helical Peptides as Vitamin D Receptor (VDR)-Coactivator Interaction Inhibitors. *Bioorganic Med. Chem.* **2015**, *23* (5), 1055–1061. https://doi.org/10.1016/j.bmc.2015.01.007.

(12) Grossmann, T. N.; Yeh, J. T. H.; Bowman, B. R.; Chu, Q.; Moellering, R. E.; Verdine, G. L. Inhibition of Oncogenic Wnt Signaling through Direct Targeting of β-Catenin. *Proc. Natl. Acad. Sci. U. S. A.* **2012**, *109* (44), 17942–17947. https://doi.org/10.1073/pnas.1208396109.

(13) Bernal, F.; Tyler, A. F.; Korsmeyer, S. J.; Walensky, L. D.; Verdine, G. L. Erratum: Reactivation of the P53 Tumor Suppressor Pathway by a Stapled P53 Peptide (Journal of the American Chemical Society (2007) 129, (2456-2457)). *J. Am. Chem. Soc.* **2007**, *129* (16), 5298. https://doi.org/10.1021/ja076886p.

(14) Baek, S.; Kutchukian, P. S.; Verdine, G. L.; Huber, R.; Holak, T. A.; Lee, K. W.; Popowicz, G. M. Structure of the Stapled P53 Peptide Bound to Mdm2. *J. Am. Chem. Soc.* **2012**, *134* (1), 103–106. https://doi.org/10.1021/ja2090367.

(15) Guardiola, S.; Díaz-Lobo, M.; Seco, J.; García, J.; Nevola, L.; Giralt, E. Peptides Targeting EGF Block the EGF-EGFR Interaction. *ChemBioChem* **2016**, *17* (8), 702–711. https://doi.org/10.1002/cbic.201500525.

(16) Bayó-Puxan, N.; Rodríguez-Mias, R.; Goldflam, M.; Kotev, M.; Ciudad, S.; Hipolito, C. J.; Varese, M.; Suga, H.; Campos-Olivas, R.; Barril, X.; Guallar, V.; Teixidó, M.; García, J.; Giralt, E. Combined Use of Oligopeptides, Fragment Libraries, and Natural Compounds: A Comprehensive Approach to Sample the Druggability of Vascular Endothelial Growth Factor. *ChemMedChem* **2016**, *11* (8), 928–939. https://doi.org/10.1002/cmdc.201500467.

(17) Lane, D. P. P53 Guardian of the Genome. *Nature* **1992**, *358* (6381), 15–16.

(18) Kato, S.; Han, S.-Y.; Liu, W.; Otsuka, K.; Shibata, H.; Kanamaru, R.; Ishioka, C. Understanding the Function-Structure and Function-Mutation Relationships of P53 Tumor Suppressor Protein by High-Resolution Missense Mutation Analysis. *PNAS* **2003**, *100* (14), 8424–8429.

(19) Kim, J.; Yu, L.; Chen, W.; Xu, Y.; Wu, M.; Todorova, D.; Tang, Q.; Feng, B.; Jiang, L.; He, J.; Chen, G.; Fu, X.; Xu, Y. Wild-Type P53 Promotes Cancer Metabolic Switch by Inducing PUMA-Dependent Suppression of Oxidative Phosphorylation. *Cancer Cell* **2019**, *35* (2), 191-203.e8. https://doi.org/10.1016/j.ccell.2018.12.012.

(20) Liang, S.-H.; Clarke, M. F. *Regulation of P53 Localization*; 2001; Vol. 268.

(21) Fischer, N. W.; Prodeus, A.; Tran, J.; Malkin, D.; Gariepy, J. Association between the Oligomeric Status of P53 and Clinical Outcomes in Li-Fraumeni Syndrome. *J. Natl. Cancer Inst.* **2018**, *110* (12). https://doi.org/10.1093/jnci/djy114.

(22) Krois, A. S.; Ferreon, J. C.; Martinez-Yamout, M. A.; Dyson, H. J.; Wright, P. E.

Recognition of the Disordered P53 Transactivation Domain by the Transcriptional Adapter Zinc Finger Domains of CREB-Binding Protein. *Proc. Natl. Acad. Sci. U. S. A.* **2016**, *113* (13), E1853–E1862. https://doi.org/10.1073/pnas.1602487113.

(23) Nicholls, C. D.; McLure, K. G.; Shields, M. A.; Lee, P. W. K. Biogenesis of P53 Involves Cotranslational Dimerization of Monomers and Posttranslational Dimerization of Dimers. Implications on the Dominant Negative Effect. *J. Biol. Chem.* **2002**, *277* (15), 12937–12945. https://doi.org/10.1074/jbc.M108815200.

(24) Garcia Pindado, J. Synthesis of Biaryl Bicyclic Peptides for Recognition of Protein Surfaces. *TDX (Tesis Dr. en Xarxa)* **2017**.

(25) McCormick, F.; Clark, R.; Harlow, E.; Tjian, R. SV40 T Antigen Binds Specifically to a Cellular 53 K Protein in Vitro. *Nature* **1981**, *292*, 63–65.

(26) Friedman, P. N.; Chen, X.; Bargonetti, J.; Prives, C. The P53 Protein Is an Unusually Shaped Tetramer That Binds Directly to DNA. *Proc. Natl. Acad. Sci. U. S. A.* **1993**, *90* (8), 3319–3323. https://doi.org/10.1073/pnas.90.8.3319.

(27) Jeffrey, P. D.; Gorina, S.; Pavletich, N. P. Crystal Structure of the Tetramerization Domain of the P53 Tumor Suppressor at 1.7 Angstroms. *Science (80-.).* **1995**, *267* (5203), 1498–1502. https://doi.org/10.1126/science.7878469.

(28) Clore, G. M.; Omichinski, J. G.; Sakaguchi, K.; Zambrano, N.; Sakamoto, H.; Appella, E.; Gronenborn, A. M. High-Resolution Structure of the Oligomerization Domain of P53 by Multidimensional NMR. *Science (80-.).* **1994**, *265* (5170), 386–391. https://doi.org/10.1126/science.8023159.

(29) Stommel, J. M.; Marchenko, N. D.; Jimenez, G. S.; Moll, U. M.; Hope, T. J.; Wahl, G. M. A Leucine-Rich Nuclear Export Signal in the P53 Tetramerization Domain: Regulation of Subcellular Localization and P53 Activity by NES Masking. *EMBO J.* **1999**, *18* (6), 1660–1672. https://doi.org/10.1093/emboj/18.6.1660.

(30) Bista, M.; Freund, S. M.; Fersht, A. R. Domain-Domain Interactions in Full-Length P53 and a Specific DNA Complex Probed by Methyl NMR Spectroscopy. *PNAS* **2012**, *109* (39). https://doi.org/10.1073/pnas.1214176109/-/DCSupplemental.

(31) Prives, C.; Hall, P. A. The P53 Pathway. *Journal of Pathology*. January 1999, pp 112–126. https://doi.org/10.1002/(SICI)1096-9896(199901)187:1<112::AID-PATH250>3.0.CO;2-3.

(32) Weinberg, R. L.; Veprintsev, D. B.; Fersht, A. R. Cooperative Binding of Tetrameric P53 to DNA. *J. Mol. Biol.* **2004**, *341* (5), 1145–1159. https://doi.org/10.1016/j.jmb.2004.06.071.

(33) D'Abramo, M.; Bešker, N.; Desideri, A.; Levine, A. J.; Melino, G.; Chillemi, G. The P53 Tetramer Shows an Induced-Fit Interaction of the C-Terminal Domain with the DNA-Binding Domain. *Oncogene* **2016**, *35* (25), 3272–3281. https://doi.org/10.1038/onc.2015.388.

(34) Gencel-Augusto, J.; Lozano, G. P53 Tetramerization: At the Center of the Dominant-Negative Effect of Mutant P53. *Genes Dev.* **2020**, *34* (17–18), 1128–1146.

https://doi.org/10.1101/gad.340976.120.

(35) Tidow, H.; Melero, R.; Mylonas, E.; Freund, S. M. V; Grossmann, J. G.; Carazo, J. M.; Svergun, D. I.; Valle, M.; Fersht, A. R. Quaternary Structures of Tumor Suppressor P53 and a Specific P53-DNA Complex. *PNAS* **2007**, *104* (30), 12324–12329.

(36) Rajagopalan, S.; Huang, F.; Fersht, A. R. Single-Molecule Characterization of Oligomerization Kinetics and Equilibria of the Tumor Suppressor P53. *Nucleic Acids Res.* **2011**, *39* (6), 2294–2303. https://doi.org/10.1093/nar/gkq800.

(37) McLure, K. G.; Lee, P. W. K. How P53 Binds DNA as a Tetramer. *EMBO J.* **1998**, *17* (12), 3342–3350. https://doi.org/10.1093/emboj/17.12.3342.

(38) Gaglia, G.; Guan, Y.; Shah, J. V.; Lahav, G. Activation and Control of P53 Tetramerization in Individual Living Cells. *Proc. Natl. Acad. Sci. U. S. A.* **2013**, *110* (38), 15497–15501. https://doi.org/10.1073/pnas.1311126110.

(39) Fischer, N. W.; Prodeus, A.; Malkin, D.; Gariépy, J. P53 Oligomerization Status Modulates Cell Fate Decisions between Growth, Arrest and Apoptosis. *Cell Cycle* **2016**, *15* (23), 3210–3219. https://doi.org/10.1080/15384101.2016.1241917.

(40) Gaglia, G.; Lahav, G. Constant Rate of P53 Tetramerization in Response to DNA Damage Controls the P53 Response . *Mol. Syst. Biol.* **2014**, *10* (10), 753. https://doi.org/10.15252/msb.20145168.

(41) Ono, W.; Hayashi, Y.; Yokoyama, W.; Kuroda, T.; Kishimoto, H.; Ito, I.; Kimura, K.; Akaogi, K.; Waku, T.; Yanagisawa, J. The Nucleolar Protein Myb-Binding Protein 1A (MYBBP1A) Enhances P53 Tetramerization and Acetylation in Response to Nucleolar Disruption. *J. Biol. Chem.* **2014**, *289* (8), 4928–4940. https://doi.org/10.1074/jbc.M113.474049.

(42) Meng, X.; Yue, J.; Liu, Z.; Shen, Z. Abrogation of the Transactivation Activity of P53 by BCCIP Down-Regulation. *J. Biol. Chem.* **2007**, *282* (3), 1570–1576. https://doi.org/10.1074/jbc.M607520200.

(43) Xu, J.; Zhou, X.; Wang, J.; Li, Z.; Kong, X.; Qian, J.; Hu, Y.; Fang, J. Y. RhoGAPs Attenuate Cell Proliferation by Direct Interaction with P53 Tetramerization Domain. *Cell Rep.* **2013**, *3* (5), 1526–1538. https://doi.org/10.1016/j.celrep.2013.04.017.

(44) Lee, I. H.; Kawai, Y.; Fergusson, M. M.; Rovira, I. I.; Bishop, A. J. R.; Motoyama, N.; Cao, L.; Finkel, T. Atg7 Modulates P53 Activity to Regulate Cell Cycle and Survival During Metabolic Stress. *Science (80-.).* **2012**, *336* (6078), 225–228. https://doi.org/10.1126/science.1218395.

(45) Rajagopalan, S.; Jaulent, A. M.; Wells, M.; Veprintsev, D. B.; Fersht, A. R. 14-3-3 Activation of DNA Binding of P53 by Enhancing Its Association into Tetramers. *Nucleic Acids Res.* **2008**, *36* (18), 5983–5991. https://doi.org/10.1093/nar/gkn598.

(46) van Dieck, J.; Teufel, D. P.; Jaulent, A. M.; Fernandez-Fernandez, M. R.; Rutherford, T. J.; Wyslouch-Cieszynska, A.; Fersht, A. R. Posttranslational Modifications Affect the Interaction of S100 Proteins with Tumor Suppressor P53. *J. Mol. Biol.* **2009**, *394* (5), 922–930. https://doi.org/10.1016/j.jmb.2009.10.002.

(47) van Dieck, J.; Fernandez-Fernandez, M. R.; Veprintsev, D. B.; Fersht, A. R. Modulation of the Oligomerization State of P53 by Differential Binding of Proteins of the S100 Family to P53 Monomers and Tetramers. *J. Biol. Chem.* **2009**, *284* (20), 13804–13811. https://doi.org/10.1074/jbc.M901351200.

(48) Lui, K.; Saeed Sheikh, M.; Huang, Y. *Regulation of P53 Oligomerization by Ras Superfamily Protein RBEL1A*; 2015; Vol. 6.

(49) S-Y Foo, R.; Nam, Y.-J.; Jason Ostreicher, M.; Metzl, M. D.; Whelan, R. S.; Peng, C.-F.; Ashton, A. W.; Fu, W.; Mani, K.; Chin, S.-F.; Provenzano, E.; Ellis, I.; Figg, N.; Pinder, S.; Bennett, M. R.; Caldas, C.; Kitsis, R. N. Regulation of P53 Tetramerization and Nuclear Export by ARC. *PNAS* **2007**, *104* (52), 20826–20831.

(50) Sakaguchi, K.; Sakamoto, H.; Lewis, M. S.; Anderson, C. W.; Erickson, J. W.; Appella, E.; Xie, D. Phosphorylation of Serine 392 Stabilizes the Tetramer Formation of Tumor Suppressor Protein P53. *Biochemistry* **1997**, *36* (33), 10117–10124. https://doi.org/10.1021/bi970759w.

(51) Yakovlev, V. A.; Mikkelsen, R. B. Protein Tyrosine Nitration in Cellular Signal Transduction Pathways. *J. Recept. Signal Transduct.* **2010**, *30* (6), 420–429. https://doi.org/10.3109/10799893.2010.513991.

(52) Nomura, T.; Kamada, R.; Ito, I.; Chuman, Y.; Shimohigashi, Y.; Sakaguchi, K. Oxidation of Methionine Residue at Hydrophobic Core Destabilitizes P53 Tetrameric Structure. *Biopolymers* **2009**, *91* (1), 78–84. https://doi.org/10.1002/bip.21084.

(53) Laptenko, Oleg Shiff, Idit Freed-Pastor, Will Zupnik, Andrew Mattia, Melissa Freulich, Ella Shamir, Inbal Kadouri, Noam Kahn, Tamar Manfredi, James Simon, Itamar Prives, C. The P53 C-Terminus Controls Site-Specific DNA Binding and Promotes Structural Changes within the Central DNA Binding Domain. *Mol Cell.* **2015**, *57(6)*, 1034–1046.

(54) Moll, U. M.; Petrenko, O. The MDM2-P53 Interaction. **2003**, *1* (December), 1001–1008.

(55) Hjerpe, R.; Aillet, F.; Lopitz-Otsoa, F.; Lang, V.; Torres-Ramos, M.; Farrás, R.; Hay, R. T.; Rodríguez, M. S. Oligomerization Conditions Mdm2-Mediated Efficient P53 Polyubiquitylation but Not Its Proteasomal Degradation. *Int. J. Biochem. Cell Biol.* **2010**, *42* (5), 725–735. https://doi.org/10.1016/j.biocel.2010.01.010.

(56) Lang, V.; Pallara, C.; Zabala, A.; Lobato-Gil, S.; Lopitz-Otsoa, F.; Farrás, R.; Hjerpe, R.; Torres-Ramos, M.; Zabaleta, L.; Blattner, C.; Hay, R. T.; Barrio, R.; Carracedo, A.; Fernandez-Recio, J.; Rodríguez, M. S.; Aillet, F. Tetramerization-Defects of P53 Result in Aberrant Ubiquitylation and Transcriptional Activity. *Mol. Oncol.* **2014**, *8* (5), 1026–1042. https://doi.org/10.1016/j.molonc.2014.04.002.

(57) Katz, C.; Low-Calle, A. M.; Choe, J. H.; Laptenko, O.; Tong, D.; Joseph-Chowdhury, J. S. N.; Garofalo, F.; Zhu, Y.; Friedler, A.; Prives, C. Wild-Type and Cancer-Related P53 Proteins Are Preferentially Degraded by MDM2 as Dimers Rather than Tetramers. *Genes Dev.* **2018**, *32* (5–6), 430–447. https://doi.org/10.1101/gad.304071.117.

(58) Muscolini, M.; Montagni, E.; Caristi, S.; Nomura, T.; Kamada, R.; Di Agostino, S.;

Corazzari, M.; Piacentini, M.; Blandino, G.; Costanzo, A.; Sakaguchi, K.; Tuosto, L. Characterization of a New Cancer-Associated Mutant of P53 with a Missense Mutation (K351N) in the Tetramerization Domain. *Cell Cycle* **2009**, *8* (20), 3396–3405. https://doi.org/10.4161/cc.8.20.9910.

(59) Muscolini, M.; Montagni, E.; Palermo, V.; Di Agostino, S.; Gu, W.; Abdelmoula-Souissi, S.; Mazzoni, C.; Blandino, G.; Tuosto, L. The Cancer-Associated K351N Mutation Affects the Ubiquitination and the Translocation to Mitochondria of P53 Protein. *J. Biol. Chem.* **2011**, *286* (46), 39693–39702. https://doi.org/10.1074/jbc.M111.279539.

(60) Jansson, M.; Durant, S. T.; Cho, E. C.; Sheahan, S.; Edelmann, M.; Kessler, B.; La Thangue, N. B. Arginine Methylation Regulates the P53 Response. *Nat. Cell Biol.* **2008**, *10* (12), 1431–1439. https://doi.org/10.1038/ncb1802.

(61) Itahana, Y.; Ke, H.; Zhang, Y. P53 Oligomerization Is Essential for Its C-Terminal Lysine Acetylation. *J. Biol. Chem.* **2009**, *284* (8), 5158–5164. https://doi.org/10.1074/jbc.M805696200.

(62) Bullock, A. N.; Fersht, A. R. Rescuing the Function of Mutant P53. *Nat. Rev. Cancer* **2001**, *1* (1), 68–76. https://doi.org/10.1038/35094077.

(63) Ano Bom, A. P. D.; Rangel, L. P.; Costa, D. C. F.; De Oliveira, G. A. P.; Sanches, D.; Braga, C. A.; Gava, L. M.; Ramos, C. H. I.; Cepeda, A. O. T.; Stumbo, A. C.; De Moura Gallo, C. V.; Cordeiros, Y.; Silva, J. L. Mutant P53 Aggregates into Prion-like Amyloid Oligomers and Fibrils: Implications for Cancer. *J. Biol. Chem.* **2012**, *287* (33), 28152–28162. https://doi.org/10.1074/jbc.M112.340638.

(64) Kamada, R.; Nomura, T.; Anderson, C. W.; Sakaguchi, K. Cancer-Associated P53 Tetramerization Domain Mutants: Quantitative Analysis Reveals a Low Threshold for Tumor Suppressor Inactivation. *J. Biol. Chem.* **2011**, *286* (1), 252–258. https://doi.org/10.1074/jbc.M110.174698.

(65) Senitzki, A.; Safieh, J.; Sharma, V.; Golovenko, D.; Danin-Poleg, Y.; Inga, A.; Haran, T. E. The Complex Architecture of P53 Binding Sites. *Nucleic Acids Res.* **2021**, *49* (3), 1364–1382. https://doi.org/10.1093/nar/gkaa1283.

(66) de Oliveira, G. A. P.; Petronilho, E. C.; Pedrote, M. M.; Marques, M. A.; Vieira, T. C. R. G.; Cino, E. A.; Silva, J. L. The Status of P53 Oligomeric and Aggregation States in Cancer. *Biomolecules*. MDPI AG April 1, 2020. https://doi.org/10.3390/biom10040548.

(67) Mateu, M. G.; Fersht, A. R. Nine Hydrophobic Side Chains Are Key Determinants of the Thermodynamic Stability and Oligomerization Status of Tumour Suppressor P53 Tetramerization Domain. *EMBO J.* **1998**, *17* (10), 2748–2758. https://doi.org/10.1093/emboj/17.10.2748.

(68) Chène, P.; Bechter, E. Cellular Characterisation of P53 Mutants with a Single Missense Mutation in the β-Strand 326-333 and Correlation of Their Cellular Activities with in Vitro Properties. *J. Mol. Biol.* **1999**, *288* (5), 891–897. https://doi.org/10.1006/jmbi.1999.2738.

(69) Kawaguchi, T.; Kato, S.; Otsuka, K.; Watanabe, G.; Kumabe, T.; Tominaga, T.; Yoshimoto, T.; Ishioka, C. The Relationship among P53 Oligomer Formation, Structure and Transcriptional Activity Using a Comprehensive Missense Mutation Library. *Oncogene* **2005**, *24* (46), 6976–6981. https://doi.org/10.1038/sj.onc.1208839.

(70) Imagawa, T.; Terai, T.; Yamada, Y.; Kamada, R.; Sakaguchi, K. Evaluation of Transcriptional Activity of P53 in Individual Living Mammalian Cells. *Anal. Biochem.* **2009**, *387* (2), 249–256. https://doi.org/10.1016/j.ab.2009.01.030.

(71) Giacomelli, A. O.; Yang, X.; Lintner, R. E.; McFarland, J. M.; Duby, M.; Kim, J.; Howard, T. P.; Takeda, D. Y.; Huong Ly, S.; Kim, E.; Gannon, H. S.; Hurhula, B.; Sharpe, T.; Goodale, A.; Fritchman, B.; Steelman, S.; Vazquez, F.; Tsherniak, A.; Aguirre, A. J.; Doench, J. G.; Piccioni, F.; M Roberts, C. W.; Meyerson, M.; Getz, G.; Johannessen, C. M.; Root, D. E.; Hahn, W. C.; Aog, B.; Aog, G.; Genet Author manuscript, N. Mutational Processes Shape the Landscape of TP53 Mutations in Human Cancer HHS Public Access Author Manuscript. *Nat Genet* **2018**, *50* (10), 1381–1387. https://doi.org/10.1038/s41588-018-0204-y.Mutational.

(72) Palmero, E. I.; Schüler-Faccini, L.; Caleffi, M.; Achatz, M. I. W.; Olivier, M.; Martel-Planche, G.; Marcel, V.; Aguiar, E.; Giacomazzi, J.; Ewald, I. P.; Giugliani, R.; Hainaut, P.; Ashton-Prolla, P. Detection of R337H, a Germline TP53 Mutation Predisposing to Multiple Cancers, in Asymptomatic Women Participating in a Breast Cancer Screening Program in Southern Brazil. *Cancer Lett.* **2008**, *261* (1), 21–25. https://doi.org/10.1016/j.canlet.2007.10.044.

(73) Ribeiro, R. C.; Sandrini, F.; Figueiredo, B.; Zambetti, G. P.; Michalkiewicz, E.; Lafferty, A. R.; DeLacerda, L.; Rabin, M.; Cadwell, C.; Sampaio, G.; Cat, I.; Stratakis, C. A.; Sandrini, R. An Inherited P53 Mutation That Contributes in a Tissue-Specific Manner to Pediatric Adrenal Cortical Carcinoma. *Proc. Natl. Acad. Sci. U. S. A.* **2001**, *98* (16), 9330–9335. https://doi.org/10.1073/pnas.161479898.

(74) Schneider, K.; Zelley, K.; Nichols, K. E.; Garber, J. *Li-Fraumeni Syndrome*; University of Washington, Seattle, Seattle (WA), 1993.

(75) DiGiammarino, E. L.; Lee, A. S.; Cadwell, C.; Zhang, W.; Bothner, B.; Ribeiro, R. C.; Zambeti, G.; Kriwacki, R. W. A Novel Mechanism of Tumorigenesis Involving PH-Dependent Destabilization of a Mutant P53 Tetramer. *Nat. Struct. Biol.* **2002**, *9* (1), 12–16. https://doi.org/10.1038/nsb730.

(76) Park, J. H.; Li, J.; Starost, M. F.; Liu, C.; Zhuang, J.; Chen, J.; Achatz, M. I.; Kang, J. G.; Wang, P. yuan; Savage, S. A.; Hwang, P. M. Mouse Homolog of the Human TP53 R337H Mutation Reveals Its Role in Tumorigenesis. *Cancer Res.* **2018**, *78* (18), 5375–5383. https://doi.org/10.1158/0008-5472.CAN-18-0016.

(77) Jeffers, J. R.; Pinto, E. M.; Rehg, J. E.; Clay, M. R.; Wang, J.; Neale, G.; Heath, R. J.; Lozano, G.; Lalli, E.; Figueiredo, B. C.; Pappo, A. S.; Rodriguez-Galindo, C.; Chen, W.; Pounds, S.; Ribeiro, R. C.; Zambetti, G. P. The Common Germline TP53-R337H Mutation Is Hypomorphic and Confers Incomplete Penetrance and Late Tumor Onset in a Mouse Model A C. *Cancer Res.* **2021**, *81* (9), 2442–2456.

https://doi.org/10.1158/0008-5472.CAN-20-1750.

(78) Mantovani, F.; Collavin, L.; Del Sal, G. Mutant P53 as a Guardian of the Cancer Cell. *Cell Death and Differentiation*. Nature Publishing Group January 1, 2019, pp 199–212. https://doi.org/10.1038/s41418-018-0246-9.

(79) BYKOV, VLADIMIR J.N. ISSAEVA, Natalia SHILOV, ALexandre HULTCRANTZ, Monica PUGACHEVA, Elena CHUMAKOV, Peter BERGMAN, Jan WIMAN, K. G.; SELIVANOVA, G. Restoration of the Tumor Suppressor Function to Mutant P53 by a Low-Molecular-Weight Compound. *Nat. Med.* **2002**, *8* (3).

(80) Gordo, S.; Martos, V.; Santos, E.; Mené Ndez §, M.; Bo, C.; Giralt, E.; De Mendoza, J. Stability and Structural Recovery of the Tetramerization Domain of P53-R337H Mutant Induced by a Designed Templating Ligand. *PNAS* **2008**, *105* (43), 16426–16431.

(81) Kamada, R.; Yoshino, W.; Nomura, T.; Chuman, Y.; Imagawa, T.; Suzuki, T.; Sakaguchi, K. Enhancement of Transcriptional Activity of Mutant P53 Tumor Suppressor Protein through Stabilization of Tetramer Formation by Calix[6]Arene Derivatives. *Bioorganic Med. Chem. Lett.* **2010**, *20* (15), 4412–4415. https://doi.org/10.1016/j.bmcl.2010.06.053.

(82) Gordo, S.; Martos, V.; Vilaseca, M.; Menéndez, M.; De Mendoza, J.; Giralt, E. On the Role of Flexibility in Protein-Ligand Interactions: The Example of P53 Tetramerization Domain. *Chem. - An Asian J.* **2011**, *6* (6), 1463–1469. https://doi.org/10.1002/asia.201000938.

(83) Gabizon, R.; Brandt, T.; Sukenik, S.; Lahav, N.; Lebendiker, M.; Shalev, D. E.; Veprintsev, D.; Friedler, A. Specific Recognition of P53 Tetramers by Peptides Derived from P53 Interacting Proteins. *PLoS One* **2012**, *7* (5), 1–11. https://doi.org/10.1371/journal.pone.0038060.

(84) Gabizon, R.; Friedler, A. Allosteric Modulation of Protein Oligomerization: An Emerging Approach to Drug Design. *Front. Chem.* **2014**, *2* (MAR), 1–15. https://doi.org/10.3389/fchem.2014.00009.

(85) Ciudad Fernández, S. Cyclic Peptides and Small Proteins in Molecular Recognition, 2016.

(86) Craik, D. J.; Fairlie, D. P.; Liras, S.; Price, D. The Future of Peptide-Based Drugs. *Chem. Biol. Drug Des.* **2013**, *81* (1), 136–147. https://doi.org/10.1111/cbdd.12055.

(87) Gordo Villoslada, S.; Giralt Lledó, E.; Universitat de Barcelona. Departament de Química Orgànica. *Use of Calix[4]Arenes to Recover the Self-Assembly Ability of Mutated P53 Tetramerization Domains*; Universitat de Barcelona, 2008.

(88) Pinto, E. M.; Billerbeck, A. E. C.; Villares, M. C. B. F.; Domenice, S.; Mendonça, B. B.; Ana Latronico, A. C. Founder Effect for the Highly Prevalent R337H Mutation OfTumor Suppressor P53 in Brazilian Patients with Adrenocortical Tumors. *Arq Bras Endocrinol Metab* **2004**, *48* (5), 647–650.

(89) Kelly, S. M.; Jess, T. J.; Price, N. C. How to Study Proteins by Circular Dichroism.

Biochimica et Biophysica Acta - Proteins and Proteomics. August 10, 2005, pp 119–139. https://doi.org/10.1016/j.bbapap.2005.06.005.

(90) Leney, A. C.; Heck, A. J. R. Native Mass Spectrometry: What Is in the Name? *J. Am. Soc. Mass Spectrom.* **2017**, *28* (1), 5–13. https://doi.org/10.1007/s13361-016-1545-3.

(91) Wilm, M.; Mann, M. Analytical Properties of the Nanoelectrospray Ion Source. *Anal. Chem.* **1996**, *68* (1), 1–8. https://doi.org/10.1021/ac9509519.

(92) Verentchikov, A. N.; Ens, W.; Standing, K. G. Reflecting Time-of-Flight Mass Spectrometer with an Electrospray Ion Source and Orthogonal Extraction. *Anal. Chem.* **1994**, *66* (1), 126–133. https://doi.org/10.1021/ac00073a022.

(93) May, J. C.; McLean, J. A. Ion Mobility-Mass Spectrometry: Time-Dispersive Instrumentation. *Analytical Chemistry*. American Chemical Society February 3, 2015, pp 1422–1436. https://doi.org/10.1021/ac504720m.

(94) Smith, D. P.; Knapman, T. W.; Campuzano, L.; Malham, R. W.; Berryman, J. T.; Radford, S. E.; Ashcroft, A. E. Deciphering Drift Time Measurements from Travelling Wave Ion Mobility Spectrometry- Mass Spectrometry Studies. *Eur. J. Mass Spectrom.* **2009**, *15* (2), 113–130. https://doi.org/10.1255/ejms.947.

(95) Jurchen, J. C.; Williams, E. R. Origin of Asymmetric Charge Partitioning in the Dissociation of Gas-Phase Protein Homodimers. *J. Am. Chem. Soc.* **2003**, *125* (9), 2817–2826. https://doi.org/10.1021/ja0211508.

(96) Ciudad, S.; Puig, E.; Botzanowski, T.; Meigooni, M.; Arango, A. S.; Do, J.; Mayzel, M.; Bayoumi, M.; Chaignepain, S.; Maglia, G.; Cianferani, S.; Orekhov, V.; Tajkhorshid, E.; Bardiaux, B.; Carulla, N. Aβ(1-42) Tetramer and Octamer Structures Reveal Edge Conductivity Pores as a Mechanism for Membrane Damage. *Nat. Commun.* **2020**, *11* (1), 1–14. https://doi.org/10.1038/s41467-020-16566-1.

(97) López, A.; Tarragó, T.; Vilaseca, M.; Giralt, E. Applications and Future of Ion Mobility Mass Spectrometry in Structural Biology. *New J. Chem.* **2013**, *37* (5), 1283–1289. https://doi.org/10.1039/c3nj41051j.

(98) Mora, P.; Carbajo, R. J.; Pineda-Lucena, A.; Sánchez Del Pino, M. M.; Pérez-Payá, E. Solvent-Exposed Residues Located in the β-Sheet Modulate the Stability of the Tetramerization Domain of P53-A Structural and Combinatorial Approach. *Proteins Struct. Funct. Genet.* **2008**, *71* (4), 1670–1685. https://doi.org/10.1002/prot.21854.

(99) Wishart, D. S.; Bigam, C. G.; Holm, A.; Hodges, R. S.; Sykes, B. D. 1H, 13C and 15N Random Coil NMR Chemical Shifts of the Common Amino Acids. I. Investigations of Nearest-Neighbor Effects. *J. Biomol. NMR* **1995**, *5* (1), 67–81. https://doi.org/10.1007/BF00227471.

(100) Ferrage, F.; Zoonens, M.; Warschawski, D. E.; Popot, J. L.; Bodenhausen, G. Slow Diffusion of Macromolecular Assemblies by a New Pulsed Field Gradient NMR Method. *J. Am. Chem. Soc.* **2003**, *125* (9), 2541–2545. https://doi.org/10.1021/ja0211407.

(101) Marsh, J. A.; Forman-Kay, J. D. Sequence Determinants of Compaction in Intrinsically Disordered Proteins. *Biophys. J.* **2010**, *98* (10), 2383–2390. https://doi.org/10.1016/j.bpj.2010.02.006.

(102) Wilkins, D. K.; Grimshaw, S. B.; Receveur, V.; Dobson, C. M.; Jones, J. A.; Smith, L. J. Hydrodynamic Radii of Native and Denatured Proteins Measured by Pulse Field Gradient NMR Techniques. *Biochemistry* **1999**, *38* (50), 16424–16431. https://doi.org/10.1021/bi991765q.

(103) Duhr, S.; Braun, D. Thermophoretic Depletion Follows Boltzmann Distribution. *Phys. Rev. Lett.* **2006**, *96* (16), 1–4. https://doi.org/10.1103/PhysRevLett.96.168301.

(104) Jerabek-Willemsen, M.; Wienken, C. J.; Braun, D.; Baaske, P.; Duhr, S. Molecular Interaction Studies Using Microscale Thermophoresis. *Assay Drug Dev. Technol.* **2011**, *9* (4), 342–353. https://doi.org/10.1089/adt.2011.0380.

(105) Jerabek-Willemsen, M.; André, T.; Wanner, R.; Roth, H. M.; Duhr, S.; Baaske, P.; Breitsprecher, D. MicroScale Thermophoresis: Interaction Analysis and Beyond. *J. Mol. Struct.* **2014**, *1077*, 101–113. https://doi.org/10.1016/j.molstruc.2014.03.009.

(106) Poon, G. M. K.; Brokx, R. D.; Sung, M.; Gariépy, J. Tandem Dimerization of the Human P53 Tetramerization Domain Stabilizes a Primary Dimer Intermediate and Dramatically Enhances Its Oligomeric Stability. *J. Mol. Biol.* **2007**, *365* (4), 1217–1231. https://doi.org/10.1016/j.jmb.2006.10.051.

(107) Chène, P. The Role of Tetramerization in P53 Function. *Oncogene* **2001**, *20*, 2611–2617.

(108) Chène, P.; Mittl, P.; Grütter, M. In Vitro Structure-Function Analysis of the β-Strand 326-333 of Human P53. *J. Mol. Biol.* **1997**, *273* (4), 873–881. https://doi.org/10.1006/jmbi.1997.1360.

(109) Zhou, N. E.; Zhu, B. -Y; Kay, C. M.; Hodges, R. S. The Two-stranded A-helical Coiled-coil Is an Ideal Model for Studying Protein Stability and Subunit Interactions. *Biopolymers* **1992**, *32* (4), 419–426. https://doi.org/10.1002/bip.360320419.

(110) Choy, N.; Raussens, V.; Narayanaswami, V. Inter-Molecular Coiled-Coil Formation in Human Apolipoprotein E C-Terminal Domain. *J. Mol. Biol.* **2003**, *334* (3), 527–539. https://doi.org/10.1016/j.jmb.2003.09.059.

(111) Kjaergaard, M.; Teilum, K.; Poulsen, F. M. Conformational Selection in the Molten Globule State of the Nuclear Coactivator Binding Domain of CBP. *Proc. Natl. Acad. Sci. U. S. A.* **2010**, *107* (28), 12535–12540. https://doi.org/10.1073/pnas.1001693107.

(112) Dijkstra, M. J. J.; Fokkink, W. J.; Heringa, J.; van Dijk, E.; Abeln, S. The Characteristics of Molten Globule States and Folding Pathways Strongly Depend on the Sequence of a Protein. *Mol. Phys.* **2018**, *116* (21–22), 3173–3180. https://doi.org/10.1080/00268976.2018.1496290.

(113) Kuwajima, K. The Molten Globule, and Two-State vs. Non-Two-State Folding of Globular Proteins. *Biomolecules* **2020**, *10* (3).

https://doi.org/10.3390/biom10030407.

(114) Kuusk, A.; Boyd, H.; Chen, H.; Ottmann, C. Small-Molecule Modulation of P53 Protein-Protein Interactions. *Biol. Chem.* **2020**, *401* (8), 921–931. https://doi.org/10.1515/hsz-2019-0405.

(115) Martinell, M.; Salvatella, X.; Fernández-Carneado, J.; Gordo, S.; Feliz, M.; Menéndez, M.; Giralt, E. Synthetic Ligands Able to Interact with the P53 Tetramerization Domain. Towards Understanding a Protein Surface Recognition Event. *ChemBioChem* **2006**, *7* (7), 1105–1113. https://doi.org/10.1002/cbic.200500555.

(116) Schrödinger Release 2017-3: Maestro, Schrödinger, LLC, New York, NY, 2017.

(117) Schrödinger Release 2017-3: Glide, Schrödinger, LLC, New York, NY, 2017.

(118) Harder, E.; Damm, W.; Maple, J.; Wu, C.; Reboul, M.; Xiang, J. Y.; Wang, L.; Lupyan, D.; Dahlgren, M. K.; Knight, J. L.; Kaus, J. W.; Cerutti, D. S.; Krilov, G.; Jorgensen, W. L.; Abel, R.; Friesner, R. A. OPLS3: A Force Field Providing Broad Coverage of Drug-like Small Molecules and Proteins. *J. Chem. Theory Comput.* **2016**, *12* (1), 281–296. https://doi.org/10.1021/acs.jctc.5b00864.

(119) Friesner, R. A.; Murphy, R. B.; Repasky, M. P.; Frye, L. L.; Greenwood, J. R.; Halgren, T. A.; Sanschagrin, P. C.; Mainz, D. T. Extra Precision Glide: Docking and Scoring Incorporating a Model of Hydrophobic Enclosure for Protein-Ligand Complexes. *J. Med. Chem.* **2006**, *49* (21), 6177–6196. https://doi.org/10.1021/jm051256o.

(120) Friesner, R. A.; Banks, J. L.; Murphy, R. B.; Halgren, T. A.; Klicic, J. J.; Mainz, D. T.; Repasky, M. P.; Knoll, E. H.; Shelley, M.; Perry, J. K.; Shaw, D. E.; Francis, P.; Shenkin, P. S. Glide: A New Approach for Rapid, Accurate Docking and Scoring. 1. Method and Assessment of Docking Accuracy. *J. Med. Chem.* **2004**, *47* (7), 1739–1749. https://doi.org/10.1021/jm0306430.

(121) Halgren, T. A.; Murphy, R. B.; Friesner, R. A.; Beard, H. S.; Frye, L. L.; Pollard, W. T.; Banks, J. L. Glide: A New Approach for Rapid, Accurate Docking and Scoring. 2. Enrichment Factors in Database Screening. *J. Med. Chem.* **2004**, *47* (7), 1750–1759. https://doi.org/10.1021/jm030644s.

(122) Schrödinger Release 2017-3: Desmond Molecular Dynamics System, D. E. Shaw Research, New York, NY, 2017. Maestro-Desmond Interoperability Tools, Schrödinger, New York, NY, 2017.

(123) Shaw, D. E. Desmond User's Guide Desmond Version 3.0 / Document Version 0.5.3. **2011**, No. April.

(124) Martos Riaño, V. Polycationic Multivalency : Protein Recognition and Cell Uptake via Oligoguanidinium Scaffolds, 2009.

(125) Ghisaidoobe, A. B. T.; Chung, S. J. Intrinsic Tryptophan Fluorescence in the Detection and Analysis of Proteins: A Focus on Förster Resonance Energy Transfer Techniques. *Int. J. Mol. Sci.* **2014**, *15* (12), 22518–22538. https://doi.org/10.3390/ijms151222518.

(126) Van De Weert, M.; Stella, L. Fluorescence Quenching and Ligand Binding: A Critical Discussion of a Popular Methodology. *J. Mol. Struct.* **2011**, *998* (1–3), 144–150. https://doi.org/10.1016/j.molstruc.2011.05.023.

(127) Jeannerat, D. Rapid Multidimensional NMR: High Resolution by Spectral Aliasing. *eMagRes* **2011**, *2011*. https://doi.org/10.1002/9780470034590.emrstm1187.

(128) Jeannerat, D. High Resolution in Heteronuclear 1H-13C NMR Experiments by Optimizing Spectral Aliasing with One-Dimensional Carbon Data. *Magn. Reson. Chem.* **2003**, *41* (1), 3–17. https://doi.org/10.1002/mrc.1118.

(129) Camilloni, C.; De Simone, A.; Vranken, W. F.; Vendruscolo, M. Determination of Secondary Structure Populations in Disordered States of Proteins Using Nuclear Magnetic Resonance Chemical Shifts. *Biochemistry* **2012**, *51* (11), 2224–2231. https://doi.org/10.1021/bi3001825.

(130) Nguyen, L. T.; Chau, J. K.; Perry, N. A.; de Boer, L.; Zaat, S. A. J.; Vogel, H. J. Serum Stabilities of Short Tryptophan- and Arginine-Rich Antimicrobial Peptide Analogs. *PLoS One* **2010**, *5* (9), 1–8. https://doi.org/10.1371/journal.pone.0012684.

(131) Boöttger, R.; Hoffmann, R.; Knappe, D. Differential Stability of Therapeutic Peptides with Different Proteolytic Cleavage Sites in Blood, Plasma and Serum. *PLoS One* **2017**, *12* (6), 1–15. https://doi.org/10.1371/journal.pone.0178943.

(132) Ding, Y.; Ting, J. P.; Liu, J.; Al-Azzam, S.; Pandya, P.; Afshar, S. Impact of Non-Proteinogenic Amino Acids in the Discovery and Development of Peptide Therapeutics. *Amino Acids* **2020**, *52* (9), 1207–1226. https://doi.org/10.1007/s00726-020-02890-9.

(133) Fominaya, J.; Bravo, J.; Rebollo, A. Strategies to Stabilize Cell Penetrating Peptides for in Vivo Applications. *Ther. Deliv.* **2015**, *6* (10), 1171–1194. https://doi.org/10.4155/tde.15.51.

(134) Eissler, S.; Kley, M.; Bächle, D.; Loidl, G.; Meier, T.; Samson, D. Substitution Determination of Fmoc-Substituted Resins at Different Wavelengths. *J. Pept. Sci.* **2017**, *23* (10), 757–762. https://doi.org/10.1002/psc.3021.

(135) Kreutzer, A. G.; Salveson, P. J. *Standard Practices for Fmoc-Based Solid-Phase Peptide Synthesis in the Nowick Laboratory (Version 1.6.1)*; 2015.

(136) Kaiser, E.; Colescott, R. L.; Bossinger, C. D.; Cook, P. I. Color Test for Detection of Free Terminal Amino Groups in the Solid-Phase Synthesis of Peptides. *Anal. Biochem.* **1970**, *34* (2, 4), 595–598.

(137) Christensen, T. A Qualitative Test for Monitoring Coupling Completeness in Solid Phase Peptide Synthesis Using Chloranil. *Acta Chem. Scand. B* **1979**, *33*, 763–766.

(138) Palasek, S. A.; Cox, Z. J.; Collins, J. M. Limiting Racemization and Aspartimide Formation in Microwave-Enhanced Fmoc Solid Phase Peptide Synthesis. *J. Pept. Sci.* **2007**, *13* (3), 143–148. https://doi.org/10.1002/psc.804.

(139) Gutsche, C. D.; Levine, J. A. Calixarenes. 6. Synthesis of a Functionalizable

Calix[4]Arene in a Conformationally Rigid Cone Conformation. *J. Am. Chem. Soc.* **1982**, *104* (9), 2652–2653. https://doi.org/10.1021/ja00373a060.

(140) Arduini, A.; Fabbi, M.; Mantovani, M.; Mirone, L.; Pochini, A.; Secchi, A.; Ungaro, R. Calix[4]Arenss Blocked in a Rigid Cone Conformation by Selective Functionalization at the Lower Rim. *J. Org. Chem.* **1995**, *60* (5), 1454–1457. https://doi.org/10.1021/jo00110a055.

(141) Casnati, A.; Pirondini, L.; Pelizzi, N.; Ungaro, R. New Tetrafunctionalized Cone Calix[4]Arenes as Neutral Hosts for Anion Recognition. *Supramol. Chem.* **2000**, *12* (1), 53–65. https://doi.org/10.1080/10610270008029804.

(142) Feichtinger, K.; Sings, H. L.; Baker, T. J.; Matthews, K.; Goodman, M. Triurethane-Protected Guanidines and Triflyldiurethane-Protected Guanidines: New Reagents for Guanidinylation Reactions. *J. Org. Chem.* **1998**, *63* (23), 8432–8439. https://doi.org/10.1021/jo9814344.

(143) Hopper, J. T. S.; Oldham, N. J. Collision Induced Unfolding of Protein Ions in the Gas Phase Studied by Ion Mobility-Mass Spectrometry: The Effect of Ligand Binding on Conformational Stability. *J. Am. Soc. Mass Spectrom.* **2009**, *20* (10), 1851–1858. https://doi.org/10.1016/j.jasms.2009.06.010.

(144) Ruotolo, B. T.; Benesch, J. L. P.; Sandercock, A. M.; Hyung, S. J.; Robinson, C. V. Ion Mobility-Mass Spectrometry Analysis of Large Protein Complexes. *Nat. Protoc.* **2008**, *3* (7), 1139–1152. https://doi.org/10.1038/nprot.2008.78.

(145) Rubinson, K. A. Practical Corrections for p(H,D) Measurements in Mixed H2O/D2O Biological Buffers. *Anal. Methods* **2017**, *9* (18), 2744–2750. https://doi.org/10.1039/c7ay00669a.

(146) Hess, B.; Bekker, H.; Berendsen, H. J. C.; Fraaije, J. G. E. M. LINCS: A Linear Constraint Solver for Molecular Simulations. *J. Comput. Chem.* **1997**, *18* (12), 1463–1472. https://doi.org/10.1002/(SICI)1096-987X(199709)18:12<1463::AID-JCC4>3.0.CO;2-H.

(147) Parrinello, M.; Rahman, A. Polymorphic Transitions in Single Crystals: A New Molecular Dynamics Method. *J. Appl. Phys.* **1981**, *52* (12), 7182–7190. https://doi.org/10.1063/1.328693.

(148) Daura, X.; Gademann, K.; Jaun, B.; Seebach, D.; Van Gunsteren, W. F.; Mark, A. E. Peptide Folding: When Simulation Meets Experiment. *Angew. Chemie - Int. Ed.* **1999**, *38* (1–2), 236–240. https://doi.org/10.1002/(sici)1521-3773(19990115)38:1/2<236::aid-anie236>3.0.co;2-m.

(149) Schrödinger Release 2017-3: Protein Preparation Wizard; Epik, Schrödinger, LLC, New York, NY, 2017; Impact, Schrödinger, LLC, New York, NY; Prime, Schrödinger, LLC, New York, NY, 2017.

(150) Schrödinger Release 2017-3: LigPrep, Schrödinger, LLC, New York, NY, 2017.